Design of an in-ear EEG device to detect consciousness levels and be used in monitoring anaesthesia levels of a patient in a medical setting.

by

Carel Wessels

Thesis presented in partial fulfilment of the requirements for the degree of Master of Engineering in Electronic Engineering in the Faculty of Engineering at Stellenbosch University

Supervisor: Prof. W. J. Perold
Co-supervisor: Prof. P. R. Fourie

April 2019

Declaration

By submitting this thesis electronically, I declare that the entirety of the work contained therein is my own, original work, that I am the sole author thereof (save to the extent explicitly otherwise stated), that reproduction and publication thereof by Stellenbosch University will not infringe any third party rights and that I have not previously in its entirety or in part submitted it for obtaining any qualification.

Date: April 2019

Abstract

Design of an in-ear EEG device to detect consciousness levels and be used in monitoring anaesthesia levels of a patient in a medical setting.

C. Wessels

Department of Electrical and Electronic Engineering,
University of Stellenbosch,
Private Bag X1, Matieland 7602, South Africa.

Thesis: MEng (Electronic)

April 2019

There is, as of yet, no feasible and real-time monitor that can accurately determine the level of conciousness experienced by a patient while under some form of general anaesthesia. Existing systems, such as the bispectral indexing (BIS) as well as expiratory vapour measurement techniques such as minimum alveolar concentration (MAC), are both limited in accuracy and in usability. The existing methods use empirical, statistical and historical means to derive at a consciousness indication, rather than a theoretical approach. A system that can accurately monitor levels of anaesthesia (or consciousness) is crucial for eliminating the health risks associated with the overdosing or underdosing of an anaesthetic.

Auditory evoked potentials (AEPs) are the brain's electrical responses, measurable using an electroencephalography (EEG) set-up, to auditory stimulus. Such responses give an indication of the neurological pathway that an auditory signal takes from the eardrum to the processing thereof in the frontal cortex. It also provides an indication of the brains ability to process the information throughout the pathway. Changes in these responses, from a less-obtrusive in-ear electrode, could potentially be utilised to detect the brain's consciousness of the auditory signal and, therefore, the overall consciousness of the patient.

In the clinical trials completed, a characteristic peak latency, namely P_a, of the AEPs was compared to existing measures of anaesthesia and was shown to remarkably outperform the BIS's ability to perceive consciousness. It also produced a more linear response than the commonly used expiratory values (being an indirect measure) and showed potential for better differentiating between all of the different levels of anaesthesia. The research completed could be instrumental in the development of a baseline consciousness monitor that would be beneficial to the health and safety of anaesthetised patients worldwide.

Uittreksel

Ontwerp van 'n binneoor EEG-toestel om bewussynsvlakke te meet en gebruik te word in die monitering van narkose vlakke van 'n pasiënt in 'n mediese omgewing.

("Design of an in-ear EEG device to detect consciousness levels and be used in monitoring anaesthesia levels of a patient in a medical setting.")

C. Wessels

Departement van Elektries en Elektroniese Ingenieurswese,
Universiteit van Stellenbosch,
Privaatsak X1, Matieland 7602, Suid Afrika.

Tesis: MIng (Elek)

April 2019

Daar is nog nie 'n monitor ontwikkel wat die vlakke van bewustheid akkuraat en deurlopend kan bepaal wanneer 'n pasiënt 'n algemene narkose prosedure ondergaan nie. Bestaande stelsels, soos die bispektrale indeks (BIS) en ekspirasie dampmetingstegnieke, soos die minimum alveolêre konsentrasie (MAC), is beide beperk in akkuraatheid en bruikbaarheid. Bestaande metodes gebruik empiriese, statistiese en historiese hulpmiddels om 'n bewussynsindikasie te bepaal, eerder as om 'n teoretiese benadering te volg. 'n Stelsel wat akkuraat die vlakke van narkose (bewussyn) kan monitor, is noodsaaklik om die gesondheidsrisiko's wat betrokke is by die oordosering of onderdosering van narkose, uit te skakel.

Ouditief-ontlokte potensiale (AEP's) is die brein se elektriese reaksie, meetbaar met behulp van 'n elektro-enfalografiese (EEG) opstelling, na 'n ouditiewe stimulus. Hierdie lesing gee 'n aanduiding van die neurologiese pad wat 'n ouditiewe sein volg vanaf die gestimuleerde oordrom tot waar dit in die frontale korteks van die brein verwerk word. Dit dui ook die brein se vermoë, asook moontlike onvermoë (vertragings), om hierdie inligting neurologies te verwerk aan. Geïnduseerde stimuli, deur gebruik te maak van 'n nie-obstruktiewe in-oor-elektrode, kan potensieel aangewend word om die brein se bewussyn van die gehoorsein en dus die algehele bewussyn van die pasiënt te bepaal.

In die kliniese proewe wat voltooi is, is 'n pieklatensie, naamlik (P_a), van die AEP's vergelyk met bestaande narkose-maatstawwe. Daar is bevind dat dit opvallend beter presteer as die BIS se vermoë om bewussynvlakke te bepaal. Dit het ook 'n meer lineêre lesing geproduseer as die algemeen gebruikte ekspirasie waardes (wat 'n indirekte maatstaf

is) en het potensiaal getoon om al die vlakke van narkose beter te onderskei. Die voltooide navorsing kan instrumenteel wees in die ontwikkeling van 'n basislyn bewussyn monitor, wat voordelig aangewend kan word om die gesondheid en veiligheid van narkose pasiënte wêreldwyd te verseker.

Acknowledgements

I would like to express my sincere gratitude to the following people and the organisations that are mentioned in the paragraphs below.

Two of the anaesthesiologists from Stellenbosch MediClinic, being Dr Johan Lourens and Dr Dietrich Eberhard Von Durckheim, who assisted me with identifying feasible patients for clinical trials and arranged for such tests to be done during their surgical procedure. Their expert interpretations of anaesthesia machine parameters were of vital importance to the comparisons made with the findings of this dissertation. They oversaw the communication with consenting patients and assisted the primary investigator with the patient set-up of the device as well as with the performing of the tests within the theatres.

Prof Willem Jacobus Perold and Prof Pieter Rousseau Fourie, being the supervisor and co-supervisor of this dissertation, who continually gave directional guidance throughout the process. They put the investigator in contact with Prof Andreas Retief Coetzee, who should be acknowledged for putting the researcher in contact with the aforementioned anaesthetists.

Bursary funding of the lead investigator for the second year of research, was provided by the Council for Scientific and Industrial Research (CSIR). A partial departmental bursary for the first year of study, was provided by the Department of Electronic and Electrical Engineering of Stellenbosch University.

Although not pertaining to scientific input, a sincere gratitude is extended to Dr Simon Barnes, for the proof-reading and suggestion of linguistic changes to better convey the findings of this documentation.

Dedications

First and foremost,
Praise and Glory be unto ***God****,*
for providing me with the talent, character and capability to complete this thesis.
My help truely comes from the Lord.

Hierdie tesis word opgedra aan my ***Pa, Carel****, en my* ***Ma, Juriehanna****.*
Dankie vir al julle ondersteuning en liefde oor die jare.

Dankie aan my twee sussies, ***Jurica*** *en* ***Illezé****.*
Al is ek vêr van die huis af, het ek julle altyd baie lief.

Finally, I wish to extend my thanks to my extended family, my close-friends and my Pastor. All of your support over the last two years has been sincerely appreciated.

Contents

List of Figures

List of Tables

Nomenclature

Abbreviations

3D	Three dimensional
ABS	Acrylonitrile butadiene styrene
AC	Alternating current
ADC	Analogue-to-digital converter
AEP	Auditory evoked potential
AGND	Analogue ground
BAEP	Brainstem auditory evoked potential
CAD	Computer aided design
CNV	Cognitive negative variant
CSIR	Council for Scientific and Industrial Research
DC	Direct current
DGA	Depth of general anaesthesia
EEG	Electroencephalography
EKG	Electrocardiograms
EMI	Electro-magnetic interference
EMG	Electromyography
EP	Evoked potential
EDC	Expiratory desflurane concentration
ESC	Expiratory sevoflurane concentration
FFT	Fast Fourier transform
HEX	Hexadecimal
IC	Integrated circuit
ICU	Intensive care unit
IDE	Integrated development environment
MAC	Minimum alveolar concentration
MEM	Melted extrusion modelling
MRI	Magnetic resonance imaging
MS	Multiple sclerosis

PCB	Printed circuit board
PLA	Polylactic acid
PPF	Peak power frequency
SD	Secure digital (in microSD card)
SEP	Somatosensory evoked potential
TIVA	Total intravenous anaesthesia
USB	Universal serial bus
VEP	Visually evoked potential
WiFi	Wireless fidelity

Constants

π = 3.14159265359...

Variables

σ	Conductivity	[S/m]
(x, y, z)	Three dimensional Cartesian coordinate	[m]
r	Three dimensional Cartesian vector	[m]
$\bar{J}^i$	Impressed current density	[A/m^3]
ϕ	Electric potential	[V]
$\bar{S}_j$	Regional boundaries	[m^3]
v	Volume	[m^3]
f_c	Cut-off frequency	[Hz]
N_p	Number of samples per period	[Samples]
E_p	Erroneous period time offset	[s]
T_{min}	Minimum period of synchronisation signal	[μs]
t_{click}	Time length of click pulse	[ms]
DC_{signal}	Duty cycle of a signal with the name "signal"	[%]
V_{s1}	ADC step size channel 1	[nV]
V_{s2}	ADC step size channel 2	[nV]
f_L	Low-frequency cut-off	[Hz]
f_H	High-frequency cut-off	[Hz]
P_x & N_x	Characteristic + and − peak latency and amplitude at x	[μV & ms]

Vectors and Tensors

r	Three dimensional Cartesian coordinate, see equation (2.3)

Chapter 1

Introduction

This chapter provides an introduction to and an overview of the system to be designed, so as to motivate the technological innovation presented in this dissertation.

1.1 Problem statement

In today's anaesthesiology industry, there is yet to exist a real-time and feasible consciousness monitoring device that is cross compatible with patients. Instead, vital sign monitoring (including parameters such as blood pressure, heart rate and oxygen saturation that is made available using a pulse-oximeter) is currently used as indicative information of sedation, but is by no means a direct measure. Anaesthetic overdosing lengthens the recovery process of a patient and may result in complications effecting the health of the patient. An underdose of an anaesthetic, in contrast, risks the patient being conscious during painful and critical surgery, which causes complications that could even result in death. It becomes clear that an accurate consciousness monitoring device is of vital importance to the field and forms the basis of the work presented in this thesis.

1.2 Background information

Electroencephalography (EEG) is the name given to conducting measurements of the electrical activity within the brain. Historically, such signals have mostly been measured using electrodes placed on the scalp. The first human-based EEG research records date back to the early 1900's [1]. There is thus no doubt that such technology has existed for quite some time. One of the first evoked-natured studies, was conducted on animals of the class mammalian (more specifically dogs) by a Russian physiologist. He measured evoked potentials by experimentally inducing brain seizures on the subjects and monitoring the potential on the scalp of the animals. He successfully managed to correlate the seizures to spikes within the potential-time plots. Such monitoring systems are commonly made up of reference potentials, bias potentials as well as a series of measurement channels from which data is obtained.

Measuring EEG signals from within the ear (ear EEG or in-ear EEG) is, however, a much more recent innovation on the original invention. The first in-ear reference records only date back to patents from the United States of America at the end of the year 2007. Such sensor placement offers certain advantages over its earlier scalp counterparts, all of which will be discussed in the following section.

Even in modern day anaesthesiology there exists no baseline system that can, in all cases, give an accurate indication of the level of conciousness that a patient has. The bispectral index (BIS) analysis, later defined and although being an algorithm based on electrical brain activity, has historically been shown to often give false information compared with what is clearly observed. Other methods, such as the monitoring of expired anaesthetic agent concentration, provide a better indication of consciousness and are preferred over the BIS value by many anaesthetists.

The BIS values, are determined from an unpublished, empirical (or observational) approach to measuring the cortical frequency spectrum. The empirical, as opposed to theoretically based, nature thereof could be the reason for its significant downside. In practice, many anaesthesiologists opt to not even set-up a BIS during a surgical procedure.

1.3 Significance and motivation

Due to the obtrusive nature of the standard scalp EEG set-up, it has, thus far, not been commercially feasible for the broader perspective of applications. The design of a device that can be truly wearable, without complicated electrode attachment sequences, is therefore of great interest to the larger field of potential commercial applications. Anaesthesia monitoring, is one such field, where the consciousness of patients can be monitored pre-, intra- and post- surgery to ensure that the most efficient recovery process is obtained.

In terms of anaesthesia, the expiratory sedating agent concentration, although using a historically structured guideline, is not a true measure of patient consciousness. The concentration measured is indicative of the concentration of anaesthetic present in the patient's body. Using historical statistical information about age-matched patients, for the same drug, conclusions are made regarding the state of conciousness of the patient. Variability in patient characteristics (such as age, gender and build), as well as the fact that not all anaesthetics are in a measurable expiratory gaseous or vapour form, motivates the need for the design of a device that can incorporate a more direct method for measuring consciousness.

1.4 Research questions

Upon understanding the background of the problem, one can determine research questions that are intended to to be answered during the investigative procedure. The research questions are as follows:

- To what extent is it possible to develop a non-obtrusive, in-ear EEG system that can potentially be used as a consciousness monitor for the anaesthesia industry?
- Which more theoretical approach that could possibly be used, as opposed to empirical bispectral index frequency analysis, for better determining anaesthesia levels?
- Are there potentially further research fields in which such a system could become a viable solution and what could these possibly be?
- What can further research include, to ensure greater rigidity for such a system, if it is successfully verified?

1.5 Assumptions, definitions and limitations

From first perspective, there are certain assumptions that are implied in the initial approach to the design. One such assumption is that, due to the in-ear nature of the EEG system, the surgery of a patient will not be obstructed by the in-ear device. If auditory stimulation is used to evoke a response, one also assumes that the patient has fully functional hearing capabilities in the ear stimulated. Another assumption is that patients will generally consider an in-ear device to be non-obtrusive to their personal space, which may not always be the case.

Limitations of the device to be designed, and verified, will be discussed in Chapter 3. For convenience, any definition of terminology that is irregular, will be done so upon the use thereof.

1.6 Theory base and general literature review

EEG has been around for quite some time, as evident from [1], where Hans Berger, a researcher from Germany, studied the first human EEG signals in 1924. This followed the discovery, by the physician Richard Caton (in 1875), that brain tissue exhibited electrical activity in rabbits and monkeys. In-ear or ear EEG, being a new trend in the field of brain monitoring, provides various advantages over standard on-scalp measurements, but also comes with a cost. There exists a large database of EEG recordings from various medical departments as outlined in [2], but most of these are from conventional 10-20 electrode placement systems and also do not necessarily have the stimulus being investigated. It therefore remains valuable for validating data that is derivative of auditory stimulus (being the chosen method of analysis in Chapter 2), ear EEG as well as acquisition during

anaesthesia (being the field of investigation). It is necessary to have all of these factors present during the data so as to ensure that meaningful results can be obtained.

Automatic sleep monitoring with ear EEG was investigated in [3]. The shortcoming of the approach, used in this finding, was that it analysed raw EEG waves and simply looked at the power spectrum of the frequency bands to draw conclusions about sleep states. This approach is somewhat similar to that of the bispectral index (BIS). Nevertheless, the findings were indicative that ear EEG analysis could be used as an indication of sleep or wakefulness, but with decreasing accuracy as one introduces more sleep deepness states. This results in a more complex decision. The findings in [4] and [5] are similar, being from the same source, and show how auditory evoked potentials, measured from the within the ear, can be obtained. These publications compared on-scalp Auditory Evoked Potentials (AEPs) to the same AEPs taken within the ear. They substantiated the feasibility of ear EEG as a viable way of obtaining and further researching evoked responses, as well as their applications for in-ear electrodes. In [5], it is noted that one can expect a decreased amplitude in the responses obtained from an in-ear electrode, relative to the same standard on-scalp recordings (between 10dB to 20dB attenuation). However, both responses have a similar signal-to-noise ratio, which therefore maintains the feasibility of accurately extracting the waveform.

A study done in [6] shows that a certain characteristic feature in AEPs can vary, in both amplitude and latency, from patient to patient. What this means for the current investigation is that one should incorporate a referential based system when analysing such signals from different source patients. In simple terms, a differential AEP waveform (input from a baseline measurement) may prove to be a better input, for future designed machine learning algorithms, than merely a single AEP waveform.

The material in [7] shows various filters, algorithms as well as techniques one should consider when processing EEG signals. It provides a theoretical background, detailed derivations as well examples of both EEG and event related potentials. This information will be of vital importance when optimising the data analytical algorithms of the designed system.

Having provided an overview of the supporting research in this section, the following section provides a summary of what can be expected from every other chapter in this dissertation.

1.7 Overview

This chapter introduces and motivates the driving force behind the investigation presented in this dissertation. It sets the foundation for the literature study, designs, implementation, experimental procedures and discussion of findings presented in the chapters that follow. For the remainder of the chapters, one can expect that:

- Chapter 2 presents an in-depth literature study in order to conceptualise a potential solution to the problem at hand. It paints a picture that will motivate the direction of the design chapters that follow.
- Chapter 3 methodically shows how the literature, and knowledge gathered thereby, will be utilised for implementing the solution detailed in the chapters thereafter.
- Chapter 4 describes the electrodes of which the final system will comprise, whilst also handling the design and implementation of the ease-of-use of such electrodes.
- Chapter 5 divides the remainder of the hardware system into executable and verifiable subsystems, which are realised and validated in the sections of that chapter.
- Chapter 6 implements the software algorithms, sequences and firmware alterations that are critical to processing the EEG data on-route to the output result. Each subcomponent is also validated individually in order to ensure its functionality.
- Chapter 7 presents the clinical results of the anaesthesia patients tested after the system was successfully implemented.
- Chapter 8 summarises the meaning of the results presented in Chapter 7. This chapter also discusses, in detail, any final aspects required to complete the greater overview of the research findings.
- Chapter 9 brings forth recommendations for prospective studies that may be aligned with the findings of the research in this thesis.
- Chapter 10 briefly concludes the dissertation and reiterates the main findings.

Chapter 2

Literature Study

This chapter discusses all the literature analysed as well as the value that it contributed to the completion of this thesis.

2.1 Introduction

The word electroencephalography (EEG) is used to describe the measuring of electrical activity of the brain using electrodes placed on the scalp. The electrodes effectively act as transducers to transform the ionic electrical nature of the brain function to a measurable potential difference signal. In [8] Swartz presents the history of EEG in detail and describes how the earliest recorded concepts are traced back to a British physician, known as Richard Caton, who presented his work in 1875 on the phenomena that rabbit and monkey exposed cerebral hemispheres exhibit electrical nature.

Schmitt who further proposes the history of EEG in [1] describes how the human brain has well over 10^8 cells which forms a network of storing, handling and processing to make up one of the most complex biological systems. Despite the complexity of the neurological system, the larger summation effect due to changes in electrical charge distribution within the regions of brain, can be measured using simple EEG electrode transducers. Despite being able to detect changes in the charge distribution of larger neuron groups, these electrodes are not able to detect charge changes within a lesser grouping of specific cells. Even modern day EEG technology is far from detecting these signals, since the cellular level communication is both too numerous and too minuscule in charge variation, relative to the larger groups.

According to [9] there have been many claims that neuron numbers are deterministic of computation ability, as well as findings indicating that the human brain contains 100 billion neuron cells and about a trillion glial cells. Despite these claims, the absolute number of these cells remains largely unknown. In [9] it was found that the human brain contains on average 86.1 ± 8.1 billion neurons and 84.6 ± 9.8 billion nonneuronal cells. An isotropic fractionator, which uses a quantification method that calculates density in-

dependent of volume and relates that to measured volumes, was employed to calculate this.

The majority of the neurons in the central nervous system (which includes the brain, brainstem as well as the spinal cord) are of multipolar neuron type, as depicted in Fig. 2.1. In the Neuroanatomy handbook by Patestas and Gartner [10], these multipolar neurons are described as neurons consisting of a single axon with multiple dendrites. These multiple dendrites allows for an integration of this neuron with more than one other neuron and ultimately increases the number of charge polarities that the elementary component can exhibit.

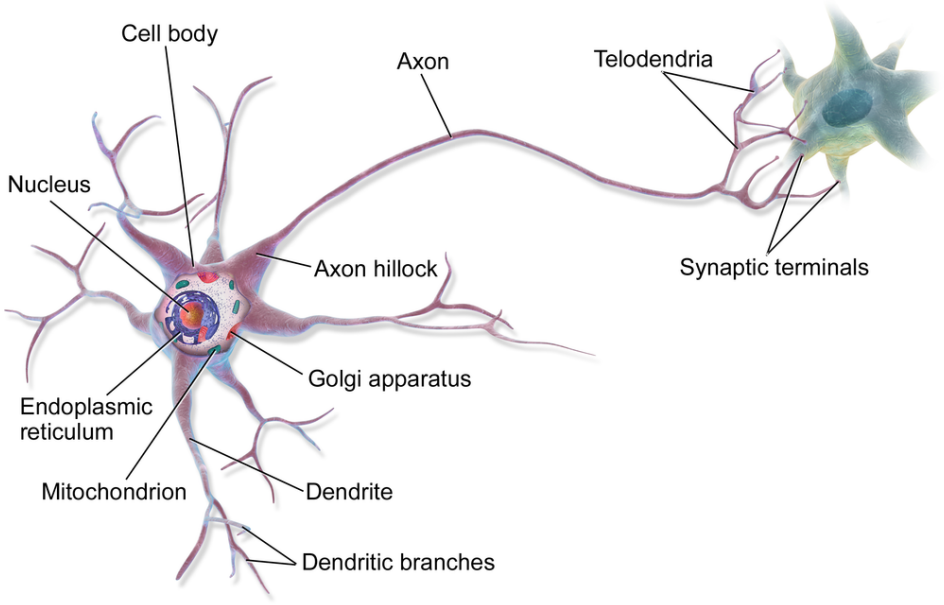

Figure 2.1: Diagram depicting a multipolar neuron [11]

Evoked potentials (EP) are derivative of EEG, as mentioned in [12], and are a description of the mind's reaction to a sensory stimulus that is usually applied by medium of sight (visually evoked potential or VEP), sound (auditory evoked potential or AEP) and touch (somatosensory evoked potential or SEP). The literature also often refers to these induced electrical activities as event related potentials (ERP). Although, this term is often used to dictate a more complex averaging approach where the resulting waveform is more specific to the unique event that is being tested.

Having dealt with the basic biological reason for the signals being present on the scalp, as a result of the summation and propagation of the neural cellular activity, literature more applicable to the application at hand can now be focused on.

2.2 Anaesthesia and monitoring thereof

This section provides an overview of anaesthesia monitoring techniques. Types of anaesthesia and anaesthetics are discussed in later sections (see Section 2.6.5). The focus here is placed on monitoring techniques as well as their shortcomings.

2.2.1 Introduction

General anaesthesia [13], and the successful application thereof, is of great importance in modern day surgical procedures. Successful anaesthesia requires the patient to display reversible loss of consciousness (commonly associated with the regions of the brain shown in Fig. 2.2) with lack of movement, unawareness, lack of response to painful surgical actions as well as an inability to recall the intraoperative events. Inadequate anaesthetic application may result in intrasurgical patient awareness and recall ability (if they were underdosed) or extensive recovery and risk of further complications (in the case of being overdosed). Incidences of inadequate anaesthesia exist largely due to the current limited ability to monitor conciousness [14].

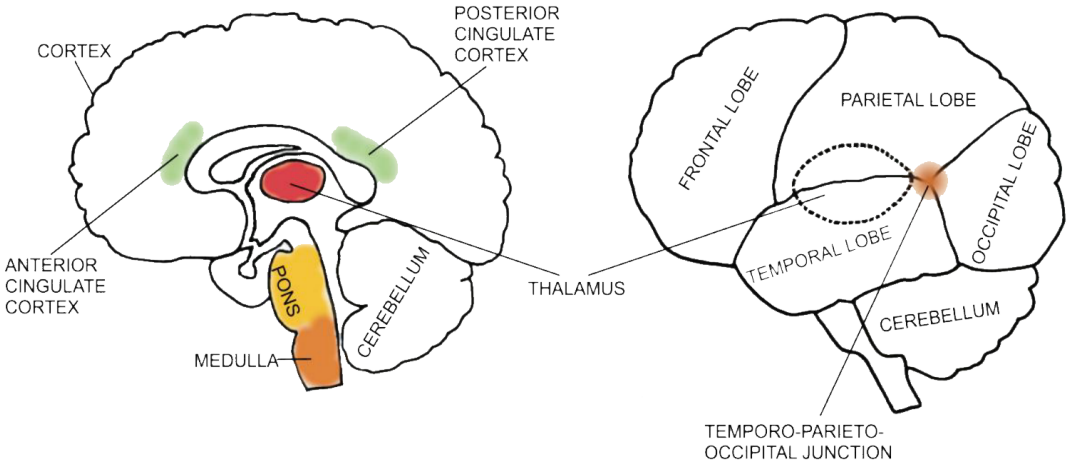

Figure 2.2: Regions of the brain, shown in colour, that relate to a state of conciousness. The spinal cord, brainstem (orange), pons (yellow), thalamic nuclei (red) and regions of the cortex (green) are the nervous system areas that undergo regulation during anaesthesia [13]

It is inherently problematic and challenging to validate newly designed anaesthesia monitoring systems, since there is as of yet no real gold standard [15] of true conciousness measurement to compare these new measurements with. A consensus aimed at deriving the minimum required performance of such a system, resulting from the definition of a validation method, would prove useful in determining the clinical feasibility of many

evoked potential and EEG based trials [16]. A few of the current methods for monitoring DGA (or depth of general anaesthesia) are discussed in the following sections.

2.2.2 Bispectral analysis

Bispectral analysis/index (BIS) is a statistically derived, empirical parameter that is calculated using weighted coefficients of various time-domain, frequency-domain and higher order spectral subparameters [17], [18]. The BIS utilises input from a single channel electrode placed on the forehead to output a dimensionless score between 0 and 100, where 100 signifies full conciousness and 0 represents full unconsciousness [13]. The exact details of the algorithm have not yet been released by the developing company, Aspect Medical Systems. In essence, a shift of dominant higher frequency components in the awake state of a patient, to predominant low frequency components during the anaesthetised state of a patient, is observed. The algorithm relies predominantly on this observational data to output an index giving an indication of apparent conciousness.

There are, however, shortcomings to such a technique [19]. Ketamine (an anaesthetic agent) does not change the value of BIS even if the patient has all the other signals of being unconscious. On the contrary, when ketamine is applied during total intravenous (applied by means of a vein) anaesthesia with fentanyl and propofol, there is an unexpected increase in the BIS value. The explanation is likely due to hypoperfusion (or drop in blood flowing through an organ) as a result of the multiple anaesthetics being present.

Application with another agent, xenon, has been recorded to have patients awake whilst the BIS value seemingly signifies deep anaesthesia. The effect of nitrous oxide on raw and evoked EEG signals is varied and therefore unpredictable. Figure 2.3 shows a comparison of EEG frequency bands (see Section 2.4.2 for the definition of these bands) during pentobarbital and ketamine anaesthesia. The changes observed contribute to the reasoning behind the abnormal BIS values output during certain anaesthetic applications.

Raw EEG, and therefore BIS outputs, are susceptible to internal (such as head muscles [20]) and external sources (hospital equipment and mains) of electromagnetic interference (EMI). Averaging, as long as the stimulus rate is not a precise factor of the EMI frequency, removes most internal and external sources of interference. Other design considerations such as shielding can be used to attenuate or remove external sources of EMI.

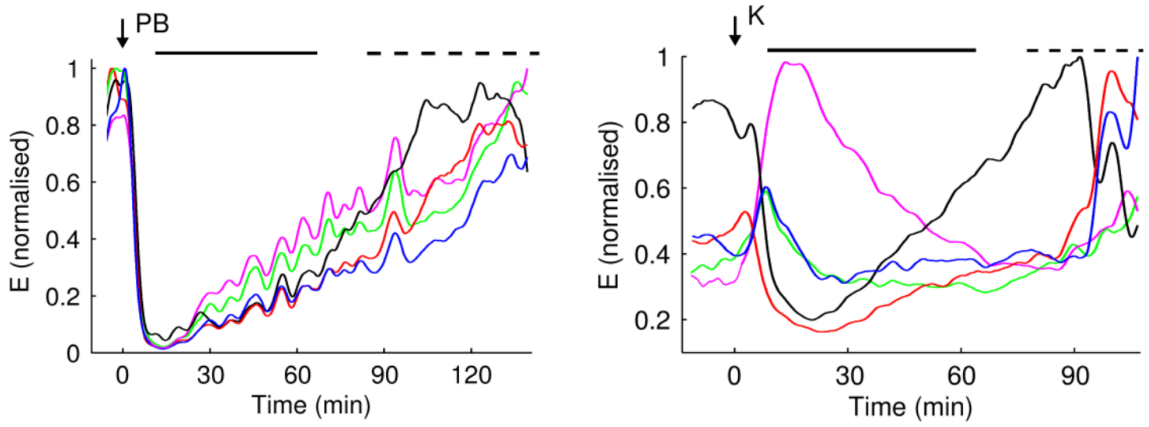

(a) Pentobarbital (PB), like most general anaesthetics, increases the activity of γ-aminobutyric acid type A receptors ($GABA_A$) which induces anaesthesia

(b) Ketamine (K), like xenon and nitrous acid, produce anaesthesia by acting upon other receptors in the brain (such as the N-methyl-D-aspartate excitatory receptor)

Figure 2.3: Relative normalised spectral power changes during anaesthesia procedures. The solid line represents deep anaesthesia, the dotted line represents shallow anaesthesia and the arrow represents the commencement of application. Legend to colour plot frequencies: black (δ), red (θ), blue (α), green (β) and violet (γ) [13]

2.2.3 Concentration of anaesthetic

Another intrasurgical medium of monitoring a patient is measuring the concentration of anaesthesia present in the patients body. The intravenous or inhalation concentrations of anaesthetics, that go into the subject, can be controlled by the machine applying it, but this is by no means an accurate measure of DGA, due to its input and not sensed nature. A high concentration applied to initiate anaesthesia does not indicate a deeply anaesthetised patient. Concentrations needed for loss of conciousness also vary substantially with age, health and other patient-related variables [16], [21], [22]. These differences in pharmacodynamics (drug effect and mechanism in body) again provide motivation for the need for a system capable of detecting clinical state transitions (concious to unconscious and visa versa).

Another intuitive system involves measuring the concentration of anaesthetic drug present in the body, giving a far better indication of the level of sedation than the input concentration. One such a monitoring set-up, found in many modern anaesthetic machines, involves detecting the concentration of agent present in the expiratory air (as opposed to the inspiratory breaths). These concentrations are often recorded as a percentage composition concentration for gas and vaporised agents or milligram per millilitre (mg/ml) for other liquids and solids. Although providing a better indication of sedation,

the problem with such a measurement is that it still provides no direct measure of conciousness (rather an indication of how much agent is present in the body) and is therefore not considered a true DGA measuring method.

2.3 Ten-twenty system electroencephalography

Standards for electrode placement schemes, for EEG systems on the scalp, have been designed to promote comparability of research in the field. The most commonly used system is the ten-twenty layout as modernly standardised by Klem in [23]. The system obtains its name through the 10% and 20% relative spacings used to locate electrode placement points after identifying anatomical landmarks on the head. The nasion, being the distinct depressed concave region between the eyebrows above the nasal bridge, is connected via the midline of the scalp to the inion, being a crest or characteristic convex point at the back of the scull for creating the first referential geometry. A second referential line is drawn from the one tragus (the small cartilage that is found on the anterior of the pinna, see Fig. 2.4) to the opposite tragus and cuts the middle-point of the first reference on the midline.

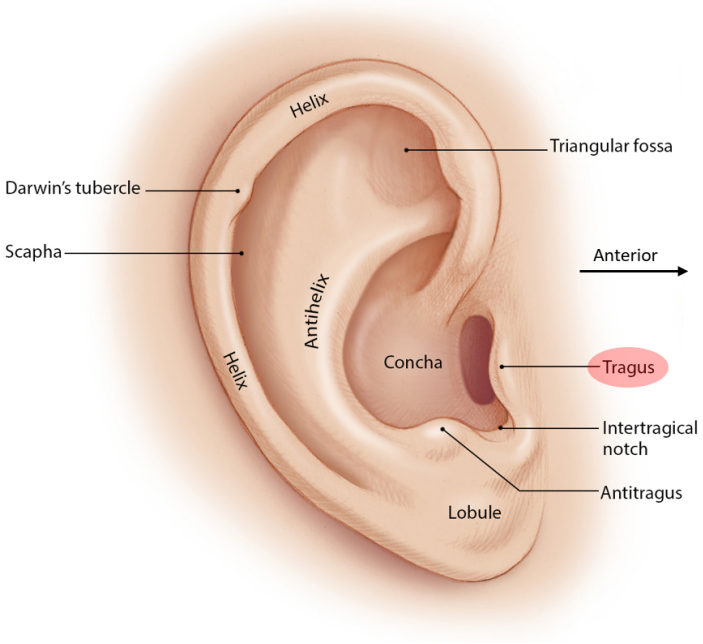

Figure 2.4: Diagram depicting a pinna (exterior ear) anatomy [24]

Conceptually these two referential geometries are divided into segments

$$S = \{10\%, 20\%, 20\%, 20\%, 20\%, 10\%\} \tag{2.1}$$

where S is the subsequent section spacing percentages of the relative full distance between adjacent reference points. Figure 2.5 depicts the original diagram, by Jasper [25], for the

system. As can be seen from the figure, the electrodes were erroneously depicted to be situated interior to the skull instead of exteriorly. The described system set-up process is modernly detailed in the manual of Trans Cranial Technologies obtainable at [26], where one can clearly see that the standard minimal set-up contains about 21 electrode positions, with even more extensive set-up topologies that utilize the void space between electrodes for even more sensor points.

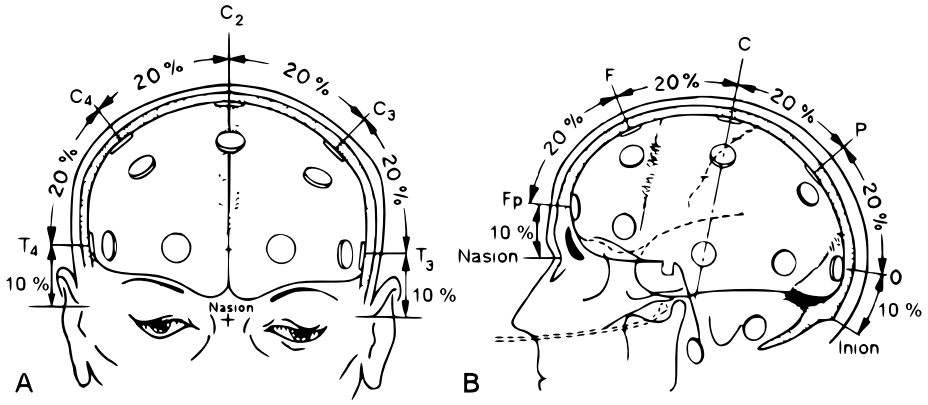

Figure 2.5: Original figure illustrating the international 10-20 system [25]

Attaching 21 electrodes along with possible ground and bias points becomes an obtrusive as well as time-extensive process. Using less electrodes means losing the ability to originate signals to a specific area of the brain.

This trade-off can be described using the analogy of the pond which is often used in the literature and clearly described in chapter 3 of [27]. Imagine the brain being a circular pond and each processed calculation or brain event being like an object thrown into the pond. These objects cause a ripple in the water, that propagates away from the source, just like a brain process causes an electrical 'ripple' that propagates outwards. An EEG electrode placed on the scalp is like a sensor positioned somewhere on the circumference of the pond to detect the ripples.

If a tyre is thrown into the pond, it will produce a characteristic ripple at the position of the sensor. The challenge, however, arises when it is not known what, where and when something was thrown into the pond. In such a scenario, what was thrown into the pond and where and when this occurred, can only be guessed with a low level of certainty, since there is not enough information available. Adding more and more sensors around the circumference of the pond, which in the case of the EEG would be like adding more electrodes to the head, would give increasingly more accurate information on where exactly an object was thrown into the pond. Once it has been more accurately narrowed down to a region of the pond, the time can also be predicted using knowledge of water ripple propagation velocity as well as by correlating the relative times that each sensor detected

the characteristic ripple.

Now imagine that the object being detected is not the only object being thrown into the pond at one time, but that there is in fact a multitude of simultaneous events happening at any given moment. It is important to note that although having more sensors may give a better indication of the location and time that the event happened, the increased number of sensors are still unable to determine , with sufficient certainty, what the object was that caused the ripple.

The other downside of such a layout is its obtrusive nature due to a large number of electrodes that all need to make skin contact with the scalp, especially areas that are often covered with hair. Hair therefore needs to be either moved away or trimmed to allow the electrodes to make sufficient (having low enough contact impedance) contact with the skin. In-ear electrodes are a recent trend for reducing such an invasive property, but inherently calls for techniques other than increasing the quantity of electrodes to solve the "when, what and where" dilemma discussed in the previous paragraph.

2.4 Conventional methods

The contents of this section are predominantly from [28] in which Malmivuo creates a clear referential explanation of conventional EEG methods.

2.4.1 General information

It is generally understood that neuron groups produce some electric field source that is able to propagate outwards due the conductivity of the matter around the source. To better understand how such propagation occurs, models have been developed to provide a mathematical explanation. Considering that the matter is inhomogeneous, one needs to note that propagation is not uniform in all the possible radial directions. When modelling the propagation of an electric macroscopic volume source, in an inhomogeneous volume conductor, one can start by understanding the derived equation for a homogeneous infinite volume given by

$$4\pi\sigma\phi = \int_v \bar{J}^i \bullet \bigtriangledown \left(\frac{1}{r}\right) dv \tag{2.2}$$

where σ is the conductivity of the medium, $\bar{J}^i$ is the impressed current density that arises from from averaging the dipole elements of all the neuron cells involved in the volume of the source, ϕ is the scalar electric potential, r is effectively the distance of the field point from the source given by $r = \sqrt{(x-x^{'})^2 + (y-y^{'})^2 + (z-z^{'})^2}$ where (x, y, z) is the source Cartesian coordinate and $(x^{'}, y^{'}, z^{'})$ is the coordinate of the field point. The term $\bar{J}^i \bullet \bigtriangledown \left(\frac{1}{r}\right)$ represents the current density/flow through a volume V, using Cartesian coordinates. The integral thus determines the quantified flow for a specific volume v. To

account for an inhomogeneous environment the equation can be altered to:

$$4\pi\sigma\phi(r) = \int_v \bar{J}^i \bullet \bigtriangledown \left(\frac{1}{r}\right) dv + \sum_j \int_{sj} \left(\sigma_j^{''} - \sigma_j^{'}\right) \phi \bigtriangledown \left(\frac{1}{r}\right) \bullet d\bar{S}_j. \tag{2.3}$$

The inhomogeneous volume conductor can be divided into a finite number of volumetric boundaries denoted by $\bar{S}_j$. On the boundaries there should be a continuous electric potential ϕ as well as a normal component of current density. The second term in equation (2.3) effectively sums up the effect of each different homogeneous region to produce an overall effect of the inhomogeneities on the volume. The first term is exactly the same as equation (2.2) and represents the contribution of the volume source. Finally the term $\left(\sigma_j^{''} - \sigma_j^{'}\right)$ represents the difference in conductivity on each boundary S_j. It can be noted that for a solely homogeneous volume, that implicitly has a constant conductivity, it follows that $\left(\sigma_j^{''} - \sigma_j^{'}\right) = 0$ which in turn implies that $\sum_j \int_{sj} \left(\sigma_j^{''} - \sigma_j^{'}\right) \phi \bigtriangledown \left(\frac{1}{r}\right) \bullet d\bar{S}_j = 0$. Equation (2.3) can therefore be reduced back to (2.2)

2.4.2 Frequency spectrum approach

Although equation (2.3) can principally derive EEG, the complexity of the brain system has made it near impossible to determine the source function $\bar{J}^i$ and feasibly use such an approach in practical applications. The model can, however, be successfully applied to simpler sensor set-ups such as electrocardiograms (EKG) that measures the electrical signal of the heart as well as electromyography (EMG) that likewise measures signals produced by skeletal muscles. As a result, quantitative EEG studies have become largely statistical and clinical EEG largely empirical. One such an approach is to observe the frequency power spectrum as shown by a normal measurement in Fig. 2.6.

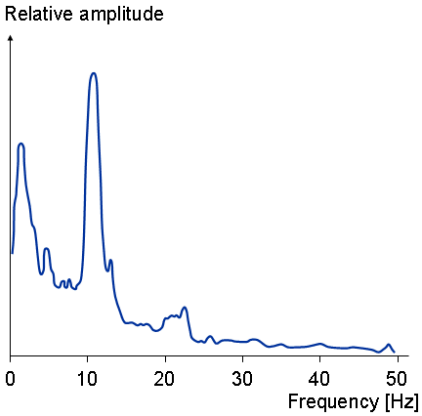

Figure 2.6: Frequency spectrum of normal EEG signals [28]

The frequencies of importance usually lie between 0.5 Hz and 50 Hz in the power analysis of an EEG. The relative levels of all the different frequency bands, as well as the area they originate from, provides insight into the mental state of a subject or patient.

Table 2.1 summarises the historically derived bands as well as providing an indication of the associated phenomena or sources thereof based on observation over time.

Table 2.1: Table showing the frequency bands of note when analysing the brain EEG

Name	**Frequency range (Hz)**	**General occurrence**
Delta (δ)	$0.5 - 4$	Infants, sleeping adults, usually frontally in adults, usually posteriorly in children.
Theta (θ)	$4 - 8$	Children, sleeping adults, drowsiness of older children and adults, meditation, focal disturbance, relaxed and creative states.
Alpha (α)	$8 - 13$	Occipitally, usually posterior in adults, high amplitude in dominant hemisphere, closing of eyes and relaxation.
Beta (β)	$13 - 30$	Frontally and parietally, symmetrically both hemispheres, motor behaviour, active state, busy state, anxious thinking and active concentration. Usually absent or attenuated when cortical damage has occurred in region.
Gamma (γ)	$30 - 50$	Binding of different neuron populations together for motor or cognitive function. Usually low relative power.

Having observed the normal frequency spectrum in Fig. 2.6, it may be useful to visualise how the different bands commonly occur in the time domain. Figure 2.7 provides sample waveforms of the various frequency divisions introduced in Table 2.1. Additionally, an example of spike behaviour close to 3 Hz, observed in a patient who was experiencing an epilepsy petit mal (or absence) seizure, during which subjects commonly loose consciousness for a time usually shorter than 15 seconds, was provided.

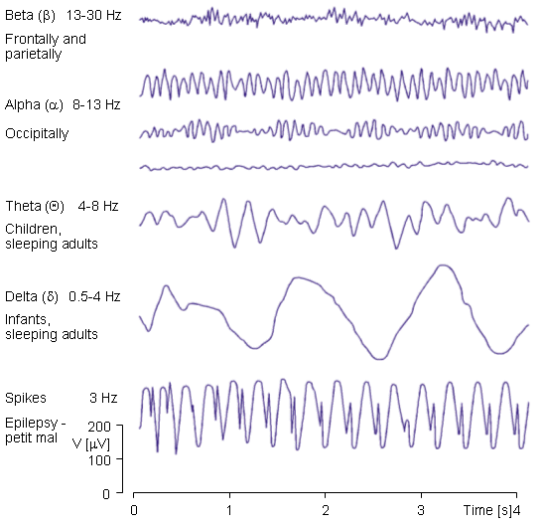

Figure 2.7: Frequency bands used in conventional observations [28]

2.4.3 Measuring set-up

One of the fundamental principles in measuring voltage signals is having a reference potential (usually referred to as ground) to which the recorded potential is compared, producing a potential difference (or voltage). An electrostatic potential is the potential energy per unit charge of a point. A potential difference is the work done moving a unit positive charge between two points against the electric force. Figure 2.8 depicts two of the standard set-ups used in recording EEG potential differences, namely bipolar in Fig. 2.8a and unipolar in Fig. 2.8b.

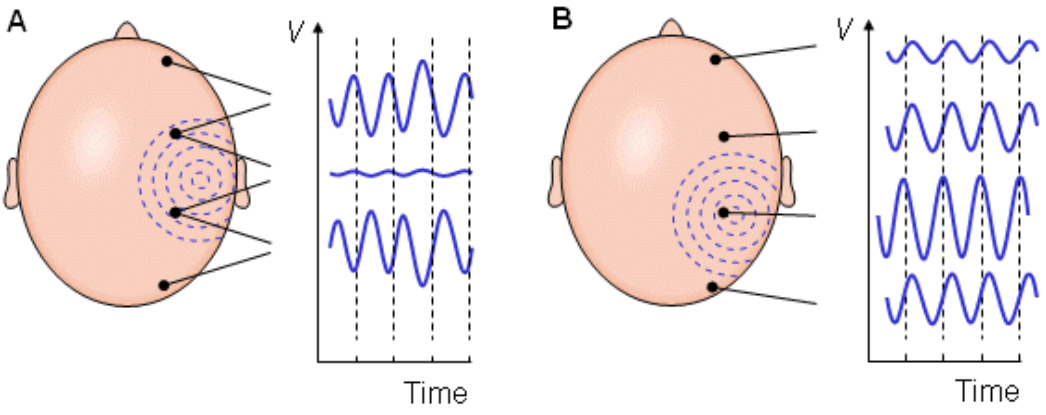

(a) Bipolar **(b)** Unipolar

Figure 2.8: Recording methods from electrodes [28]

The bipolar configuration measures the potential difference between two electrodes, while unipolar measurements takes the voltage between an electrode and either an average potential of all the electrodes or some electrode (referred to as the reference or ground electrode) chosen for its electrically neutral properties. The circular dotted blue lines in Fig. 2.8 represents a specific EEG frequency source. Due to both interior electrodes being close to the source in Fig. 2.8a and relatively in-phase, the signal measured between these is small in nature. The exterior electrodes, measured relative to the internal ones, produce a larger signal amplitude due to the larger signal difference, based on the distance from the source. These signals are inverted due to the alternation of differential positive and negative inputs.

A unipolar set-up more accurately represents the activity per region. The closer an electrode in Fig. 2.8b comes to the source of the bioelectric generated frequency, the larger the amplitude, as would be expected from the model of equation (2.3). Due to the propagation time and phase of the signal, one can like-wisely expect an phase offset at the electrode location.

2.5 In-ear electroencephalography

The last decade has seen a clear rise in investigations into in-ear EEG applications, as is evident from an IEEE Xplore search of the term. Section 2.5.1 analyses a few such studies.

2.5.1 Previous studies and findings

One of the most recent studies, in [29], contains research by Nakamura pertaining to the use of an in-ear EEG device in becoming a wearable biometric identification device. The research involves the use of robust power spectral density and autoregressive analysis to uniquely identify signatures of individual wearers. The recording duration of the EEG data was set to 60 seconds and tested over 15 subjects. A half total error rate of 17.2% and accuracy of 95.7% was achieved, which for an initial proof-of-concept, is substantially impressive.

Likely the most relevant research to the work of this thesis (contextually this will become clear once Section 2.6 has also been read) was done by Kidmose (both in [4] and [5]), who set out to verify whether it is feasibly possible to obtain event related potentials (ERPs) from an in-ear and non-obtrusive electrode set-up. It was found that, although evoked potential amplitudes were almost 20 dB lower than those of their vertex counterparts, a similar signal-to-noise ratio is maintained.

Furthermore, the investigated in-ear evoked potentials of visual, somatosensory and auditory stimulus origin had a strong resemblance to the standard temporal lobe evoked potentials. It was noted, in the articles, that some differences were also observed due to the inhomogeneous characteristic of brain matter. The overall conclusion that was drawn, is that it is possible to record evoked potentials from within the ear.

Although the papers identified potential in the future use of in-ear evoked potentials, it by no means investigated any specific uses thereof. This thesis thus aims to further validate the findings of Kidmose and possibly identify its potential in an end user market (such as anaesthesiology), in which it could become industry-disruptive.

2.5.2 In-ear anatomy

In order to understand the obtained sensor data and successfully design a system that records EEG data from within the ear, it is necessary to study the anatomy of the ear to make appropriate design choices as well as understand the origin of recorded data. The textbook by Marieb [30] gives a detailed background of the required anatomy and contains a useful labelled diagram, as shown by Fig. 2.9.

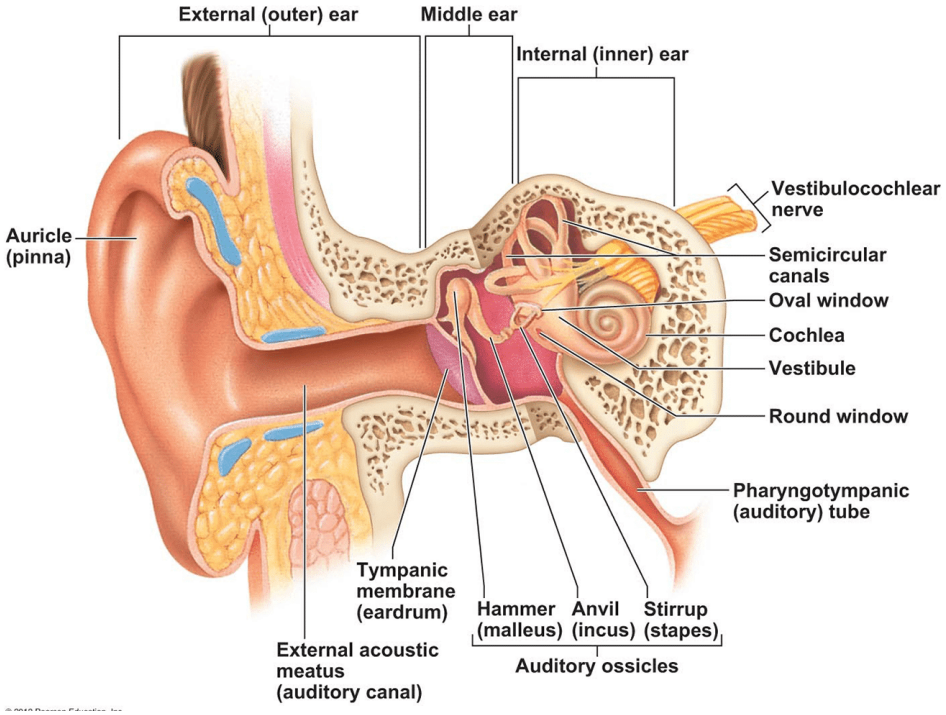

Figure 2.9: Diagram depicting the cross sectional anatomy of the ear [30]

From the figure it is seen that the external acoustic meatus (or auditory canal) is a roughly circular tube that leads from concha (labelled in Fig. 2.4) to the tympanic membrane (commonly known as the eardrum). As acoustic waves collide with the membrane, it produces motor oscillations which transmit the oscillatory behaviour onto the cochlea via medium of the auditory ossicles. The auditory ossicles are essentially a series of three bones (also known as the ear bones) which are able to mechanically transfer the kinetic behaviour from the one side to the other. The cochlea is responsible for the conversion of the kinetic oscillatory energy into electrical energy which is sent to the auditory cortex of the brain my medium of the vestibulocochlear nerve.

The average diameter of the auditory canal is given by [31] to be between 8 mm to 10 mm. From the structural geometry output in [32] the average length of the canal is given to be 25 mm with an approximate diameter of 7 mm. The canal is described to flow in a slightly sigmoid shape in most of the observed individuals and the cross sectional geometry is stated to be more accurately characterised as an ellipse, which is a contributing reason for the slight discrepancy in diameter measurements found in the literature.

2.5.3 EEG measurements extended analogy

In expanding the analogy of the pond, from Section 2.3, let it be required that it is not favourable to have multitudes of sensors distributed around the circumference of the pond,

but rather a single sensor. This requirement correlates to designing an EEG system that is non-obtrusive as well as non-complex to set-up. In order to produce a system that is still able to produce some meaningful information from the vast pool of signals, one needs to develop an approach that solves some of the dilemmatic questions that arise from having such a simplified system.

Conceptualise a scenario where the item thrown into the pond as well as its location and time are fixed, i.e. it is no longer the system that attempts to detect whether and where a tyre was thrown into the pond, but a system that knows it can expect a tyre to be thrown at a certain location of the pond at a certain time. The sensor information is therefore guaranteed to contain ripple information as a result of the tyre. Although it is known that the tyre was thrown into the pond at a specific time interval and location, the apparatus has no knowledge of whether other large objects where also thrown into the pond at the same time.

It can therefore not be concluded that the ripple information sensed is solely as a result of the tyre. On the contrary, a large or even majority portion of the signal can actually be attributed to different sources depending on the relative size and proximity of the objects. How does it thus become possible to obtain the response that can be exclusively attached to the tyre? Mathematically, if the object can be repetitively thrown into the pond at a known constant frequency, one can find an average of the period that mostly correlates to the effect of the tyre (with perhaps minimal residual noise remaining due to time limitations of measurements).

This analogy effectively introduced what is known as evoked potentials. It detects the components of EEG that arise from stimulus such as electric, visual, auditory or somatosensory. These components are usually well below the noise level of all the ambient EEG activity and are therefore not readily distinguishable until a train of stimulus data has been obtained and the period average has been determined. This motivates research into such an approach as done in the following section.

2.6 Evoked Potentials

Walsh [33] presents the clinical role of evoked potentials (EPs) in the modern day health-care industry. This section outlines the ideas and key concepts obtained from the presented article.

2.6.1 Background and Introduction

The neuro-electric response of the brain to almost any sensory stimulus can be recorded in a non-invasive and simply set-up fashion. The averaging of evoked potentials was first employed by Dawson [34] in 1947. The clinical value of an evoked potential system is

- to demonstrate a patient with abnormalities in processing sensory information when historical or neurological examinations are questionable;
- to reveal a subclinical effect on a sensory system, especially one where demyelination (or damaging of nerve protective sheaths caused by a disease) is occurring and produces attenuation or even elimination of nerve impulses;
- To assist in defining the anatomic arrangement of the neurology system and become valuable when evaluating the pathophysiology of a disease (the disordering of physiological processes due to diseases or injury); and
- in monitoring a patient's neurological state and changes thereof.

The most commonly used variants of evoked potentials in industry are those that are evoked using pattern reversal visual stimulus (VEPs, see Section 2.6.2), short latency somatosensory stimulus (SEPs, see Section 2.6.3) and a division of auditory stimulation that focuses on the impulses of the brainstem (BAEP, see Section 2.6.4). Other less common clinical approaches are auditory responses with a larger latency that targets receiving more of the cognitive function information, contingent negative variant (CNV) and sensory potentials induced by stimulating regions with a CO_2 laser.

A arbitrary example of how a typical evoked potential response is observed is given by Fig. 2.10. Note that the example was created for referential purposes only and is by no means an actual recorded signal.

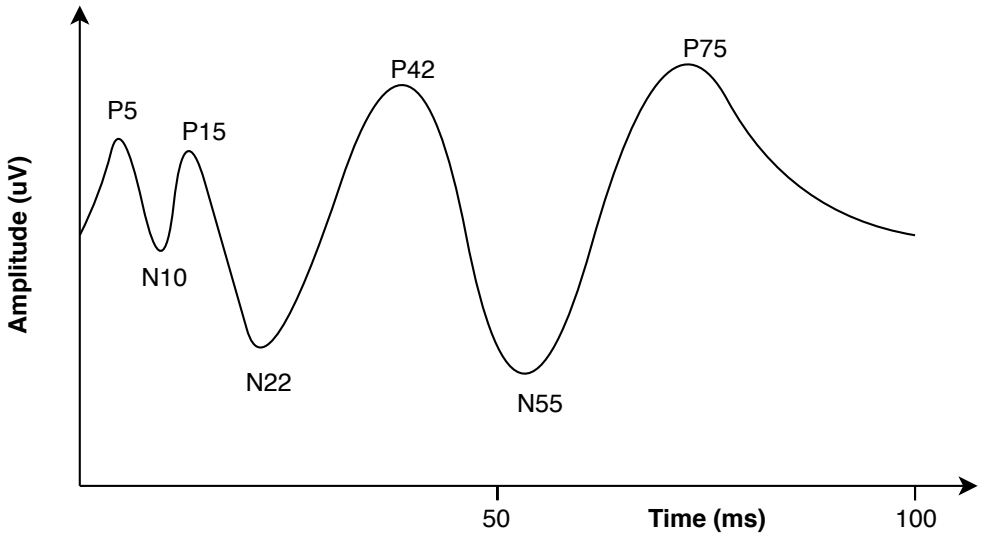

Figure 2.10: An example of an evoked response for some arbitrary stimulus

Evoked responses can be easily classified both in terms of latency (time from stimulus onset to specific response) and magnitude. One of the naming conventions for characteris-

tic crests and troughs throughout the response, is that crests receive the letter P (denoting a positive peak) and troughs receive the letter N (denoting a negative peak). The number that follows the letter is indicative of the time in ms after which that local minimum or maximum usually occurs in the EPs of like-wise nature. Another conventional naming technique involves naming the crests with sequential capital Roman numerals, which is especially used when analysing BAEPs.

It can be deduced from the $100ms$ period of Fig. 2.10 that the frequency of stimulation is likely $f = \frac{1}{P} = \frac{1}{0.1s} = 10$ Hz and that P5, N10 and P15 are the initial neuro-electric responses to the stimulus occurring in the sensory nerves closest to the source of stimulation. The remaining wave characteristics from N22 to P75 are more delayed responses resulting from either the transmission or processing of the stimulus, depending on the specific example studied.

EPs have several advantages over detailed neurological evaluations. Such recordings are often more objective as well as sensitive and it is possible to use them on patients that are either anaesthetised or comatose. The latter advantage, along with the constant upgrading and optimisation of the technology, has led to new applications in the intensive care unit (ICU) as well as surgical theatre, whilst magnetic resonance imaging (MRI) systems have predominantly been replacing older EP equipment in the assessment of multiple sclerosis (or MS, being the damage or weakening of nerve myelin coverings). EEG systems can obtain electrical information in relative real-time as opposed to other techniques that often contain much larger latencies from event to detection of the corresponding effects.

The disadvantages of EPs are that they are mostly disease unspecific, they dynamically change with age, they require some form of patient cooperation to obtain artefact-free data as well as being susceptible to end organ diseases (for example, VEPs are affected by ocular disease, SEPs are abnormal in subjects with peripheral neuropathy and BAEPs are subject to the absence of conductive and sensorineural deafness).

The three predominantly discussed EPs in this section are further studied and characterised in the following sections to provide application specific background and insight.

2.6.2 Visually Evoked Potentials

VEPs provide diagnostic ability for patients with visual abnormalities such as demyelinating disease, optic neuritis and several other optic neuropathies. The stimulus is of pattern reversal type, where a black and white checkerboard, spanning at least the central 20°–30°of the visual field, periodically inverts black and white squares to induce a visual response. The averaged signal waveform is thus a result of the reversal of the pattern.

Figure 2.11 demonstrates monocular (right side of figure) and binocular (left side of figure) responses to a full field stimulus. There are three VEP electrode channels

placed posteriorly on the occipital region with the ground electrode positioned mid frontal. Electrodes are also placed close to each eye to record the average activity in that region. The monocular recordings show the unused/obstructed eye electrode signal tending to ground as it is not stimulated. The square pulse on the bottom left gives indication of scale and also indicates that the y-axis has been inverted (resulting in inversion of P and N labels). VEPs normally contain a prominent positive component roughly 100 ms after the time of reversal at P100 which is also normally preceded by a trough at N75. The stimulated eye(s) proximity electrodes normally have a P50 and N95 component resulting from optical nerve activity.

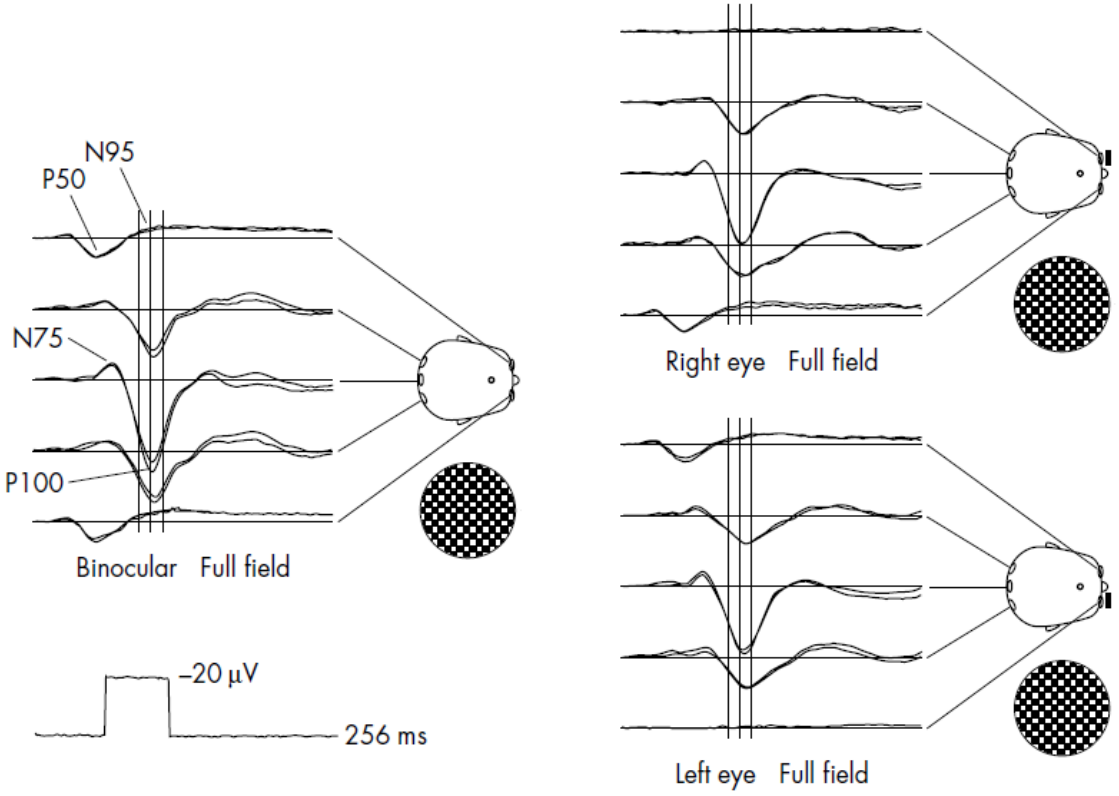

Figure 2.11: Visually evoked responses based on full field pattern reversal where the vertical lines represent the mean latency of P100 with its 99.5% confidence intervals (± 2.5 SDs) [33]

The vertical lines represent the mean and 99.5% confidence intervals of P100 latency, as determined from normal subjects. If P100 occurs outside of the bounds of the interval, it can usually be deduced that there is visual abnormality present in the patient. Figure 2.12 shows some of the abnormalities that deviate from the normal measurements of 2.11.

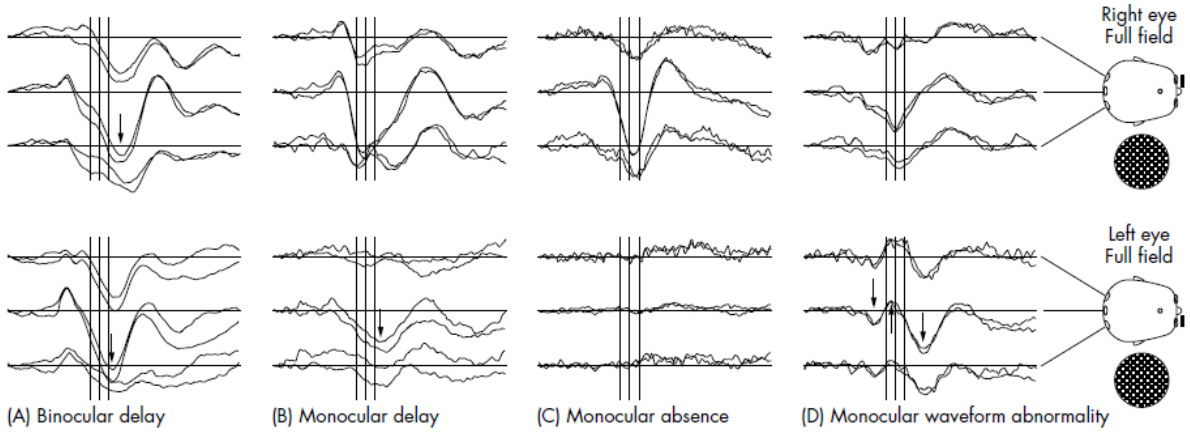

Figure 2.12: Visually evoked responses for commonly occurring abnormalities based on full field pattern reversal stimulus [33]

In Fig. 2.12, part (A) depicts the phenomenon of having the P100 latency prolonged (to the extent that it falls outside the confidence interval) binocularly, part (B) marks the same phenomenon but only occurring monocularly in the left eye, part (C) marks the irregularity of having a predominantly absent response monocularly in the left eye and part (D) again marks an abnormally shaped monocular response in that of the left eye. Any impairment of the conduction in the retino-striate path will likely cause the above-mentioned affects on the latency, amplitude and shape of the VEP waveform, which can be associated with demyelination regardless of the specific disease. Traumatic brain injuries are believed to cause diffuse axonal injury and therefore also effects nerve conduction to an extent related to injury severity. Other studied causes of nerve conduction loss include toxic causes such as tobacco-alcohol amblyopia as well as nutritional causes such as vitamin B12 deficiency.

2.6.3 Short Latency Somatosensory Evoked Potentials

SEP responses, from percutaneous (that is through the skin) electrical stimulation of the upper limbs (for example the median nerve), are usually completed within 30 ms and lower limbs (such as the tibial nerve) within 60 ms. The source of the waveform is likely the successive activation of synaptic and action potentials from bioelectric generators within the dorsal–lemniscus (being the central nervous system pathway carrying information such as fine touch and vibrations to the primary somatosensory cortex) and thalamo–cortical (the pathways from the thalamus [35], which lies between the midbrain and cortex and functions as a relay of sensory signals to the cortex, where the perception of the sensory signals is processed). Figure 2.13 epitomises the responses that can be expected from SEP tests, both normal and abnormal.

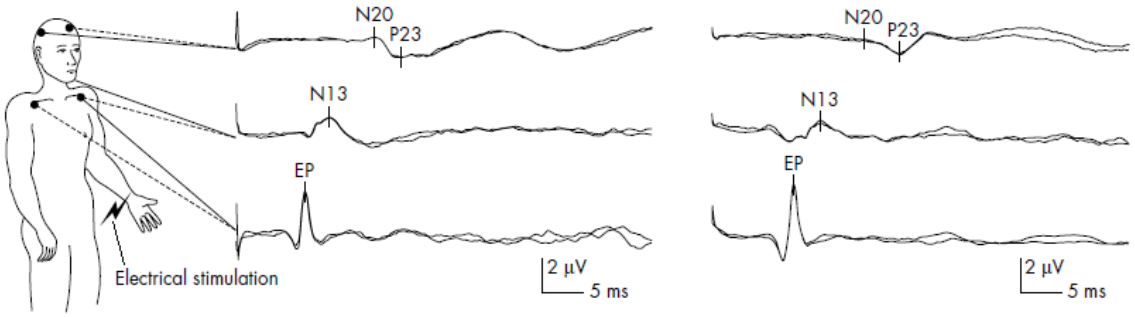

(a) Stimulation on the median nerve with both right and left showing normal SEPs

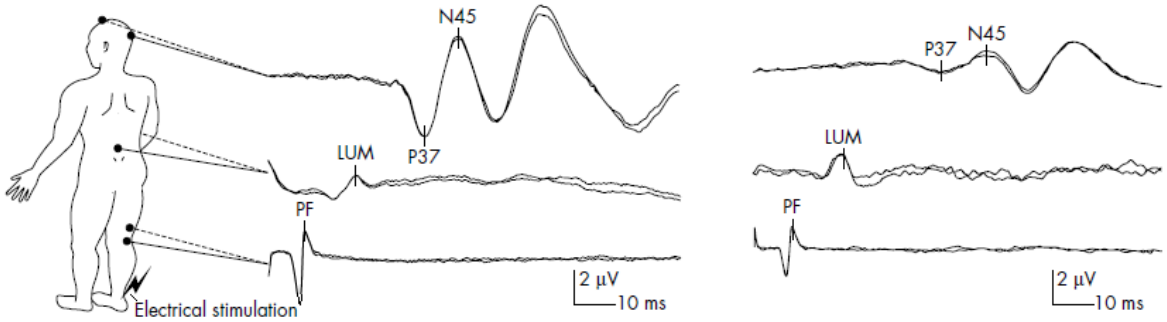

(b) Stimulation on the tibial nerve with the left showing a normal SEP, while the right shows scalp potentials with a dispersed P37 and an extended latency

Figure 2.13: Examples of somatosensory evoked potentials (SEPs) from electrical stimulation of both median and tibial nerves with bipolar recordings taken at three respective coordinate pairs for each set-up [33]

Figure 2.13a shows a standard test set-up and expected output of two normal patients who underwent a SEP with median nerve stimulation. The bottom of the three waveforms shows the bipolar response between two chest electrodes and indicates propagation of the impulse along the media nerve en route to the somatosensory cortex. The top waveform shows the healthy locations of characteristic N20 and P23 peaks on both patients (two averaged SEPs superimposed per patient).

Figure 2.13b reveals the difference between a normal tibial stimulated SEP (left) and abnormal SEP (right). Again, the bottom of the three waveforms are recorded from nerve impulses, within the tibial nerve, en route to the brain. On the left overlaid tests, for a normal patient, it is evident that there exists strong and timely P37 and N45 components, whilst the right shows an attenuated response as well as a delayed latency before the onset of the response.

SEPs are typically used to investigate multiple sclerosis patients, myoclonus (describing a medical sign often unrelated to disease diagnostics, whereby sudden involuntary muscle jerks and twitches, being positive myoclonus, or sudden lapses in concentration, being negative myoclonus, occur [36]), used as an intrasurgical sensory pathway integrity

monitoring method whilst correcting spinal curvatures (such as scoliosis and kyphosis) as well as a prognosis guide during post-traumatic and anoxic-ischaemic (brain injury due to oxygen deprivation) as a result of their lower susceptibility to metabolism changes and sedating agents.

2.6.4 Brainstem Auditory Evoked Potentials

BAEP waveforms are usually recorded from the vertex (anatomical surface where the four bones of the skull meet superiorly) with reference to the ipsilateral mastoid (the crest bone behind each ear) of the ear being stimulated by means of auditory click sounds. The reference electrode (for the unipolar set-up) is also commonly attached to the lobules (see Fig. 2.4) of the ear. The output averaged waveform usually contains distinct peaks that can be correlated to various regions of neuron activity as the signal travels from the cochlea to the primary auditory cortex. Figure 2.14 shows the likes of what can be expected when measuring BAEPs.

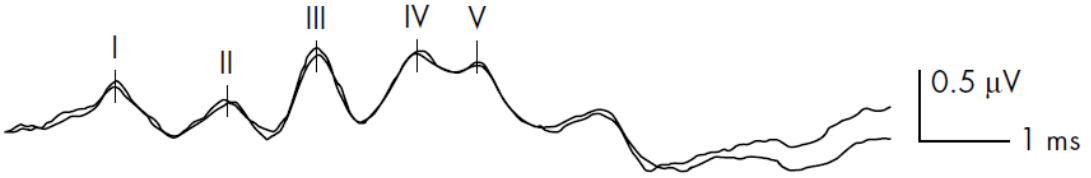

(a) Normal BAEP obtained from using an alternating click approach

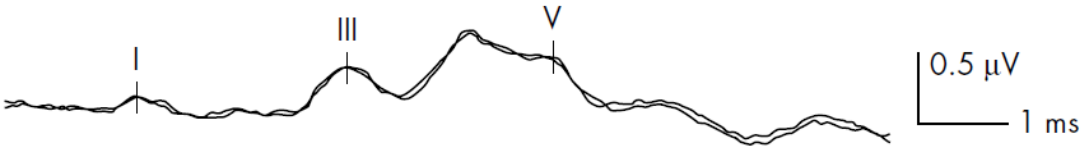

(b) Abnormal BAEP sourced from a patient diagnosed with an acoustic neuroma showing poorly formed waveforms and prolonged I–III as well as III–V inter-peak latencies

Figure 2.14: Examples of brainstem auditory evoked potentials (BAEPs) using the previously mentioned Roman numeral numbering system [33]

A normal BAEP usually contains 5 prominent peaks, as shown in the superimposed plots of Fig. 2.14a, followed by two less prominent peaks (sometimes labelled VI and VII accordingly). The probable origins of these characteristic peaks are summarised in Table 2.2, with their usual latency after onset of click stimulation.

Figure 2.14b provides a scenario in which an abnormal BAEP waveform is observed. It can be seen that both the individual latencies as well as inter-peak latencies have been prolonged from that of the normal response. The prominence of all three initial peaks have been subdued, with peak II being almost completely neutralised. Peak IV and V,

although not being suppressed much in terms of amplitude, have been altered in both shape and delay.

Table 2.2: Table showing the probable physiology origin of peaks for a brainstem auditory evoked potential waveform

Peak	Usual latency (in ms)	Physiology position origin
I	1–2	The distal portion of the acoustic nerve (segment near cochlea) also referred to as the vestibulocochlear nerve (labelled in Fig. 2.9) or eighth cranial nerve
II	2–3	The proximal portion of the vestibulocochlear nerve (closest to brainstem) along with the cochlear nucleus where the auditory nerve forms its first synapses on the surface of the brainstem
III	3–4	Multiple generators including the ipsilateral olivary complex, medial nucleus of trapezoid body as well as superior olives contralaterally
IV	4.5–5	Likely the lateral lemniscus
V	5–6	The lateral lemniscus along with the contralateral inferior colliculus found in the lower parts of the midbrain
VI	6–8	Probably due to the medial geniculate nucleus or from inferior colliculus projections
VII	8–10	Most likely the primary auditory cortex

Electric response audiometry based on BAEPs is often preferred over formal audiometry, especially when the latter is to be done in a patient who is unable to cooperate (such as infants). BAEPs are clinically useful in investigating subjects with possible MS, especially when the demyelination affects the brainstem. They can also be used to detect silent lesions, which are damaged tissues or organ regions (in this case being nervous tissue) that don't produce noticeable symptoms or enhance an MRI scan.

During an excision of posterior fossa tumour operation, BAEPs are useful for monitoring the integrity of the brainstem and auditory nervous pathways, to better ensure successful surgery. Similar to that of SEPs, BAEPs are also used in the prognosis of comatose patients who are in ICU as a result of trauma or brain oxygen deprivation. Structural lesions causing hearing loss can cause the response seen in Fig. 2.14b. It is possible to record BAEPS with anaesthetised patients with slight stimulation alteration due to their relative resistance to anaesthetic agents.

2.6.5 Effect of anaesthesia on EPs

Anaesthesia is a controlled state in which there is temporary loss of sensation and conciousness due to certain drug applications. Various anaesthetics (agents/drugs that cause anaesthesia) are known to effect the brain in different ways, but ultimately numb the patient from feeling pain during surgery. Local anaesthetics numb a specific region of operation where a patient is fully aware of all other senses except the physical sensation of the surgical area. General anaesthesia, being the type relevant to the study presented in this thesis, induces the whole body into a state of unconsciousness. In [37] the previously investigated effect, of isoflurane (a general anaesthetic agent applied via inhalation) on the evoked potentials (EPs), is studied by Sebel.

The effect on VEPs is shown in Fig. 2.15, where the control represents the test before application and the increasing percentages represent the increasing percentage concentration of isoflurane in the inspired air. Every concentration was applied for 15 minutes. Evidently there is a clear change in both the extended latency and reduced amplitudes, of the N75 as well as P100 marks, as the concentration of the agent increases. The stimuli were 2 Hz flashes for 128 repetitions.

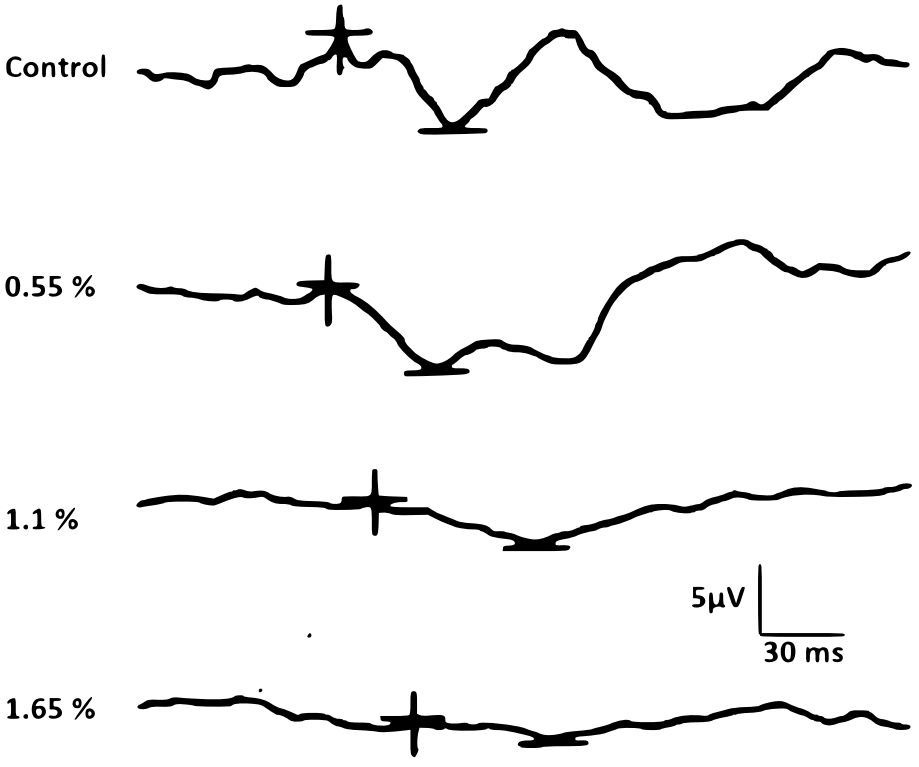

Figure 2.15: Plots showing the effect of isoflurane on VEP waveforms (adapted from [37])

In Fig. 2.16, similar changes were observed in the measurement of SEPs, with median

nerve stimulation using 100 μs constant current, 2 Hz pulses for 256 repetitions. Both the N20 and P23 aforementioned exhibited a slight extension in latency and a larger decrease in amplitude (to the extent where P23 has almost completely disappeared)

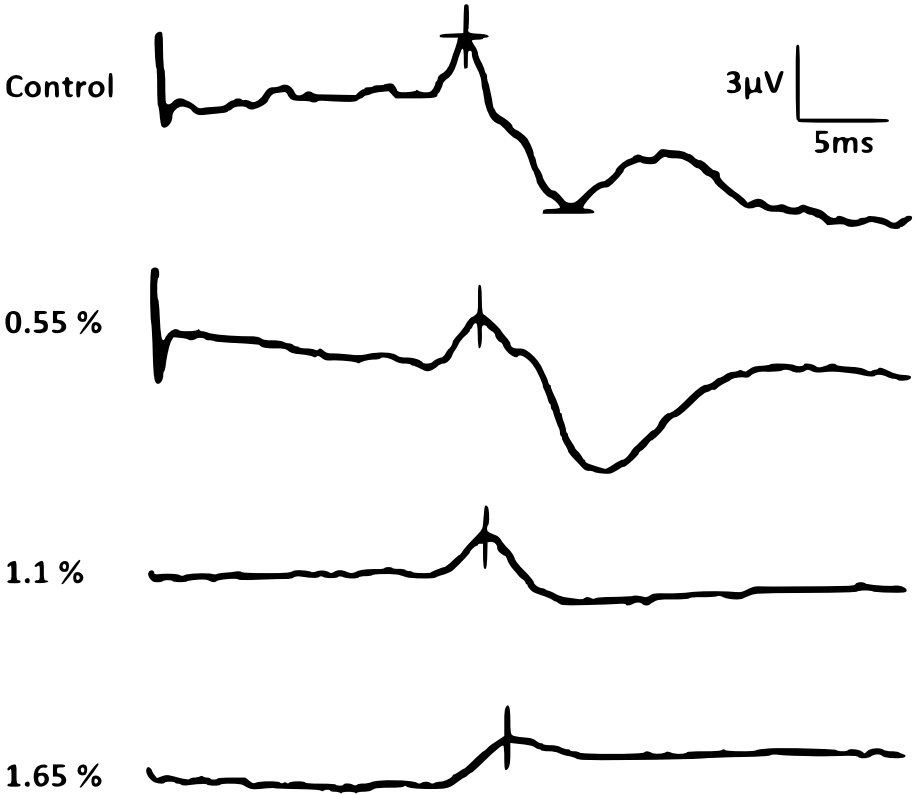

Figure 2.16: Plots showing the effect of isoflurane on SEP waveforms (adapted from [37])

BAEPs are by far the most resistant to anaesthetic application, as seen in Fig. 2.17. Although some latency lengthening and small decreases in amplitude could be suggested, they are small and distorted relative to the changes of SEPs and VEPs. On the contrary, it has been shown that anaesthetics such as alfaxolone/alfadolone [38] and etomidate [39] have no effect on the BAEPs. Conveniently speaking, it would be beneficial to have stimulation and measurement in the same region (i.e. ear region) to encourage the compact and non-obtrusive design of such a envisioned system. This motivated further investigation into auditory stimulation for the purpose of anaesthesia monitoring.

Sebel does mention in [37] that more latent auditory responses exist that are more susceptible to the state of anaesthesia. In [40] the three different latency-based divisions of auditory evoked potentials (AEPs) are described. These include BAEPs, followed by middle latency auditory evoked potentials (MLAEPs) and finally long latency auditory evoked potentials (LLAEPs).

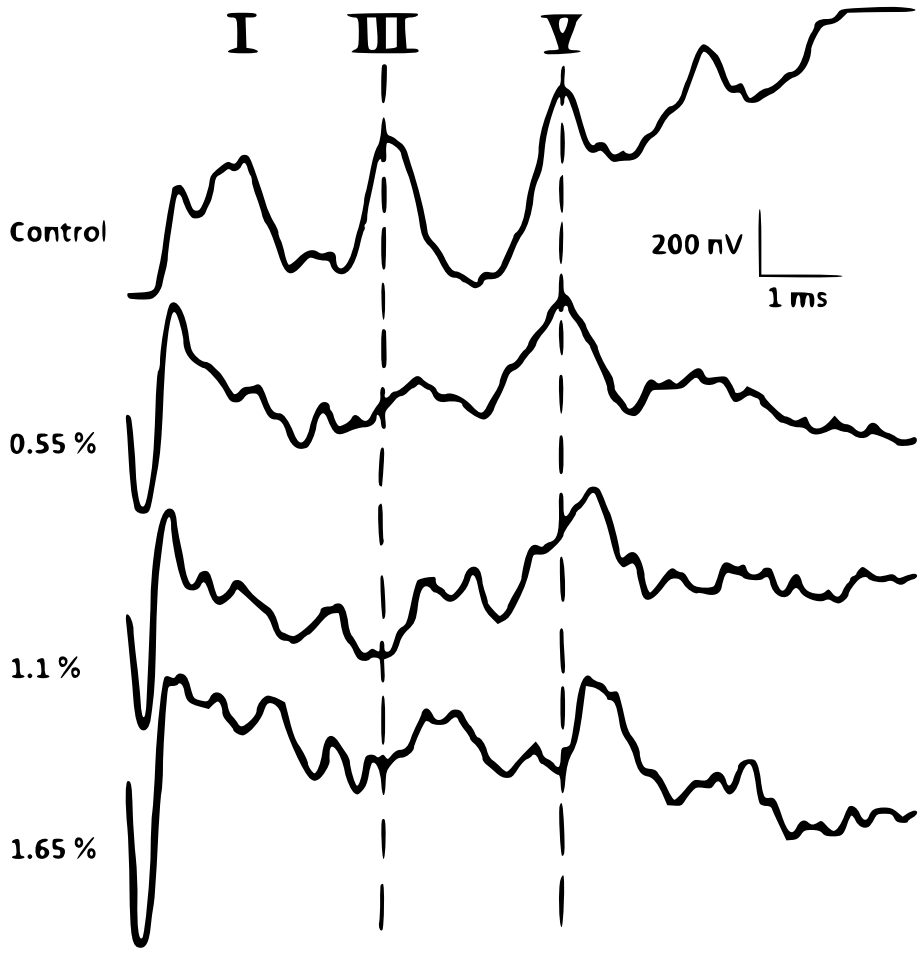

Figure 2.17: Plots showing the effect of isoflurane on BAEP waveforms (adapted from [37])

Table 2.3 defines the latency, origin and effect of anaesthesia on the various auditory evoked potential waveform segments. MLAEPs are sensitive to changing levels of anaesthesia as opposed to LLAEPs that are excessively susceptible and quickly lost, even with initial drug application. From this information, it can be deduced that MLAEPs will give the best indication of the level of intra and post-surgical sedation.

Table 2.3: Table summarising auditory evoked potential subgroups

AEP division	Latency interval (in ms)	Physiology origination	Anaesthesia influence
BAEP	0–10	Acoustic nerve and brainstem (detailed in Table 2.2)	Very resistant to anaesthesia
MLAEP	10–100	Primary auditory cortex of temporal lobe, medial geniculate and thalamus [41]	Sensitive to anaesthesia states
LLAEP	100–1000	Frontal cortex and association areas	Very susceptible to anaesthesia and lost completely (being fully attenuated)

The normal MLAEP, as measured from the vertex, has a waveform as represented by Fig. 2.18. It can be noted that the short latency BAEP (although now sampled at a lower frequency and therefore not showing all the peaks) is still present, as would be expected.

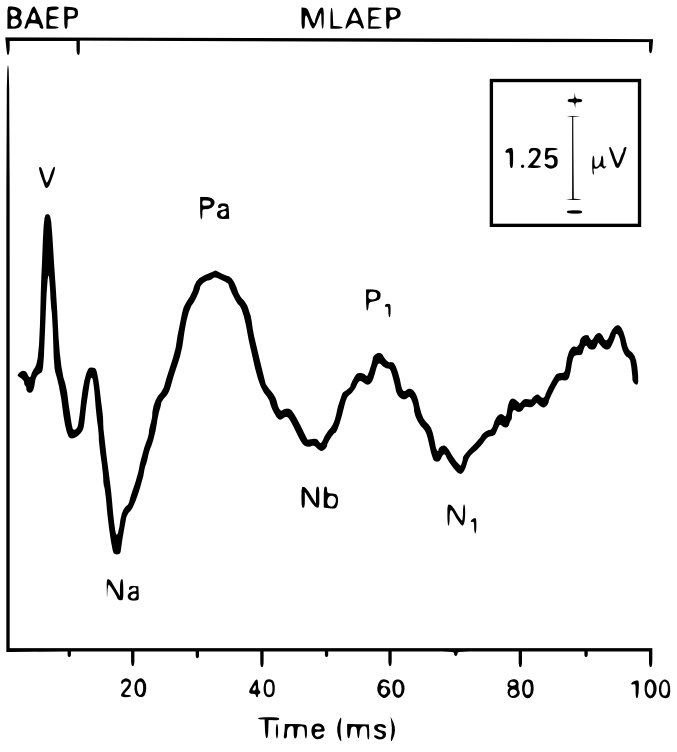

Figure 2.18: Plot showing a normal AEP (with both the BAEP and MLAEP segments) [42]

Figure 2.19 shows the effect of midazolam anaesthetics on the MLAEP. In [42] the findings show that although there is no clear trend in amplitude attenuation, a latency delaying effect of component Pa is caused by the anaesthesia.

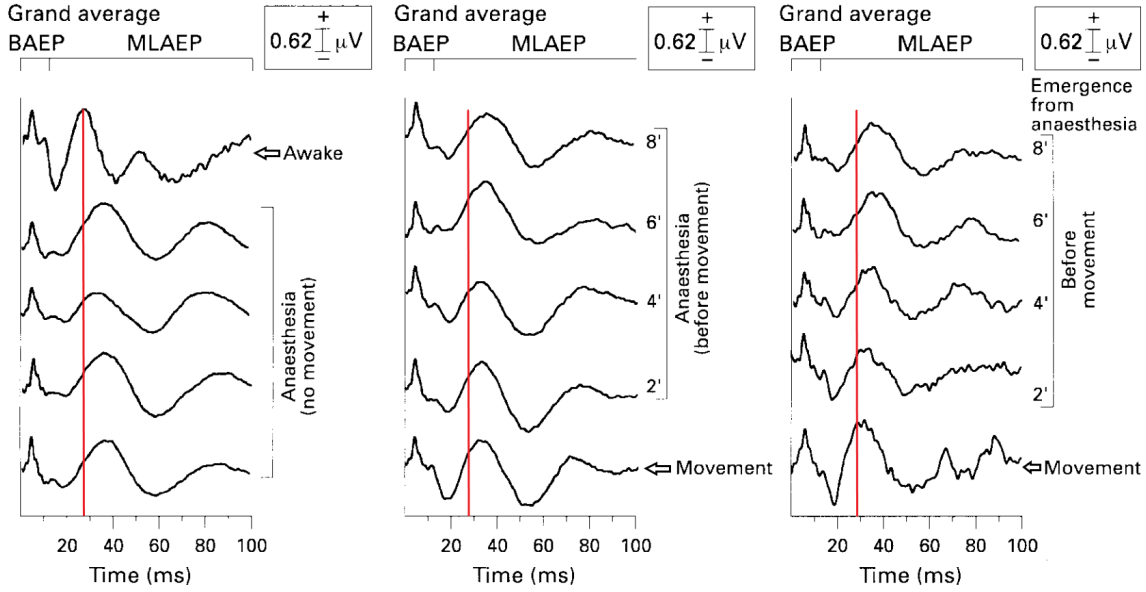

Figure 2.19: Plot showing how anaesthesia levels effect the MLAEPs of a patient (adapted from [42])

From these findings, it was concluded that midazolam preserves cortical function in an auditory sense, although delaying the process to a observable extent. Measurements in Fig. 2.19 were taken at minute intervals before patient movements (such as eye opening or muscle movements) as well as before anaesthesia in the 'awake' state. It was observed that intervals of movement (especially the latter, which required greater cortical function to follow a movement instruction) had a similar response to that of the 'awake' state.

Based on various other studies [43]–[52], it is evident that various general anaesthetic agents exist that effect both the latency and amplitude components of MLAEPs. These include enflurane, isoflurane, propofol, halothane, sevoflurane, etomidate, desflurane, thiopentone and Althesin (alfaxolone/alfadolone composition mixture that has since been withdrawn from the market due to severe drug reactions seen in patients). The extent to which these affect the middle latency auditory potentials can be correlated to the level of agent applied or more accurately the level of anaesthetic present in the body.

Compared to raw EEG signals, AEPs (including the useful monitoring region of MLAEPs) are much less sensitive to artefacts such as random time occurring unexplained signals. Such artefacts are removed from the MLAEP by means of continuous averaging [15]. The interval of specific middle latency importance, given by [15], is between 40 ms and 60 ms, where one of the characteristic peaks occur. This still lies within the region

specified in Table 2.3.

The use of raw EEG signals, for obtaining the depth of general anaesthesia, is for most part an empirical approach. AEPs (and other evoked potentials) are based on stronger theoretical physiology of signal pathways and therefore have a greater potential for becoming a standard of measuring consciousness. The following section discusses the chosen route of conciousness detection.

2.6.6 Conclusion with selected approach

Having obtained a background for all three of the most commonly used evoked potential methods, the route required to produce a non-obtrusive monitoring system, can now be decided upon. Visually evoked responses inherently require open eyes or bright strobes (also called flash VEP, which is unreliable in drawing inferences about the quality of visual perception) that can sufficiently penetrate through the eyelids and as such will require alterations to an anaesthesia set-up, thus complicating the process. Such evoked potentials are not commonly used for integrity monitoring during anaesthesia. Somatosensory potentials are a feasible route since they give an indication as to how conscious a patient is to electrical sensory stimulation from the limbs. This, however, requires setting-up in more than one region of the patients body being a limb- and the head- region (or more specifically, in the case of this thesis, the ear regions on the head).

Auditory evoked potentials, with specific reference to the MLAEP, have been shown by multiple studies to be feasible for measuring anaesthesia levels. Due to its convenient sensory location, it is chosen as the investigated method. One further study, conducted on rats in a veterinary setting, is given by [53] and concludes that even rats show a increased latency and decrease in both frequency and amplitude information while anaesthetics are applied. In [54] it is indicated that noteworthy parameters, that are worth analysing for the chosen auditory approach, are the peak latencies and amplitudes along with morphology index and peak power frequency (PPF) of the evoked response.

Natus Neurology [55] published a webinar [56] in which guidelines are provided for the set-up and required stimulation to be used in the recording of MLAEPs and BAEPs. The stimulus frequency was described to be selected between 8 Hz and 10 Hz. Higher frequencies cause a reduction in the amplitude of the waveforms and also have an effect on the obtainable middle latency time-domain range, whilst lower frequencies give rise to large averaging times being required to obtain a clean signal. The South African mains frequency is 50 Hz, which, being a multiple of ten, will interfere strongly with a 10 Hz averaged signal. As a result, an 8 Hz frequency (or 125 ms period) is chosen as the stimulus frequency. Figure 2.20 illustrates the auditory pulse for one period length.

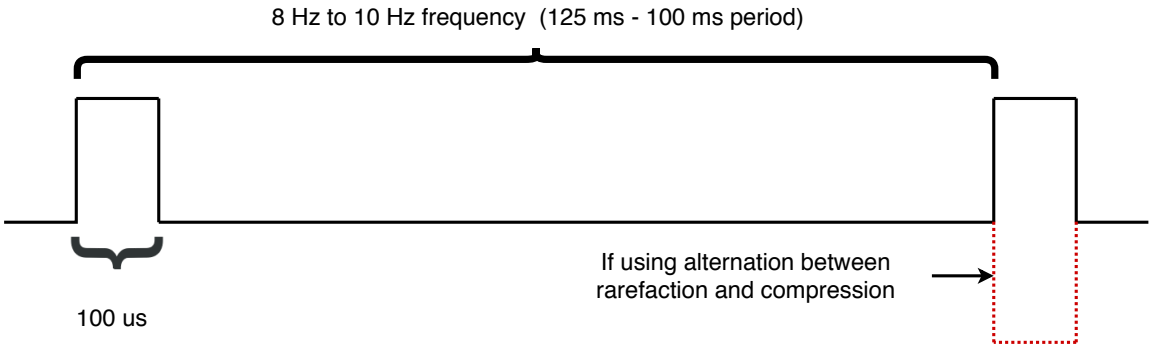

Figure 2.20: Plot illustrating the stimulus suggested by the information from [56]

The pulse width is suggested to be 100 μs and to be of square-form, which consists of frequency harmonics over a larger spectrum. The short pulse width avoids mid-latency interference of the stimulus with the evoked potential. Another suggested technique to remove any residual EMI speaker artefacts is to alternate the polarity of consecutive pulses, as shown by the dotted red line in Fig. 2.20.

2.7 Conclusion of the literature study

From having gathered an in-depth understanding of the theory and research applicable to this study, one can continue onwards to construct a methodology in Chapter 3, that incorporates this knowledge, to address the problem statement.

Chapter 3

Methodology

This chapter defines how the literature from Chapter 2 will be utilised, with available skill sets and research instruments, to design, implement and verify a functional in-ear evoked potential recording device. In the future this device could possibly be used as an anaesthesiologist's patient anaesthesia depth monitoring system.

3.1 Introduction

In order to address and derive a solution to the problem statement, from conceptualisation to design and implementation, a sequential methodology is crucial. The following sections detail such a methodical approach for this dissertation. The design approach, that will ultimately address the larger problem at hand, is outlined in the next section.

Due to the chosen structure of this document, individual and more detailed methodologies are provided in the overview and testing procedure sections of the design and results chapters. The electrode topology design method is given in Section 4.1, the remaining hardware implementation methods are found in Section 5.1, whereas the software designs are described in Section 6.1. In order to ensure successful clinical trials the testing procedure is detailed in Section 7.1. The remainder of the methods, to complete the full picture, are described in this chapter.

3.2 Research design

Figure 3.1 gives an overall view of the approach that needs to be followed to successfully realise a system that addresses the problem statement.

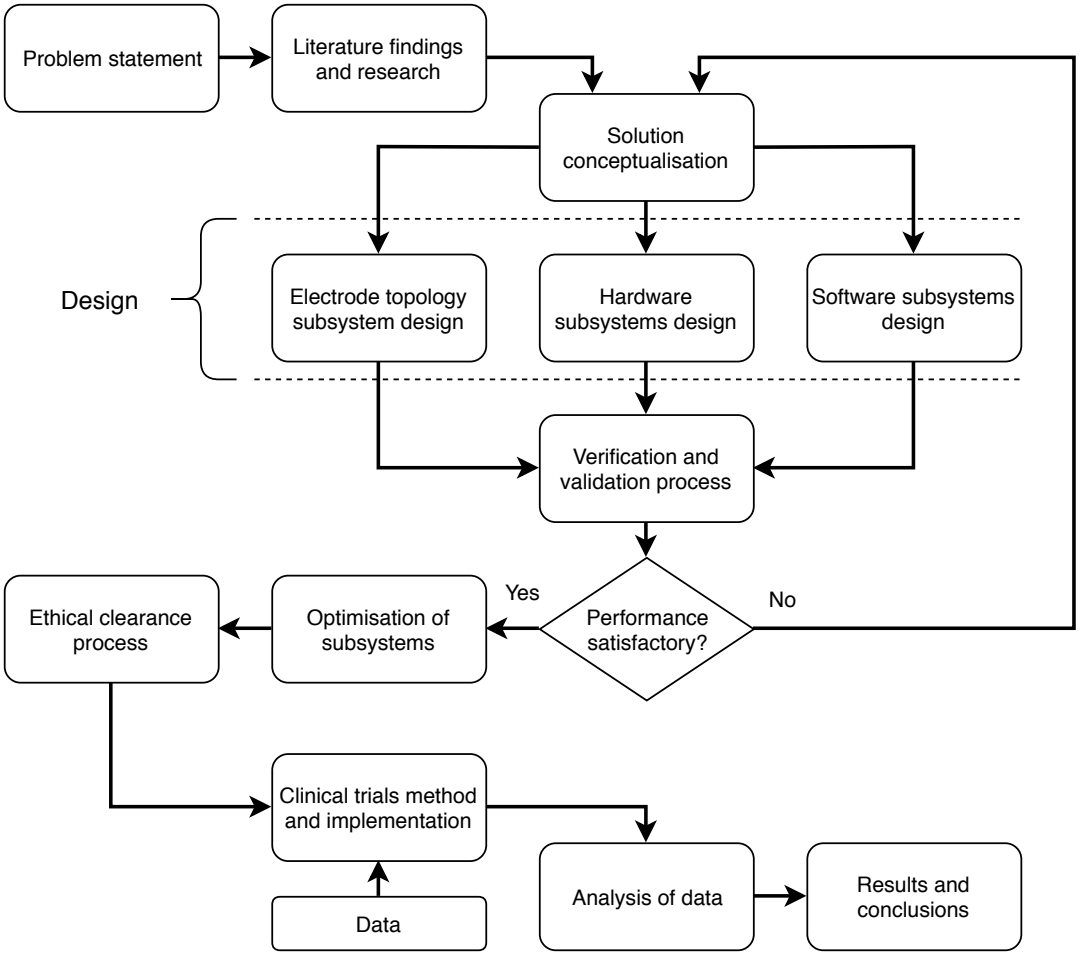

Figure 3.1: Diagram of the methodology process overview

The figure presented above represents an overview of the complete method to be followed, from start to finish. Simultaneous documentation should occur, with each step of the process, to ensure that all the aspects can be presented in this final thesis record. The detailed explanation of Fig. 3.1 is as follows:

1. Begin by clearly defining the problem statement (with all of the research questions to be addressed), as is done Chapter 1.

2. After gaining a clear understanding of the challenge at hand, commence with a full background literature study. As possible routes to a solution become evident, delve into the research on those pathways until every aspect of a solution has been researched. The outcome of this process is documented in Chapter 2.

3. Next one should conceptualise an overall design solution, followed by methodically dividing it into specific and verifiable subsystems.

4. The design and implementation of the subsystems can be divided into three main categories, being:

4.1. the design and implementation of a topology that will address the need for easily attached and detached, non-obtrusive and in-ear centred EEG electrodes (as addressed by Chapter 4);

4.2. the design and implementation of all the surrounding hardware components to accurately ensure the recording of auditory evoked potentials (addressed by Chapter 5); and

4.3. finally, successfully design and implement of all the necessary software to control data recording steps, as well as process the raw EEG data to the point where auditory evoked potentials have been obtained (which is addressed by Chapter 6).

5. Validate all the designed subsystems individually, and if it is found that the functionality of a certain component is not producing the required output to a satisfactory level, re-iterate that design with the necessary adjustments.

6. Optimise and tune the variable parameters of all of the designed systems to produce the most promising output.

7. Successfully apply for ethical clearance at the Health Research Ethics counsel 2 (HREC2) of Stellenbosch University, completing all the necessary documents and following all the appropriate protocols throughout the design process.

8. Upon successful ethical clearance, commence with the clinical trials. Define a testing procedure to ensure the comparability of the results, as is done in Section 7.1.

9. Use the validated software designed to analyse the patient clinical data.

10. Present the results (Chapter 7) of every patient tested in detail, using graphical methods to illustrate correlations of variables and discussing the significance of all the components.

11. Summarise the clinical findings and discuss the significance of the overall implementation (Chapter 8), make recommendations to anyone wishing to pursue the research further (Chapter 9) and conclude the dissertation (Chapter 10).

3.3 Research instruments and tools

In order to successfully complete the greater research task, a wide range of instruments and tools are needed throughout the entire process. As designs and research protocols are developed, new instruments become valuable in addressing, validating and assisting these thesis tasks. At the end of the design implementation, the following lists of instruments and tools, divided into three subcategories, were found to be of meaningful value.

3.3.1 Hardware instruments

Various personal, as well as laboratory and workshop equipment at Stellenbosch University, was used to compile the final hardware subsystem as represented in Fig. 5.19. The equipment needed to realise the hardware subsystems were as follows:

- UP Plus 2 3D printer [57]
- MakerBot Replicator Z18 3D printer [58]
- LPKF ProtoMat S63 PCB prototyping machine [59]
- Magnum 2004 soldering iron
- Laboratory thermal evaporator
- Stanley hot glue gun

The measuring instruments, that were used to validate the hardware subsystems and also allow for the manual recording of existing comparable anaesthesia levels for the results section, were:

- A Tektronic digital oscilloscope
- A Fluke digital multimeter
- An anaesthesia monitoring machine
- A smartphone microphone

3.3.2 Device hardware and consumable components

The instrumental products, that were either used (on the software and data processing side) or utilised (see 5.19) in the successful final hardware implementation, were as follows:

- A OpenBCI Cyton EEG data recording board with Bluetooth dongle [60]
- A SanDisk 16 GB class 10 microSD card
- A USB 3.0 Transcend microSD card reader
- A Gigabyte Aero 15 laptop with an Intel i7-8750 processor and 32 GB of random access memory (RAM) running Windows 10 Pro
- A Samsung Galaxy Note 8 smartphone
- A set of eight OpenBCI gold cup electrodes [61]
- One set of JBL T450BT Bluetooth headphones [62]

- One set of Geist 36BL Bluetooth earphones [63]
- One set of 3M Peltor X2A earmuffs [64]
- Various other miscellaneous electronic components and shielded wiring, mentioned in Chapter 5

The consumable products that were valuable to the design implementation, as well as the clinical measurement phase of the system, were found to be:

- Weaver and Company Ten20 conductive paste [65]
- Weaver and Company NuPrep skin preparation gel [66]
- Dove cotton buds
- Duracell 9 V and AA batteries
- Printer polymer filament
- Glue sticks for the hot glue gun
- Insulation tape
- Single and double sided printed circuit board (PCB) prototyping boards
- Bispectral index (BIS) electrodes set-up by anaesthetist (property of the hospital)
- Desflurane and sevoflurane anaesthetics applied by anaesthetist (property of the hospital)

3.3.3 Software instruments

Various software platforms, design tools, languages and environments were used during the completion of the research investigation. The following list provides all such programs and tools:

- Python [67]
- Anaconda (Jupyter Notebook) [68]
- MathWorks Matlab [69]
- Trimble Inc. SketchUp [70]
- Autodesk Inventor [71]
- Autodesk Eagle [72]
- Arduino integrated development environment (IDE)
- Microsoft Excel
- TeXstudio with MiKTeX

3.4 Data

Apart from the data collectable by testing the designed system on oneself, there will be two sets of patient related data collected. This will be the raw EEG or evoked potential data, described in Section 3.4.2, along with the miscellaneous data manually recorded for comparison reasons, as summarised in Section 3.4.1.

All the raw recorded and collected data and information will be saved offline on the password protected personal computer of the primary investigator. The data will be anonymous, and so will the findings of the thesis. This is done to align with ethical protocols and to protect the identity of the patients that gave consent to partake in the study.

The analysis of the data is outlined in Section 3.5, and the details thereof are fully defined in Chapter 6.

3.4.1 Patient spreadsheet data

Figure 3.2 presents a blank Microsoft Excel spreadsheet table that can be used to record anonymous patient information for comparative purposes. Information such as the date and time, patient number, surgery type and estimated duration of surgery are noted at the top of the sheet. For every EEG data file recording initiated, a line record is made to note the time, anaesthesia level, in terms of the anaesthesiologist's observation, data file name, file recording duration, bias/reference configuration, extra notes for the interval as well as the anaesthesia machine readings for that data file. Readings are taken at intervals of one minute (or thirty seconds if sharp changes are expected).

Date			Surgery type:															
Patient no			Estimated duration:															
							0	60	120	180	240	300	360	420	480	540	600	Time in seconds
Time	Anaesthesia Level	Data File	Interval Duration	Bias / Ref Swopped?	Note Time	Notes	0	1	2	3	4	5	6	7	8	9	10	Time in minutes
																		Exp Desoflurane BIS
																		Exp Desoflurane BIS
																		Exp Desoflurane BIS
																		Exp Desoflurane BIS

Figure 3.2: Excel spreadsheet layout for the recording of anonymous patient information

3.4.2 Patient designed system data

The Cyton board, chosen as the EEG recording device (see Chapter 5), has the capability to write raw EEG channel data from the analogue-to-digital converters to a text file, in a comma separated format. This will be utilised as the recording method of the electroencephalography (EEG) data containing the patients' evoked potentials. Section 6.4 details how the data will be imported and converted from these files.

3.5 Analysis

The raw data will first be processed via a series of frequency filters to collectively remove DC offsets, remove speaker interference, remove mains interference as well as remove any frequencies that are not related to the auditory evoked potential range. The filtered data is also run through algorithms to remove corrupted data from muscle twitches or other non-head-related electrical activity. The raw data is then divided and synchronised into period subsets correlating to the audio stimulus frequency. These data sets are then all averaged together to produce a single low micro- or high nano-volts waveform of stimulus period length (meaning that with an 8 hertz stimulus the waveform will be 125 ms in length). The resulting signal is known as the auditory evoked potential waveform and contains a series of peaks and valleys correlating to the activation of neuron groups (which each produce a small yet detectable electrical ripple) from the eardrum up until the auditory cortex where the stimulus is processed. The stimulus frequency allows for both brainstem auditory evoked potentials (BAEPs) and middle latency auditory evoked potentials (MLAEPs) to be recorded.

As the brain is subjected to anaesthesia, these peaks and valleys and the latency thereof are expected to defer from the normal 'awake' state. It is this change that could potentially later become the foundation of machine learning analysis for a commercial anaesthesia monitoring device. The peaks and valleys will reduce in amplitude as the neuron groups become sedated and the latency is expected to increase due to an increase in propagation time from group to group.

3.6 Limitations

Due to the two-year prescribed master's thesis duration, to bring all of the research to completion, along with the work being completed by one individual, limitations are introduced in completing all the necessary processes, completing the ethical clearance process and the testing of numerous patients. The former two were successfully completed at the end of duration, but numerous patients were limited. It was, however, found that due to the strong correlations of the final four patients tested and the voluminous nature of the data collected for each individual patient, the data gathered is implicitly considered to be a proof-of-concept. In order to implement machine learning algorithms, one will require a larger pool of data to build and verify such models.

3.7 Ethics

Ethical clearance was successfully applied for at the Health Research Ethics counsel 2 (HREC2) of Stellenbosch University, by completing all the necessary documents and following all the appropriate protocols throughout the design process. The research protocol of Appendix B and exemplary patient consent form outline given in Appendix A, were

submitted as supplementary components of the online application. The acceptance of the project in this regard, is defined in the letter of Appendix C.

3.8 Conclusion of the methodology

This, hereby, concludes the methodology of this chapter. As aforementioned, with references to the appropriate sections and chapters, individual and more detailed methods will be provided as concepts are broken down into executable tasks. The following chapters deal with the design and fabrication of the solution.

Chapter 4

Electrode topology fabrication

In order to work towards obtaining data for the analysis algorithms, the design and implementation of a fully functional electrode topology is a necessary predecessor phase. This chapter covers the implementation process from the initial design considerations to the final system.

4.1 Overview and considerations

There are three major regions of electrode placement: the channel of interest, reference node and the bias electrode. In line with the objectives of this thesis, the channel of interest is to be placed within the ear-canal which will create a potential difference signal in relation to the reference electrode. To reduce unnecessary high potential differences, the reference electrode should be placed relatively close to the channel of interest on a area that is mostly electrically neutral (least affected by electrical activity in the brain). The bias (or ground) electrode is used to reduce mains power electromagnetic interference (EMI) on both the reference and channel electrode using common mode rejection. Its placement on the user is for the most part irrelevant.

The placement of the reference node was chosen to be on the earlobe of the same ear to which the channel electrode is to be attached. The bias electrode will be placed on the contralateral earlobe to create consistency, maintain conventions and simplify the number of designed parts. As implied, the in-ear channel will be placed in contact with the walls of the ear canal. Figure 4.1 shows the configuration as described.

The printers available in the electronic workshop are the Tiertime UP Plus 2 [57] as well as the MakerBot Replicator Z18 [58]. Both printers are capable of meeting the dimensional challenge of the ear electrode topology. After prototyping with both printers, using melted extrusion modelling (MEM) technology, the UP Plus 2 was ultimately chosen. This was due to its improved accuracy when repetitively synthesizing small components without producing too many irregularities in the output.

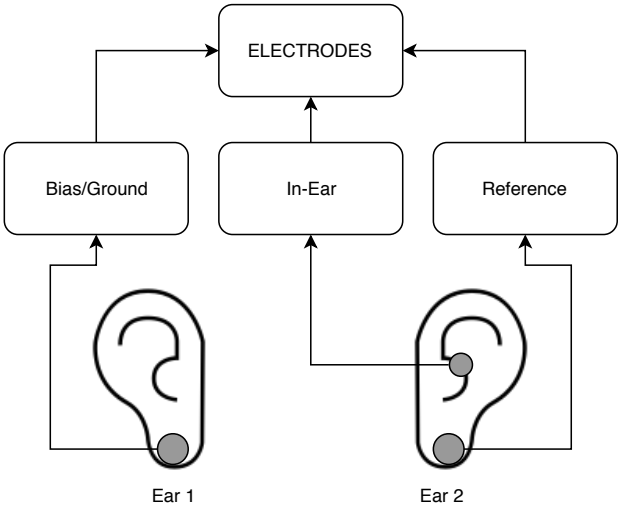

Figure 4.1: Electrode placement

4.2 Additive manufacturing of electrode holders

Additive manufacturing was selected as the means of prototyping and implementing the electrode holding parts. This process offers multiple advantages over various other manufacturing techniques, such as:

- Being inexpensive to produce once the 3D printers have been acquired (which is the case in the Electronic Workshop of the Department of Electrical and Electronic Engineering at Stellenbosch University).
- Rapid prototyping rates are attainable. The designs can easily be altered in the chosen three dimensional CAD program, set to print, and after completion extracted from the printer bed and assembled if necessary.
- The polymer materials, used by the printers, have elastic properties that are utilised during the design process.
- The polymers are non-reactive with the other chosen materials and are also not hazardous for the skin contact that will occur during normal operation.
- The polymers are electrically insulated, which is necessary to keep the contact area of the electrode at a reasonably constant value.

It was chosen to implement the computer-aided design of the components in Trimble SketchUp [70] due to previous experience with the software. A student version of Autodesk Inventor [71], which has been made available by Stellenbosch University, is also used for components that could not be completed due to the limitations of the free and trial SketchUp software. This printer can additionally print ABS (Acrylonitrile Butadiene

Styrene) thermal polymers whereas the alternative is limited to PLA (Polylactic Acid) plastics.

4.2.1 In-ear component

The first challenge was to design a component capable of easily bringing an electrode into contact with the skin of the inner-ear of a user or patient, whilst being as non-obtrusive as possible. This has previously been done by using moulds of specific patient's ears or by using memory foam ear-plugs containing a foil electrode. The use of moulds creates the need for patient specific design which both adds to the cost and the pre-testing preparation time of the system. Although cross-patient compatible, memory foam is often difficult to place deep enough into the ear-canal as well as having inconsistent placement due to the elastic nature of the material. A solution that incorporates both the comfort and cross patient compatibility of memory foam, as well as the rigidity of a sturdier plastic, is therefore of great design importance. According to [31], the average diameter of the outer ear-canal is 8 mm to 10 mm with the average for the entire canal being around 7 mm.

4.2.1.1 First iteration

The first approach, as shown in Fig. 4.2, was a mechanism that could be spring loaded so as to easily collapse whilst being pinched before entering into the ear-canal. It will thereafter expand upon release to come into contact with the inner walls of the ear. The round pad areas, where the electrodes could ultimately be placed, were designed, as shown in Fig. 4.2a, using an outer diameter of 7mm whilst leaving space for collapsing. Two pivoted points, linking the pads to corresponding bars, allow for the rounded pads to inhibit one axis of rotation. These bars are then pivoted together around their centre to again allow one relative rotational axis of freedom. A 1:10 scaled model was printed as shown in Fig. 4.2b.

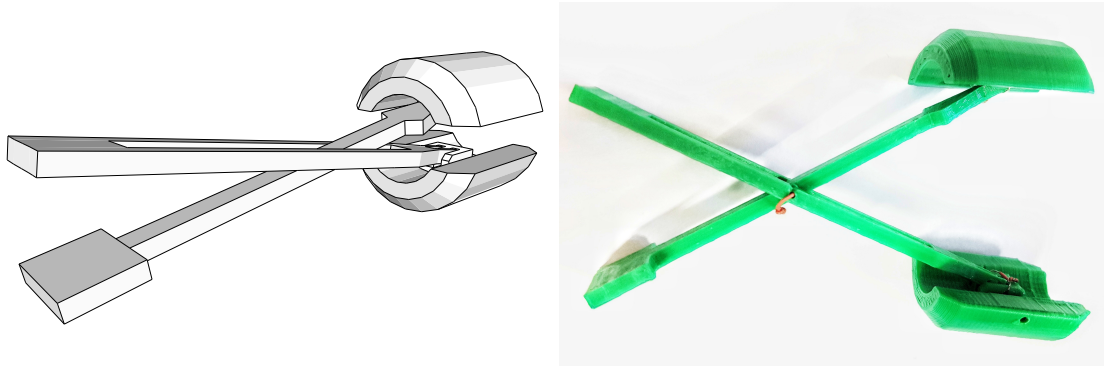

(a) Computer-aided design model

(b) Additive manufacturing realisation (10× enlargement)

Figure 4.2: First design iteration of the in-ear mechanism

The feasibility of the first iteration, for the end-user market, was analysed using certain predefined criterion, as shown in Table 4.1.

Table 4.1: Table showing the feasibility criterion and results for design iteration one

Criterion	Analysis	Outcome
Scalability	The design is difficult to scale down due to the small cross sectional area of the attaching bars. Once this is scaled down, the dimensions of various parts become too small to accurately reproduce using the available additive manufacturing machines. Machining small dimensions is also a challenging process.	In terms of scalability the first iteration is not feasible for additive manufacturing production.
Reproducibility	The 3D printing of the dimensions is not feasible. The machining of such components requires multiple specialist intervention stages and machining tools. The fully functional outcome of this design will therefore not be easily reproducible.	Not easily reproduced using machining techniques.
Cost of production	Machining is a relatively expensive process in the end-user market. The materials are also significantly pricier than the polymers used in standard additive manufacturing.	The cost of producing this iteration does not make economical sense for the goal market.
Adaptability and reusability	The small dimensions also allow for easily breakable components in some manufacturing techniques, which has a negative effect on re-usability (with the possible exception of machining with metallic materials). Adaptability is a positive factor as the three pivots, each with a rotational freedom axis, allow for flexibility around differing inner-ear geometries.	With machining as the chosen production technique, the design is adaptable and reusable.
Feasibility	The design adapts well to different geometries, but does not meet other criterion due to its small downscaled dimensions and the limitations of the available additive manufacturing printers. A design that can improve on the geometrically small and infeasible dimensions is thus a motivation for the second iteration.	

Using the analysis of this iteration, design changes were made to define a second system that could potentially solve the challenge at hand.

4.2.1.2 Second iteration

The second approach, as shown in Fig. 4.3, incorporates a similar rounded pad as the first iteration but with the pivoted point shifting to the end of the pad rather than to the

middle, as shown by Fig. 4.3a. This allows for larger bar sections that can be attached to the pads. The idea is to link the two pad centres via a spring-loaded section which will collapse upon pinching the bars connected to the corresponding pads. This will allow for it to expand again upon release within the ear. There are four component pieces linked to each other via a pivot, with each piece having one rotational degree of freedom along the same axis. The synthesized and up-scaled system (with a ratio of 1 : 10) is shown in Fig. 4.3b.

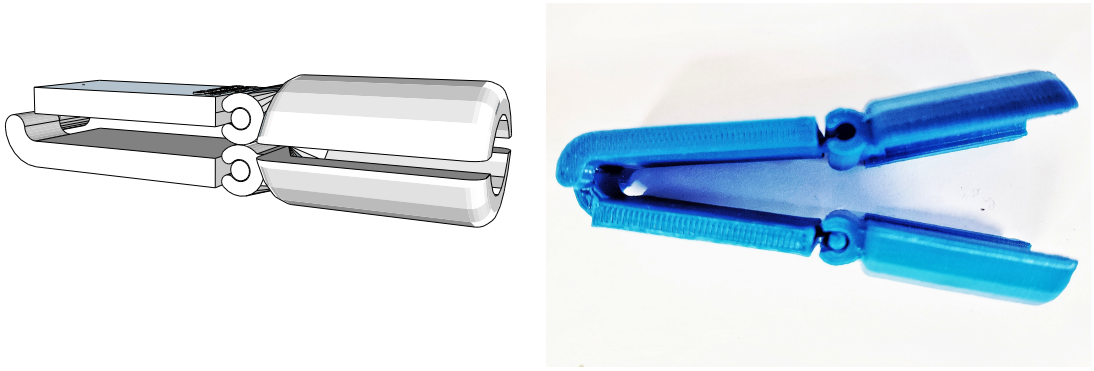

(a) Computer-aided design model

(b) Additive manufacturing realisation (10× enlargement)

Figure 4.3: Second design iteration of the in-ear mechanism

The feasibility of the second iteration was assessed in Table 4.2 using the same criterion as before. During the assessment it was found that side pivoting caused unwanted rotational geometrics when attempting to place the system into an up-scaled ear model. A design that can incorporate both the sturdiness of a larger bar together with the effectiveness of centre pivoting was therefore the motivation for another iteration.

Table 4.2: Table showing the feasibility criterion and results for design iteration two

Criterion	Analysis	Outcome
Scalability	The design is much easier to scale down for additive manufacturing, although the pivot sections require some reinforcement to strengthen the joints. The links were assisted with wiring to give them better strength when undergoing tensile and shear strain tests. The scale model designed has a bar thickness of $\approx 2mm$ which falls within an acceptable 3D printing range.	In terms of scalability, the second iteration is more feasible for additive manufacturing production than the initial concept.
Reproducibility	The dimensions are relatively feasible for 3D printing. Minor reinforcements are necessary during post-printing, to insure durability, which in turn leads to minor delays in reproducibility.	Easily printed but requires some assembling and reinforcement.
Cost of production	Inexpensive once there is access to the necessary machinery. In the end-user market there may be assembly costs involved for necessary tweaking and joint strengthening.	The cost of the polymer filament and wiring used in fabrication is minimal.
Adaptability and reusability	During mechanical testing, the side pivots on the pads were not found to be as ideal as expected. The pads tend to turn outwards under a spring load and become difficult to place into tight-fitting, circular canals. The design is easily reusable and this factor is not an issue.	The design is less adaptable than expected but has an evident reusable characteristic.
Feasibility	The design has acceptable performance in most criterion, however, pivotal reinforcement is required and there is unfavourable rotation of the pads during the force application stage.	

The following section shows the third iteration design that builds on the strengths of the first two implementations while eliminating their short-comings.

4.2.1.3 Third iteration

The area lacking in iteration one was bar volumes with dimensions that were not large enough to print properly. A solution to this, is to incorporate less void space in the model and to better utilise the given space within the model volume. Iteration three, shown in Fig. 4.4, is the optimised result of these considerations. It contains the central pad pivots of iteration one as well as further improvements to the larger bar volumes with the lateral bar pivot positioning of the second implementation. Figure 4.4a shows the CAD model of the components that can be fabricated to produce the outcome shown in Fig. 4.4b (enlarged with ratio of 1: 10). The inner centre of the pads will be linked with spring load to collapse and expand upon fitting.

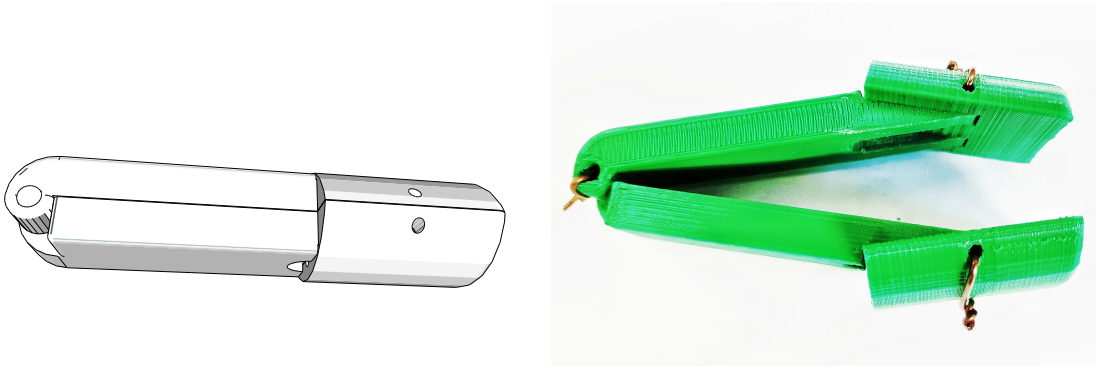

(a) Computer-aided design model

(b) Additive manufacturing realisation (10× enlargement)

Figure 4.4: Third design iteration of the in-ear mechanism

An acceptable test of scalability would be to scale down the model to observe how the printer performs for the reduced dimensions. Figure 4.5 shows three views of a synthesized and assembled system that has only been enlarged with a factor of 1: 4. As is evident from the photographs, the pivotal links have been successfully assembled using wires.

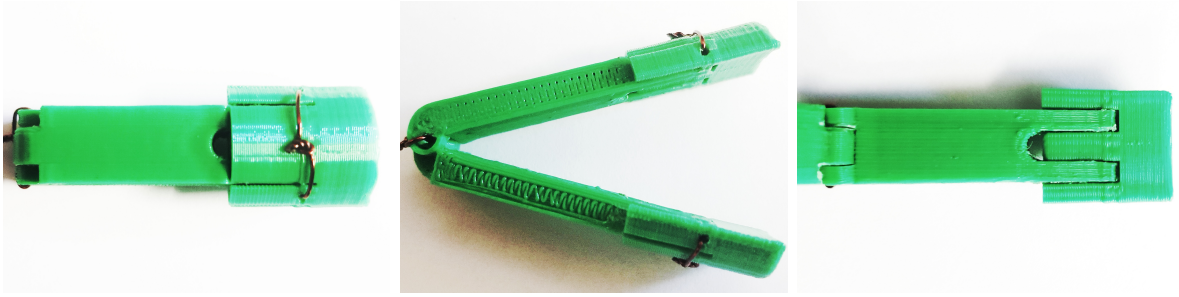

(a) Top view **(b)** Side view **(c)** Inside view

Figure 4.5: Third design iteration implementation as enlarged four times

As a true final test of scalability, the design was printed to scale as shown in Fig. 4.6. The difference between the output of the two aforementioned printers can be seen in Fig. 4.6a and Fig. 4.6b. The photographs of the *MakerBot* product indicate that there are significantly more irregularities in the to-scale print. The pads and bar components were printed with irregularities in both outputs, as illustrated in the Fig. 4.6. The model slits on the pads were not designed to be through slits, but ended up being so on the extruded implementation shown in Fig. 4.6a.

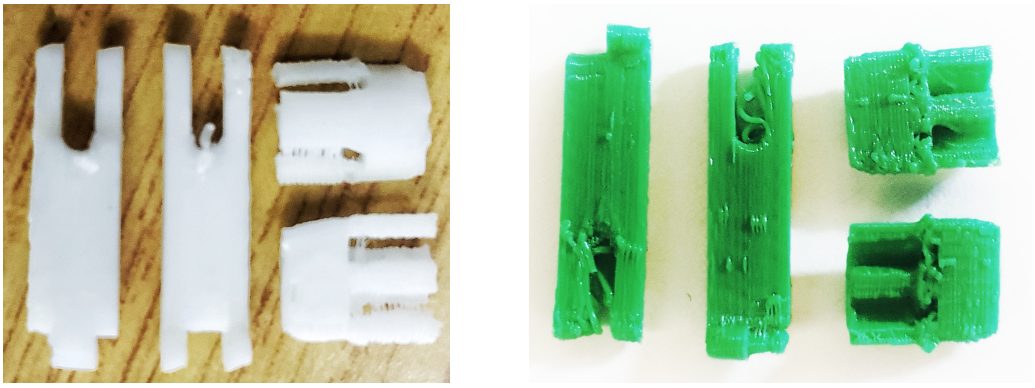

(a) Using Tiertime UP Plus 2 **(b)** Using MakerBot Replicator Z18

Figure 4.6: Actual scale print of design iteration three

Table 4.3 contains the feasibility evaluation for design iteration three. Although the scaled versions in Fig. 4.4 Fig. 4.5 are feasible to implement, the to-scale version of Fig. 4.6 has too many irregularities and weak points to be produced and assembled to a satisfiable extent. From this analysis it becomes clear that the complexity, space limitation as well as chosen manufacturing method may thus be largely incompatible. The space limitation is a model restraint, making the manufacturing type and complexity the only alterable variables. To maintain reproducibility and low cost it is logical to keep the MEM technology as the choice of production which in turn leaves only the complexity as a varying parameter. A model that has less complex joints and components is therefore the primary driving factor for a totally re-imagined design.

Table 4.3: Table showing the feasibility criterion and results for design iteration three

Criterion	Analysis	Outcome
Scalability	The third iteration is the most scalable of the three designs having the largest dimensional space for the bars, pads and linking regions and having the ability to scale down to the furthest extent without any need for alterations. It is necessary to note, however, that as shown in Fig. 4.6, the implementation still produces irregularities due to scale.	Based on the scaled implementation, it is shown that although there is a drastic improvement in additive manufacturing of the component, the irregularities still make the design only vaguely feasible.
Reproducibility	The only intervention necessary is to assemble the components, which is minimal compared to the possible addition of machining and reinforcement stages.	Easily printed but requires some assembling. Out of the three systems it requires the least effort for the assembly of the scaled down versions.
Cost of production	Not expensive once there is access to the necessary machines. In the end-user market there may be assembly costs involved for the necessary tweaking and alterations post-printing.	The cost of the polymer filament and wiring, used in fabrication, is minimal.
Adaptability and re-usability	The adaptability of the system is favourable. It is able to adjust to specific ear geometries using the two pivoted pads. The system would be largely reusable if it was not for the to-scale printed weaknesses incurred during fabrication.	As exclusive criterion, the system is favourable in both adaptability and reusability.
Feasibility	The design has acceptable performance in most criterion with the only negative factors being the irregularities in the smallest (to-scale) fabrication as well as the need for post printing assembly alterations, although the latter is minimal.	

The following section delves into the fourth and simplified iteration.

4.2.1.4 Fourth Iteration

Due to the slightly elastic nature of the printed polymers, including the ABS filament, one can utilize this characteristic material property in producing a design that requires no external spring loading or assembly (meaning a single solid printable). Although this may be at the expense of some ear adaptability, the elimination of mechanical links and joining regions will ultimately improve durability as well as scalability. By including memory foam as a buffer between the plastic and inner-ear skin, one can count the adaptability-cost as

negligible when considering the benefits arising from the simplified design approach. For strength and distribution of elastic deformation, a circular pivotal point was designed as shown in the three iterations of Fig. 4.7.

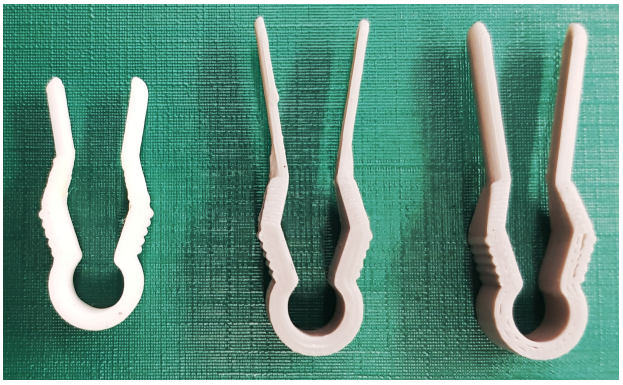

Figure 4.7: To scale in-ear electrode holder iterations. The print on the left (printed using the MakerBot [58]) had a 10mm tip. The middle print (using the UP Plus 2 [57]) shows a flat, 25mm tip. The final version on the right (also realised using the UP) shows a rounded, 25 mm tip

.

Recall that from [32] the average length of the ear-canal was given to be 25 mm. Therefore the latter two versions of Fig. 4.7 provide better depth utilisation. Due to a strength and rigidity comparison, the rounded (rather than flat), 25 mm tip design is selected as the preferred approach.

Figure 4.8 provides the Inventor [71] 3D graphical representation of the final, iteration four, printable. The exterior area following the rounded region is roughened using semi-circular prisms in order to promote grip while pinching the component closed.

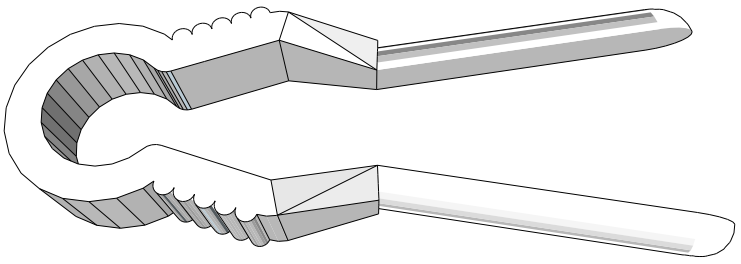

Figure 4.8: Iteration four CAD perspective

Figure 4.9 illustrates the final fabricated and assembled electrode part. The gold-plated electrode was made using a thermal evaporator with source gold pellets and then targeted unto copper foil. The copper was selected for its conductivity as well as for its solderability (gold is not easily soldered onto as it corrodes with standard zinc-tin solder and requires specialised soldering alloys). Memory foam is also incorporated into the system to maximise comfort and adaptability.

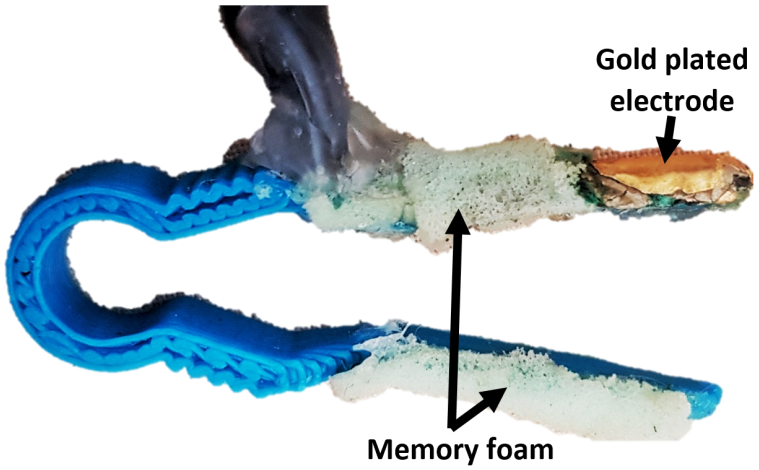

Figure 4.9: Final assembled outcome of the fourth and chosen iteration

The fourth iteration was practically tested and shown to work well with standard quick EEG tests. The next section deals with the implementation of the electrode holders to be used in attaching electrodes to the earlobe.

4.2.2 Earlobe components

A component similar to that of a clothes peg will be a convenient approach in attaching electrodes to the earlobe of a patient. In Section 4.2.1.4, an elastic deformation, spring-type design was shown to be manufacturable by means of additive extrusion. The use of such a mechanism, in the design and implementation of the peg-like component of the earlobe electrodes, could prove to be valuable.

A peg, however, requires a mechanism that is inverse to that of the forth iteration of the in-ear component. A logical approach to doing so would be to have a cross-over region to invert the peg legs between the pivotal point and the tip of the legs. The legs of the design shown in Fig. 4.8 are consequently altered to the variations shown in Fig. 4.10. The printable parts are made in such a way that there is room to bend the legs over to the opposite side, using the necessary force.

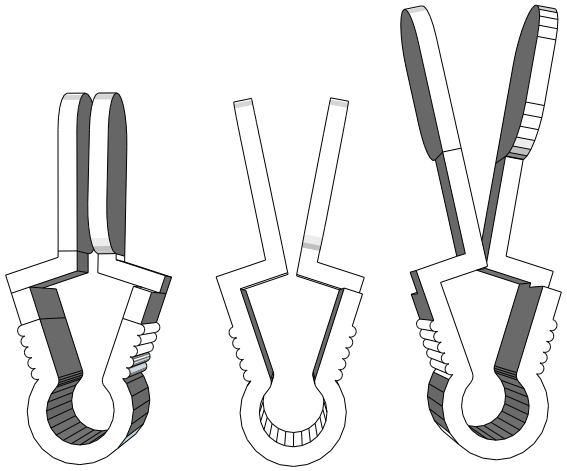

Figure 4.10: Various initial iterations of the earlobe peg

The variations of angles after the cross-over region are indicative of the trial-and-error approach that was followed to obtain an angle that would produce the best final configuration component with parallel peg legs. The trial-and-error approach was followed due to the non existence of a single, fixed pivotal point, but rather an entire circular region that effectively mimics a spring-loaded pivot. It was also observed, with further iterations, that the further the cross over was placed from the pivot, the larger the extent to which the adjusted peg could be opened (using a manual compression force).

Gold cup electrodes, bought from OpenBCI [61], were incorporated into the component. As such, a negative volume was designed into the model in order to position the electrode along with its wiring. Figure 4.11 presents the final model of the peg earlobe electrode holder. All of the edges and surface boundaries that come into contact with skin are rounded for safety and comfort. A negative cavity for the electrode wiring is included and leads the wire back up the leg.

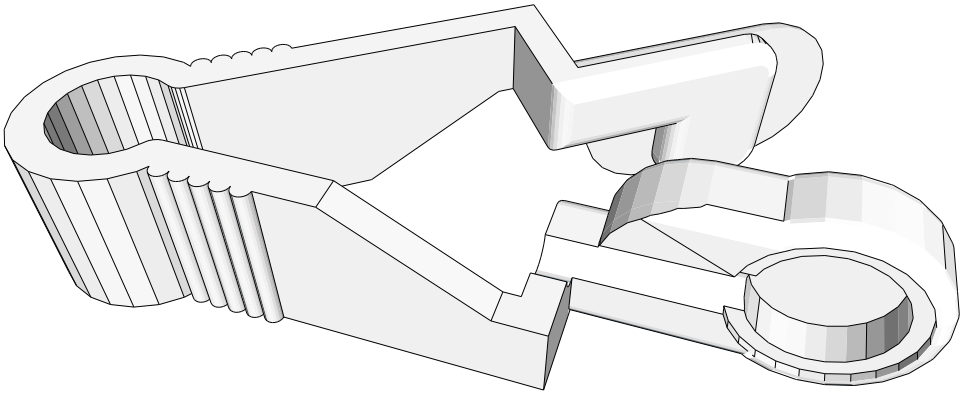

Figure 4.11: Final earlobe peg model designed in Inventor [71]

The fabricated (using the UP Plus 2 [57]) and pieced-together version of the ear peg is given in Fig. 4.12. One can note that the gold-plated cup electrode is fully contained within the peg leg volume and that soft material was added to the exterior surfaces of the peg facing the patient to once again provide optimal wearing comfort.

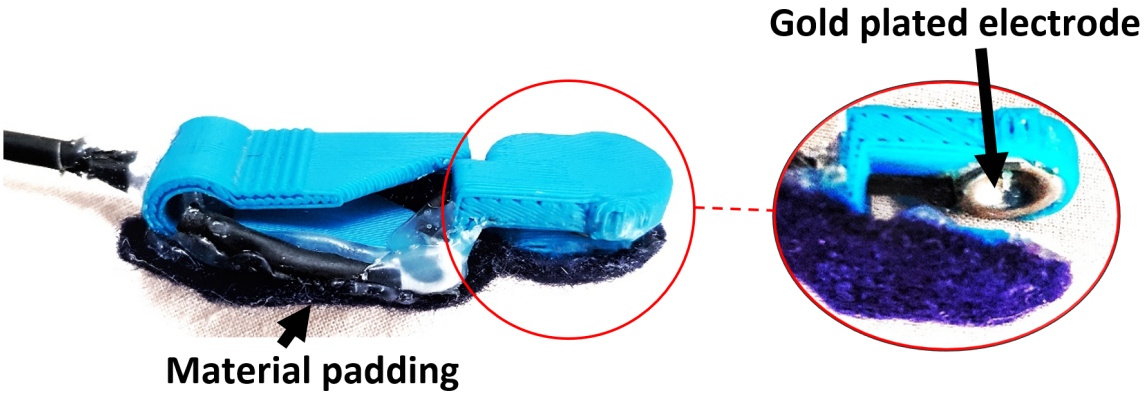

Figure 4.12: The fabricated earlobe peg electrode holder along with all of its parts and assembly

4.3 Conclusion of the electrode topology design

The designed peg was practically tested and shown to be fully functional as expected. The chapter that follows further broadens the hardware approach surrounding the now designed electrode topology.

Chapter 5

Hardware design implementation

Having successfully designed the electrode topology. It is necessary to design the remainder of the connected devices and subsystems to produce a functional end product. The overview that follows gives indication of the subsystems needed to produce a working system. A modular design approach is followed in order to individually debug and optimise the subsystems.

5.1 Overview

It is logical that one of the subsystems should be a device capable of recording (or streaming via some wireless medium) the EEG data obtained from the electrode topology. It will be required to play the audio stimulus to the ear of importance to evoke the auditory response. Therefore it is vital that an acoustic stimulation subsystem be implemented. In order to avoid bone conduction stimulation of the contralateral ear, causing unwanted artefacts in the response obtained, a white noise generating system should be designed to mask it.

All of the above-mentioned subsystems need to be contained within close proximity of a patient undergoing surgery. Longer wiring distances increase susceptibility to electromagnetic interference (EMI). A containing base structure system is therefore necessary to hold the individual subsystems together in order to simplify the presurgical set-up process. Figure 5.1 shows a system block diagram depicting the various subsystems whilst providing an indication of their proposed interconnectivity and the relevant sections detailing the design. It can be noted that from the figure, the acoustic stimulus subsystem contains a wired connection to the EEG recording device. This linkage exists in order for the EEG data to be synchronised with the stimulus, if such a need arises.

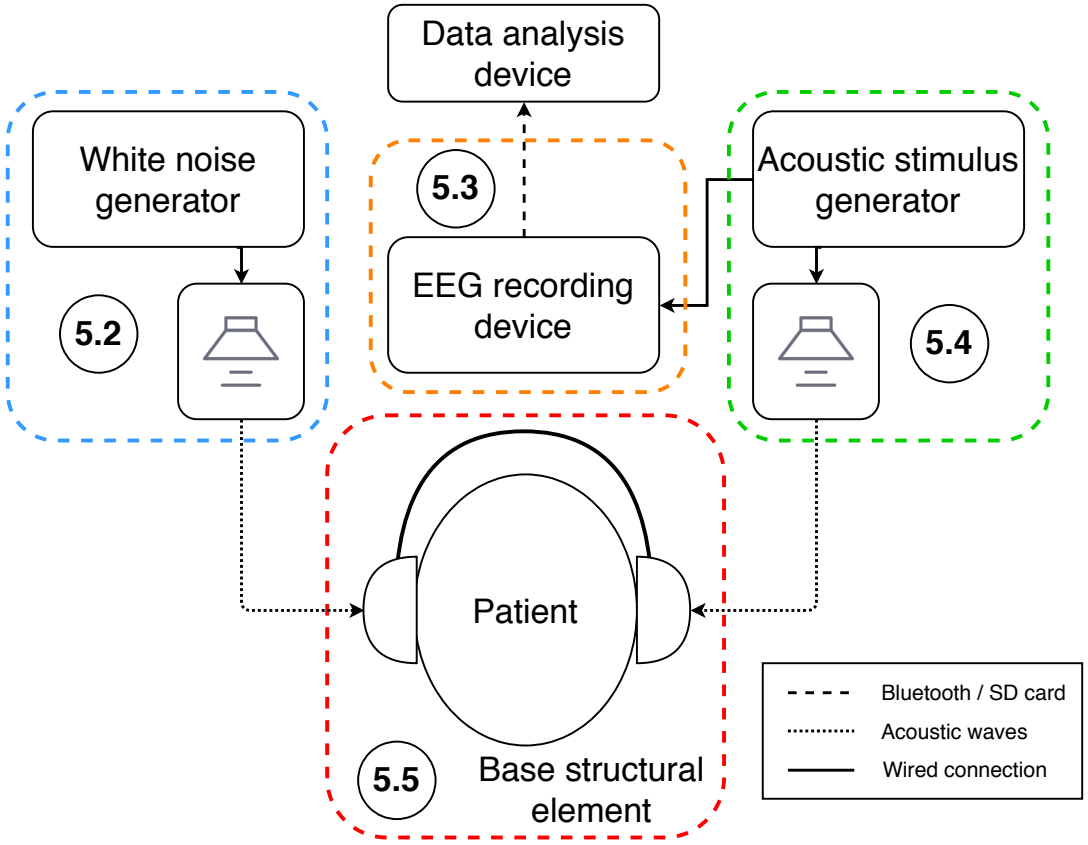

Figure 5.1: Overview of the hardware subsystems and their corresponding section numbers

The next sections contains the details of the design process required to produce these subsystems.

5.2 White noise generator

In order to maximally eliminate noise propagation to the other very sensitive subsystems, the noise generator was designed entirely separately and has its own power supply and containment housing. This section focuses on the design of such an isolated system.

5.2.1 Electronic design

In order to playback white noise, one needs to either have some form of audio player device built into the subsystem containing a white noise file, play noise remotely from a wired/wirelessly connected device or generate the white noise on-board and play the generated signal. The former two options would be over-designed implementations for the simple task at hand and would result in unnecessary expenses. The latter option,

however, is a feasible choice and is the preferred route.

One such method of achieving a white noise generator, is utilising the phenomenon that a npn-transistor exhibits random behaviour when placed in reverse bias. As the reverse voltage over the base-emitter junction surpasses the breakdown voltage, there is an increasing presence of noise observed at the emitter node. It was chosen to use a 2N3904 bipolar junction transistor as the noise source (datasheet available at [73]). It is listed in the datasheet that the minimum base-emitter breakdown voltage is:

$$B_{(BR)EBO} = 6.0V$$

Therefore a standard 9V battery is sufficient to push the junction into the breakdown region. In Fig. 5.2 the designed circuit is presented with the circuitry on the left being the white noise generating stage and the right being the audio amplifier. The 9V battery is to be connected in series with a switch to element JP1 nodes 1 and 2 (having the positive terminal leading to node 2). The switch allows turning the device on and off without needing to disconnect the battery.

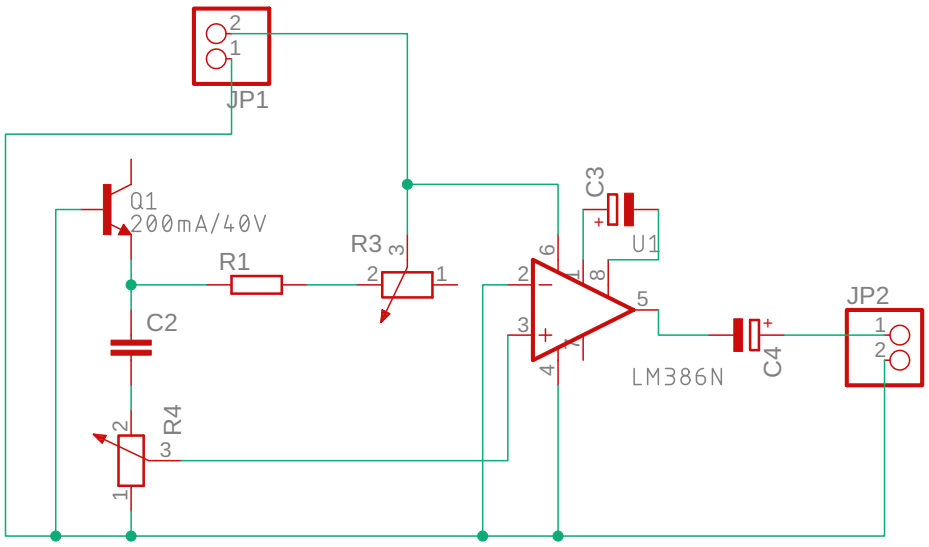

Figure 5.2: White noise circuit schematic as designed in Autodesk Eagle [72]

Due to the bipolar transistors having slight electrical variations, it is logical to make use of a potentiometer to allow tuning of the base-emitter reverse breakdown current until optimal results are obtained. The positive terminal of the battery is fed through a chosen R3 = 100kΩ potentiometer in series with a protective R1 = 10kΩ resistor, which is connected to the emitter of transistor Q1. The base of Q1 is grounded to insure that the reverse biasing is obtained. With variation of the R3 setting, the reverse current and bias of the transistor is tweaked to give optimal observable output. The reverse noise behaviour of V_E contains a DC offset that is decoupled using a small C2 = 0.1μF capacitor.

The audio amplifier was built using an LM386N low-voltage audio power integrated circuit (datasheet available at [74]). In order to control the volume of the output signal, another R4 = 10kΩ potentiometer adjusts the level of the decoupled noise signal being input to the positive specialised operational amplifier node. The negative input is connected to ground (being the negative battery terminal). Pins 6 and 4, being the source rails, are connected across the battery. Pins 1 and 8 are bridged with a C3 = 10μF electrolytic capacitor to set the gain of the amplifier to 200 [74]. Finally the output is decoupled using a C4 = 250μF electrolytic capacitor, before connecting to the 8Ω speaker attached across JP2. The capacitor and speaker produce a high-pass cut-off frequency that can be calculated using

$$f_c = \frac{1}{2\pi\tau_c} = \frac{1}{2\pi RC} \tag{5.1}$$

$$= \frac{1}{2\pi.8\Omega.250\mu F} \tag{5.2}$$

$$= 79.58 \text{ Hz}. \tag{5.3}$$

The printed circuit board (PCB) layout can then be generated and optimised from the schematic and the board can be manufactured (see Fig. 5.3). Figure 5.3a shows the copper connections on the bottom layer with components placed on the top layer. Figure 5.3b provides a photograph of the produced and soldered PCB that is ready to be tested.

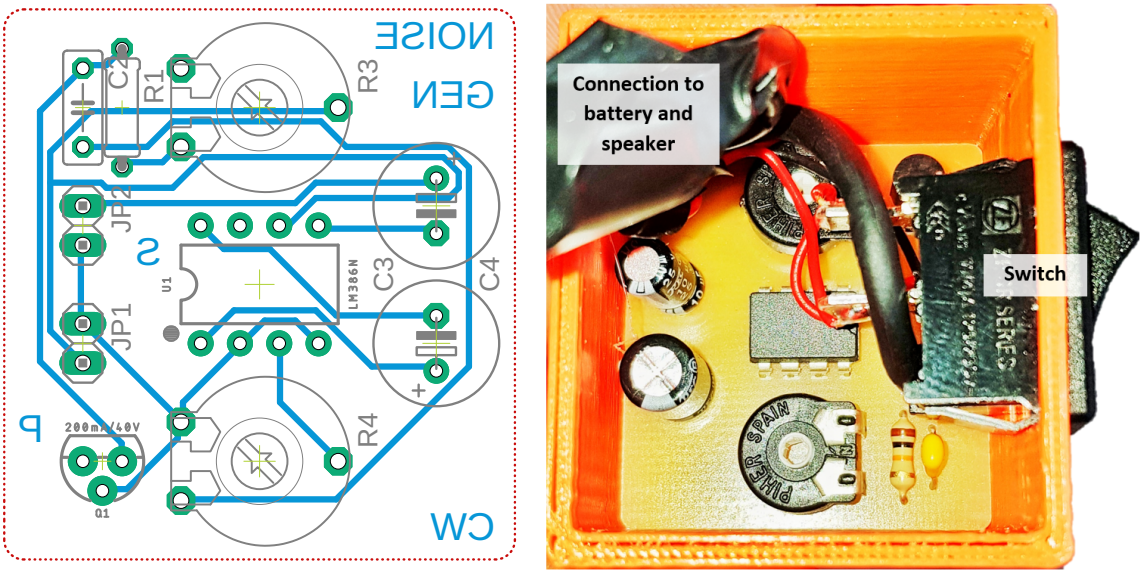

(a) PCB design in Autodesk Eagle [72] **(b)** Photograph of the prototyped design

Figure 5.3: The white noise generator PCB realisation

In order to prepare the test of the generator, initial tweaking was done whilst monitoring an oscilloscope output to find the optimal potentiometer setting. To obtain a true output representation, a smartphone microphone recorder was used to record the output

of the speaker. The audio file was then transferred to a computer where it was input into a Matlab [69] script and plotted in the frequency and time-domain, as shown in Fig. 5.4.

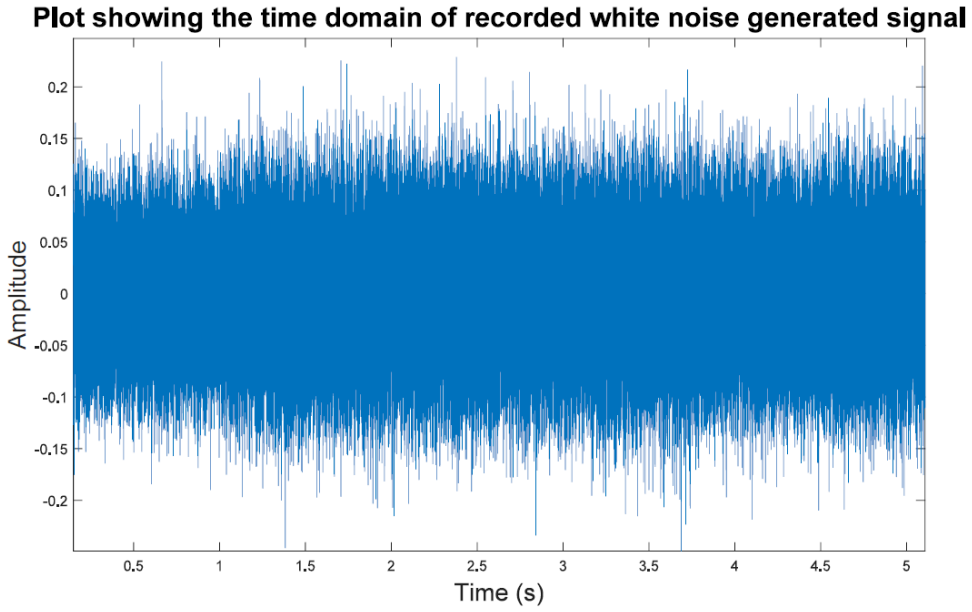

(a) Time-domain

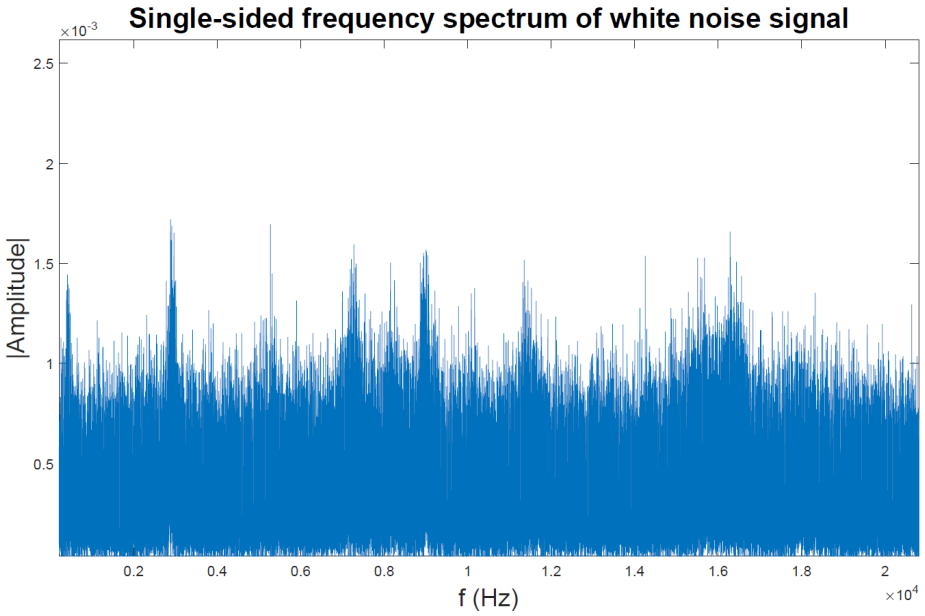

(b) Frequency-domain

Figure 5.4: Output result of the hardware system

Although the frequency-domain, plotted in Fig. 5.4b, shows slight irregularities over the half sampling rate (oversampled Nyquist frequency for audio file is $f_s = 44100$ Hz)

range, the response is more than sufficient for the application of merely being a masking noise. The time-domain is indicative of a randomly distributed signal, thus validating the design's success. The section that follows describes the design of the container within which such a system will be isolated.

5.2.2 Containment design

In accordance with conventional ethical practice and EMI reduction techniques, a containment unit was designed for the developed circuitry. Figure 5.5 summarises the components drawn up in Inventor [71], to shield the open wiring and PCB from human contact as well as to prevent the noise generated from causing outwardly propagating EMI.

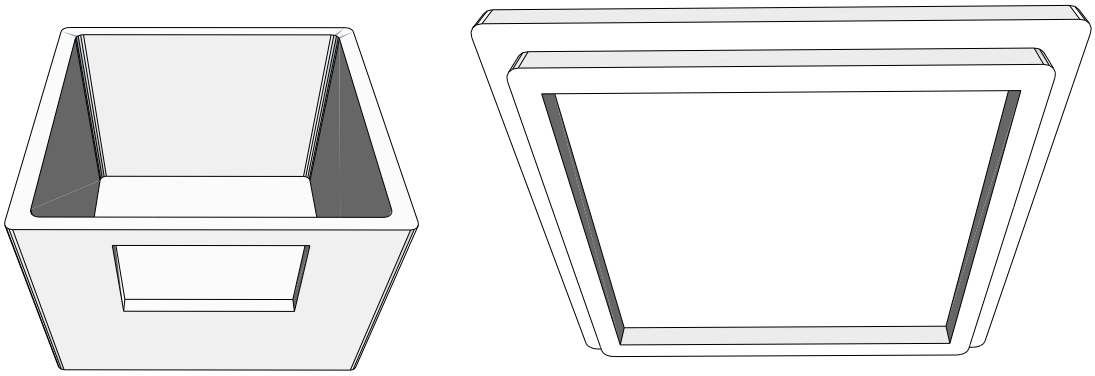

(a) The white noise PCB box with a switch hole and opening for lid (see Fig. 5.3b)

(b) Lid to the PCB box with an inside shoulder to align closure

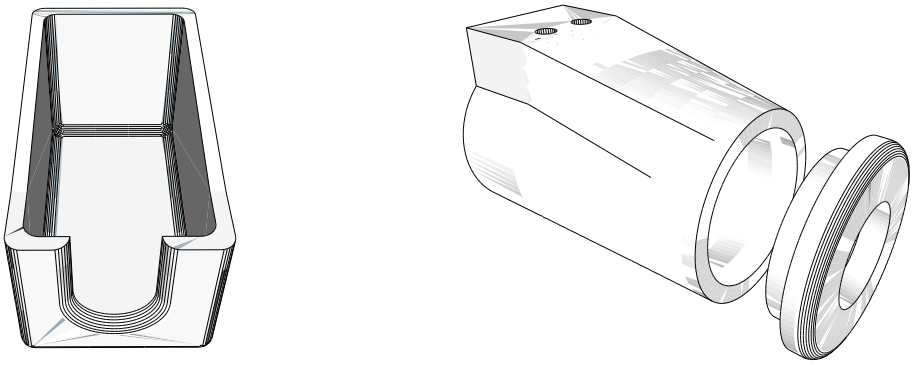

(c) Cover to surround the shielded speaker container (in Fig. 5.5d)

(d) Speaker container with two small holes for wiring and a holed lid to attach an acoustic canal to

Figure 5.5: Designed white noise generator parts in Inventor [71]

The PCB in Fig. 5.3b is placed in the container of Fig. 5.5a and closed with the part of Fig. 5.5b. Wiring from the PCB connects to an external 9V battery as well as an external speaker placed inside the part of Fig. 5.5d, which is first shielded using aluminium

tape (which is grounded to the battery negative terminal) before being covered with the printed component shown in Fig. 5.5c. The shielding ensures that the electromagnetic nature of the speaker has a minimal effect on the electrode wires within proximity of the device. An transparent acoustic channel leads the sound from the speaker to the target ear.

The final system is shown in Fig. 5.6 with all the attached parts being glued together. The switch conveniently allows for separate control of the device.

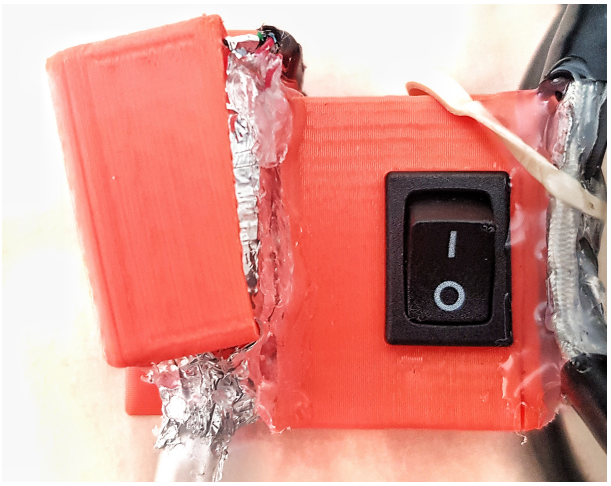

Figure 5.6: Final white noise generator system housing as fabricated using the UP Plus 2 [57]

The next section describes the design procedure for the EEG recording device.

5.3 EEG recording device

It was chosen to use an OpenBCI Cyton Biosensing board [60], portrayed in Fig. 5.7, as the means of obtaining the data from the designed electrode topology. The reason for this choice is as follows:

- It contains eight 24-bit EEG channels that are individually configurable (houses a Texas Instruments ADS1299 ADC IC [75] specialised for low-noise biopotential measurement).
- It allows for adjustment of sampling rate for the faster sampling required for evoked potentials (as opposed to standard EEG).
- The device is wirelessly controllable via means of a Bluetooth dongle and serial communication.
- The data is both streamable by means of Bluetooth or writeable to a microSD card.

- The device is compact and externally powered with a battery pack.
- OpenBCI has made the firmware open-source and has developers that have written packages and integration tools in languages such as C^{++} and Python [67].

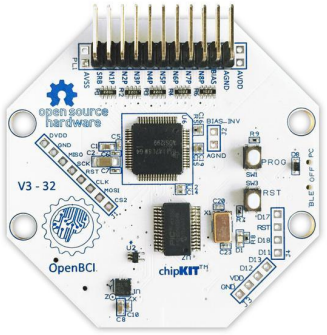

Figure 5.7: The OpenBCI Cyton [60] biosensing board

5.3.1 Electronic design

The Cyton board will receive various inputs from the different electrodes, audio stimulus generator (to synchronise the recordings) as well as communication from the controlling computer. The details of these connections are given in the integrated design described by Fig. 5.8. The peripheral pin connections, listed from top to bottom in the figure, were chosen to be as follows:

- The analogue ground (AGND – either top or bottom as they are shorted) is connected to the shielding of the wire leading specifically to the in-ear and reference electrodes. This ensures that the noise effect is ultimately reduced as far as possible in the channel of importance.
- The biasing node (BIAS – bottom pin), included to utilise common mode rejection for removing mains and other resilient interference artefacts from the active and reference electrodes, that are input into an on-board amplifier, is connected to the left earlobe electrode.
- The synchronising differential signal from the audio stimulus generator is connected to the differential nodes of channel two. Upon testing, the voltage drift caused unwanted random behaviour in the signal, and as such, the negative input was shorted to ground to eliminate the drift as well as the observed unwanted behaviour.
- The bottom pin of channel one is connected to the in-ear electrode of focus.
- The reference (SRB – bottom pin) is connected to the right earlobe electrode to be used as a reference to which the channel one potential is compared.

- A Bluetooth USB dongle, plugged into the computer, communicates with the built-in Bluetooth module on the Cyton board (found on the bottom layer).
- Included in the box of the Cyton, is a 6V (4 × 1.5V AA batteries) power supply which can be plugged into a connector on the bottom of the board.

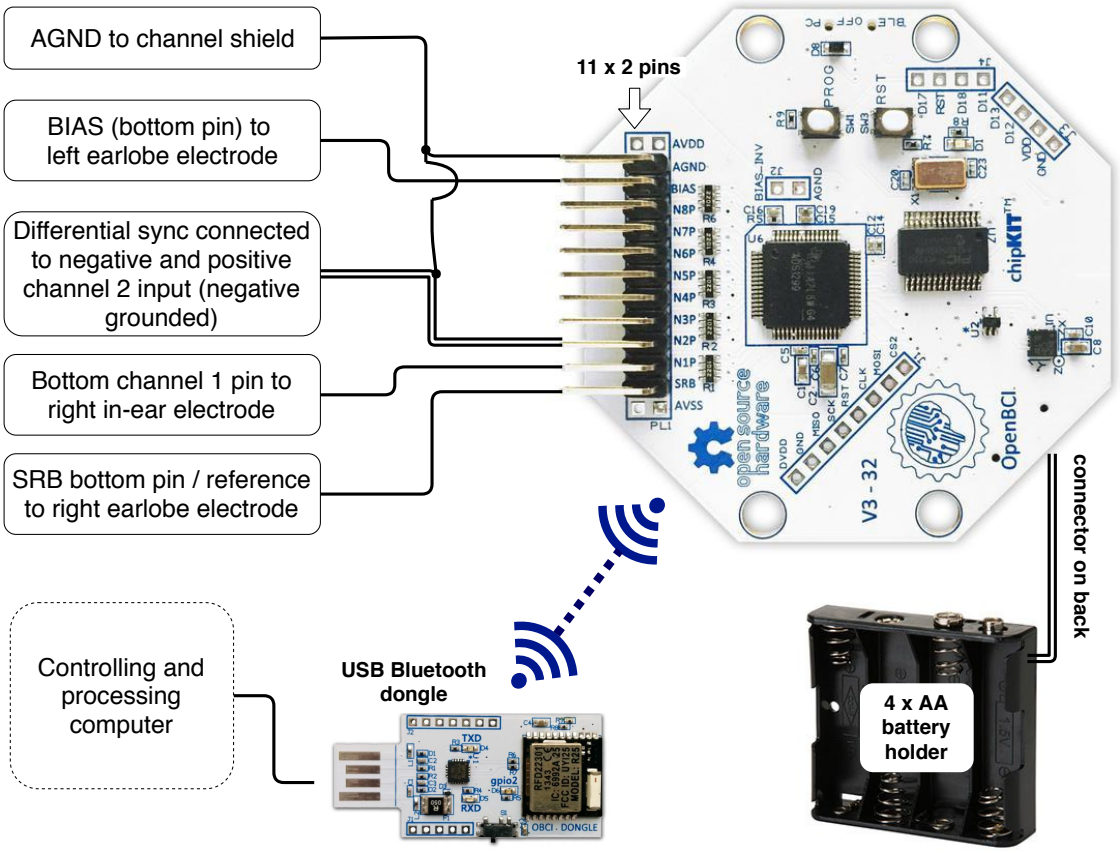

Figure 5.8: Layout depicting how the Cyton board is connected to the electrodes, surrounding subsystems and computer (three images adapted from [60])

In order to connect all of the electrodes to the Cyton [60] board, one needs to design some form of pin-out connector. Figure 5.9 shows such a pin-out for bridging the pins of the board to the wires of the various electrodes and synchronisation system. Figure 5.9a shows how the central 11×2 standard pin header is individually wired to the attaching nodes. Figure 5.9b represents the minimal board area translation of the drawn schematic. Later, in Fig. 5.12, it is shown how the pin-out connector is assembled and connected to the Cyton board. The design was then precautionarily verified using the continuity test of a multimeter.

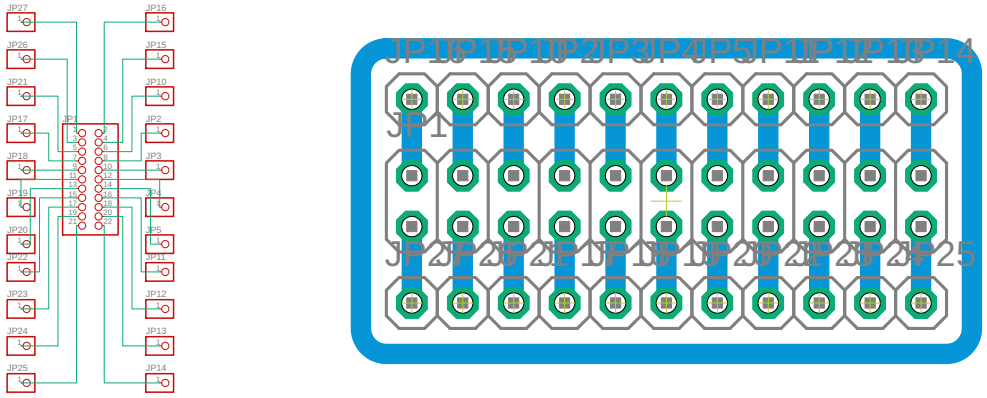

(a) Schematic (b) PCB layout

Figure 5.9: Eagle [72] designed part to conveniently switch the bias and reference electrodes

For comparison reasons, it would be valuable to design a circuit (as shown in Fig. 5.10) capable of interchangeably switching the bias (or ground) and reference electrodes.

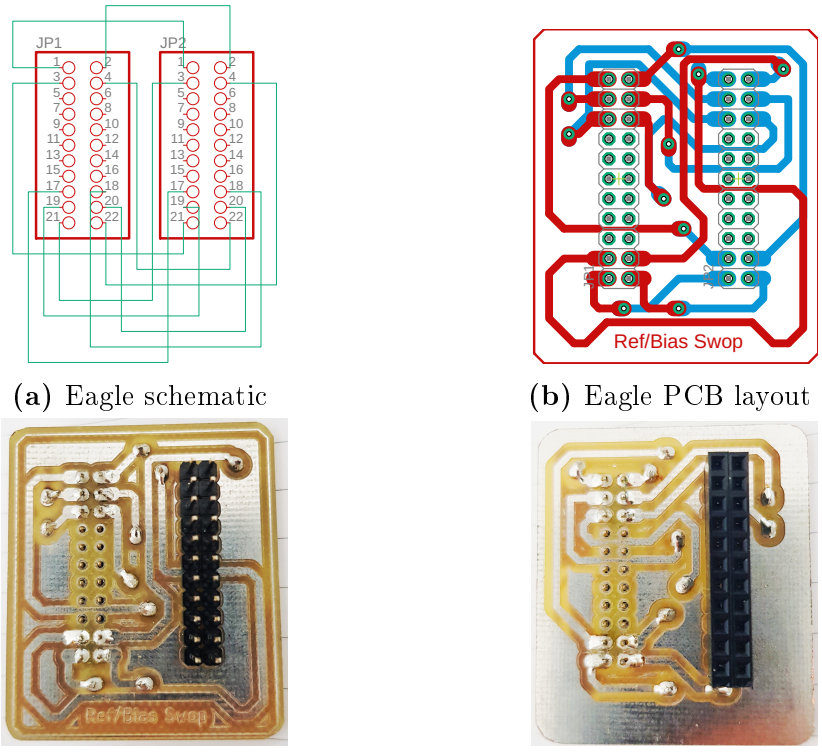

(a) Eagle schematic (b) Eagle PCB layout

(c) Prototyped top of board (d) Prototyped bottom of board

Figure 5.10: Designed part (using Eagle [72]) and fabrication (using the ProtoMat S63 [59]) to conveniently switch the bias and reference electrodes

In doing so, the auditory evoked potential will therefore be measured through the brainstem across the inner-ear and contralateral earlobe electrodes, rather than across the inner-ear and ipsilateral earlobe electrode. The pins of the bias and reference nodes are switched in the mapping of the two 11×2 headers, shown in the schematic of Fig. 5.10a, while the remainder of the pins are correspondingly linked. Due to the desired intermediate placement of the part as well as the pin-mapping, it becomes necessary to design a double sided PCB, as given in Fig. 5.10b. The two sides of the fabricated board, with soldered vias and both male and female headers, are depicted in Fig. 5.10c and Fig. 5.10d.

In validating the design, the desired pathways were verified by measuring the continuity across the ends. In order to protect and insulate the board from patient contact, a containment unit is designed in the following section.

5.3.2 Containment design

OpenBCI have made available a GitHub repository containing a printable full ten-twenty EEG helmet and board cover (link provided in [76]). The board cover can be adapted for the in-ear device of this thesis, by closing the unnecessary through-holes, strengthening some regions and removing various threaded geometries.

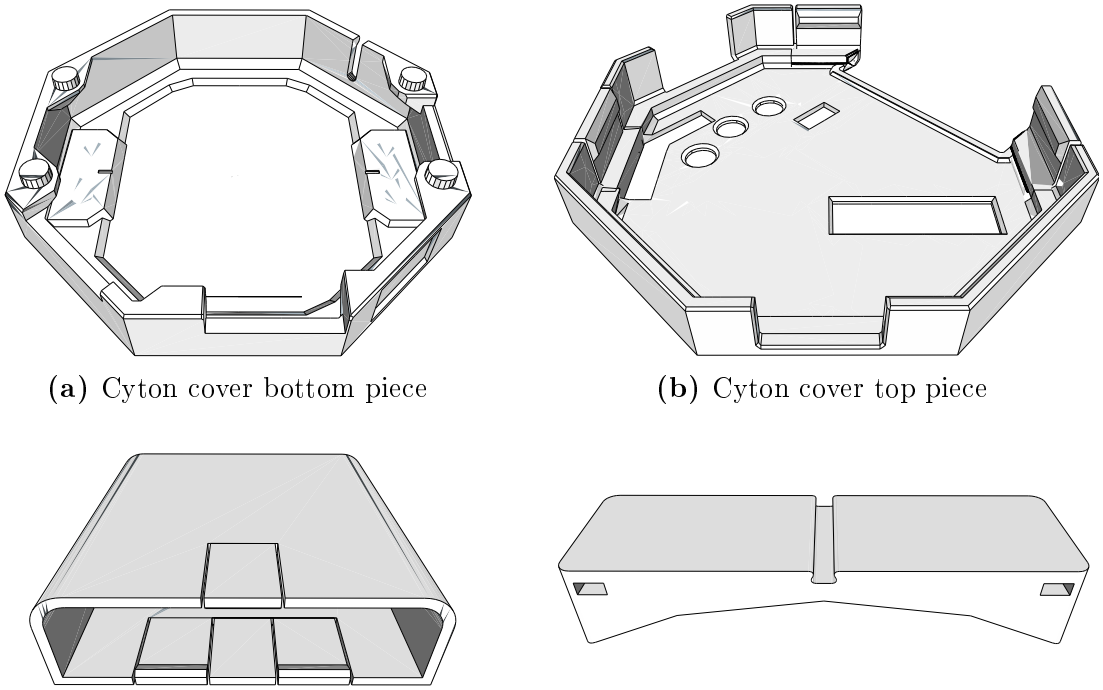

(a) Cyton cover bottom piece

(b) Cyton cover top piece

(c) Battery holder cover

(d) Stand to fix board to headphones (see Section 5.5)

Figure 5.11: Designed and adapted (using Inventor [71]) housing components for the Cyton board and related parts

Fig. 5.11, Fig. 5.11a and Fig. 5.11b show the modified models of the downloaded board top- and bottom- covers. An adjustment was also made to the GitHub design to allow for the battery wires to be lead through a slit out of the side of the cover (see the top right hand corner of Fig. 5.11a). Figure 5.11c shows the designed battery holder cover, made from taking measurements of the shipped part. To attach the board to the Peltor [64] (see Section 5.5), the curvature of the over-the-head part of the earmuffs is traced and measured to be used in designing a stand, as shown in Fig. 5.11d.

The final assembly of the design is shown in Fig. 5.12, with the board cover fixed onto the battery holder cover, which is attached to two board stands connected to the headphones by means of glued Velcro strips.

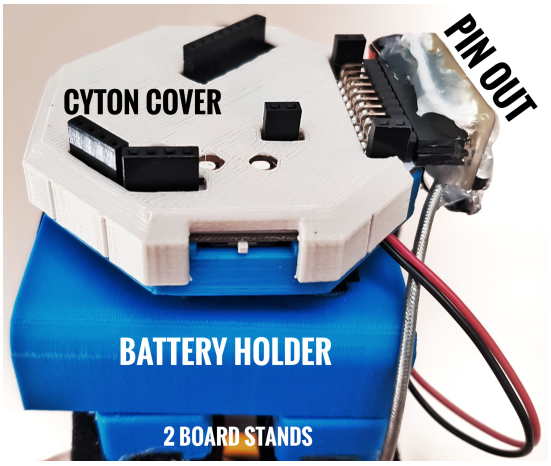

Figure 5.12: The final compilation of all the designed EEG recording components

The success validation of the electrode topology and set-up is implicit with the outputs of the software chapter that follows. The following section describes the design of the acoustic stimulator subsystem.

5.4 Acoustic stimulus generator

A critical component in the recording of auditory evoked potentials (AEPs), is the auditory stimulus (having the form as recommended in Section 2.6.6). The details of how the waveform is generated, and validation thereof, is given in Section 6.2. This subsection merely deals with the playing of such audio signals and describes how to provide the Cyton board with a signal to synchronise the recorded data with the relative latency after audio click. The reason that an audio stimulus synchronisation signal is necessary is also discussed.

5.4.1 Motivation for audio synchronisation

In the perfect world where everything is perfectly structured, in-time and on-time, there should be no need to create a signal used to synchronise the data to the stimulus. If it is known that the frequency of stimulation is 8 Hz, and the sampling frequency of the Cyton board is set to 1 kHz, it can simply be chosen that the number of samples per period is

$$N_p = \frac{\text{period of stimulus}}{\text{period of sampling}} = \frac{1/8}{1/1000} = \frac{125ms}{1ms} = 125\ samples. \tag{5.4}$$

By merely averaging together every group of 125 data samples, one should obtain a waveform representing the AEP (although perhaps being shifted in the time-domain). But in actual fact, none such perfect-world assumptions can be made and there are too many factors than need to be accounted for. Some of the factors that could be accounted for are the following:

- Clock drift – If the clock of the audio player device and recording device are not an exact factor or multiple of (or exactly equivalent to) each other, there will be a gradual drift in the time misalignment over time causing erroneously averaged evoked potentials.
- Audio sampling rate – If the audio file sample rate is not an exact multiple of the stimulus rate, a slight time-offset due to the actual realised frequency is produced. Let the sampling rate be the commonly used 44100 Hz and the stimulus rate 8 Hz, which is not a factor of the sampling rate. The time offset (E_p) for every period can be determined using the modulus operator (%) as

  $$E_p = \left(\frac{1}{8}\%\frac{1}{44100}\right) = 1.13378685 \times 10^{-5}s \tag{5.5}$$

  and therefore for a 5 minute audio file with $5 \times 60 \times 8 = 2400$ stimulus periods, the gradual time-drift due to the audio sample rate totals to $2400 \times (1.13378685 \times 10^{-5}) \approx 0.02721s = 27.21ms$, which is extremely significant and unignorable.

There are, however, factors that are predominantly unpredictable and can therefore not be accounted for without some synchronisation signal. Such factors are:

- true quartz crystal frequency having an unknown offset from the presumed frequency on the devices involved in playing the signal;
- transmission errors causing time-domain jumps in the Bluetooth streaming of the audio; and
- electronic communication errors also effecting the on-time delivery of the audio to the speaker, and as a result, causing time-offsets.

It is therefore critical to be able to sense the beginning of every stimulus in order to synchronise the averaging algorithms using this information. An astute way to address this, would be to utilise the stereo nature of an audio stream to simultaneously stimulate the ear with one channel and provide the EEG device with a synchronisable signal in the other channel. Another advantage of doing so is the ability to generate different duty cycles on the two channels, which will allow the EEG recording device to detect the stimulus onset on the synchronising channel, even if its sampling frequency is too slow to detect the duty cycle on the stimulation channel (which was the case in this thesis).

The following section describes the initial design approach to stimulate the ear and synchronise the data.

5.4.2 Initial approach

Geist 36BL Bluetooth earphones [63] were initially modified and adapted to become the audio subsystem. Figure 5.13 shows the designed circuit that, once again, uses a LM386 audio amplifier [74] based circuit for a maximum gain of 20. The component values of the amplifier circuit are R1 = R2 = 10 kΩ, R3 = 10 Ω, C1 = C2 = 250 μF and C3 = 0.05 μF.

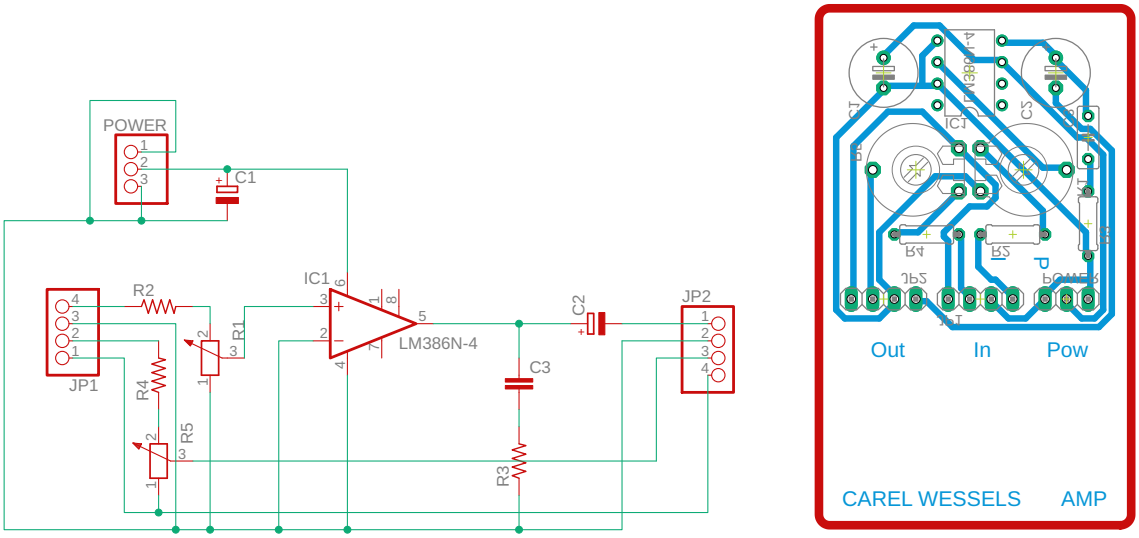

(a) Schematic **(b)** PCB layout

Figure 5.13: Eagle [72] designed expansion part, to amplify and use as synchroniser for the signals, of a Geist [63] audio device

The Geist earphone circuit is removed from its containment unit and detached from the speakers before channel one's positive and negative output is wired to pins 4 and 3 of JP1, illustrated in Fig. 5.13a. These pins are fed as input through the amplifier to obtain a desired output sound level, played on the speaker connected to pins 1 and 2 of JP2. The differential second output channel of the Geist is fed through an adjustable simple

voltage division circuit consisting of R4 = R5 = 100 kΩ. The output voltage fed into pins 3 and 4 of JP2, which is connected as the synchronisation channel to the EEG device, is therefore adjustable to 0–0.5 times the input by adjusting the potentiometer. The system Geist is powered with the included rechargeable battery and the amplifier is power with a 9V battery connected to the pin headers marked "POWER".

Figure 5.13b shows the PCB design (with space reserved at the bottom to attach the Geist 36BL circuit). The final system was fully wired to an isolated speaker and power system and contained within the designed and printed housing, as shown in Fig. 5.14.

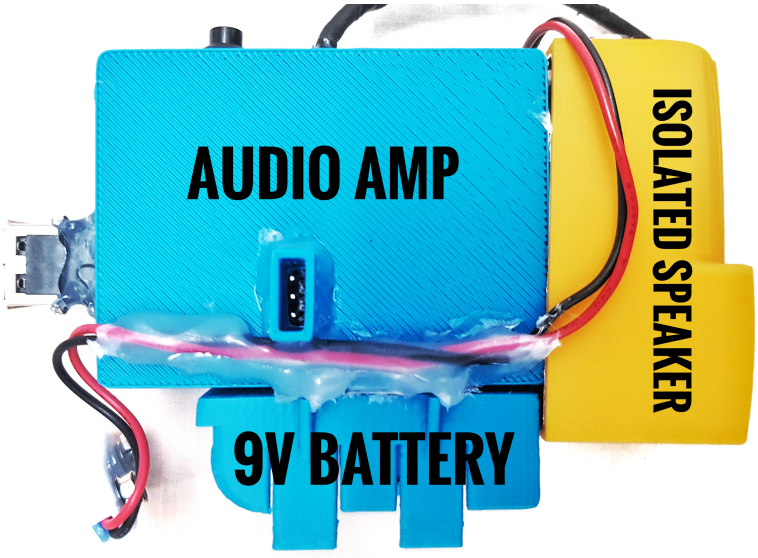

Figure 5.14: The final product of the the initial audio amplifier subsystem

It was, however, observed that the cascading of the built-in amplifier of the Geist and the designed amplifier caused irregularities in the audio output. An oscillating sound intensity, together with other irregularities, was audible when testing the sound stimulus generated by the code presented in Section 6.2. It was decided to instead design a system that does not require a second amplifier and that exhibits a satisfactory low-frequency response. The following section details such an approach.

5.4.3 Electronic design of improved system

A headphone device has louder output volume capabilities than that of an earphone, and as a result a JBL T450BT on-hear headphone [62] is selected as the replacement for the Geist. The speaker and amplifier, playing the audio stimulus, will be kept as the built-in optimised options, with the modification of the second channel to be used as the synchroniser. The circuit components, along with one speaker and all of its housing is kept, while the remainder of the device is removed and disconnected. Figure 5.15 gives the design of channel two modification circuitry similar to that of the initial approach.

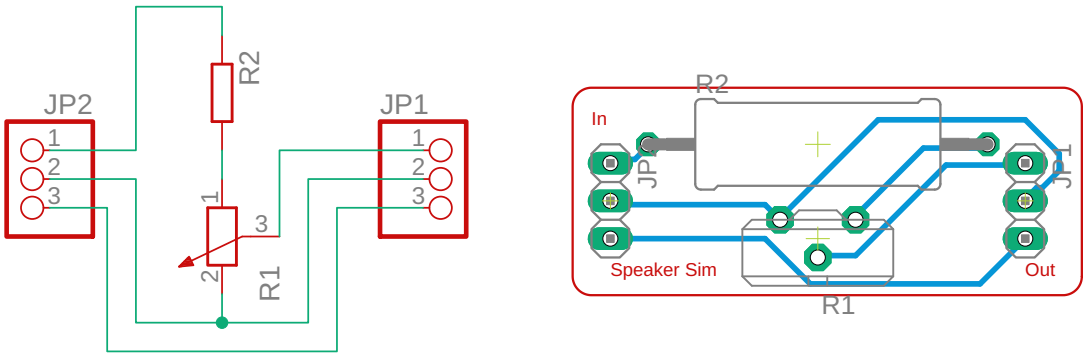

(a) Schematic **(b)** PCB layout

Figure 5.15: Eagle [72] designed part to modify the second channel to be input into the EEG recording device

Another consideration change from the first approach is that an alteration in the load that the JBL circuitry sees will cause unbalanced load irregularities. The impedance of the speaker is therefore measured with a multimeter and found to be $R_s = 32\Omega$, which is mimicked by the $R1 = 25\Omega$ potentiometer in series with the $R2 = 7.5\Omega$ resistor. The current protection of the EEG device (and conveniently also a reduction in EMI generation of the wiring leading to it) is applied in the software of Section 6.2 by dramatically decreasing the amplitude of the synchronisation channel of the stereo signal (also evident in Fig. 5.16).

In Fig. 5.15a, the nodes that did lead to the removed speaker are connected to JP2 pin 1 and 2. This is passed through a simple voltage division circuit and wired as a differential signal to the EEG device by means of JP1 pin 1 and 2. The whole shielding system, consisting of the speaker container wrapped in foil as well as the wiring shield, is connected to ground (negative node of the JBL's battery) by means of JP2 pin 3 which is directly bridged to JP1 pin 3.

5.4.4 Verification of design

To fully verify the audio stimulus generator's functionality, it can be connected to an oscilloscope and observed in the time-domain. Figure 5.16 shows the measurement of both the speaker signal and amplitude decreased, duty cycle increased synchronisation signal. It can be noted that from the x-axis scale, the frequency of 8 Hz (125 ms pulse spacing) is obtained as designed in Section 6.2.

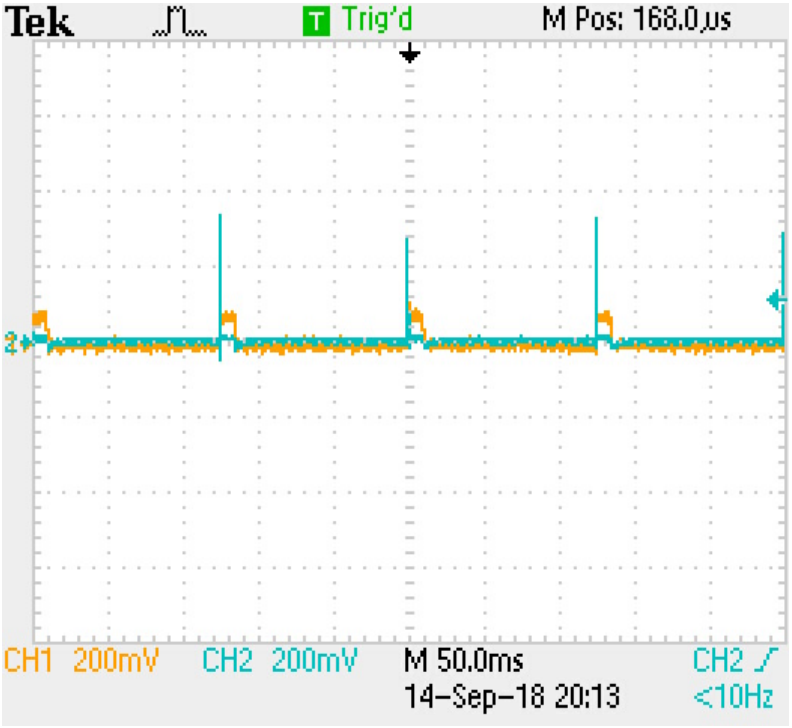

Figure 5.16: Oscilloscope measurements of the two audio stimulus channels used for synchronisation (yellow-orange) and sound stimulation (cyan)

5.4.5 Containment design

Figure 5.17 models the designed assembly of printable components that have been created to cover the designed audio generator in its entirety. The interior surfaces of all the components are covered with aluminium foil tape to act as shielding that is also shorted to the ground node. The speaker sound can be carried to the ear by means of an auditory canal attached to the leftmost part.

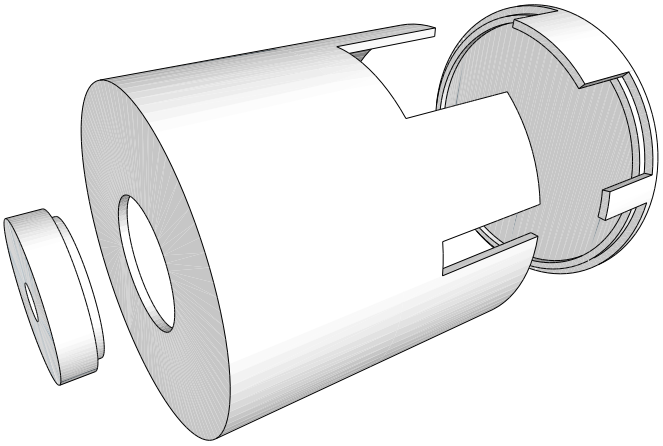

Figure 5.17: The Inventor [71] designed containment of the audio generator subsystem

The differential synchronisation signal is routed to the EEG recording device by means of shielded wiring. The final assembly of the subsystem attached to the Peltor earmuffs is shown by Fig. 5.18.

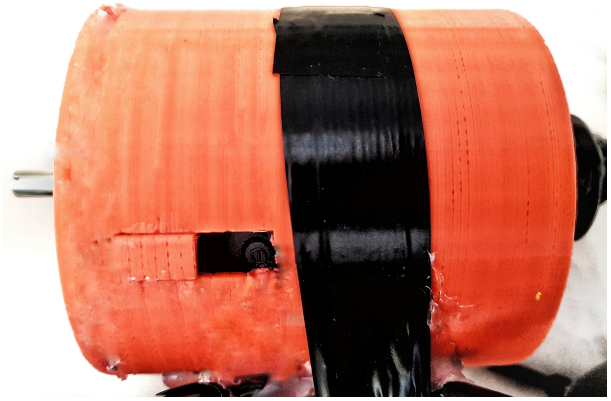

Figure 5.18: The complete optimised version of auditory stimulator with synchronisation signal

5.5 Base structural element

It was decided to use a 3M Peltor X2A [64] 31dB noise blocking earmuff as the structural component to attach all the hardware subsystems to. The passive noise cancelling nature of the earmuff attenuates external noise in the region of the ears, so that the white noise and auditory stimulus is the predominant sound delivered to the respective eardrums. The final hardware system in entirety is shown in Fig. 5.19.

Figure 5.19: Entire hardware system perspective

The auditory canals are placed through drilled holes on both sides and the surrounding gaps closed with a hot glue gun. The white noise generator (bottom), EEG recording device (left), audio stimulus generator (top) and all the electrodes of the designed topology (right) are shown attached to the Peltor (centre) in the figure.

5.6 Conclusion of the hardware designs

The following chapter details the software design components of the thesis, which integrate with the hardware of the last two chapters.

Chapter 6

Software design implementation

This chapter deals with the design and successful implementation of the software aspects integrated with the hardware described in Chapter 4 and Chapter 5. Its functionality and detailed design are of vital importance to meeting the objectives of this dissertation.

6.1 Overview

Figure 6.1 illustrates which software components are necessary to obtain a working product as well as how they communicate and integrate with the hardware of the previous two chapters. The key software subsystems are:

- the generation of an auditory stimulus, both unipolar and bipolar, to induce an electrical response in the auditory nervous pathway (see Section 6.2);
- the control of sequences that will set channel settings, prompt the user to set parameters (such as sampling frequency) and control the microSD recording process (see Section 6.3);
- the importation and conversion of the 24-bit hex-values from a structured text file to arrive at the raw EEG data (see Section 6.4);
- the synchronisation and signal detection to identify the starting positions of each stimulus pulse in order to later implement successful averaging (see Section 6.5);
- filtering of the raw data to obtain a clean and usable averaging input (see Section 6.6); and
- the averaging algorithm that utilises the starting position of the stored stimulus to produce the evoked potential waveform (see Section 6.7).

It is chosen to implement the software in an Anaconda Jupyter Notebook [68] environment running Python [67]. The filtering modules, modular execution, powerful data-processing capability, existing GitHub OpenBCI libraries [77], user interface and tool-sets available make it the preferred choice over Matlab and C^{++}.

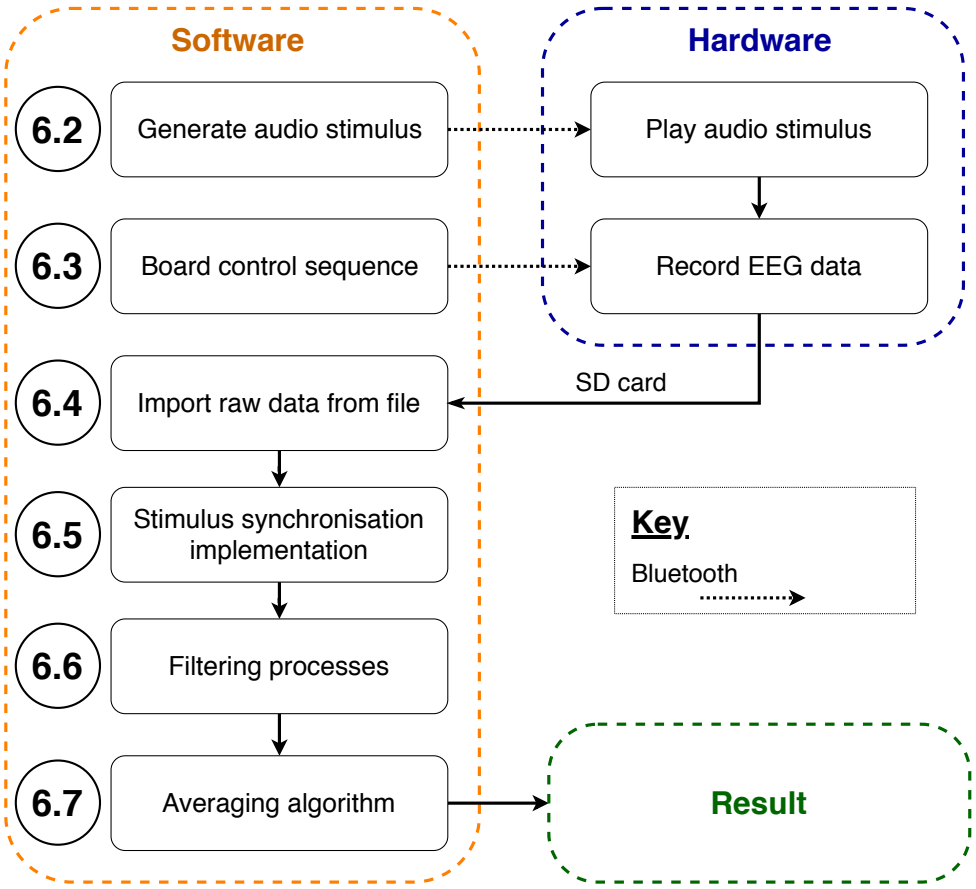

Figure 6.1: Overview of the software subtasks and their corresponding section numbers

6.2 Generate audio stimulus

The first system designed is a audio generator script which is outlined and validated in this section.

6.2.1 Overview

As discussed in Section 2.6.6, the optimal stimulus required to produce a middle latency auditory evoked potential (MLAEP), that is not frequency specific, is a click (or also often referred to as a pip) that occurs at a frequency between 8 Hz to 10 Hz and is of 100μs duration. The literature also suggested that an alternation of stimulus polarity will reduce the speaker and wiring artefacts in the final averaged system. The alternation technique may have an observable negative effect on the amplitude of the MLAEP waveforms and therefore the code will be designed to account for both stimulation formats.

6.2.2 Design

Figure 6.2 presents the design of the audio stimulation along with its synchronisation on the second audio channel of the stereo configuration.

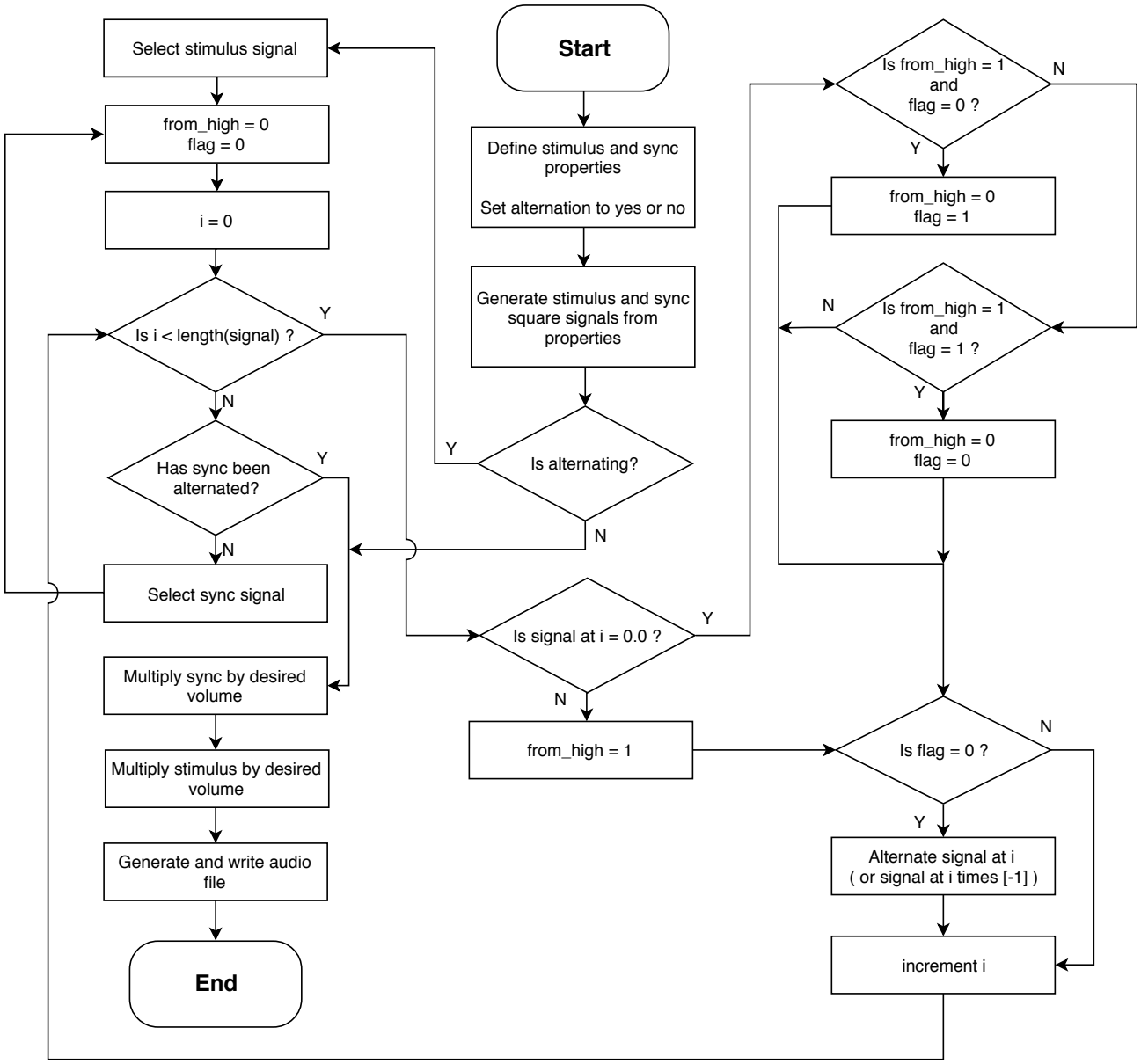

Figure 6.2: Software design flowchart of the audio stimulus and synchronisation (sync) signal generator

Due to the maximum achievable sampling rate writeable to the microSD card of the Cyton [60] being $F_s = 2$ kHz (higher only upon purchasing an additional WiFi streaming module), the synchronisation duty cycle needs to be selected appropriately. It can be

determined that due to the sampling selection, the click (square-shaped high pulse) length of the synchronisation signal should be strictly greater than

$$T_{\text{min}} = \frac{1}{F_s} = \frac{1}{2000} = 0.0005s = 500\mu s. \tag{6.1}$$

This is five times longer than the stimulation pulse and therefore can not be of the same duty cycle. There is no restriction on the length of the pulse in the second channel and it is therefore chosen to be 100 times larger than the first stimulation channel, meaning that the selected click length is

$$t_{\text{click}} = 100 \times 100\mu s = 10000\mu s = 10ms. \tag{6.2}$$

From the chosen pulse widths, with frequency of 8 Hz (not being a factor of the mains 50 Hz, as mentioned in Section 2.6.6), the corresponding duty cycles can be determined using

$$DC_{\text{signal}} = \frac{\text{click duration}}{\text{total period duration}}. \tag{6.3}$$

The duty cycle of the synchronisation channel DC_{sync} is determined to be

$$DC_{\text{sync}} = \frac{10ms}{\frac{1}{2\text{kHz}}} = 0.08 = 8\% \tag{6.4}$$

whereas the duty cycle of the audio stimulation channel DC_{stim} can likewise be calculated to be

$$DC_{\text{stim}} = \frac{100\mu s}{\frac{1}{2\text{kHz}}} = 0.0008 = 0.08\%. \tag{6.5}$$

Additionally the volume of the stimulation channel clicks is chosen to be at a maximum (16-bit two's compliment data values having a maximum of $(2^{15} - 1) = 32768$) and the synchronisation channel volume, for interference limiting purposes, is chosen to have a volume of one-hundredth of the stimulus volume (correlating to a rounded integer of 328).

6.2.3 Implementation

The Python implementation, of the flow-diagram with the chosen parameters, can be found in Appendix D. The next section verifies the output of the implementation.

6.2.4 Verification

Figure 6.3 is a visual verification of the implemented software's ability to generate an audio stimulus, along with its synchronisation signal, in both a bipolar and a unipolar fashion. Note the scale difference for both signals showing the 16-bit representation of each.

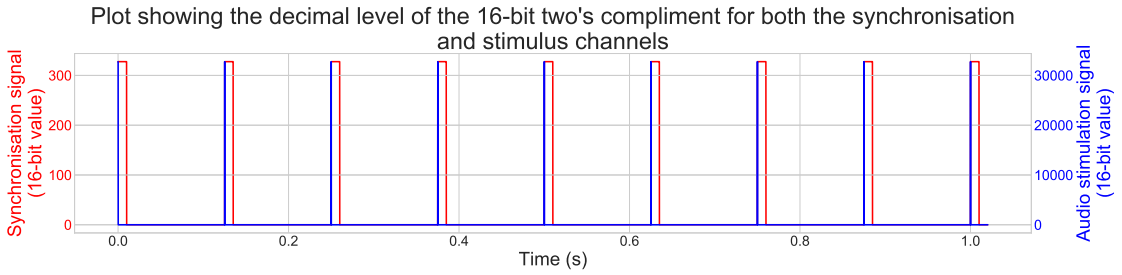

(a) Unipolar stimulus generation

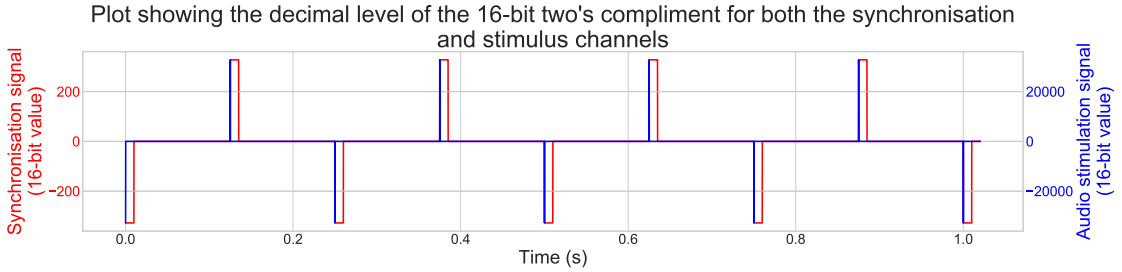

(b) Bipolar stimulus generation

Figure 6.3: Verification of the software's ability to generate both bipolar and unipolar audio stimulus (with aligned synchronisation)

Figure 6.3a shows the unipolar and Fig. 6.3b the bipolar version of both the stimulation (blue) and synchronisation (red). To verify that the correct frequency is being generated, the fast Fourier transform (FFT) of both the polar and unipolar signals are generated and plotted as shown in Fig. 6.4.

In Fig. 6.4a, it is evident that there is an 8 Hz component with all of the expected square-form relating harmonics.

In 6.4b, due to the alternating nature of the signal, its initial component shifts to 4 Hz, with a harmonic spacing of the fundamental 8 Hz component. It can also be observed that there is no DC component present at 0 Hz, due to the net-zero voltage of the bipolar signal.

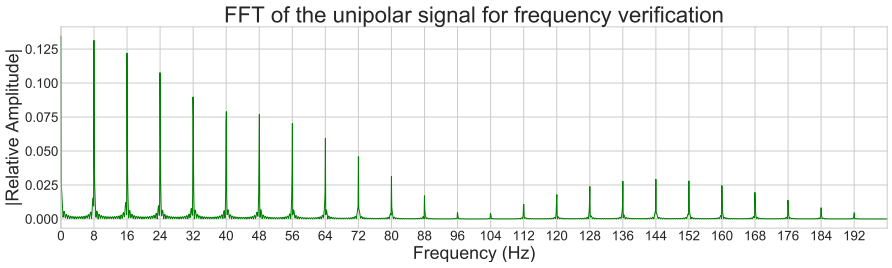

(a) Unipolar stimulus generation with components starting at 8 Hz

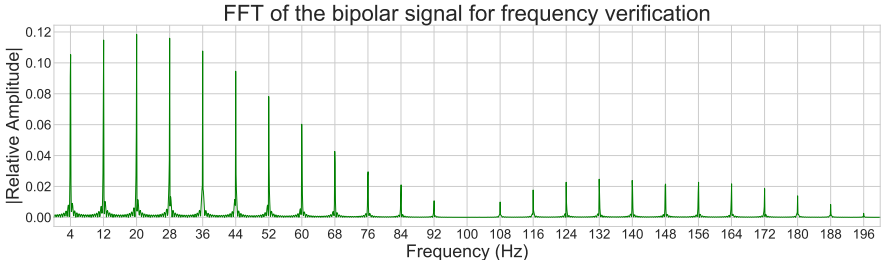

(b) Bipolar stimulus generation with components starting at 4 Hz

Figure 6.4: Frequency-domain representation of a synchronisation signal showing the clear 8 Hz-spaced square-form harmonics

Visual confirmation, that the designed for duty cycles have been obtained through software generation, is provided in Figure 6.5.

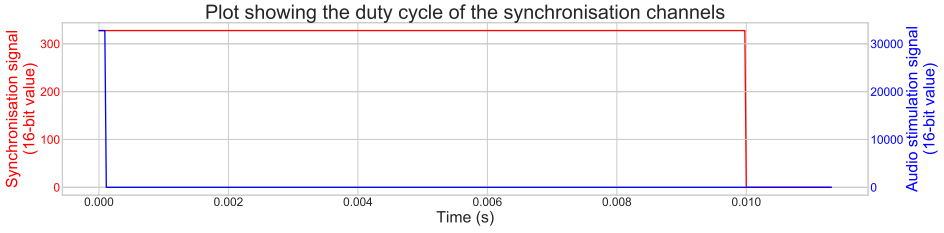

(a) Duty cycle of the synchronisation channel ($\frac{10\text{ms}}{125\text{ms}} = 0.08 = 8\%$)

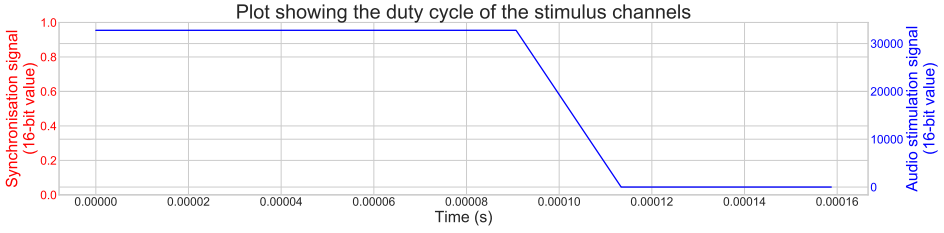

(b) Duty cycle of the stimulus channel ($\frac{100\mu\text{s}}{125\text{ms}} = 0.0008 = 0.08\%$)

Figure 6.5: Verification of the duty cycle output for both of the generated signals

The signal can then be played on the audio stimulus player designed in the previous chapter. The hardware output can be measured on an oscilloscope and all of the param-

eters can be matched to their corresponding expected values. Figure 6.6, along with the previously presented measurements in Fig. 5.16, confirm the successful hardware-software integration.

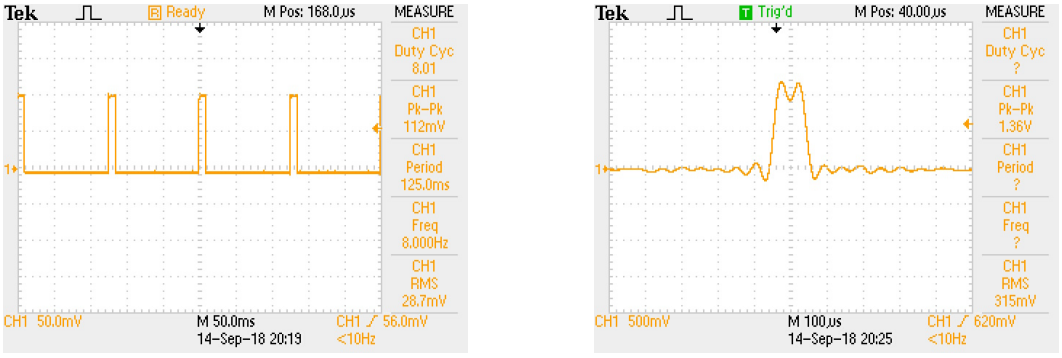

(a) Duty cycle of the synchronisation channel ($\frac{10\text{ms}}{125\text{ms}} = 0.08 = 8\%$)

(b) Duty cycle of the stimulus channel ($\frac{100\mu\text{s}}{125\text{ms}} = 0.0008\%$)

Figure 6.6: Verification of the final hardware duty cycle (and also frequency and period) output for both of the generated signals

From the right hand panes of Fig. 6.6a and Fig. 6.6b, it can be observed that the desired pulse durations of 10ms and 100μs, were obtained for the synchronisation and stimulus channels respectively. The board control sequence is implemented next.

6.3 Board control sequence

The second system implemented interfaces with and controls the Cyton [60] board's setting and data acquisition phase.

6.3.1 Overview

The design of the board control sequence (which records data with the necessary channel settings, sampling rate and duration) is discussed in this section. OpenBCI have made available Python packages on GitHub [77] to control the communication timings and serial protocols for board-computer interfacing. These packages are used to design the subsystem, together with the serial commands (provided on the software development kit website [78]) for setting and controlling the recordings.

6.3.2 Design

A flowchart was developed to describe the board control sequence software, which sequentially sets parameters and allows for the recording of data for a pre-defined period of time. The order of the steps was optimised during the implementation phase, but is already reflected as such in Fig. 6.7.

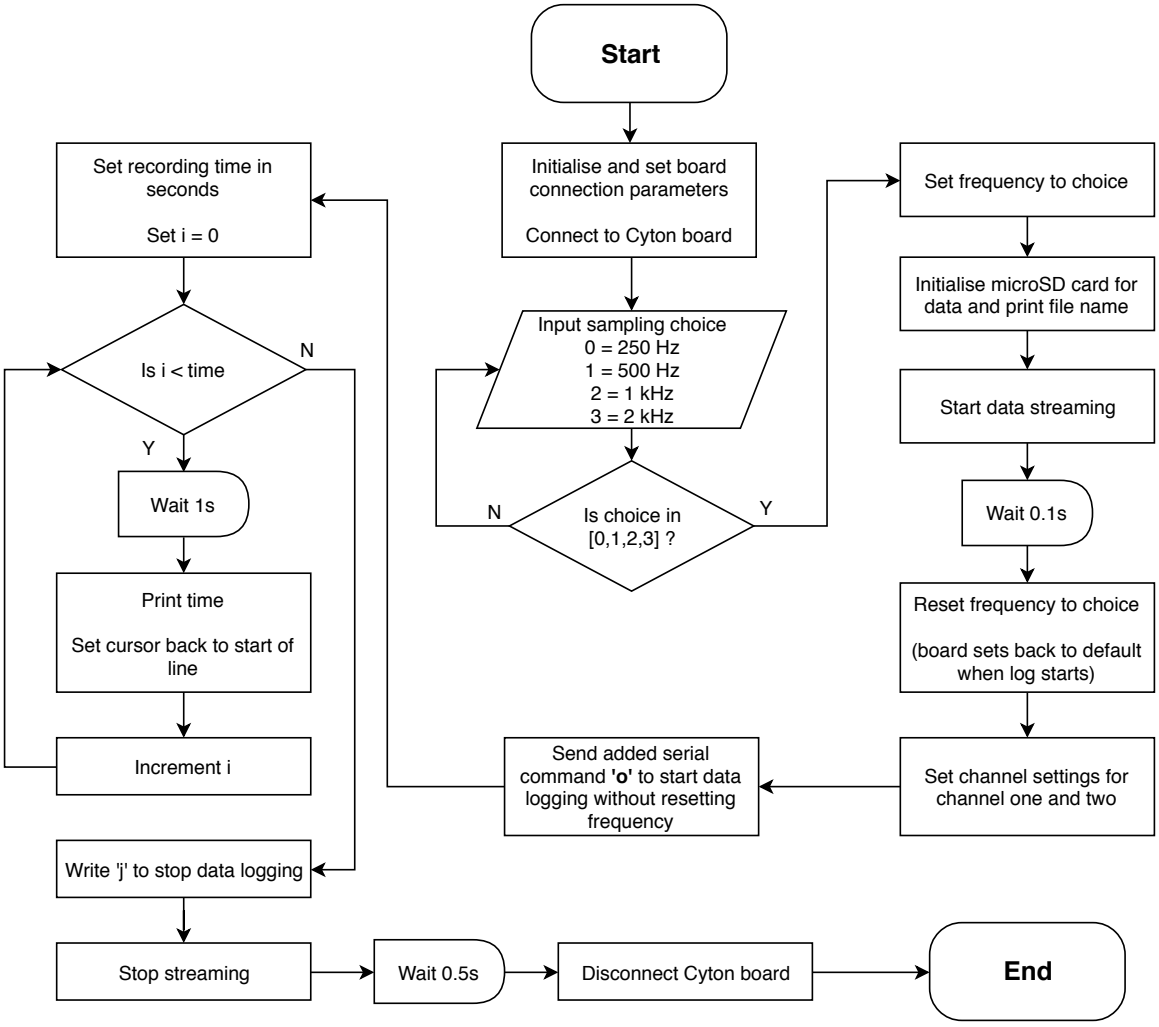

Figure 6.7: Software design flowchart of the Cyton [60] board control sequence for recording data

6.3.3 Implementation

Upon implementing the board control software, it was discovered that in order to protect the Bluetooth modules from damage, the module is continually reset back to a sampling rate of 250 Hz, unless an OpenBCI WiFi add-on module is detected. This inherently posed a problem for the success of the project, as 250 Hz sampling would not suffice to obtain clear distinguishable evoked potentials. This happens regardless of whether one wishes to write the information to a capable microSD or not. After deeply analysing the Arduino firmware sketches (utilising a C^{++} language), the responsible lines of code were identified.

In order to protect the board's Bluetooth module, as well as the provided USB dongle, the data streaming via this medium is switched off as is shown by the commenting out of

the line in Listing 6.1.

Listing 6.1: Commenting-out the board streaming command in "SDBoard.ino"

```
void loop()
{
        if (board.streaming)
        {
                ...
                // EDIT made - Stop board from streaming over Bluetooth
                // board.sendChannelData();
        }
}
```

Listing 6.2 shows the remainder of the changes made to the firmware to ensure that data is written to the microSD card at higher sampling rates.

Listing 6.2: Adding serial command in "SD_Card_Stuff.ino" to start data stream (or in this case only data logging) without resetting the sample rate

```
char sdProcessChar(char character)
{
        switch (character)
        {
                case 'A': // 5min
                        ...
                case 'L': // 24hr
                case 'a': // 512 blocks
                        fileSize = character;
                        SDfileOpen = setupSDcard(character);
                        break;
                ...
                case 'b':
                        if(SDfileOpen)
                        {
                                stampSD(DEACTIVATE);
                        }
                        break;
                // ADDED code start ----------------------
                case 'o':
                        if(SDfileOpen)
                        {
                                stampSD(DEACTIVATE);
                        }
                        break;
                // ADDED code end ------------------------
                default:
                break;
        }
        return character;
}
```

The serial command 'b' [78] is used to begin the logging of the data to the microSD card, but also triggers checks for a WiFi module and the resetting of the sampling frequency. In order to bypass these checks, an unused serial command 'o' was added to the firmware to mimic the command 'b', without triggering the extra checks and resetting of the ADC rate. The board was re-flashed with the updated firmware and the implementation could continue.

Channel one is switched-on and linked with the bias and reference electrodes. Due to the small nature of the evoked signals, the gain thereof in the ADS1299 [75] is set to a maximum value of $G_1 = 24$, meaning that with the ADC reference voltage of $V_{ref} = 4.5V$ and a 24-bit two's compliment resolution of the values, the step size of the ADC channel 1 (V_{s1}) is

$$V_{s1} = \frac{V_{ref}}{G_1.(2^{23} - 1)} = 2.23517445 \times 10^{-8} \approx 22.352\ nV. \tag{6.6}$$

Channel two is switched-on, delinked from both the bias and reference electrodes and set to differential input mode. Due to the significantly larger nature of the synchronisation signal, the gain thereof in the ADS1299 [75] is set to a minimum value of $G_2 = 1$, meaning that with the same ADC reference voltage and 24-bit two's compliment resolution, the step size of the ADC channel 2 (V_{s2}) is

$$V_{s2} = \frac{V_{ref}}{G_2.(2^{23} - 1)} = 5.36441867 \times 10^{-7} \approx 536.442\ nV. \tag{6.7}$$

Due to the changes made, the order in which the serial commands should be sent to the Cyton (to maintain the proper channel settings and allow for the faster sampling rate) was obtained by a trial-and-error approach (observing and verifying the output and if not satisfactory, re-iterating the sequence). Figure 6.7 provides the optimised implementation design with its realisation being included in Appendix D.

6.3.4 Verification

The validation of the subsystem will not involve observation of actual data (which will be done from Section 6.4 onwards), but more of a verification that there is successful communication with the Cyton board and that there is no resetting of the sampling frequency. The realised implementation produces the output as given in Fig. 6.8. The output screen shows the successful control of board connection, frequency selection and setting, microSD set-up with file initiation, recording timing, verification that the frequency stayed constant at the set value throughout and finally the disconnection from the board (which produces a warning by nature).

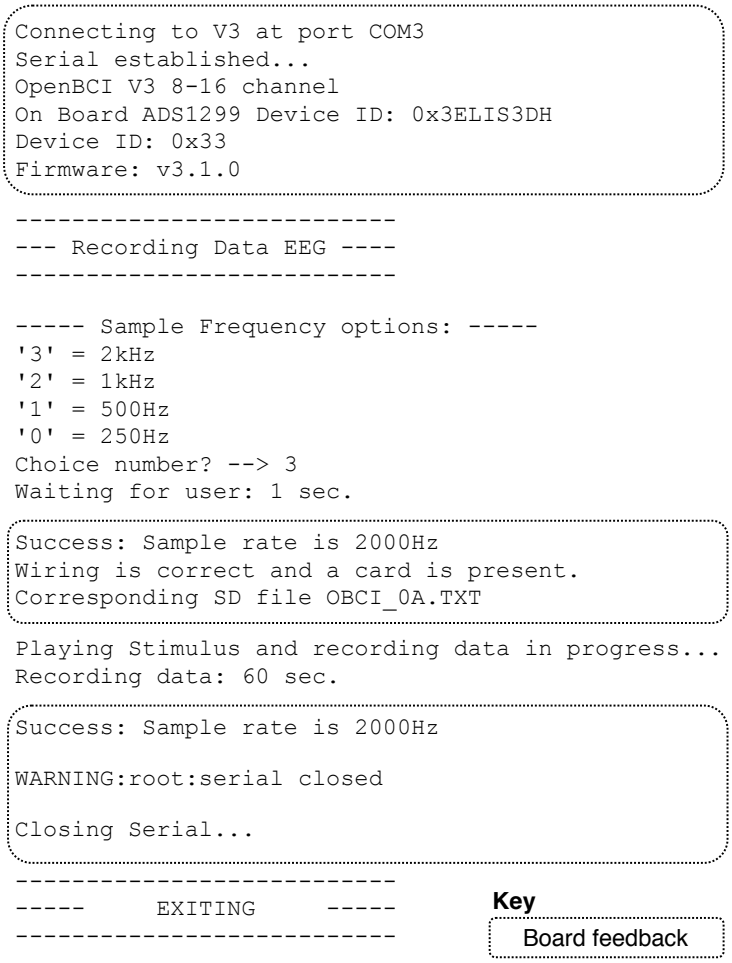

Figure 6.8: Example of board control sequence verification, copied from the communication cell output of the Jupyter Notebook [68]. Note that the data received from the board is shown within dotted borders. The remainder of the input and output is generated by the designed code.

6.4 Import raw data from file

The next step would be to connect the microSD card from the Cyton to a computer for data importation.

6.4.1 Overview

The format of the data files are comma separated structured lists. Each line contains: a two digit board mode ('00' meaning default mode), 6-digit hexadecimal data values for each of the channels (one to eight) and occasionally an additional three parameters of four hexadecimal digits each, representing accelerometer data in the three axes. An example of the file contents is given by Fig. 6.9.

```
%STOP AT
00022BF5
00,000000,000000,000000,000000,000000,000000,000000,000000,FD20,E130,0760
00,000000,000000,000000,000000,000000,000000,000000,000000
00,000000,000000,000000,000000,000000,000000,000000,000000
00,000000,000000,000000,000000,000000,000000,000000,000000,FD00,E160,0770
00,000000,000000,000000,000000,000000,000000,000000,000000
00,000000,000000,000000,000000,000000,000000,000000,000000
00,000000,000000,000000,000000,000000,000000,000000,000000
00,000000,000000,000000,000000,000000,000000,000000,000000
00,000000,000000,000000,000000,000000,000000,000000,000000
%STOP AT
00022FC5
00,CEA89B,FFF929,000000,000000,000000,000000,000000,000000
00,CEA444,FFF925,000000,000000,000000,000000,000000,000000
00,CE9F2F,FFF919,000000,000000,000000,000000,000000,000000
00,CE9969,FFF919,000000,000000,000000,000000,000000,000000
00,CE9365,FFF924,000000,000000,000000,000000,000000,000000
00,CE8D08,FFF91E,000000,000000,000000,000000,000000,000000
00,CE8671,FFF919,000000,000000,000000,000000,000000,000000
00,CE7FAC,FFF921,000000,000000,000000,000000,000000,000000
00,CE78AB,FFF91B,000000,000000,000000,000000,000000,000000
00,CE7191,FFF922,000000,000000,000000,000000,000000,000000
00,CE6A7F,FFF926,000000,000000,000000,000000,000000,000000,FCF0,E170,0790
00,CE6349,FFF928,000000,000000,000000,000000,000000,000000
00,CE5C67,FFF932,000000,000000,000000,000000,000000,000000
00,CE5581,FFF92F,000000,000000,000000,000000,000000,000000
```

Figure 6.9: Extract of a data file named OBCI_0A.txt

6.4.2 Design

The channel data values are of 6-digit two's complement hexadecimal format. This equivalently converts to a 24-bit binary digit, with the first bit representing the sign of the data and also how the remainder of the data should be interpreted. Upon researching available conversion libraries it was discovered that a standard conversion function for a 24-bit digit does not exist, with the closest library being a 16-digit or 32-digit to decimal converter package. It therefore becomes necessary to convert the 24-bit digit to an equivalent 32-bit representation.

From the theoretical knowledge of two's complement format, one can create a check to determine whether the first binary character is a '1' or a '0' and add either a respective 'FF' or '00' to the beginning of the hexadecimal value to convert it into standard form. One such an approach to check the value, is using a standard hexadecimal-to-decimal conversion on the first two hex values of the digit and then testing whether the output is greater than 127 (or $2^7 - 1$). If true, the first digit is an 'F' and one should append 'FF' to the beginning of the digit to equate it to 32-bit representation. If false, the first digit is anything excluding an 'F' and one should append '00' to the beginning of the digit to like-wisely equate it.

The decimal values can be converted to a uV value by multiplying it by the ADC step size equations of Section 6.3.3. The flowchart in Fig. 6.10 represents the full design of the subsystem used to import the converted data of both channel one and two into arrays.

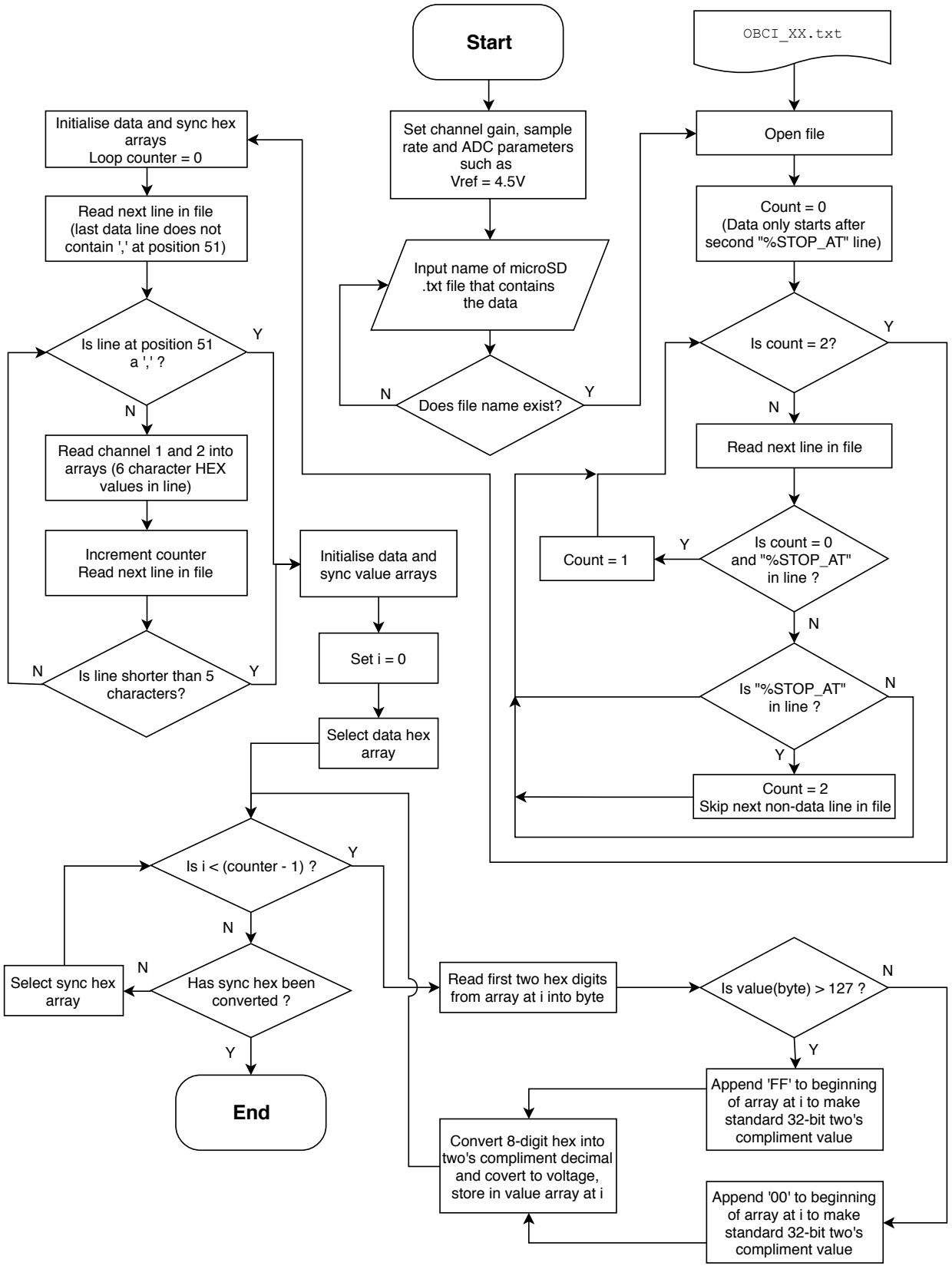

Figure 6.10: Software design flowchart of the data file import algorithm and conversion of 24-bit hexadecimal (hex) values into voltages

6.4.3 Implementation

The implementation of the data importing component, outlined in the flowchart, is attached in Appendix D.

6.4.4 Verification

The text feedback of the implemented Python cell is given by 6.11. The sample number matches the expected value (to a satisfactory extent, taking into account communication delays).

```
-------------------------
----- Importing data ----
-------------------------

PLEASE ENTER THE TEXT FILE HEX NUMBER (EXAMPLE '02' or 'C6')? --> B9

Success! Opened file at C:/Users/Carel/Documents/Data Files - Masters/OBCI_B9.txt

Success! Data imported with 359645 values

-------------------------
-------- Exiting --------
-------------------------
```

Figure 6.11: Example of the data import verification copied from the file reading cell output of the Jupyter Notebook [68]. The parameters were set for three minutes of recording at 2 kHz, which verifies that the sample number of 359 645 is close to the expected number of (2 kHz $\times$ 180 s = 360 000)

The imported data can be verified by passing it through a simple band-pass filter (see Section 6.6) to remove the DC components and frequencies above half that of the sampling rate. The time-domain and frequency-domain of the filtered signal is shown in Fig. 6.12.

The time-domain correlates to that which can be expected when observing a raw EEG signal. Likewise the frequency-domain shows the majority of the information being in the domain below 50 Hz, which is characteristic of raw EEG data. Shielding and various hardware design considerations have contributed to the low amplitude (yet visible) of the 50 Hz interference frequency. Implicitly, the fact that the 50 Hz spike frequency appears where it should in the spectrum is verification that the desired sampling frequency (assumed to be 2kHz in plotting the FFT) is obtained in the data.

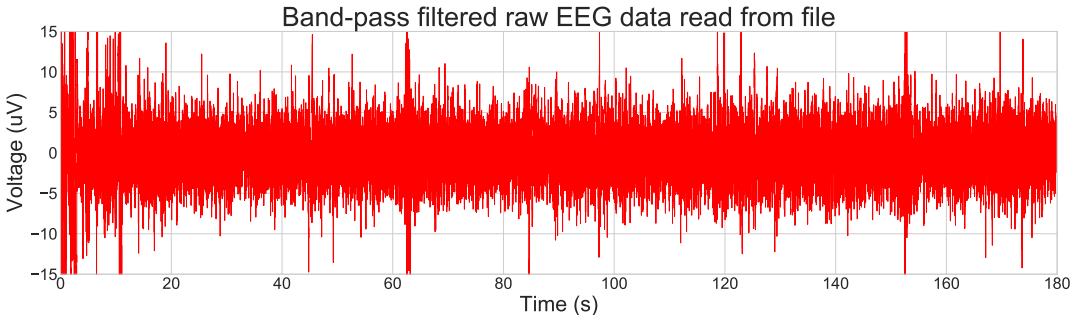

(a) Time-domain

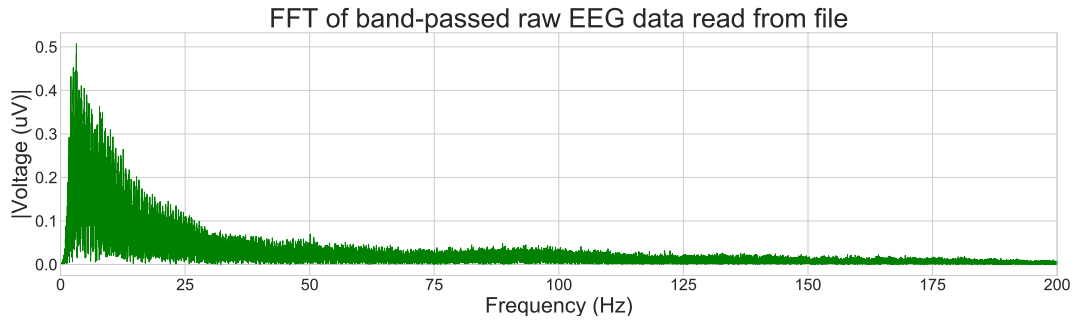

(b) Frequency-domain

Figure 6.12: Verification of the EEG data, read and converted from hexadecimal to μV, in the file of Fig. 6.11 that has been band-pass filtered with $f_L = 2$ Hz and $f_H = 800$ Hz

6.5 Stimulus synchronisation implementation

The ability to detect the stimulus start positions, from the use of the simultaneously generated synchronisation signal, is the design addressed in this section.

6.5.1 Overview

The ability to detect the stimulus start positions in a bipolar signal implies that the simplified unipolar stimulation is also detectable (effectively the sole difference between the two signals, programmatically speaking, is a simple absolute value function). A rising- or falling- edge threshold approach can be used on a preprocessed signal to store the locations of the stimulus start positions (in terms of sample numbers) in an array. These sample numbers correlate directly to the sample numbers of the in-ear data channel as they are synchronously recorded on the ADS1299.

6.5.2 Design

The necessary preprocessing would be a band-pass filter (Section 6.6) to remove aliasing higher frequencies and DC offsets, followed by an absolute value to convention the peaks

to a single side (or make unipolar), followed by a square of the signal to increase the amplitudinal spacing between the noise rail and the pulse peaks. Figure 6.13 shows the designed flowchart for detecting the falling edges of a negative squared signal (correlating to a rising edge of a positive square) that lies below a determined threshold. This is then the sample position considered to be five samples before the initial onset of stimulus.

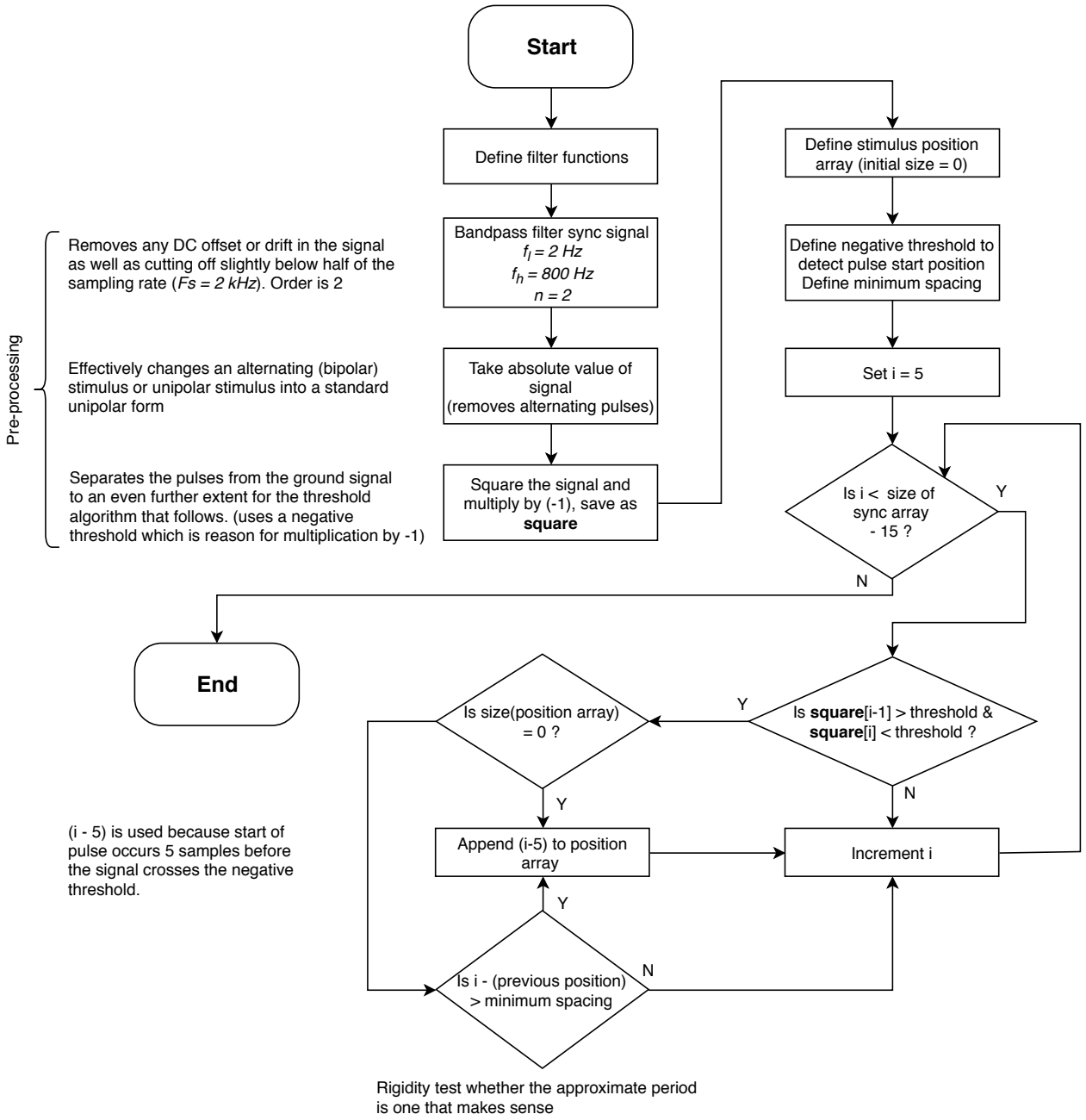

Figure 6.13: Software design flowchart of the synchronisation (sync) signal pulse position detector algorithm

6.5.3 Implementation

The design is implemented in a Jupyter Notebook cell using the same script as all of the Python implementations provided in Appendix D.

6.5.4 Verification

Verification of the detection ability, as well as the effect of each pre-processing step, is plotted in the series of frequency-domain spectra of 6.14 and time-domain figures of Fig. 6.15.

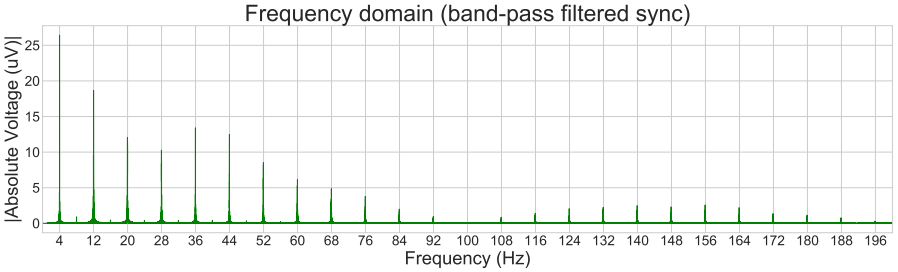

(a) Frequency-domain of band-passed signal ($f_L = 2$ Hz and $f_H = 800$ Hz)

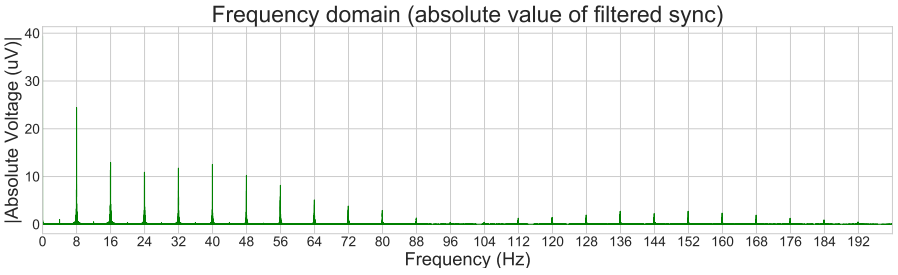

(b) Frequency-domain of absolute-valued signal in Fig. 6.14a

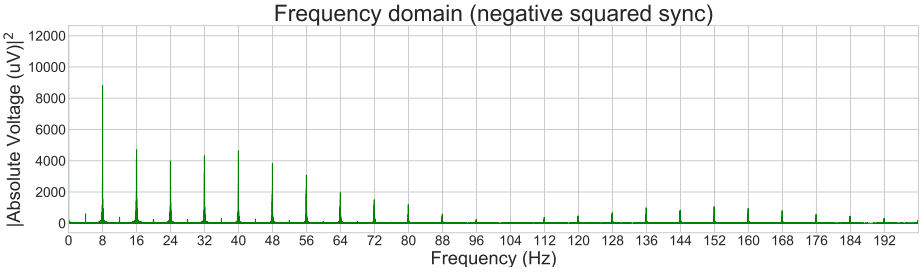

(c) Frequency-domain negative of squared signal in Fig. 6.14b

Figure 6.14: Frequency-domain verification of bipolar (and therefore also unipolar) synchronisation detection

A short calculation was written to calculate the average frequency detected. This was achieved by first calculating the average of all the period time-differences, for the 10-minute recording used in Fig. 6.15, and then taking its inverse to obtain the frequency. This resulted in an average detected frequency of 7.9991592 Hz.

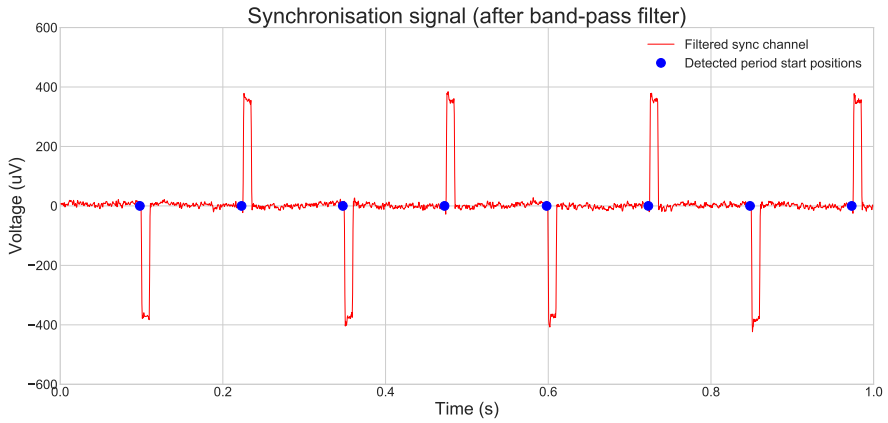

(a) Time-domain of band-passed signal ($f_L = 2$ Hz and $f_H = 800$ Hz)

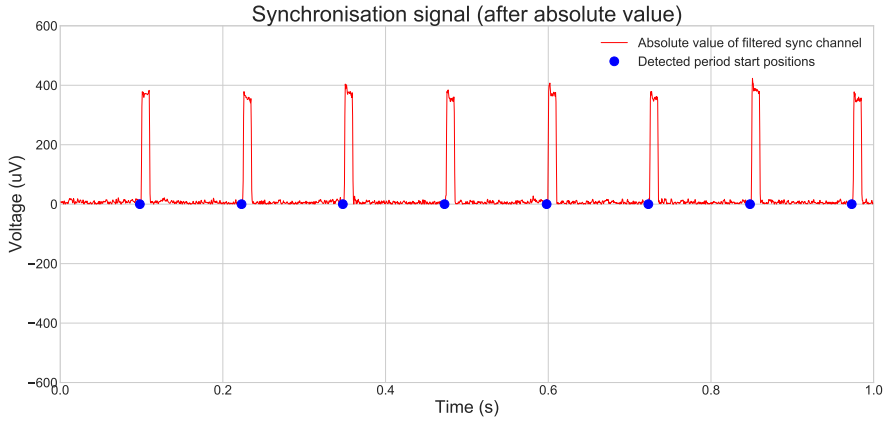

(b) Time-domain of absolute-valued signal in Fig. 6.15a

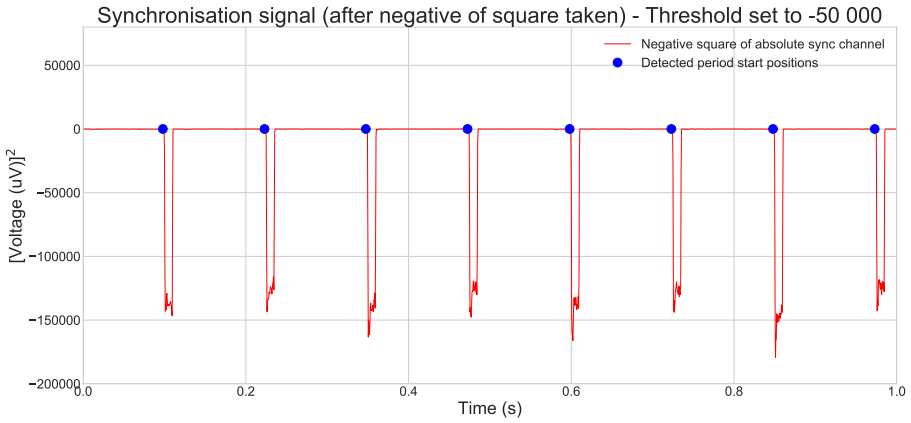

(c) Time-domain negative of squared signal in Fig. 6.15b

Figure 6.15: Time-domain verification of bipolar (and therefore also unipolar) synchronisation detection and processing of the second channel

The band-pass filter effectively removes its necessary DC and aliasing components, as seen in Fig. 6.14a and Fig. 6.15a, while the frequency-domain matches that of the theoretically generated bipolar one in Fig. 6.4b. The absolute value is successfully applied to the signal, as shown in Fig. 6.15b, and causes its frequency-domain, shown in Fig. 6.14b, to expectedly correlate with that of a unipolar spectrum, theoretically presented in Fig. 6.4a. Although the squaring application does not indicate an observably large effect on the spectrum of Fig. 6.14c, the time representation of Fig. 6.15c shows a much flatter ground rail relative to the signal pulses. This is used in falling edge detection with a threshold of -50000 uV^2. All of the time-domain plots are superimposed with blue dots representing the detected start positions of the stimuli. The dots correlate to the correct samples and the subsystem design is therefore verified.

6.6 Filtering processes

In order to clean the data from noise related interference or focus on a specific frequency band, a series of filter functions are to be designed for convenient use.

6.6.1 Overview

Python has built-in functions to assist in implementing numerous filter types. Butterworth type filters are chosen for their flat amplitude response (compared to another common Chebyshev type). A slightly more complex filter implementation is that of a comb filter for attenuating all the harmonics of a interfering frequency in a signal. A critical design choice is the use of forward-reverse filtering to eliminate phase offsets, induced by filtering, that will have a significantly detrimental effect on evoked potential timings. Figure 6.16 is a block diagram drawn to represent how such filtering is applied (which is unique to digital filtering, since an inversion of the time axis is not achievable by means of purely analogue circuitry).

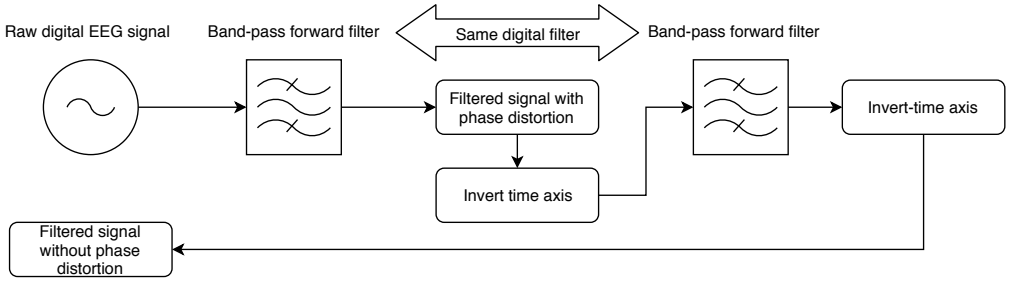

Figure 6.16: The application of a forward-reverse filtering approach to obtain a linear phase response

Python contains a function called "filtfilt" that is used to apply the forward-reverse filtering. Figure 6.17 graphically shows the difference between normal filtering (applied forward twice shown by red plot) and forward-reverse filtering (filter applied once forward

and once reversed by black plot) as compared to the input noisy signal shown by the blue plot. It goes without saying that the latency nature of evoked potentials requires a filter response as show by the blue plot

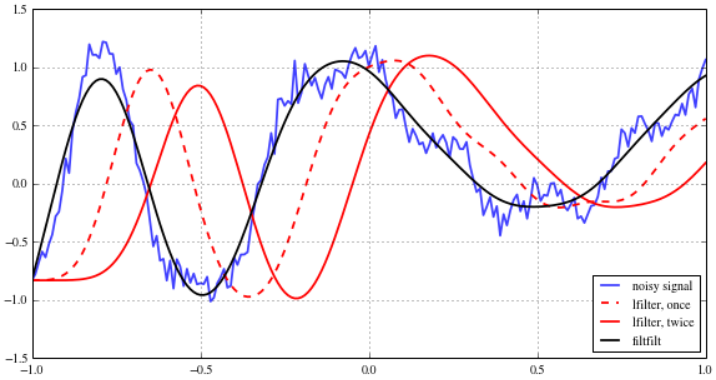

Figure 6.17: Example of practical filtfilt implementation (Image obtained from [79])

6.6.2 Design

In order to design a comb filter response, the fundamentals are first discussed. It is known that a pole-zero diagram can be used to depict a filter. A pole-zero diagram with one zero on the unit circle and one pole just inside the unit circle, as shown on the left of Fig. 6.18, creates a notch filter with a notch width proportional to the distance between the pole and the zero. For the placement on the real axis, the frequency of occurrence will be at 0 Hz (or DC).

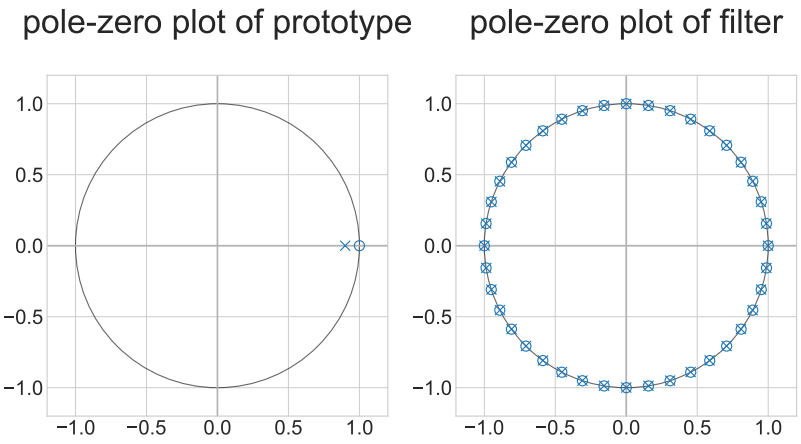

Figure 6.18: The pole-zero diagram of both the prototype notch filter (left) and the designed comb filter (right)

It can now be calculated that with a sampling rate of $F_s = 2$ kHz and a desired attenuation of all the 50Hz harmonics in a frequency band, there should be $N_{p/z} = \frac{F_s}{50\text{Hz}} = 40$ of both poles and zeroes evenly spaced around the unit circle, as shown in the plot to the right of Fig. 6.18. It may seem that the poles and zeroes are both on the unit circle, but the poles are slightly interior thereto in order to create a sharp and narrow notch at the harmonic frequencies. Such a plot can now be converted to a series of numerator and denominator coefficients and a filter generated therefrom.

A flowchart of the designed filtering algorithm is provided in Fig. 6.19, along with function descriptions of the purposing for each filter.

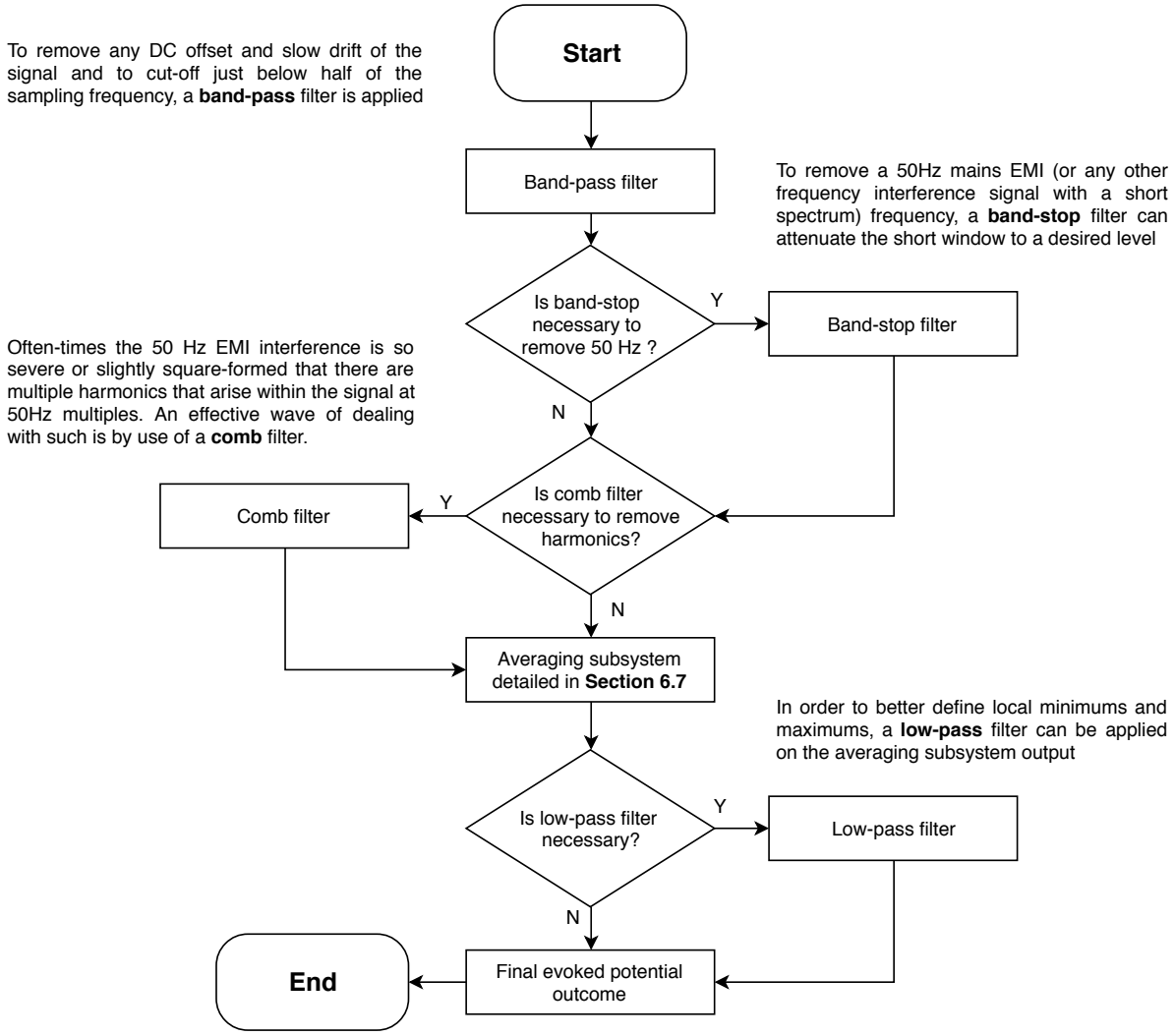

Figure 6.19: Software design flowchart of the filtering processes and their relative possible application regions (if required)

6.6.3 Implementation

The filters are encapsulated in functions provided in Appendix D and their transfer functions, with test frequency scenarios, are given in Fig. 6.20.

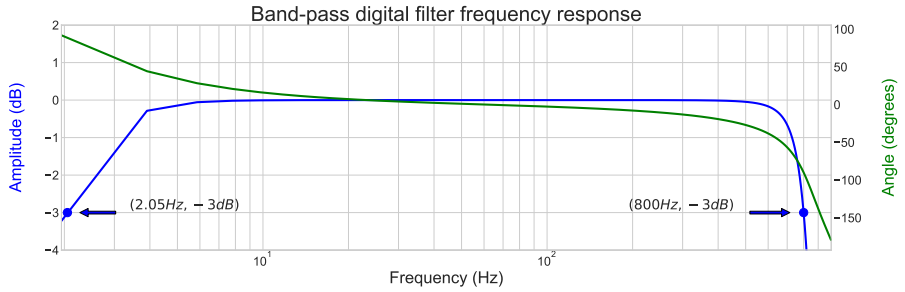

(a) Example of band-pass response ($f_L = 2$ Hz, $f_H = 800$ Hz and order $= 2$)

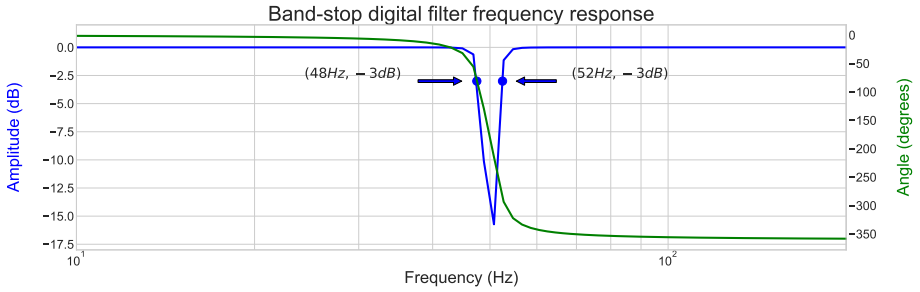

(b) Example of band-stop response ($f_L = 48$ Hz, $f_H = 52$ Hz and order $= 2$)

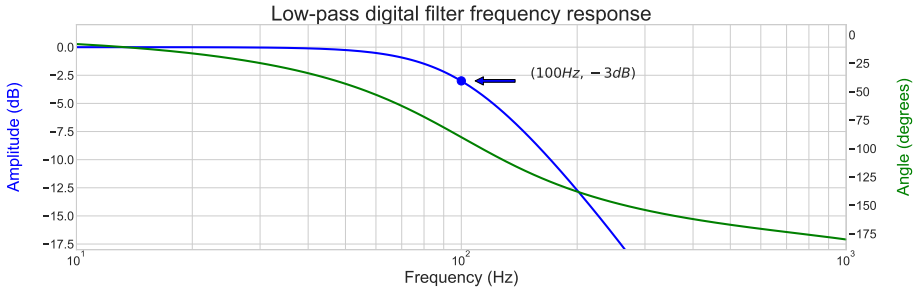

(c) Example of low-pass response ($f_H = 100$ Hz and order $= 2$)

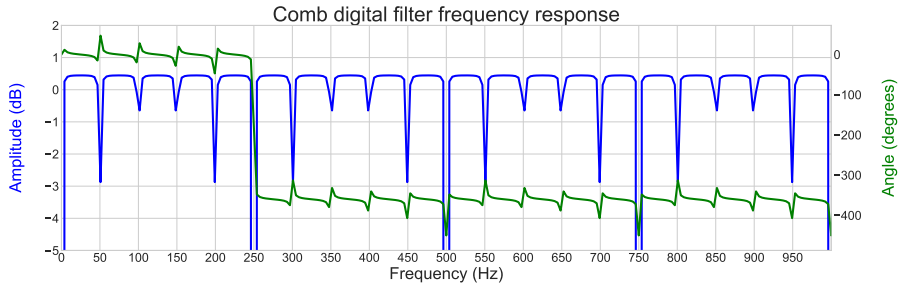

(d) Example of comb response ($f_N = 50.n.\text{Hz},$ where n $\in \{\mathbb{N}\}$)

Figure 6.20: Frequency response of the designed filters showing both phase and amplitude effect along with marked -3dB cut-off points

6.6.4 Verification

The filters are verified by applying data through them in a forward-reverse nature using the filtfilt function, as is shown in Fig. 6.21.

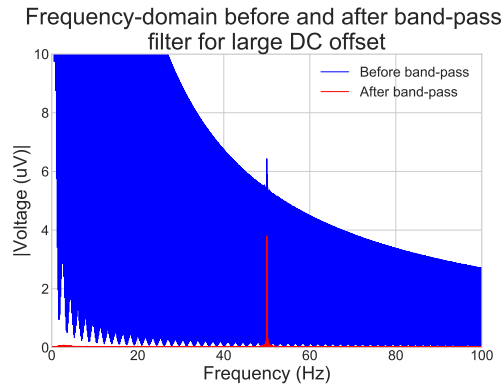

(a) Band-pass frequency-domain

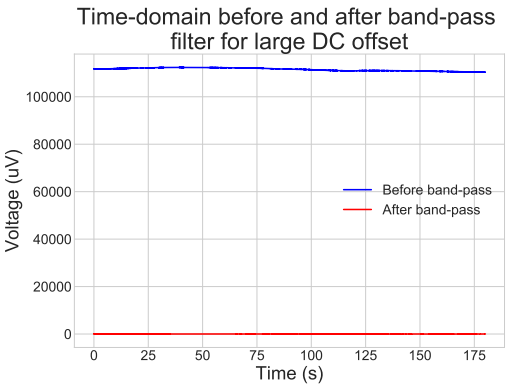

(b) Band-pass time-domain

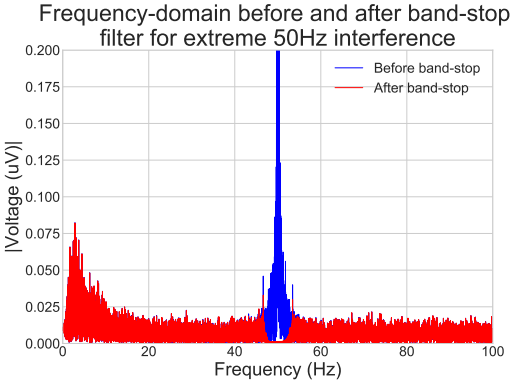

(c) Band-stop frequency-domain

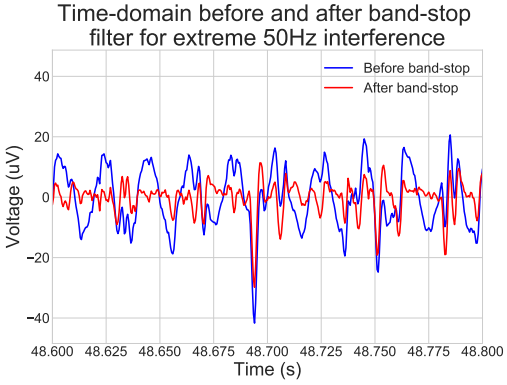

(d) Band-stop time-domain

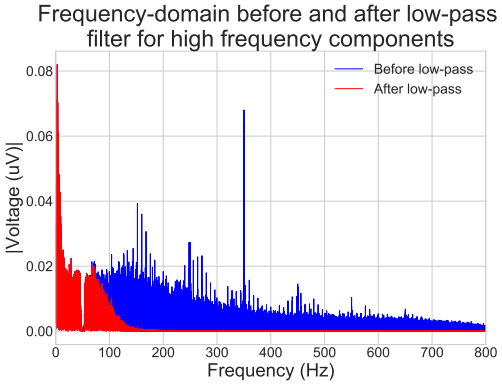

(e) Low-pass frequency-domain

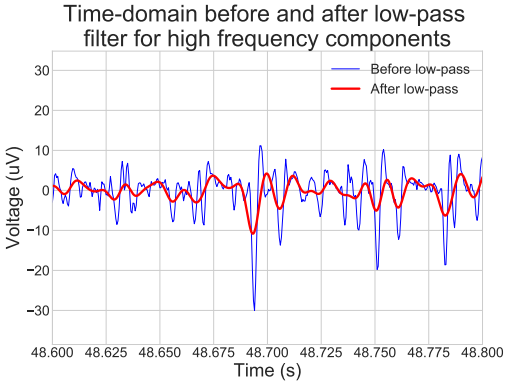

(f) Low-pass time-domain

Figure 6.21: Filter verification applications (showing both before and after measurements in both time- and frequency- domains) for miscellaneous data files recorded over the design phase

The same verification can be applied to the designed comb filter as shown in Fig. 6.22

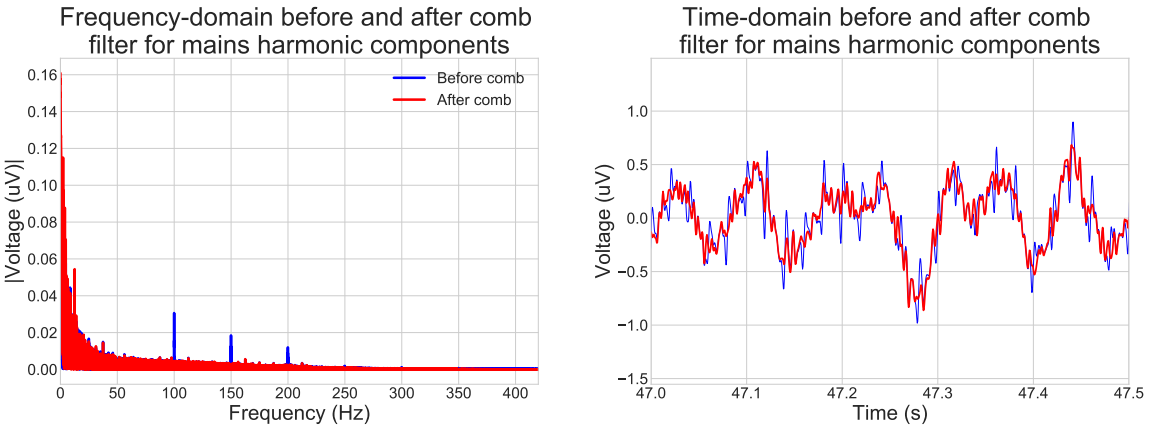

(a) Comb filter frequency-domain **(b)** Comb filter time-domain

Figure 6.22: Comb filter verification application (showing both before and after in both time- and frequency- domains) for mains with harmonics interfered data file

The filters are confirmed to work as expected and observation of the time-domain showed no evident shift in the phase of any filtered signal. The design of the final software stage is now able to commence.

6.7 Averaging algorithm

In order to derive the evoked potentials from the simultaneously played auditory stimulus, the averaging of period lengths, aligned with period onset, needs to be implemented.

6.7.1 Overview

An algorithm that can average all of the data obtained within a specified time into a single period, with the stimulus onset being fixed to a certain location (usually the first) sample, is of vital importance to the evoked potential derivation. Furthermore, a spike period exclusion algorithm can be implemented to clean larger than usual amplitudes from the data, that may somewhat distort the average.

6.7.2 Design

A flowchart of the designed averaging algorithm, with its cleaning application, is given in Fig. 6.23. Only periods confined within a certain boundary are allowed to pass onto the averaging process, thus removing artefacts such as accidental electrode touches or large muscle artefacts.

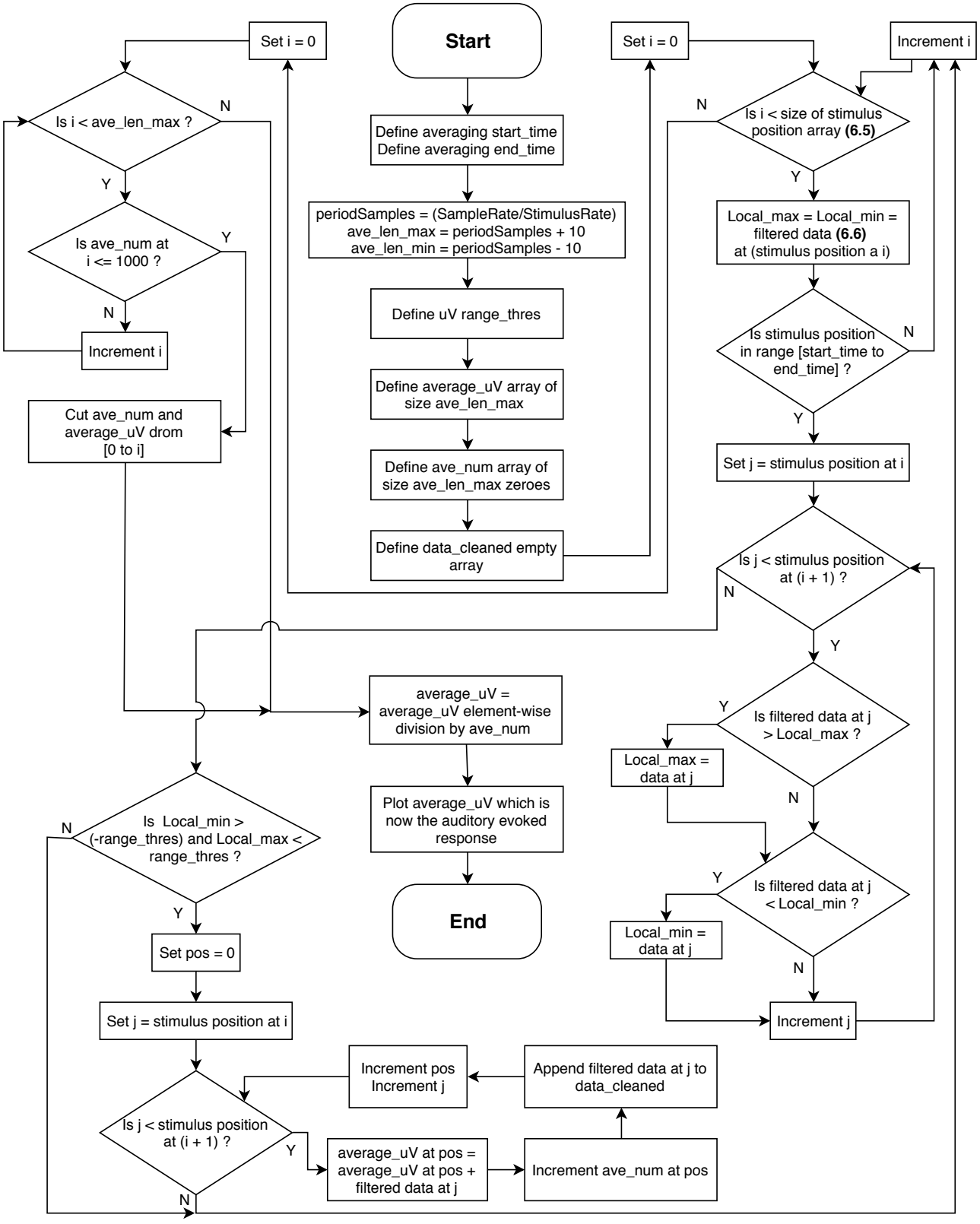

Figure 6.23: Software design flowchart of the averaging algorithm (along with amplitude cleaning and period checking mechanisms) to obtain the auditory evoked potential (AEP)

6.7.3 Implementation

Due to the unique approach followed and successful functionality of the designed averaging method, the final commented Python code is provided in Fig. 6.24 (also see Appendix D).

```
#-----------------------------------------------------------
# Code for implementing averaging on the filtered data
#-----------------------------------------------------------
import numpy as np                                  # Import the numpy array library

start_time = int(len(data_uv_comb)*(0/2))           # Define the start time in sample number terms
end_time = int(len(data_uv_comb)*(2/2))             # Define the end time in sample number terms

ave_len_max = int(SAMPLE_RATE/pip_rate)+10          # Define the maximum allowable period sample length
ave_len_min = int(SAMPLE_RATE/pip_rate)-10          # Define the minimum allowable period sample length
average_uV = np.zeros(ave_len_max)                  # Initialise a length max array of zeroes for the evoked response
ave_num = np.zeros(ave_len_max)                     # Array to track how many periods are added to average_uV
ave_range=8.0                                       # Maximum threshold offset in uV from zero (remove spikes)
ave_thres=ave_range*2                               # Maximum (max - min) range for any period in uV (remove spikes)
cut_periods = 5                                     # The amount of periods to cut from start and end (filter effects)
data_uV_cleaned = []                                # Empty array to hold all the cleaned data from start_ to end_time

data_uv_ave=data_uv_comb                            # Select data to be averaged (This case comb filter output)

local_min=0                                         # Initialise local period minimum
local_max=0                                         # Initialise local period mamimum

for i in range(0,period_count-2-cut_periods):
    local_max=data_uv_ave[stim_pos[cut_periods+i]]  # Redefine local period maximum to first value in a period
    local_min=data_uv_ave[stim_pos[cut_periods+i]]  # Redefine local period minimum to first value in a period

    # Test that the period lies within the start and end time specified
    if stim_pos[cut_periods+i] >= start_time and stim_pos[cut_periods+i+1] <= end_time:

        # Find the local minimum and maximum for the period and store into the variables
        for j in range(stim_pos[cut_periods+i],stim_pos[cut_periods+i+1]):
            if data_uv_ave[j] > local_max:
                local_max = data_uv_ave[j]
            if data_uv_ave[j] < local_min:
                local_min = data_uv_ave[j]

        # Test whether the data for period's range falls within the desired "spikeless" range, if so add to arrays
        if (local_max-local_min) < ave_thres and local_max < ave_range and local_min > (-ave_range):
            pos = 0
            if (stim_pos[cut_periods+i+1] - stim_pos[cut_periods+i]) < ave_len_max and (stim_pos[cut_periods+i+1] - \
                                        stim_pos[cut_periods+i]) > ave_len_min:
                for j in range(stim_pos[cut_periods+i],stim_pos[cut_periods+i+1]):
                    average_uV[pos]=average_uV[pos]+data_uv_ave[j]
                    ave_num[pos] += 1
                    data_uV_cleaned.append(data_uv_ave[j])
                    pos += 1

# Cut the average_uV array to only include index values that contain more than a thousand values
for i in range(0,len(ave_num)):
    if ave_num[i] <= 1000:
        ave_num = ave_num[:i]
        average_uV = average_uV[:i]
        break

# Divide the summed signals by the number of signals in each index to obtain the evoked potential average
average_uV = np.divide(average_uV,ave_num)

print("Done averaging - Evoked Potential Ready")


```

Figure 6.24: Python [67] averaging and cleaning algorithm as implemented in a Jupyter Notebook [68] environment

6.7.4 Verification

Verification of the cleaning component of the design is evidenced by the removal (and therefore time shortening) of signal spikes in Fig. 6.25.

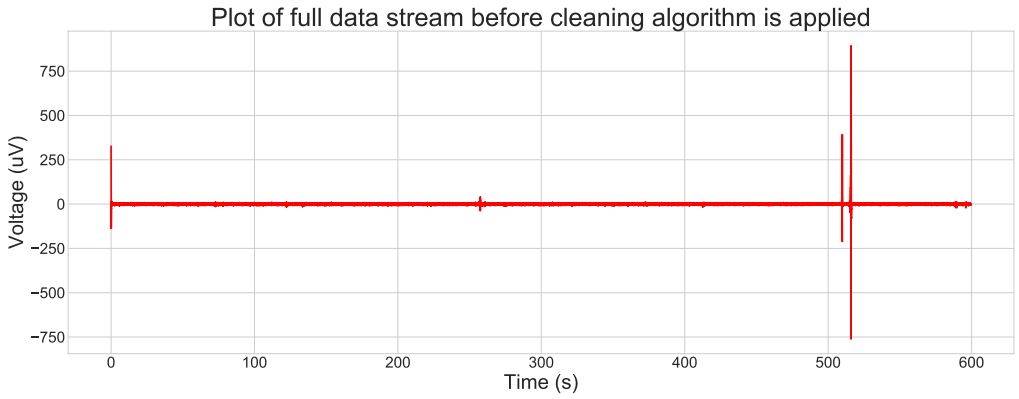

(a) Signal before period cleaning algorithm is applied showing several spikes over the full 10 minute recording

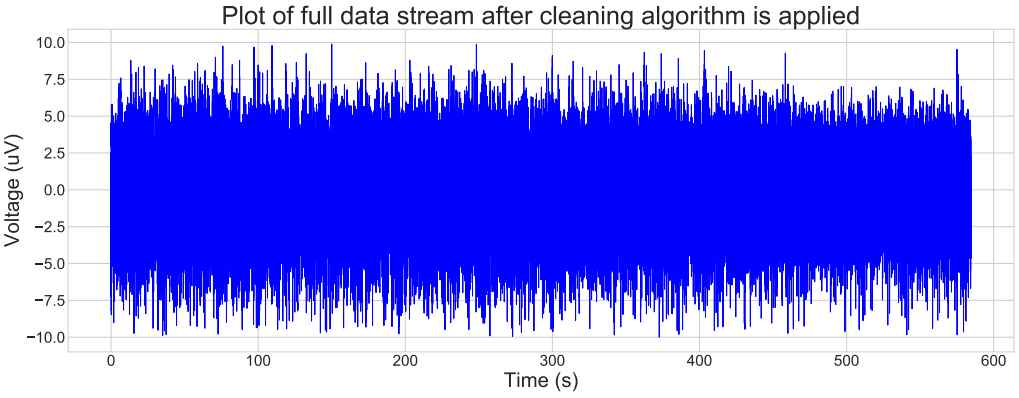

(b) Signal after period cleaning algorithm is applied showing the removal of whole periods which are not confined within a specified range (in this case from -10μV to 10μV)

Figure 6.25: Verification of the period spike cleaning algorithm with notable shortening of full signal duration

Figure 6.26 illustrates the successful evoked potential output and averaging implementation. It is shown in Fig. 6.26a that the auditory evoked potential measured within the ear exhibits a similar nature, yet not exactly the same response as provided in the literature on evoked potential, measured from the vertex of the head. This can be expected due to the electrically inhomogeneous properties of the brain and skull. The output can be optimised by tuning the parameters and filters to a satisfactory extent.

Figure 6.26b shows the difference on the averaged signal and therefore also the averaging of interference, generated by bipolar (band-pass red signal) and unipolar (absolute value blue signal) stimulation. The alternating bipolar signal has a net cancellation effect, whereas the unipolar implementation has an obvious resilience in the averaging of the signal.

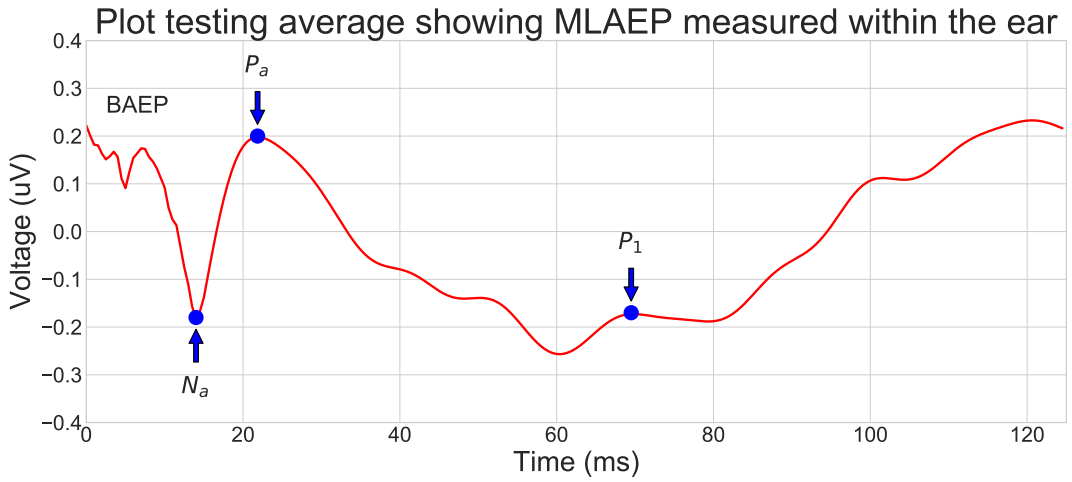

(a) Output of the period averaging algorithm on the in-ear data to produce the middle latency auditory evoked potential (comparable to, but not from the same origin as Fig. 2.18)

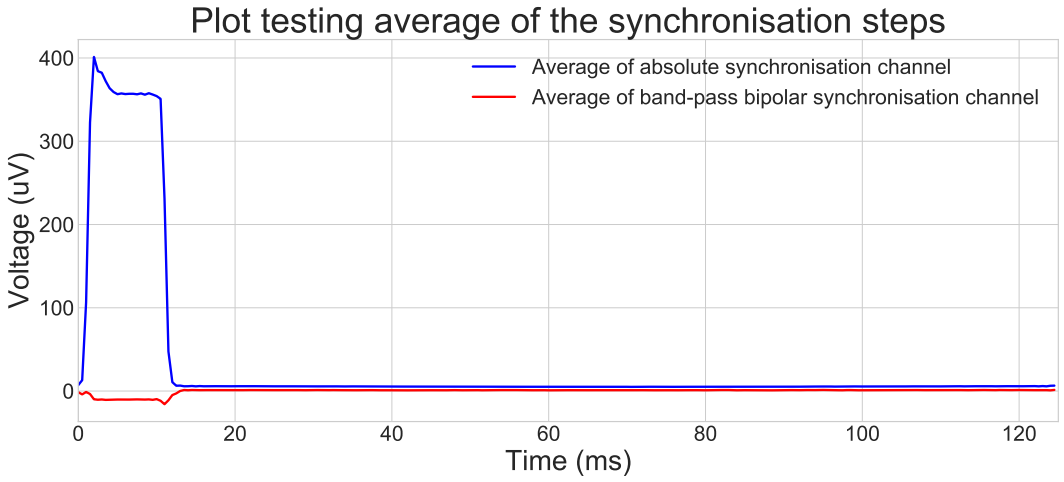

(b) The output of the averaging algorithm for the band-pass and absolute synchronisation signal from Fig. 6.15

Figure 6.26: Verification of the averaging algorithm when applied to the two channels

6.8 Conclusion of the software designs

That concludes the design of the software as well as the overall design process. The device is now ready for clinical trials which are presented in the next chapter.

Chapter 7

Results

The actual testing phase of the developed device, within the medical industry, could now commence. This chapter covers and details the results obtained from such tests.

7.1 Clinical preparation and testing procedure

In order to complete a successful experimental procedure, to validate the potential of the designed device, one needs to define a series of steps and control measures to ensure that valuable results will be output. A detailed list of such steps is given below:

1. Preliminary preparation phase consisting of:
    1.1. ensuring that the designed system is comfortable to wear (even over extended periods of time);
    1.2. applying for ethical clearance at the Health Research Ethics counsel 2 (HREC2) of Stellenbosch University;
    1.3. waiting for the approval of said application ensuring that all protocols are followed; and
    1.4. upon receiving approval, making contact with appropriate and willing anaesthesiologists to make arrangements for such tests to be done in theatre and to learn how the procedures are done.
2. Preclinical preparation, a day before the surgery is due to take place, one should:
    2.1. ensure that the patient undergoing a non-interfering suitable anaesthesia procedure receives a copy (and translator if needed) of the consent form drawn-up as a supplementary document to the ethical application;
    2.2. ensure the wiring of the electrodes are still conductive by means of a continuity test;
    2.3. test the battery voltages and charge the appropriate hardware subsystems to ensure that all of the voltages are at satisfactory levels;

2.4. make arrangements with the doctor on duty regarding the time to arrive and set-up at the corresponding hospital; and

2.5. create a formatted spreadsheet in which the corresponding information such as patient expiratory anaesthetic as well as the bispectral index, measured throughout the procedure at specified time intervals, can be recorded from the anaesthesia machine.

3. On the day of the clinical trial the steps to follow are to:

3.1. arrive early at the hospital with the device, communication dongle, laptop and microSD card to set-up and check that everything is in order for recording;

3.2. speak to the patient explaining the exact procedure and answer any questions they may have, and if they are willing to participate, have them sign the consent form;

3.3. open the Jupyter Notebook script on the laptop and plug the OpenBCI dongle into the USB port;

3.4. insert the microSD card into the Cyton EEG recording device;

4. Once the patient enters into the operation theatre and is ready for set-up:

4.1. start by preparing the earlobes and inner-ear of the patient for electrode attachment by cleaning it with Weaver NuPrep [66] (formulated product for EEG electrode skin preparation) placed on cotton buds;

4.2. place the earmuff device over the patient's head, not yet covering the ears and having the in-ear electrode component on the right-hand side of the patient (unless auditory impairment is diagnosed in that ear, in which case the left-ear is chosen), so as to bring the electrodes into the proximity of the attachment regions;

4.3. cover the in-ear region and fill the cup gold electrodes with Weaver Ten20 [65] conductive paste, so as to ensure that a conductivity pathway is formed between the skin and the electrodes;

4.4. securely attach the peg electrodes (reference and ground) to both earlobes;

4.5. pinch and insert the in-ear electrode into the patient's right-hand ear canal insuring a comfortable fit;

4.6. carefully place the earmuffs over the ears, taking care not to have the electrodes detach or slip out of their positions;

4.7. switch-on the EEG recording device, stimulus Bluetooth player and white noise generator;

4.8. start playing the bipolar stimulus file from a smartphone device connected to the Bluetooth audio subsystem;

4.9. move aside to an area where the anaesthesia machine's display can be clearly seen and the BIS value as well as expiratory anaesthetic agent concentrations (and possibly other anaesthesiologist recommended parameters) are clearly visible;

4.10. commence with the EEG recording process from the controlling laptop, taking note and manually recording the BIS, minimum alveolar concentration (MAC, as described in Section 7.5.1), expiratory sevoflurane concentration (ESC) or expiratory desflurane concentration (EDC) and monitor values (found on the monitor as shown in Fig. 7.1) that are applicable for the current surgical iteration, in intervals of one minute for a specific ten minute EEG recording file, identified by its name as sent by the Cyton;

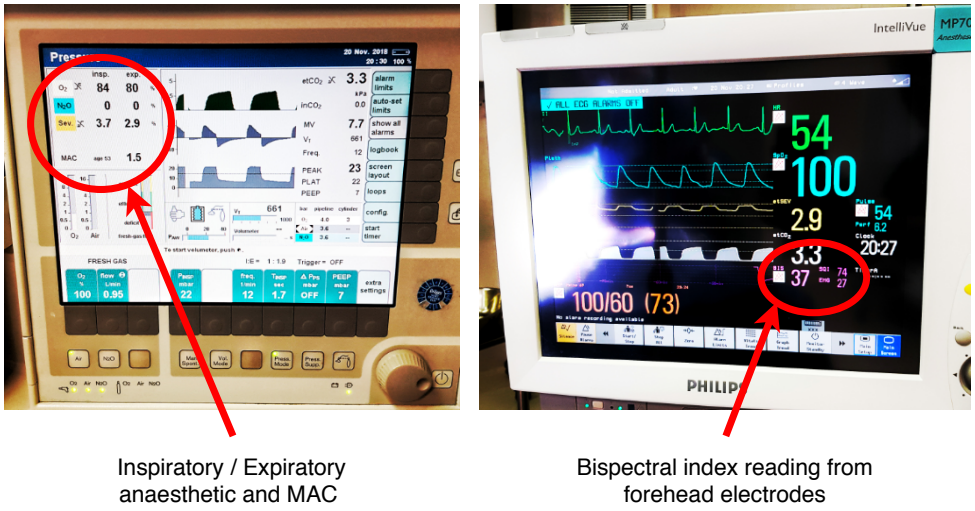

Figure 7.1: Key anaesthesia monitoring machine areas for recording in the spreadsheet (layout provided in Chapter 3)

4.11. repeat the previous step after each ten minute interval is complete, up until the time the patient needs to be moved out of theatre after the surgery is completed and sufficient anaesthesia recovering has occurred;

4.12. carefully remove the earmuff device from the patient and create a back-up of the microSD card and the ten minute data files recorded on the laptop; and

4.13. either prepare the device for the next patient or pack up all the equipment if it was the final test for the day.

5. Postoperative tasks include:

5.1. importing, cutting and processing the data files individually to generate middle latency auditory evoked potentials (MLAEPs) from the data segments, using the software designed in Chapter 6;

5.2. correlating the MLAEPs to the anaesthesia machine values, recorded in a spreadsheet, and like-wisely correlating the machine values with each other;

5.3. identifying the MLAEP characteristics for each data segment output waveform and correlating these with the anaesthesia machine parameters;

5.4. calculating the frequency power spectrum for each in-ear recorded data segment, in order to relate changes in the EEG frequency bands with machine parameters indicative of anaesthesia depth; and finally

5.5. provide all the information gathered above as graphical patient specific results.

The output results of the clinical trials, for each of the four patients tested, are presented in the sections that follow.

7.2 Results of Patient one

The first patient was monitored on the 11^{th} of November 2018, the details of which are provided in this section.

7.2.1 Overview and background

The first patient, undergoing a surgical procedure to remove gouty arthritis (uric acid waste build-up causing the formation of sodium urate crystals in the joints) from the knuckles of their left hand, was an adult male. The operation took place at Stellenbosch MediClinic, with the general anaesthesia applied by anaesthesiologist Dr. J. Lourens. The total duration of the surgery was 39 minutes, of which 10 minutes accounted for the transition from deep anaesthesia (just as anaesthetic agent is switched-off) to a near-wakeful state (just prior to the patient exiting the theatre and regaining full conciousness).

7.2.2 Anaesthesia machine parameters

The anaesthesia machine parameters, that were manually recorded into a spreadsheet, were the bispectral index (BIS) and the expiratory sevoflurane concentration (ESC). The relationship between these two parameters at the analysis points is plotted in Fig. 7.2 and is indicative of a sigmoid form correlation.

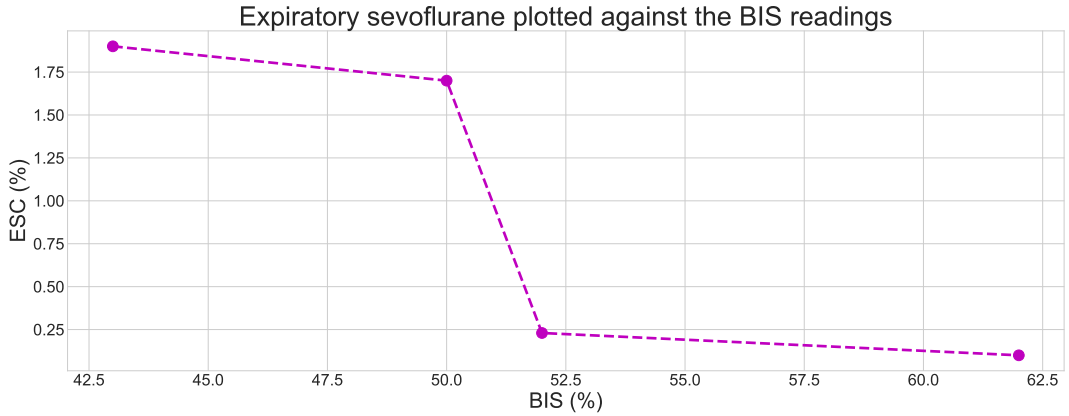

Figure 7.2: Both the recordings of the anaesthesia monitoring machine (BIS and ESC) plotted against each other for patient one

Recall that, from the literature study, a BIS value of 0% indicates zero cortical function, and a value of 100% is indicative of full cortical function. Inversely, on the other hand, an expiratory anaesthetic agent concentration that is higher represents a higher presence of anaesthesia in the patient's body and is therefore suggestive of a higher level of sedation. This accounts for the negative nature of the relationship observed in the plot.

7.2.3 Middle latency auditory evoked potentials at anaesthesia levels

The MLAEPs at various analysis points are plotted in Fig. 7.3, each at their corresponding instance of BIS and ESC, as provided in Fig. 7.2. The characteristic points are defined as N_a, P_a and N_b, as can be seen in every plot. A trend in latency (time from stimulus onset to peak time, or simply the x-axis reading of that peak since the stimulus-onset is normalised to 0 ms by the nature of the algorithm) can be seen.

An important factor to mention when observing the evoked potentials, is that a low-pass filter was applied to the evoked potential post brainstem response (or after the first 10 ms). This was done due to the relatively small nature of in-ear auditory evoked potentials obtained, relative to the standard evoked potentials mentioned in literature, causing a strong presence of high frequency noise (possibly from muscular activity, known as EMG, and other external sources). Both the placement of the electrode as well as the applied processing of the measured signals could cause discrepancies between the readings and the literature presented MLAEP values, discussed in 2.18. However, there is still a strong correlation with the more concious patient in Fig. 7.3a. The averaging time can alternatively be extended to clean the data over-time, but will result in an even larger delay when deriving an output MLAEP.

An identical filter, with cut-off frequency of 50 Hz, is applied to all four of the patient's MLAEP data in order to differentiate between peak latencies and maintain comparability. As a result, however, the forward-reverse filter (although not producing a phase or latency effect) produces an amplitude response that may alter the amplitudes of the peaks obtained. Also, any characteristic peaks, with a large frequency precedence above 50 Hz, will have their lower frequency components combined with other peaks to produce a more overall effect.

Both P_a and N_b are observed to increase in latency as the anaesthesia (and therefore unconsciousness) level is sequentially increased in Fig. 7.3a, Fig. 7.3b, Fig. 7.3c and Fig. 7.3d. To visually compare the latencies and effect on amplitude that anaesthesia has on the evoked potentials, these will be extracted and plotted against the anaesthesia machine parameters in the sections that follow. It is again crucial to note that, due to the nature of both the BIS (being an empirical approach) and ESC, the values are by no means a true indication of conciousness. Such a feasible and real-time conciousness measuring system is yet to be designed, but BIS and expiratory concentrations (also related to MAC from Section 7.5.1) are the best parameters currently available in theatre.

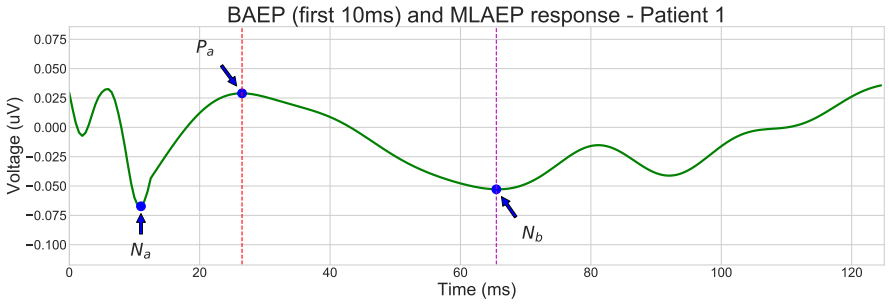

(a) MLAEP at a BIS of 62% and expiratory sevoflurane concentration of 0.1%, three minutes before patient showed signs of movement and waking

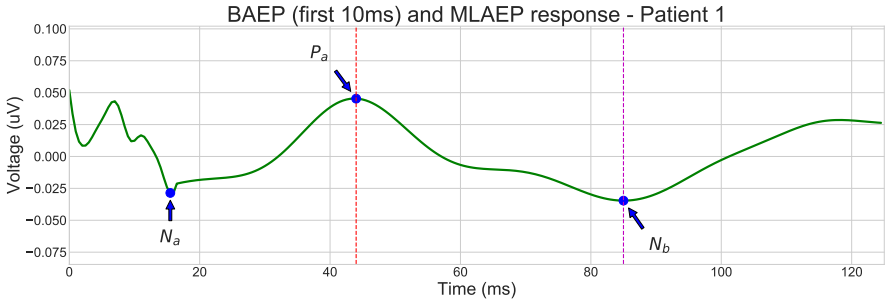

(b) MLAEP at a BIS of 52% and expiratory sevoflurane concentration of 0.23%, after anaesthesia was switched off

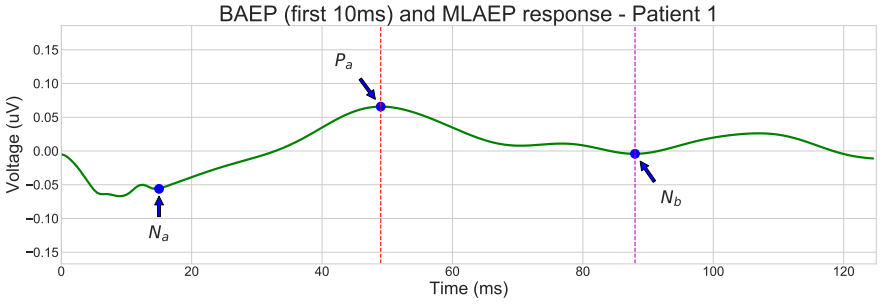

(c) MLAEP at a BIS of 50% and expiratory sevoflurane concentration of 1.7%, after anaesthesia was switched off

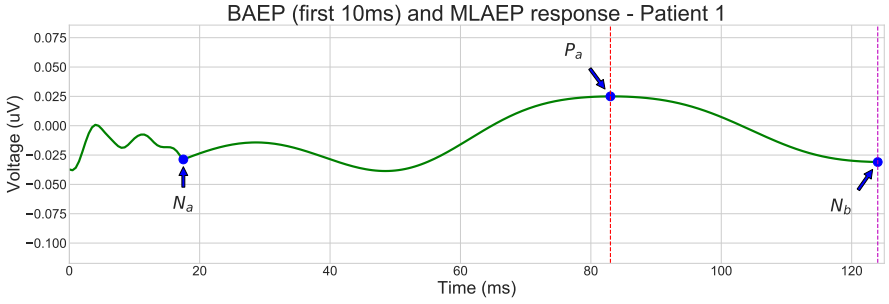

(d) MLAEP at a BIS of 43% and expiratory sevoflurane concentration of 1.9%, deeply anaesthetised patient

Figure 7.3: Averaged reverse-forward low-pass filtered MLAEPs at various levels of anaesthesia for patient one

7.2.4 Correlation of recorded MLAEP amplitudes and latencies with anaesthesia machine readings

The effect of anaesthesia on the latency of the characteristic peaks can be seen in Fig. 7.4. Peak latencies of P_a and N_b, as well as the inter-peak latency $P_a - N_a$, are most effected by anaesthesia levels.

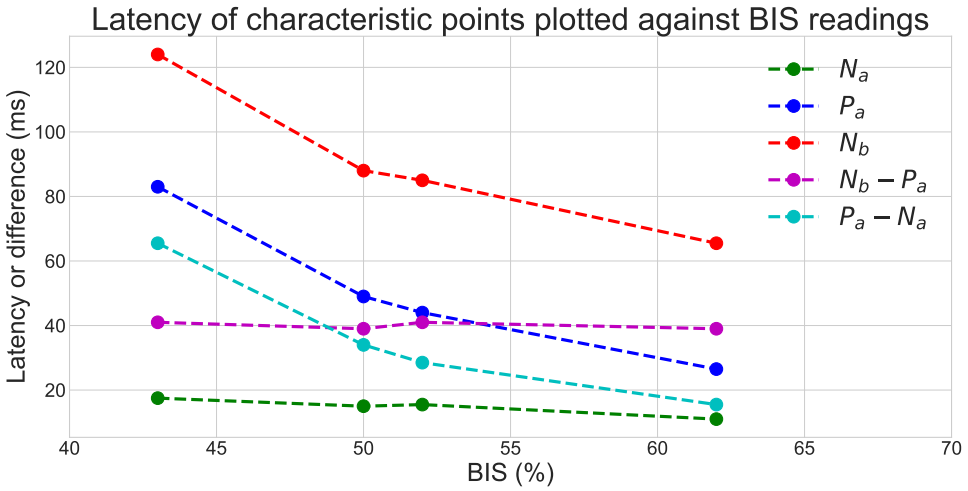

(a) Against the bispectral index

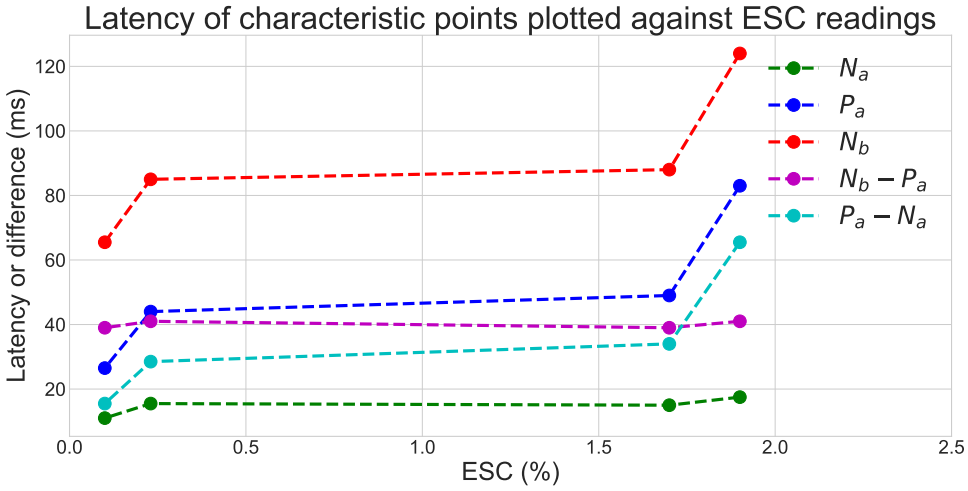

(b) Against the expiratory sevoflurane concentration

Figure 7.4: Graphs depicting changes in characteristic peak and inter-peak latencies against corresponding anaesthesia machine BIS and ESC values for patient one

The correlation of the latencies to the BIS are closely linear, as seen in Fig. 7.4a, and

seemingly sigmoid to the ESC shown in Fig. 7.4b. These correlations are in agreement to what would be expected when referring back to the BIS and ESC relationship in Fig. 7.2. Longer latencies relate to deeper levels of anaesthesia, which is consistent with the literature.

The brainstem auditory evoked potential (BAEP) peak N_a is less effected by anaesthesia. On the contrary, it is difficult to identify the exact latency of this peak due to the sampling rate not being high enough to measure BAEPs (requiring a sampling rate of 6000 Hz or higher [56]). The unfiltered higher frequency nature of the initial segment also results in the prevalence of the high-frequency noise.

Similarly, yet less linearly, the amplitude difference between peaks P_a and N_b is also noted to decrease with increasing levels of anaesthesia, for patient one in Fig. 7.5. This corresponds to what is expected from the theory of the literature.

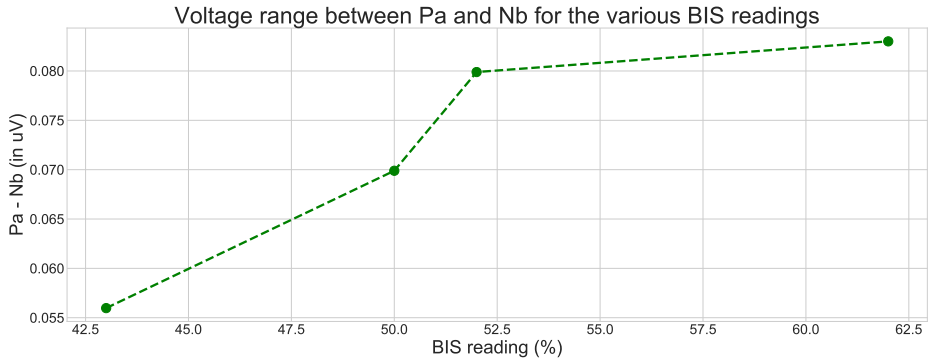

(a) Against the bispectral index

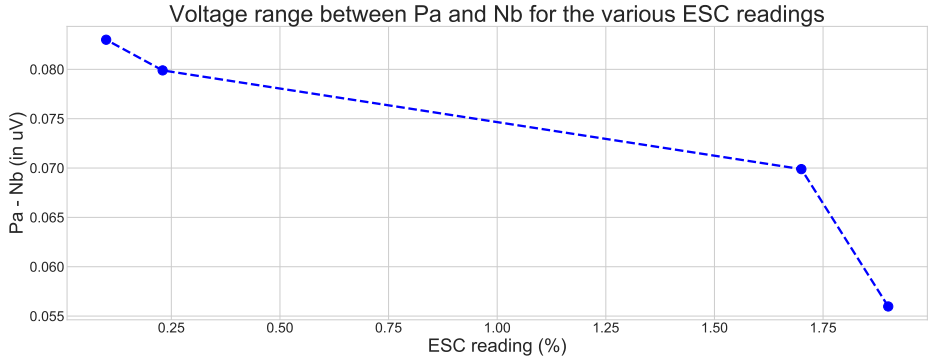

(b) Against the expiratory sevoflurane concentration

Figure 7.5: Graphs depicting changes in the inter-peak voltage difference between P_a and N_b against corresponding anaesthesia machine BIS and ESC values for patient one

As the anaesthesia effect on the nervous system increases, the auditory cortex's ability to process the auditory signals becomes delayed and less prominent, as is seen by the increase in latency and decrease in amplitude of the MLAEPs.

Another advantage of using the in-ear approach with evoked potentials, is that it remains possible to additionally analyse the usual EEG spectral information. This is done at the various anaesthesia levels in the next section.

7.2.5 In-ear spectral power at anaesthesia levels

The average spectrum of the anaesthesia levels' segmented data, prior to the low-pass filters, are calculated and averaged over the specific EEG band domains, namely delta (0 Hz-4 Hz), theta (4 Hz-8 Hz), alpha (8 Hz-13 Hz), beta (13 Hz-30 Hz) and gamma (30 Hz-50 Hz). The average normalised power of each band, for every measured state of anaesthesia, is illustrated in Fig. 7.6.

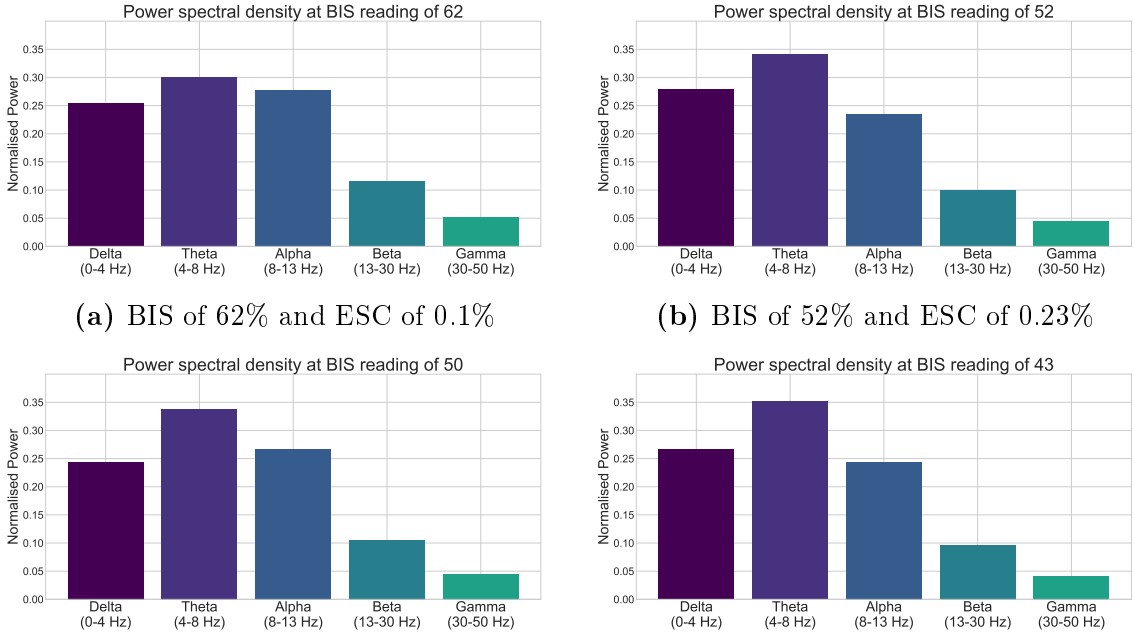

(a) BIS of 62% and ESC of 0.1%

(b) BIS of 52% and ESC of 0.23%

(c) BIS of 50% and ESC of 1.7%

(d) BIS of 43% and ESC of 1.9%

Figure 7.6: Power spectral density of different anaesthesia levels at quoted bispectral indices (BIS) and expiratory sevoflurane concentrations (ESC) for patient one

Although slight changes in band power for anaesthesia levels are evident, it is unclear from the bar graphs how the bands change with increasing levels of sedation. To better represent this correlation, the average spectral band amplitudes are plotted over the recorded BIS and ESC readings.

7.2.6 Correlation of spectral power with anaesthesia machine readings

Figure 7.7 generally shows a gradual decrease, for all of the frequency bands, as BIS decreases (in Fig. 7.7a) and ESC increases (in Fig. 7.7b).

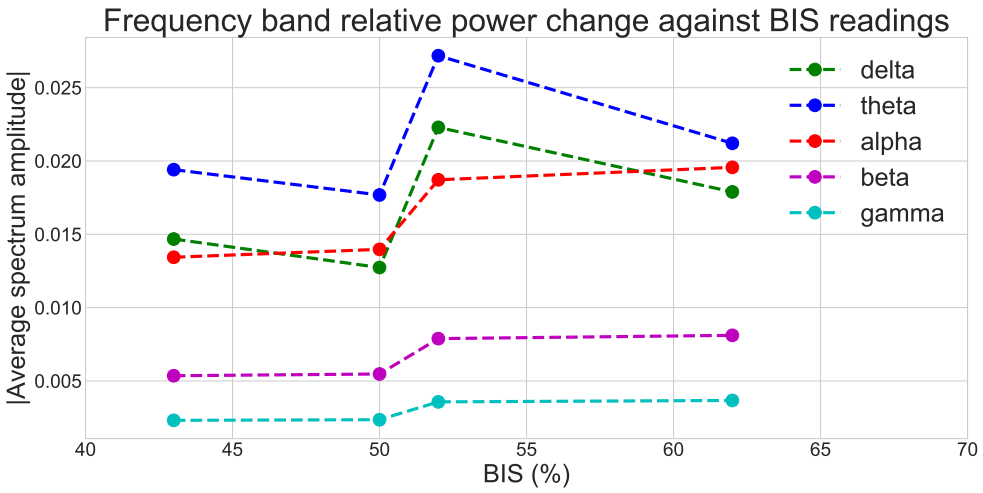

(a) MLAEP at a BIS of 62% and expiratory sevoflurane concentration of 0.1%

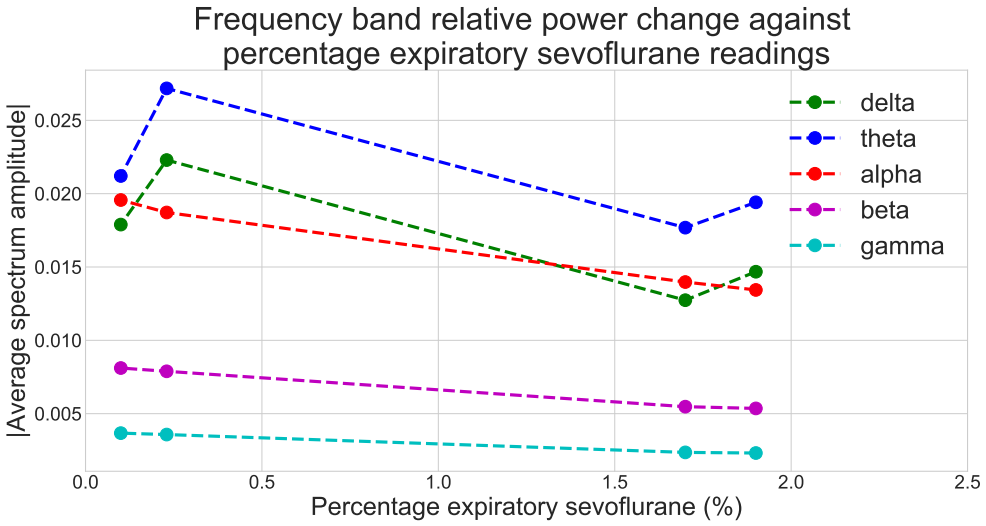

(b) MLAEP at BIS of 52% and expiratory sevoflurane concentration of 0.23%

Figure 7.7: Graphs depicting changes in EEG frequency band average amplitudes against corresponding anaesthesia machine BIS and ESC values for patient one

The low frequency delta and theta bands increase in prominence, relative to the other bands, as anaesthesia levels deepen. This is expected since there is a known general shift

to the lower frequencies with the sedation and even sleep (or less concious) states.

7.3 Results of Patient Two

The second patient was monitored on the evening of the 20^{th} of November 2018, the details of which are provided in this section.

7.3.1 Overview and background

The second patient, who was undergoing a cholecystectomy operation (being the use of a camera and other specialised surgical tools to extract the gallbladder from the abdomen, commonly due to gallstone formations), was an adult female. The operation took place at Stellenbosch MediClinic, with the general anaesthesia applied by anaesthesiologist Dr D.E. Von Durckheim. The total duration of the surgery was 43 minutes, of which 7 minutes accounted for the transition from deep anaesthesia (just as anaesthetic agent is switched-off) to a near-wakeful state (before the patient is transported out of the theatre and regains full conciousness).

7.3.2 Anaesthesia machine parameters

The anaesthesia machine parameters for the second patient were, as with patient one, the BIS and the ESC. The relationship between these two parameters at the analysis points is given in Fig. 7.8 and seems to show a broken correlation. It was practically observed that the parameter at fault, was the BIS. The patient showed signs of regaining consciousness before the BIS could give such indication.

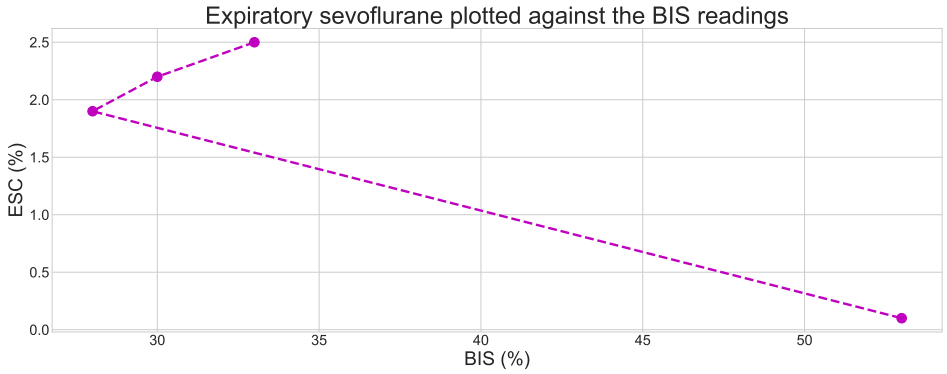

Figure 7.8: Both the recordings of the anaesthesia monitoring machine (BIS and ESC) plotted against each other for patient two

7.3.3 Middle latency auditory evoked potentials at anaesthesia levels

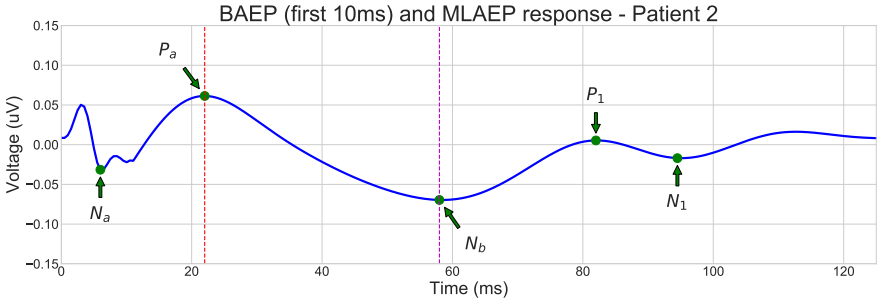

(a) MLAEP at a BIS of 53% and expiratory sevoflurane concentration of 0.1%, one minute before patient showed signs of movement and responsiveness

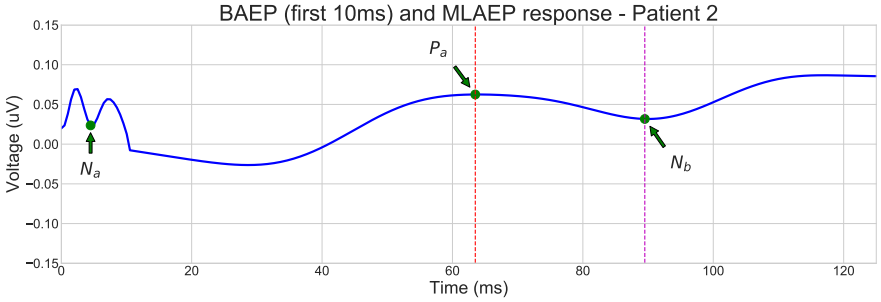

(b) MLAEP at a BIS of 28% and expiratory sevoflurane concentration of 1.9%, after anaesthesia was switched off

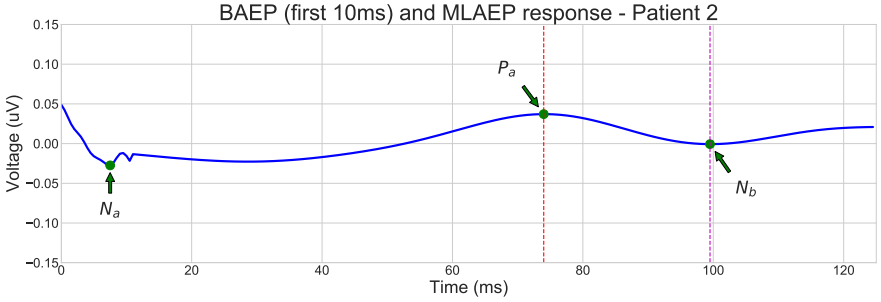

(c) MLAEP at a BIS of 30% and expiratory sevoflurane concentration of 2.2%, after anaesthesia was switched off

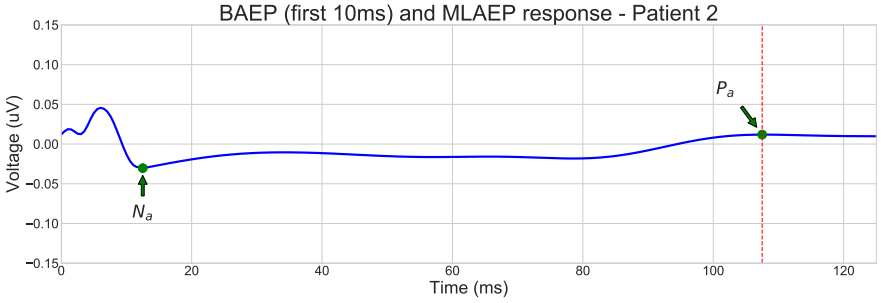

(d) MLAEP at a BIS of 33% and expiratory sevoflurane concentration of 2.5%, deeply anaesthetised patient

Figure 7.9: Averaged reverse-forward low-pass filtered MLAEPs at various levels of anaesthesia for patient two

The MLAEPs at various analysis points are plotted in Fig. 7.9. The plots are again done with each corresponding to the instances of BIS and ESC from Fig. 7.8. The characteristic points are similar to the first patient (N_a, P_a and N_b) with the added delayed peaks P_1 and N_1 for the more conscious response of Fig. 7.9a. It can be noted that N_b eventually falls outside the observable domain as sedation deepens and therefore becomes undetectable.

An identical low-pass filter, with cut-off frequency of 50 Hz, is applied (as with patient one). Similar trends as before are also protruding. There is again, as with the first patient, a decreasing inter-peak amplitude ($P_a - N_b$) as well as delays in the latencies of the same characteristic peaks (and troughs), as the patient's anaesthesia level is raised sequentially higher in Fig. 7.9a, Fig. 7.9b, Fig. 7.9c and Fig. 7.9d. The MLAEPs were ordered from top-to-bottom, in increasing order of ESC, as in this instance it was found to be a more accurate monitor of the depth of general anaesthesia (DGA) as compared to the BIS, which is supported by the data plotted in Fig. 7.8.

7.3.4 Correlation of recorded MLAEP amplitudes and latencies with anaesthesia machine readings

The effect of anaesthesia, on the latency of the characteristic peaks, can be seen in Fig. 7.10. Due to the erroneous nature of the BIS, too much attention should not be given to Fig. 7.10a. Figure 7.10b is indicative of half of a sigmoid function, which correlates to the expected relationship as produced in Fig. 7.4b. The peak latencies of P_a and N_b, as well as the inter-peak latency $P_a - N_a$, are again most effected by anaesthesia levels. P_a evidently produces the largest gradient and is beginning to emerge as the most promising characteristic. Due to N_b falling outside of the detectable range in Fig. 7.9d, only three points and differences therewith can be plotted.

The latency N_a, due to its aforementioned inaccurate detection ability, is unreliable and can thus not be used as a potential DGA for the designed system. The resilient nature of the brainstem's responses to the effects of anaesthesia are clearly presented in the literature. The inter-peak latency $N_b - P_a$, due to the low-pass effects and also limited detectability of N_b, does like-wise not present evidence of reliable anaesthesia depth detection capability.

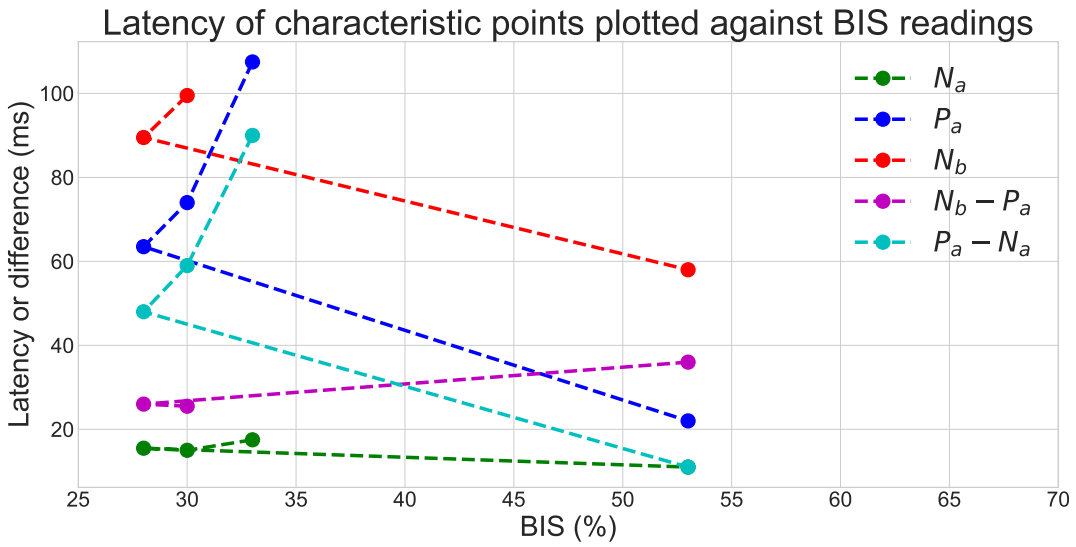

(a) Against the bispectral index

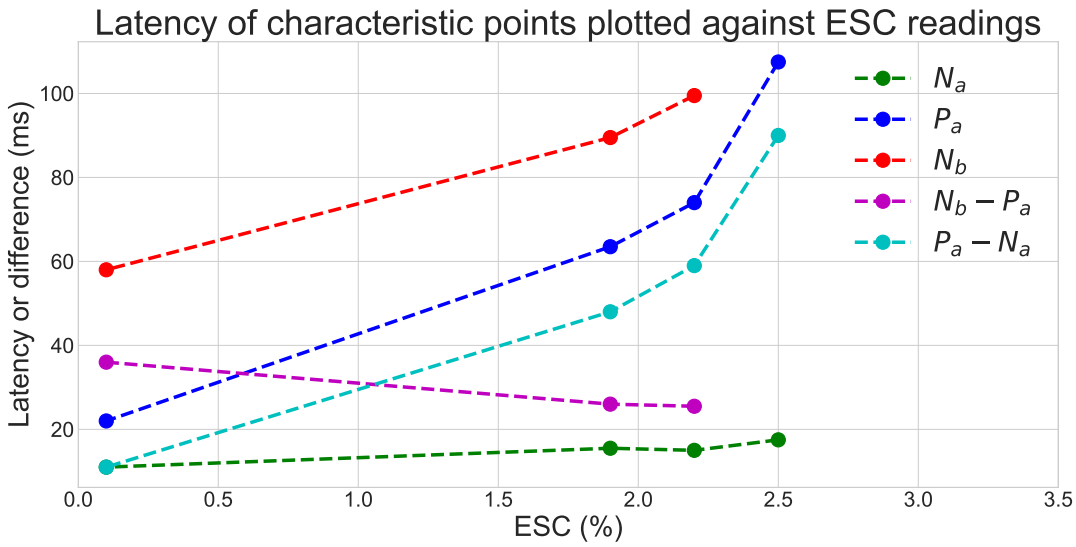

(b) Against the expiratory sevoflurane concentration

Figure 7.10: Graphs depicting changes in characteristic peak and inter-peak latencies against corresponding anaesthesia machine BIS and ESC values for patient two

The amplitude difference between peaks P_a and N_b again generally decreases with increasing levels of anaesthesia for patient two, as shown in Fig. 7.11. Upon first view, it may seem that the BIS in Fig. 7.11a is almost perfectly directly proportional to the amplitude difference, until one notices that the two bottom left-hand points are switched.

Figure 7.11b shows the amplitude difference plotted against the expiratory sevoflurane concentration (ESC). The unexpected amplitudes of the last two points can be partly attributed to the effects of the low-pass filter. The higher frequency (over 50 Hz) components, that could have slightly upped the amplitude of the point at 1.9% ESC, are attenuated by the filter. Due to the majority of the signal information laying below 50 Hz, however, the effect is minimal and a general decrease in amplitude is still observable with increasing sedation.

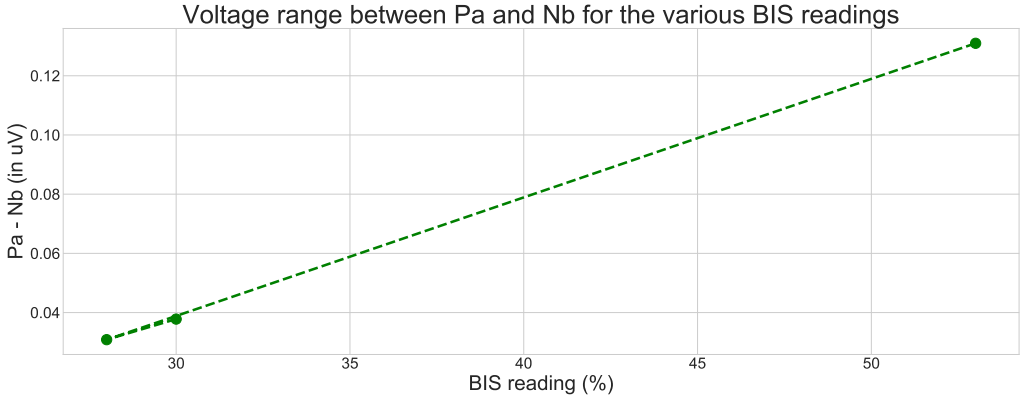

(a) Against the bispectral index

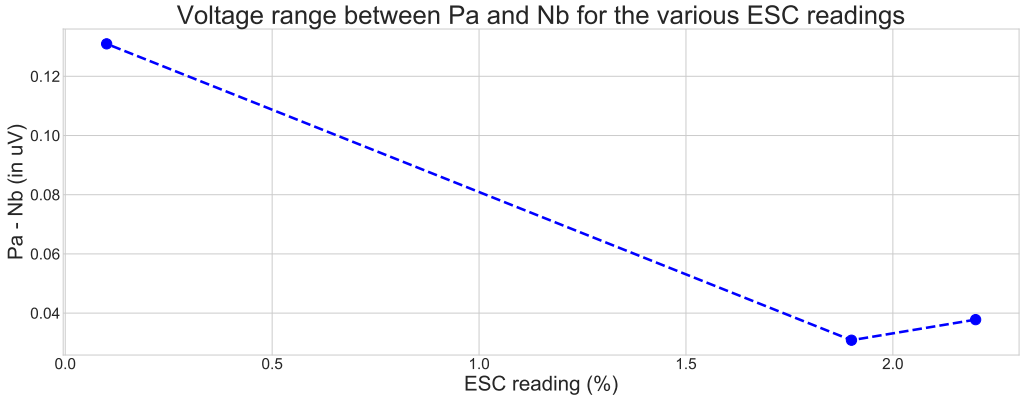

(b) Against the expiratory sevoflurane concentration

Figure 7.11: Graphs depicting changes in the inter-peak voltage difference between P_a and N_b against corresponding anaesthesia machine BIS and ESC values for patient two

The following section analyses the frequency information before the low-pass filter. It is crucial to ensure that each data segment for a patient is filtered and processed in an identical fashion so that the different tests maintain analysis capability and comparability.

7.3.5 In-ear spectral power at anaesthesia levels

The average spectra of the anaesthesia levels, from Fig. 7.8, are calculated and averaged over the specific EEG band domains, namely delta (0 Hz-4 Hz), theta (4 Hz-8 Hz), alpha (8 Hz-13 Hz), beta (13 Hz-30 Hz) and gamma (30 Hz-50 Hz). The results are presented in the bar graphs of Fig. 7.12.

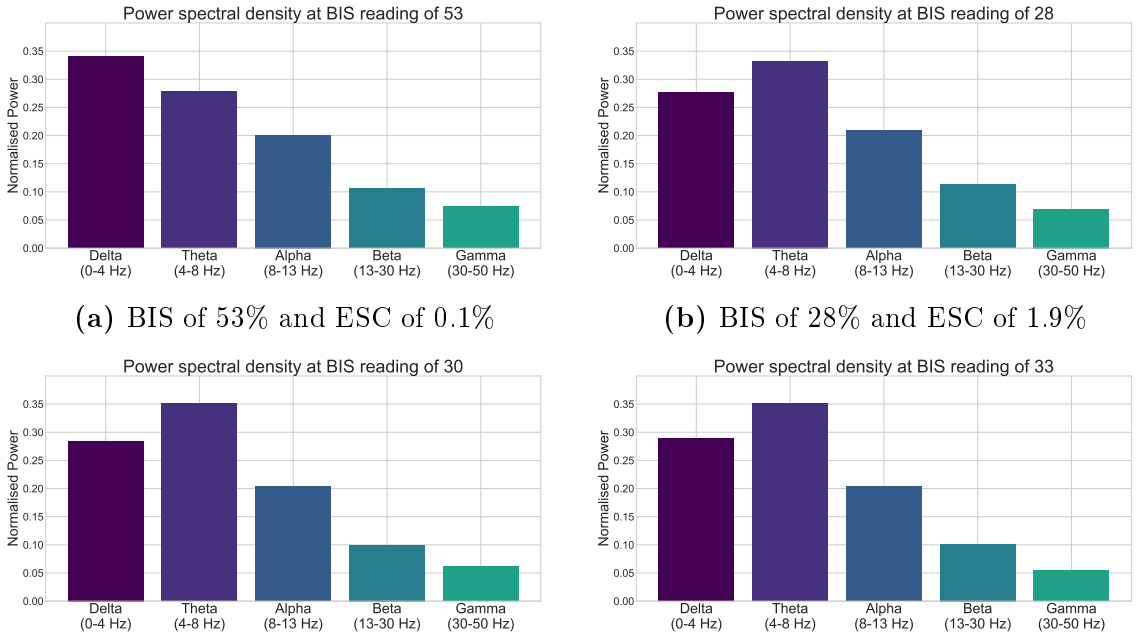

(a) BIS of 53% and ESC of 0.1%

(b) BIS of 28% and ESC of 1.9%

(c) BIS of 30% and ESC of 2.2%

(d) BIS of 33% and ESC of 2.5%

Figure 7.12: Power spectral density of different anaesthesia levels at quoted bispectral indices (BIS) and expiratory sevoflurane concentrations (ESC) for patient two

For the sake of clarity, the average spectral band amplitudes are plotted over the recorded BIS and ESC readings in the following section.

7.3.6 Correlation of spectral power with anaesthesia machine readings

The change in the average frequency spectrum amplitudes is plotted against anaesthesia machine values in Fig. 7.13. Again, the BIS plot (Fig. 7.13a) shows irregular behaviour and Fig. 7.13 is therefore noted but not analysed. In Fig. 7.13b, a general decrease in average spectrum amplitude is evident, for most of the bands, as the ESC increases.

The low-frequency theta band is the only frequency that is observed to increase in average amplitude, before being subdued by the anaesthetic at the deeper levels. There

is gradual shift, in signal composition, from the higher-frequencies to lower-frequencies. As aforementioned in Section 2.2.2, this is expected.

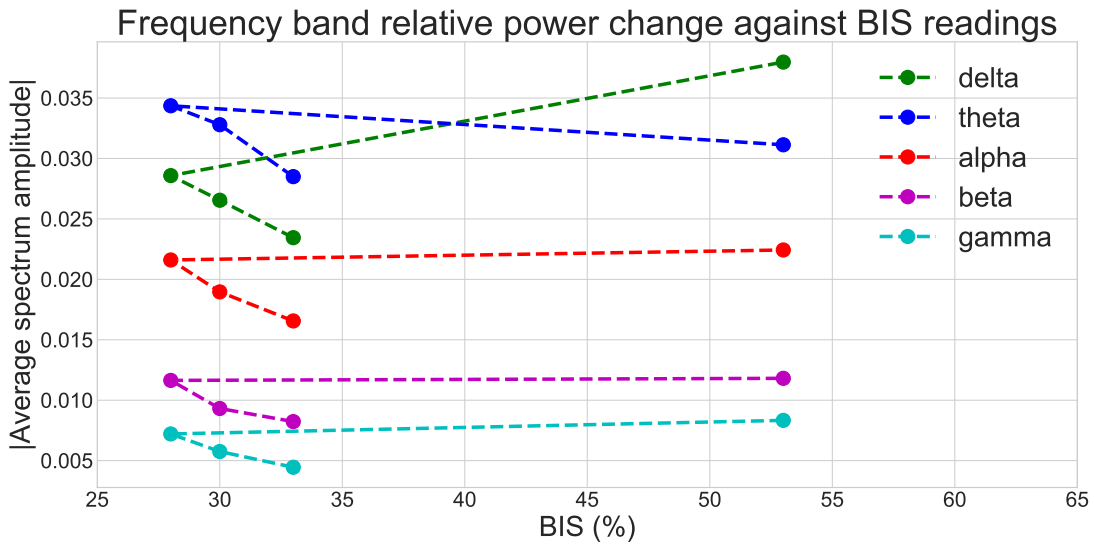

(a) Against the bispectral index

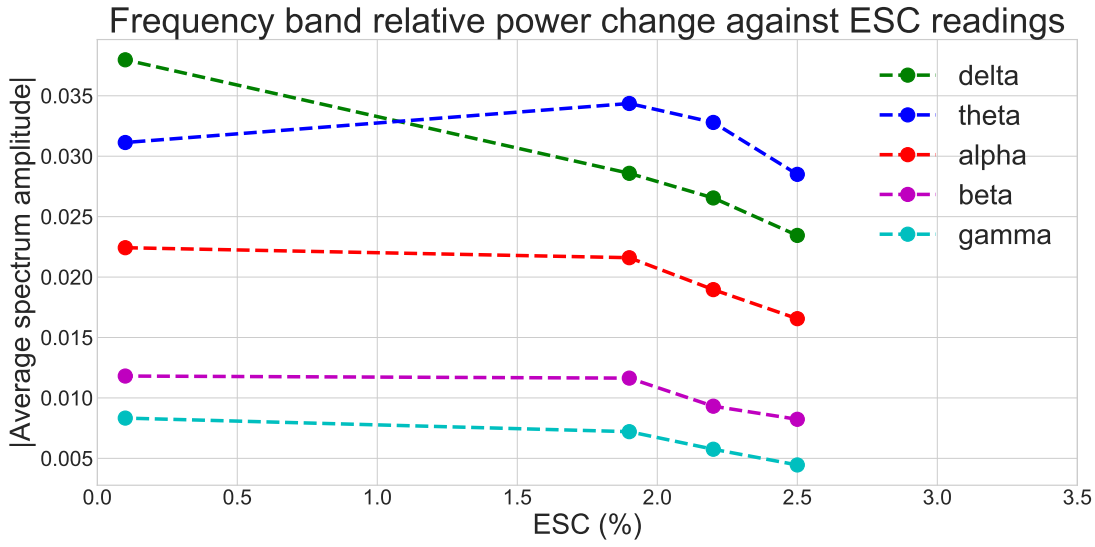

(b) Against the expiratory sevoflurane concentration

Figure 7.13: Graphs depicting changes in EEG frequency band average amplitudes against corresponding anaesthesia machine BIS and ESC values for patient two

The third patient was measured directly after the second, and as such, the device was prepared and readied for the second measurement of the day.

7.4 Results of Patient Three

The third patient was monitored on the evening of the 20^{th} of November 2018, the details of which are provided in this section.

7.4.1 Overview and background

The third patient, that underwent a appendectomy (surgery that also uses a camera and other specialised surgical tools to remove the appendix from the abdomen, almost always as an emergency response to appendicitis), was a young adult male. The operation took place at Stellenbosch MediClinic, with the general anaesthesia applied by anaesthesiologist Dr D.E. Von Durckheim. The total duration of the surgery was 30 minutes, of which 3 minutes accounted for the transition from deep anaesthesia (just as anaesthetic agent is switched-off) to a near-wakeful state (before the patient is transported out of the theatre and regains full conciousness).

Sevoflurane was used to initiate anaesthesia, which was then maintained with desflurane (being more of a pungent agent and therefore not commonly used for initiation). The reason for the change of anaesthetic were to allow for a faster recovery time.

7.4.2 Anaesthesia machine parameters

The anaesthesia machine parameters for the third patient differs from the former two, now being the same BIS with a different expiratory desflurane concentration (EDC) monitored. Desflurane concentrations need to be higher to have the same sedating effect as that of sevoflurane. The relationship between these two parameters at the analysis points, is given in Fig. 7.2 , and again shows a broken correlation. The culprit monitoring parameter was practically observed to be the BIS value, as was the case with patient number two.

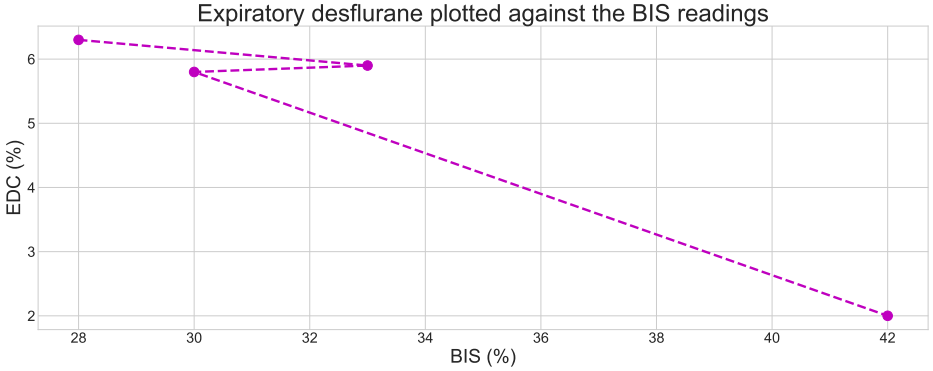

Figure 7.14: Both recordings of the anaesthesia monitoring machine (BIS and EDC) plotted against each other for patient three

7.4.3 Middle latency auditory evoked potentials at anaesthesia levels

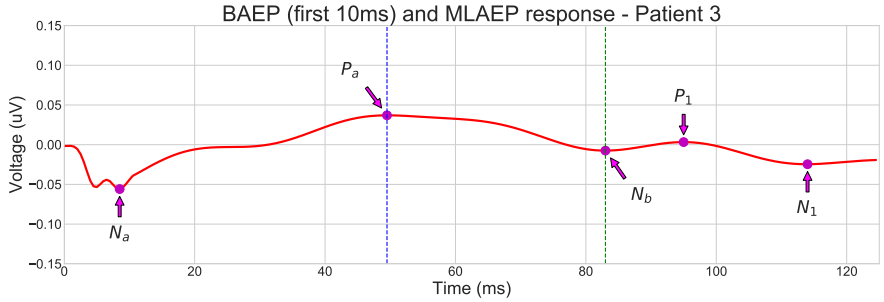

(a) MLAEP at a BIS of 42% and expiratory desflurane concentration of 2%, one minute before patient showed signs of movement and responsiveness

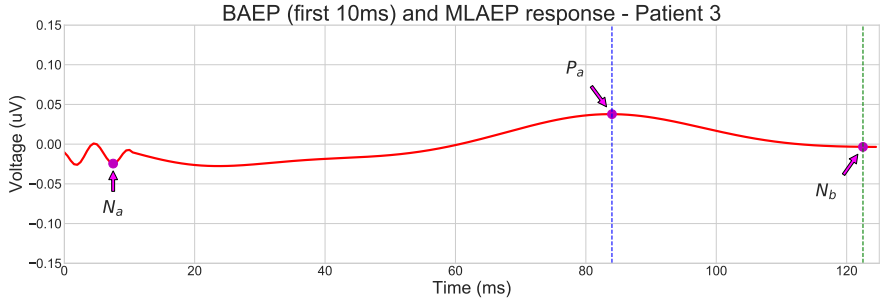

(b) MLAEP at a BIS of 30% and expiratory desflurane concentration of 5.8%, after anaesthesia was switched off

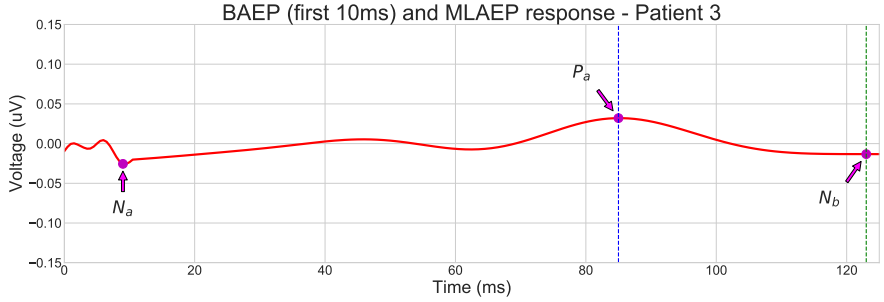

(c) MLAEP at a BIS of 33% and expiratory desflurane concentration of 5.9%, after anaesthesia was switched off

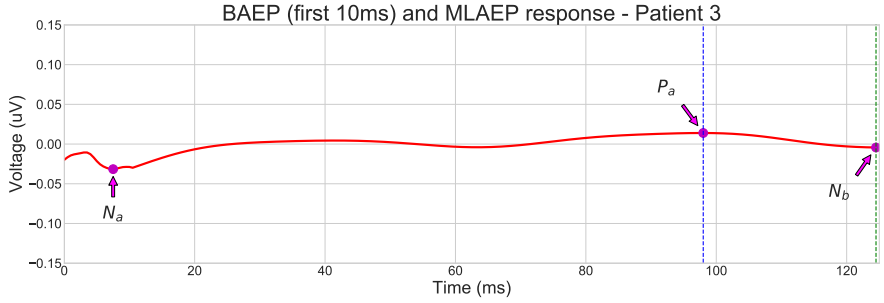

(d) MLAEP at a BIS of 28% and expiratory desflurane concentration of 6.3%, deeply anaesthetised patient

Figure 7.15: Averaged reverse-forward low-pass filtered MLAEPs at various levels of anaesthesia for patient three

The MLAEPs at various analysis points are plotted in Fig. 7.15. The characteristic points are similar to the second patient (N_a, P_a and N_b) with added delayed peaks P_1 and N_1 for the more conscious response in Fig. 7.15a. It can be noted that N_b eventually falls on the domain edge and therefore becomes somewhat effected by boundary saturation effects. It is thus expected that irregular latency changes will be exhibited in the following section.

An identical low-pass filter, with cut-off frequency of 50 Hz, is applied on the MLAEPs (not on initial BAEPs, as this would completely attenuate these high-frequency responses). Decreasing inter-peak amplitude and delays in the latencies of the same peaks, are evident as the patient's anaesthesia level climbs sequentially higher, as shown in Fig. 7.15a, Fig. 7.15b, Fig. 7.15c and Fig. 7.15d. The MLAEPs were ordered from top-to-bottom in increasing order of EDC, as it was again found to be a more accurate measure of the depth of general anaesthesia (DGA) when compared to the BIS.

The latencies observed over the noted BIS and EDC values are plotted in the following section. This allows for the analysis of the changes in latency over the suggested DGA values of the anaesthesia machine.

7.4.4 Correlation of recorded MLAEP amplitudes and latencies with anaesthesia machine readings

The effect of anaesthesia on the latency of the characteristic peaks, for patient three, can be seen in Fig. 7.16. Lagging and irregular monitor outputs are evident from the BIS plot provided in Fig. 7.16a. Figure 7.16b latencies, with specific reference to P_a and $P_a - N_a$, is again indicative of a half a sigmoid function. This follows the trend observed for both patient one and two (Fig. 7.4b and Fig. 7.10b). The effects of edge averaging saturation cause unpredictable behaviour when detecting the local minimum (or trough) latency. For this reason, the latency N_b, approaching the boundary condition, can be attributed to this unpredictable saturation.

Due to the aforementioned inaccurate detection ability of the latency N_a, any differential use thereof (with the designed system) is considered to be unreliable as a potential measure of DGA. This has already been discussed in more detail in the discussion of the results obtained for patient two.

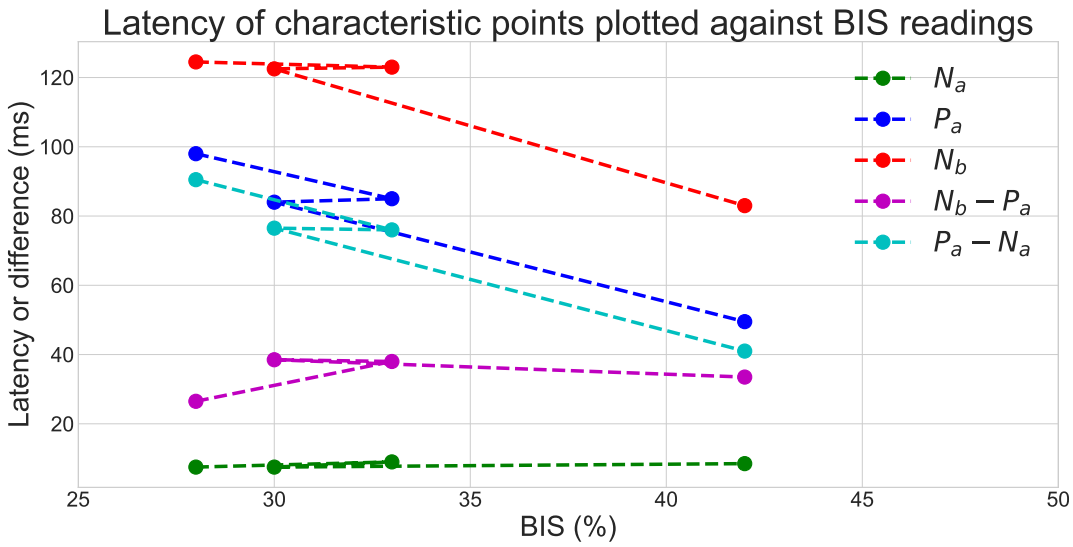

(a) Against the bispectral index

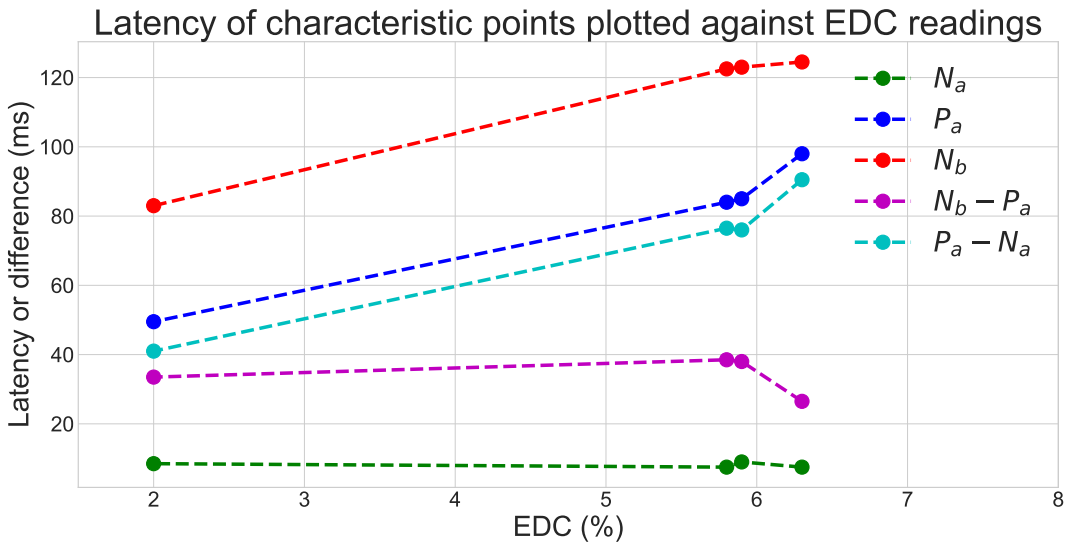

(b) Against the expiratory desflurane concentration

Figure 7.16: Graphs depicting changes in characteristic peak and inter-peak latencies against corresponding anaesthesia machine BIS and ESC values for patient three

The $P_a - N_b$ differential voltage continues to show a overall decreasing nature with increasing levels of anaesthesia, as depicted in Fig. 7.17. The BIS plot (Fig. 7.17a), however, contains very significant irregularities, especially for the middle two data values plotted at BIS values of 30% and 33%.

Figure 7.17b shows the amplitude difference plotted against the EDC, as done for patient one in Fig. 7.5b. The curve is iconic of a half sigmoid function, which confirms that the apparent correlation of expiratory anaesthetic versus anaesthesia levels is of a sigmoid-type form. This conclusion is arrived at since an approximately linear relationship between the BIS and the peak characteristics of the previous two patients was also observed, as shown in Fig. 7.4a and Fig. 7.5a. All of the curves, containing the expiratory concentrations of either desflurane or sevoflurane on its axis, seem to exhibit some full- or partial- characteristics of a sigmoid function.

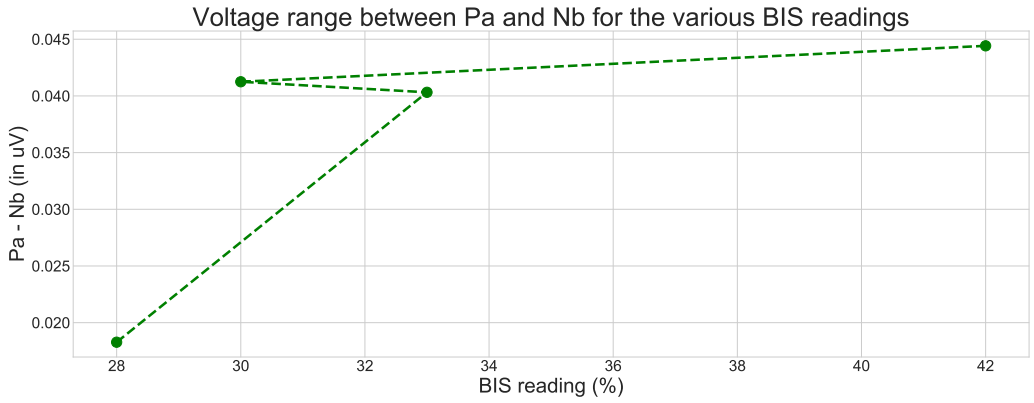

(a) Against the bispectral index

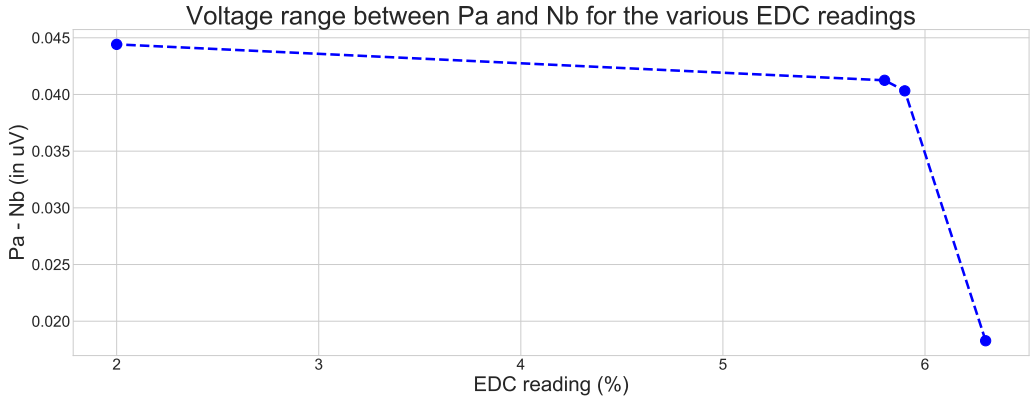

(b) Against the expiratory desflurane concentration

Figure 7.17: Graphs depicting changes in the inter-peak voltage difference between P_a and N_b against corresponding anaesthesia machine BIS and ESC values for patient three

The frequency information for patient three is presented in the following two sections.

7.4.5 In-ear spectral power at anaesthesia levels

The normalised power of the frequency bands, at each anaesthesia depth analyses, is presented in Fig. 7.18.

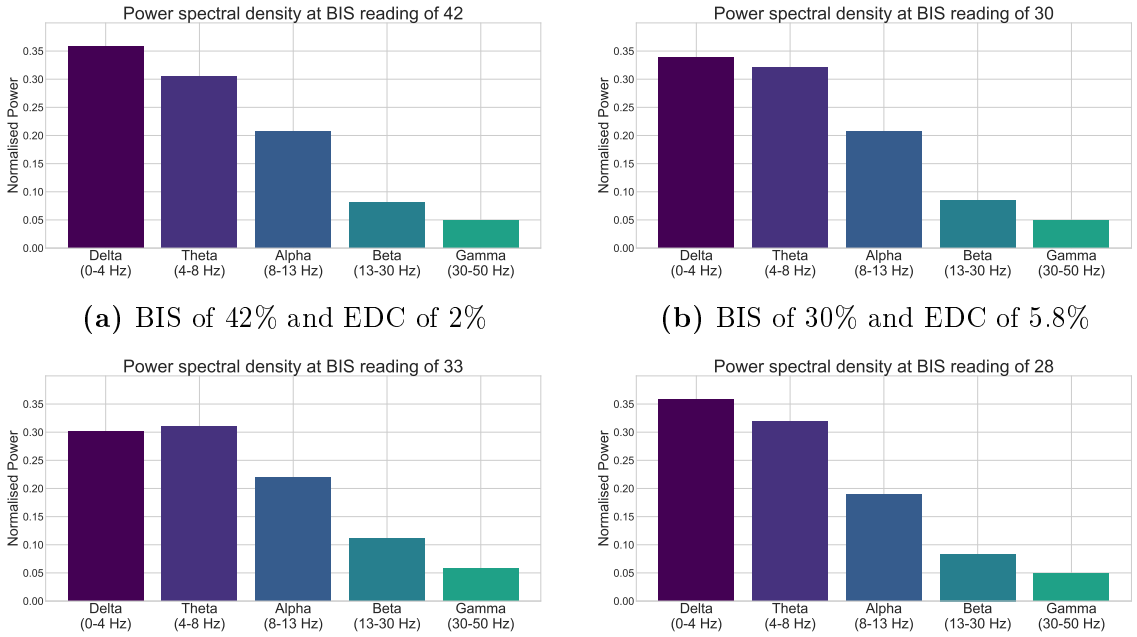

(a) BIS of 42% and EDC of 2%

(b) BIS of 30% and EDC of 5.8%

(c) BIS of 33% and EDC of 5.9%

(d) BIS of 28% and EDC of 6.3%

Figure 7.18: Power spectral density of different anaesthesia levels at quoted BIS and EDC for patient three

The normalisation applied in these bar graphs were done so as to ensure that the sum of all of the bands equates to a value of one for a certain graph. For that reason, the plots of the correlation sections contain the averages of the frequency band intervals (non normalised) , so as to better illustrate decreases in overall power as anaesthetic is applied (or increases when flushed out by the body during recovering). This were done for every patient.

7.4.6 Correlation of spectral power with anaesthesia machine readings

In Fig. 7.19, one can observe the expected irregular behaviour of the bands-BIS plot of Fig. 7.19a as well as the expected trends of the bands-EDC plot of Fig. 7.19b. The bands-EDC plot shows strong similarities with the trends observed for patients one and two, but with slight differences. Frequency-domain information is much more susceptible to both external and internal noise sources, which could be the reason for the sudden dip seen at 5.9% EDC in Fig. 7.19b as well as the overall differences observed between patients.

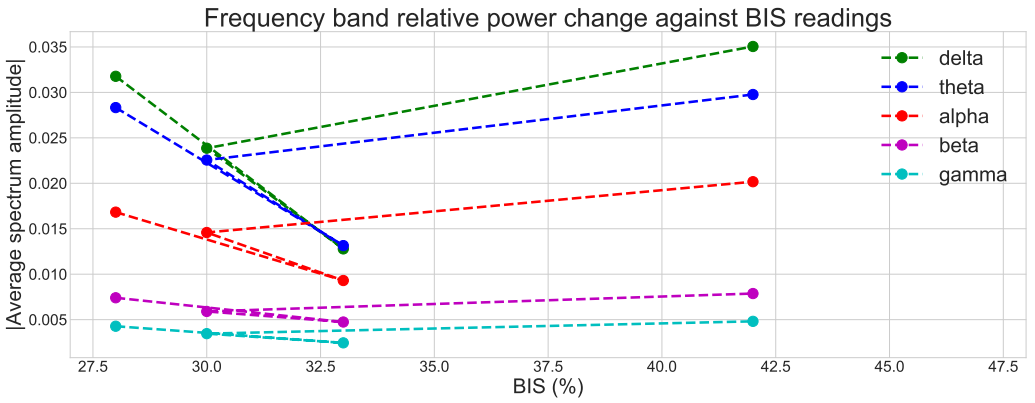

(a) Against the bispectral index

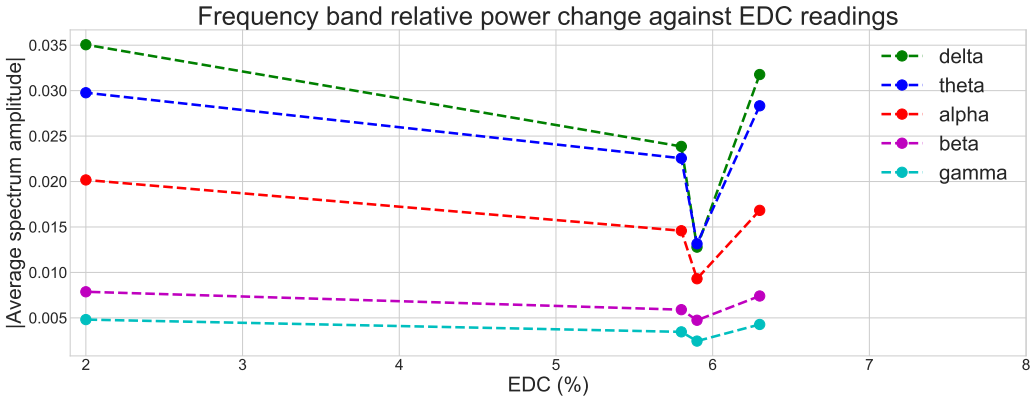

(b) Against the expiratory desflurane concentration

Figure 7.19: Graphs depicting changes in EEG frequency band average amplitudes against corresponding anaesthesia machine BIS and EDC values for patient three

An important observation that can be made is that, due to the BIS value's algorithmic dependence on the EEG frequency information (on the forehead, yet having similarities to the in-ear information), the irregular frequency information around the dip could account for the irregular BIS output.

The fourth patient was measured directly after the third one. Therefore, the device was prepared and readied for the third measurement of the day.

7.5 Results of Patient Four

The fourth patient was monitored on the 20^{th} of November 2018, the details of which are provided in this section.

7.5.1 Overview and background

The last of the four patients had a ureteroscopic laser lithotripsy (removal of ureteral stones assisted with the use of X-ray and gamma ray lasers) and was an adult male. The operation also took place at Stellenbosch MediClinic, with the general anaesthesia applied by anaesthesiologist Dr D.E. Von Durckheim. The total duration of the surgery was 40 minutes, of which 9 minutes accounted for the transition from deep anaesthesia (just as anaesthetic agent application is ceased) to a near-wakeful state (before the patient is transported out of the theatre and regains full conciousness).

Due to the previous use thereof, no more BIS monitors were stocked and available for use on the final patient. As a result, it was decided to additionally record the minimum alveolar concentration (MAC) on the anaesthesia machine along with the expiratory value of the desflurane used. One MAC represents the minimum concentration value of a specific gaseous or vapour anaesthetic that needs to be present in the lungs to historically prevent motor responses in 50% of subjects. The level of concentration is age related, and therefore dependant. For instance, one MAC of a 40-year old patient is given by $\text{MAC}_{40} = 6.6\%$ EDC $= 1.8\%$ ESC. This implicitly indicates that sevoflurane is a much more potent and volatile anaesthetic than desflurane. Elderly people and infants have lower MAC values and observations have shown that factors such as gender and build are less significant than the predominant age factor.

7.5.2 Anaesthesia machine parameters

The anaesthesia machine parameters, recorded for the last patient, are again different from all of the previous patients. The new parameters now being the EDC along with its corresponding minimum alveolar concentration (MAC) value. The relationship between these two parameters, at the analysis points, is given in Fig. 7.2 and shows an almost perfect linear correlation. This is clearly expected, since the two values are directly linked and the MAC is calculated using knowledge of the anaesthetic used, patients age and the expiratory value obtained.

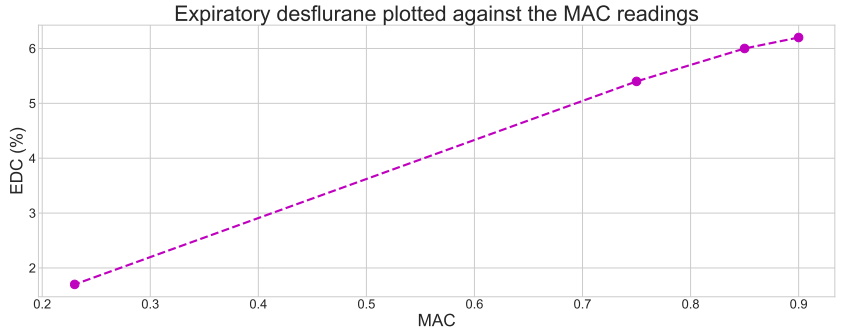

Figure 7.20: Both recordings of the anaesthesia monitoring machine (BIS and MAC) plotted against each other for patient four

7.5.3 Middle latency auditory evoked potentials at anaesthesia levels

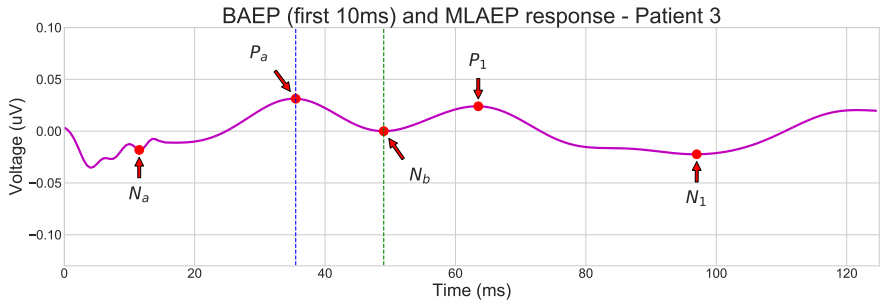

(a) MLAEP at a MAC of 0.23 and expiratory desflurane concentration of 1.7%, one minute before patient showed signs of movement and responsiveness

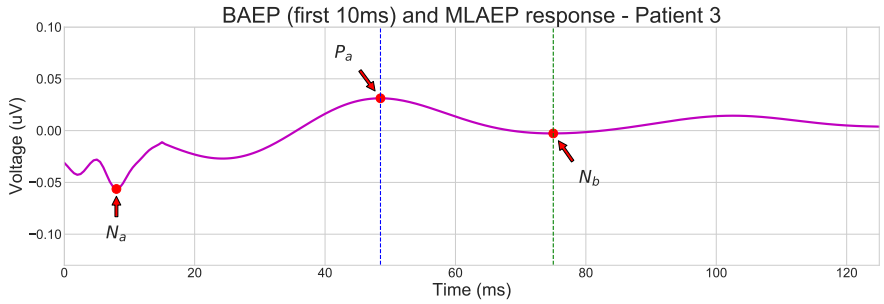

(b) MLAEP at a MAC of 0.75 and expiratory desflurane concentration of 5.4%, after anaesthesia was switched off

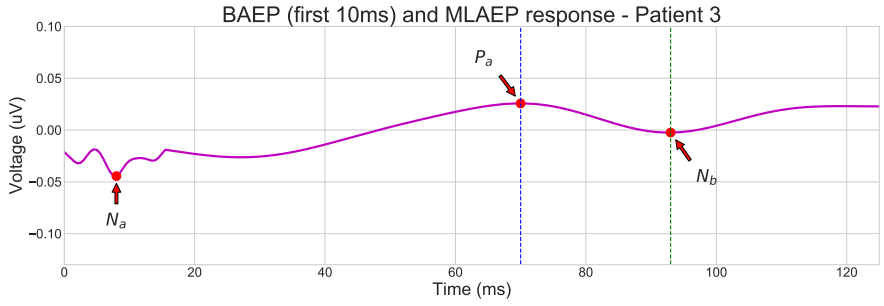

(c) MLAEP at a MAC of 0.85 and expiratory desflurane concentration of 6.0%, after anaesthesia was switched off

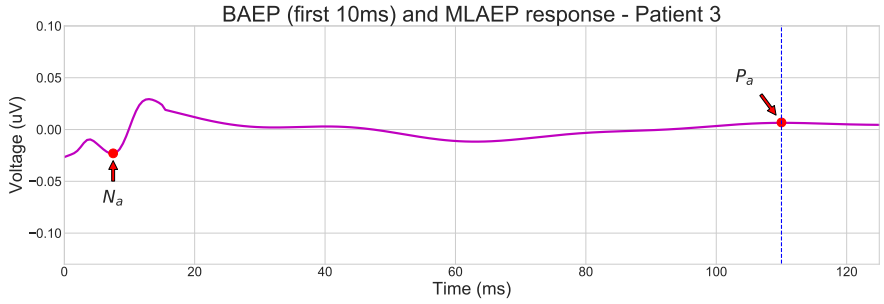

(d) MLAEP at a MAC of 0.9 and expiratory desflurane concentration of 6.2%, deeply anaesthetised patient

Figure 7.21: Averaged reverse-forward low-pass filtered MLAEPs at various levels of anaesthesia for patient four

The auditory evoked middle latency plots, for the varying depths of anaesthesia of patient four, are given in Fig. 7.21. The characteristic points N_a, P_a, and if detectable, N_b, P_1 and N_1 are labelled on the plots. Eventually at deep anaesthesia, N_b again falls outside of the boundary region and becomes undetectable.

The 50 Hz low-pass filter was implemented on the segments of the MLAEPs. It has now become clear that there exists a repeatable trend, within the evoked potentials, as anaesthesia moves sequentially higher in all of the four observed patients (from Fig. 7.21a to Fig. 7.21d for patient four).

To analyse the observed changes in latency with anaesthesia , using the machine suggested DGA, latencies over the noted MAC and EDC values are plotted in the following section. The plots are logically expected to be almost identical due to the linear relationship mentioned in the previous section.

7.5.4 Correlation of recorded MLAEP amplitudes and latencies with anaesthesia machine readings

There is an exceptionally strong relationship between the latency data obtained for patient four, provided in Fig. 7.22, and the data obtained for the previous patients. It has become clear that the delay (or otherwise know as latency) of peak P_a repetitively correlates well with the strongest expiratory sedative agent concentration, in a sigmoid-fashion, and continues to show extra-ordinary potential in being used as the basis of perhaps the first feasible and reliable DGA for anaesthesiologists.

The peak N_b and inter-peak latency $P_a - N_a$ values also maintain a strong sigmoid (or perhaps even partly exponential) correlation with both the latency-MAC and latency-EDC plots of Fig. 7.22a and Fig. 7.22b as well as with the latency-expiratory plots for the previous patients.

The values obtained for peak latency N_a and inter-peak latency $N_b - P_a$ are too inconsistent to be described as feasible characteristics for the outputs presented in this chapter and for this designed system set-up. This could possibly be attributed to the previously mentioned sampling limitations, presence of high-frequency noise as well as boundary averaging saturation.

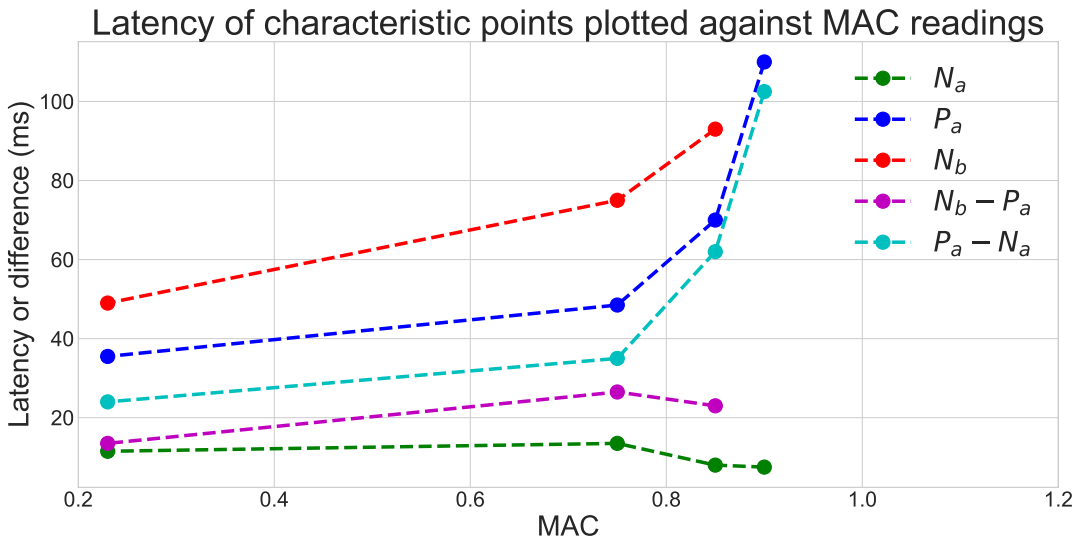

(a) Against the bispectral index

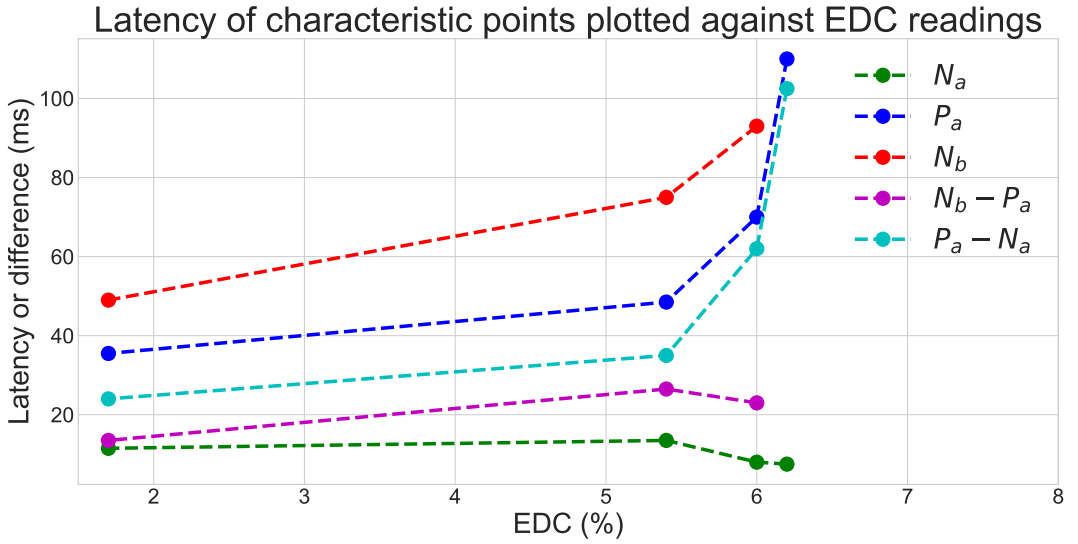

(b) Against the expiratory desflurane concentration

Figure 7.22: Graphs depicting changes in characteristic peak and inter-peak latencies against corresponding anaesthesia machine BIS and ESC values for patient four

The next plot (Fig. 7.23) presents the $N_b - P_a$ amplitude difference against the MAC (Fig. 7.23a) and EDC (Fig. 7.23b) values for the fourth patient.

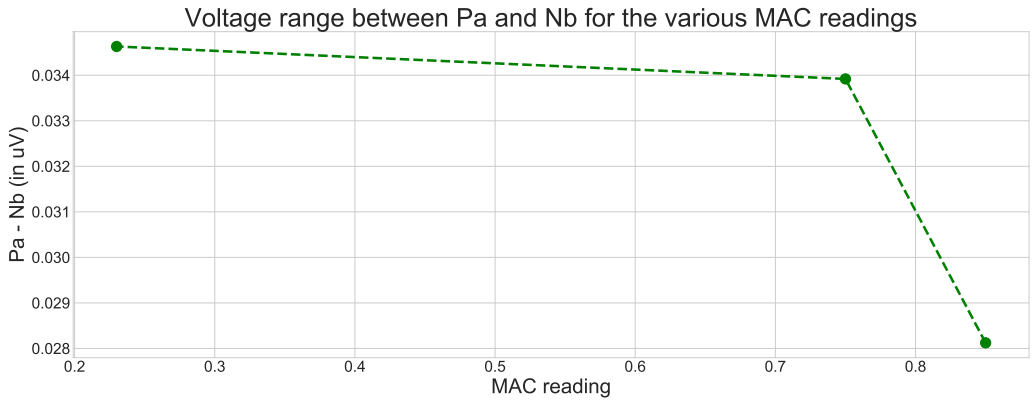

(a) Against the bispectral index

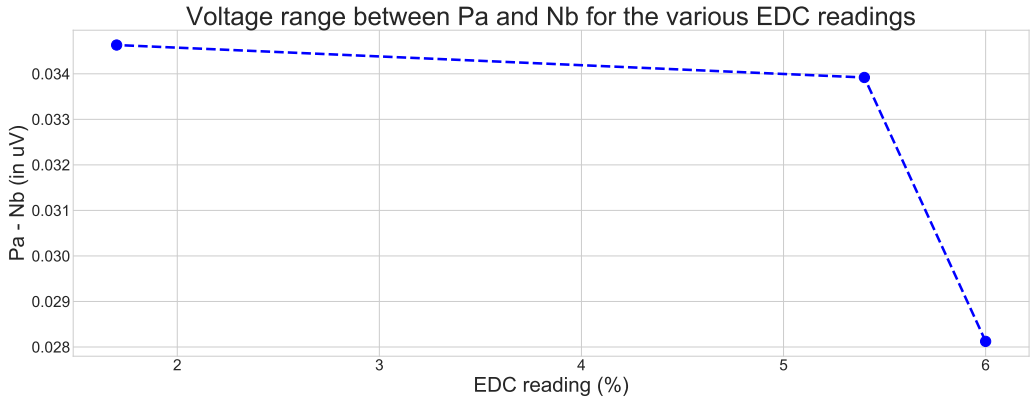

(b) Against the expiratory desflurane concentration

Figure 7.23: Graphs depicting changes in the inter-peak voltage difference between P_a and N_b against corresponding anaesthesia machine BIS and ESC values for patient four

The graphical representation of the amplitude difference, plotted against the expiratory desflurane concentration and minimum alveolar concentration, is again indicative (in terms of its form) of a sigmoid or exponential relationship between the differential amplitude and anaesthesia machine gaseous/vapour concentration measurements.

The final patients frequency information, as analysed from the designed in-ear electrode, is presented in the section that follows.

7.5.5 In-ear spectral power at anaesthesia levels

The normalised power of the frequency bands, at each anaesthesia depth analyses coordinate of Fig. 7.20 and consequently every MLAEP waveform in Fig. 7.21, is presented in Fig. 7.24.

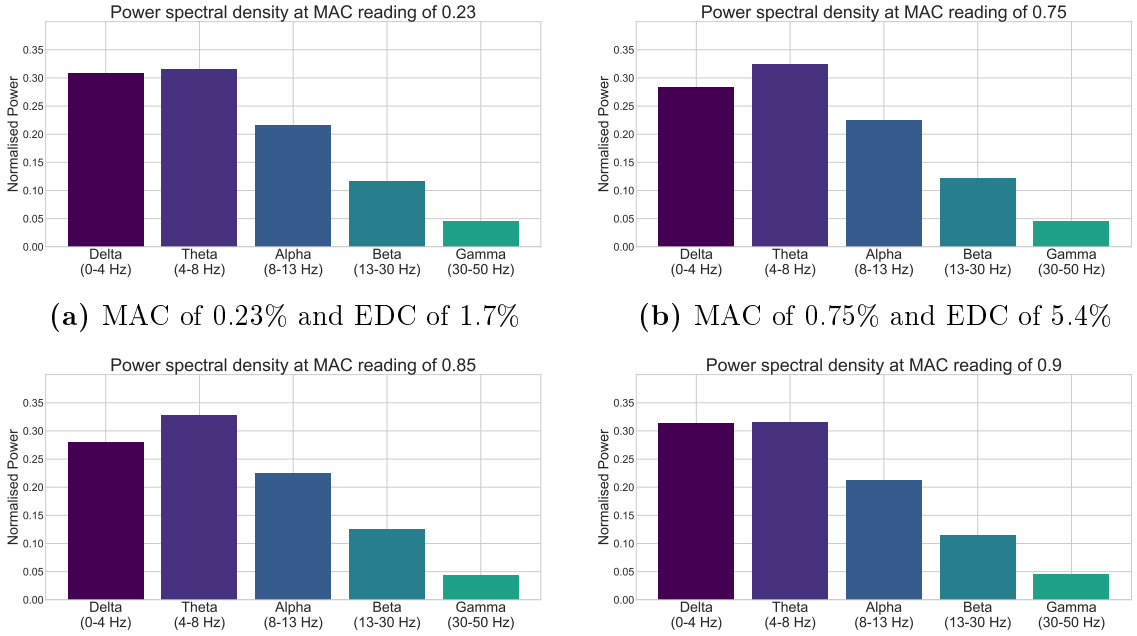

(a) MAC of 0.23% and EDC of 1.7%

(b) MAC of 0.75% and EDC of 5.4%

(c) MAC of 0.85% and EDC of 6.0%

(d) MAC of 0.9% and EDC of 6.2%

Figure 7.24: Power spectral density of different anaesthesia levels at quoted BIS and MAC for patient four

The next section better represents the last patient's frequency spectrum shift at various depths of general anaesthesia.

7.5.6 Correlation of spectral power with anaesthesia machine readings

The non normalised (and therefore having unaffected amplitude information) averaged frequency band data is plotted over the monitoring machines output readings in Fig. 7.25.

The higher-frequency alpha and beta bands, and also the lower-frequency theta bands, show similar responses. There is an initial gradual drop in average amplitude as the patient's body contains increasingly higher anaesthetic presence, followed by a sharper negative gradient as deep anaesthesia is reached.

The lowest-frequency delta band has a similar start, but actually exhibits a positive gradient as the patient enters into deep anaesthesia. This correlates well with the literature and also what has been observed from subjects that are in a state of deep sleep.

The highest-frequency gamma wave band shows a similar, yet less prominent response to the alpha and beta bands. Due to the relatively smaller nature of the amplitude of the

gamma ray, it is more likely to have a higher signal-to-noise ratio in the presence of any noise source introduced by the ambient environment.

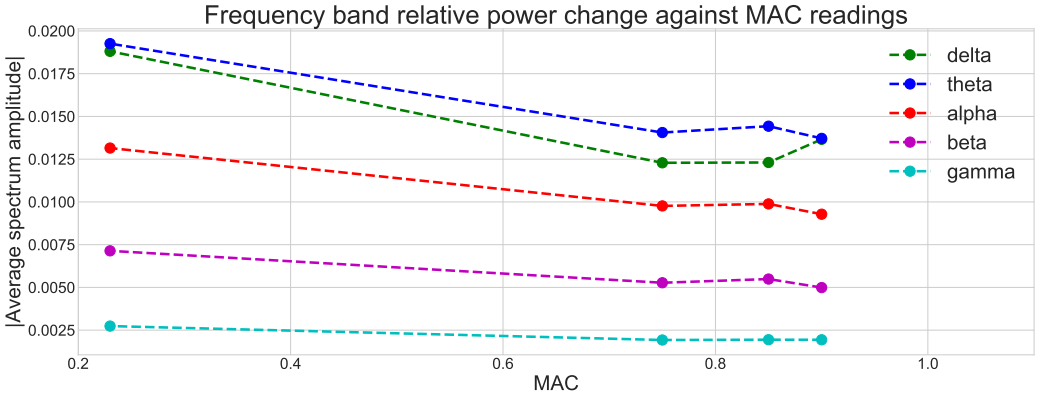

(a) Against the bispectral index

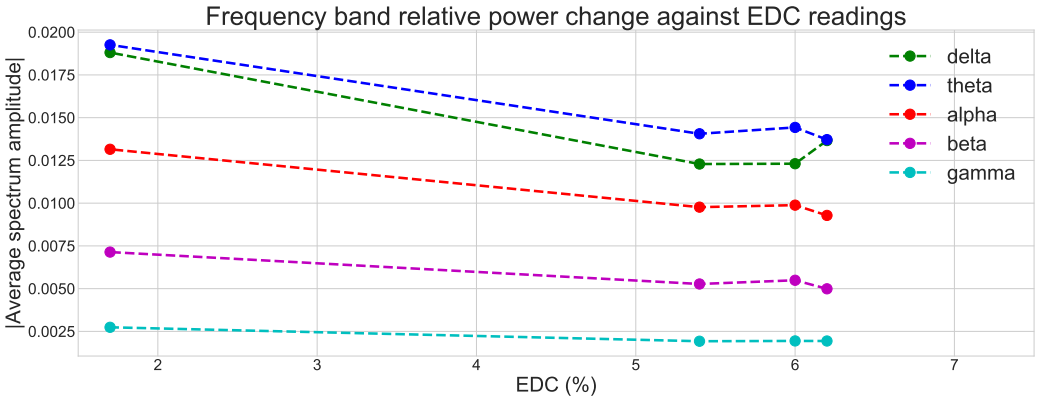

(b) Against the expiratory desflurane concentration

Figure 7.25: Graphs depicting changes in EEG frequency band average amplitudes against corresponding anaesthesia machine BIS and EDC values for patient four

7.6 Final remarks and conclusion

A general consensus, gained from the anaesthesiologists, is that they have repetitively found that the bispectral index is an inaccurate measure of anaesthesia. Descriptive words and phrases such as "delayed", "lagging" and "sudden jumps" were in the vocabulary of the doctors when asked about their opinion of the BIS. So much so, that if it was not requested to use the BIS for correlation purposes, it would not have been set-up at all. There is a dominant preference, amongst the anaesthetists, towards the monitoring and application guidelines of sedative agents via means of expiratory anaesthetic concen-

trations and their corresponding MAC values.

Expiratory anaesthetics measurement is, however, not a direct measure of consciousness. It may give indication of how much of a certain sedating drug is present in the patient's body, but the quantity needed to keep patients sedated varies substantially and often unpredictably with factors such as patient age, gender and build.

Experience in working with the medical professionals proved that it is of vital importance, to the future of the field of anaesthesiology, to derive a system capable of monitoring consciousness more accurately and within relative real-time.

The latency value P_a has shown the strongest potential for being used as a measure of depths of anaesthesia. In retrospect of the results presented in this chapter, it has out-performed the BIS in all of the initial three tests at detecting a waking (or deepened anaesthesia) patient. It is an extra-ordinary observation, since it is merely an evoked potential characteristic, whereas the BIS is a more complex algorithm that is formulated to be a measure of depth of general anaesthesia (DGA).

The discussion chapter that follows will present the information of the previous paragraph, as a summary of the results and findings, in more detail.

Chapter 8

Discussion

This chapter is supplementary to the inter-result discussions of Chapter 7. The focus, herewith, is placed on the overall perspective of the research and design project. The first section summarises the results obtained in a clear and conclusive manner.

8.1 Summary of result findings

The ultimate aim of the project was to develop a system that could potentially give a better indication of the level of consciousness, possibly throughout the pre-, intra- and post- surgery phases, that a patient undergoing general anaesthetics has. Existing methods, used in the hospital setting to address this need, have been found to be unreliable, delayed or indirect.

The bispectral index (BIS) uses an empirical, observational and frequency-based algorithm to derive at a percentage that should be indicative of cortical function. It has, however, been found to commonly output delayed and unexpected values during its practical use in the field of anaesthesiology. As mentioned in Chapter 7, it is, at least in the hospital applicable to this study, scarcely set-up and used as a measure of depth of general anaesthesia (DGA).

During the clinical trials, it was found that one especially promising parameter, being the latency of the middle latency auditory evoked potential (MLAEP) peak P_a, outperformed the BIS's ability to give an accurate indication of the depth of sedation. It was not possible, due to the design's limitations, to obtain this latency value in real-time during the surgical procedures. Regardless, it was later analysed at corresponding time intervals and compared to the average output of the anaesthesia machine's suggested depth, over the same time intervals, to show a stronger correlation to expiratory desflurane concentrations (EDC) and expiratory sevoflurane concentrations (ESC) than that of the BIS.

Figure 8.1 summarises the outperformance, in the form of comparable box and whisker plots, of the peak latency P_a over the BIS of the anaesthesia machine.

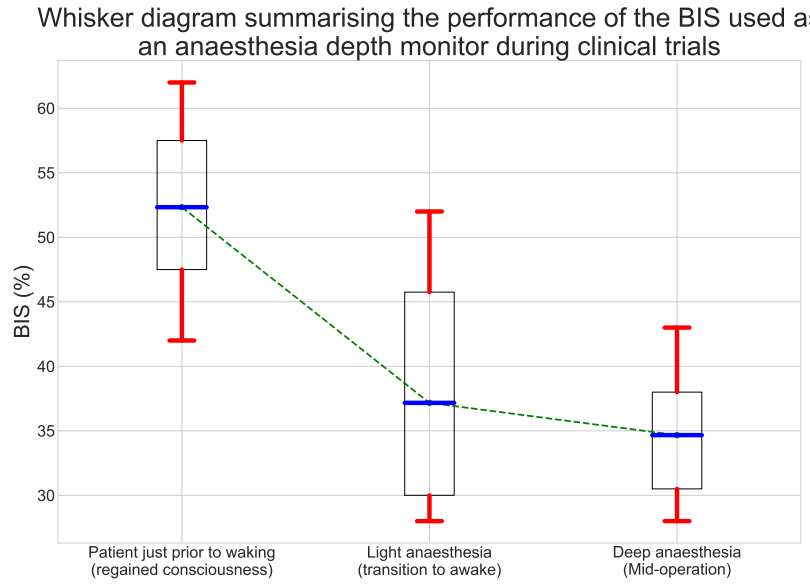

(a) The overall performance of the BIS to differentiate between the suggested conciousness levels.

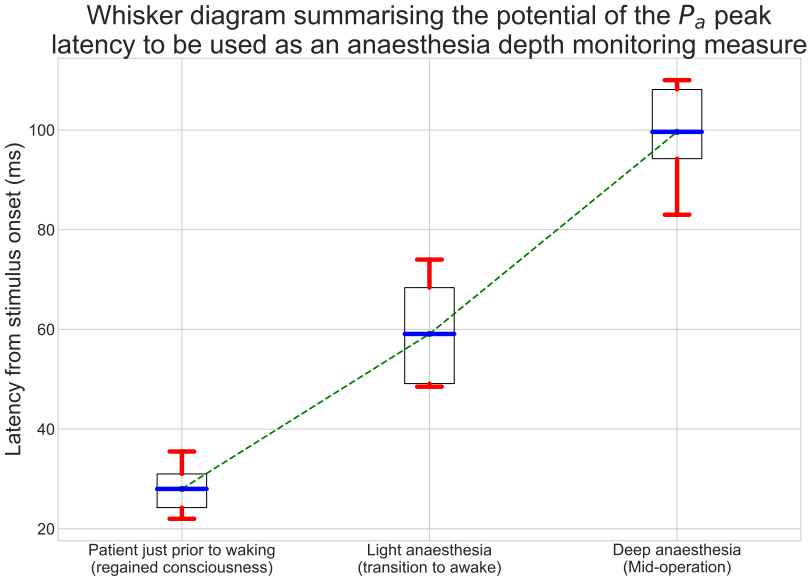

(b) The overall performance of the latency of peak P_a to differentiate between the suggested conciousness levels.

Figure 8.1: Whisker diagram summary of results showing a stronger and more accurate correlation of peak P_a latency as compared to the BIS value readings. The blue lines represent the data means and red lines the data range in every grouping

In order to derive the plots of Fig. 8.1, and due to the non-existence of a baseline consciousness measuring system, all of the data from Chapter 7 was grouped into three categories. The categories were, namely, "Patient just prior to waking (regaining consciousness)", "Light anaesthesia (transition to awake)" and "Deep anaesthesia (mid-operation)". These categories were formed, using as guidelines, the expiratory machine outputs (ESC and EDC) as well as the expert interpretation of the anaesthesiologist, to group all of the P_a latencies and BIS values into three perceived and suggested consciousness levels. Due to the limited quantity of samples, the red whiskers of the plots were instead linked to the range of the data groups (including outliers), whereas the blue centre lines of the plots (usually representing the data medians) were instead linked to the mean of the data groups. Green dotted lines were used to join the means of both plots.

The plots, speaking for themselves, show a remarkable improvement (in the tested patients' results) in the ability of a single in-ear recorded MLAEP characteristic (P_a latency) to distinguish between different levels of consciousness, when compared to that of BIS.

Figure 8.1a shows how the groupings of the average BIS, for anaesthesia level segments, strongly overlap in both their ranges and interquartile ranges. There is also a problematic relative-closeness of the means in the "Light anaesthesia" and "Deep anaesthesia" categories. A general decline in the mean percentages output by the BIS is evident as anaesthesia deepens (as would be expected), but the overall variability and range of the data is far too large to accurately conclude what level of consciousness the patient has.

On the contrary, Figure 8.1b presents a strongly preferable and exemplary model response for determining levels of consciousness, from the latency of P_a. There is a clear and distinguishable separation between the ranges of each of the categories. A strongly as well as positively linear correlation is evident from the mean plot linking the diagrams. The positive gradient is sensible since a larger latency, inherent to the delayed primary auditory cortex responses to stimulus, is expected as anaesthesia affects the mind. The interquartile ranges in the groupings, along with the overall trend observed, is indicative of a more accurate definition for the state of consciousness.

The following section discusses the possible causes of BIS inaccuracy.

8.2 Shortcomings of the BIS

Returning to the analysis of the BIS, the reason for its inaccuracy, can be attributed to various phenomena. In Section 2.2.2, it was shown that different anaesthetics can have inconsistent effects on the frequency changes that occur at various depths of anaesthesia. The BIS is predominantly dependant on this spectral information, and as such, will be susceptible to these inconsistencies.

As mentioned in the first paragraph, the BIS is dependant on information that varies with different agents and drugs. In addition to this, another factor to consider is that merely patient specific variables (such as age, gender, build and genetics) could effect the frequency response of that patient's brain to anaesthesia. Attempts have been made to remove other inference sources from the BIS inputs, such as EMG and EKG (defined in Chapter 2), but the removal techniques are not always perfect in their functionality. Resilient components of such sources can once again effect the frequency-domain of the signal and as a result, the BIS.

Sources of Electromagnetic interference (EMI) also introduce variation in spectral information, especially when such sources are not easily filtered out in narrow-band notch domains. The susceptibility of the frequency spectra to EMI, and the reliance of the BIS on the information contained within these spectra, results in the accuracy of BIS being dependant on the absence of strong interference sources. The EEG signal amplitudes are relatively small in relation to other signals. The signal-to-noise ratio is therefore implicitly decreased in the presence of EMI noise.

The expiratory anaesthetic concentration monitors are also limited in the information that they can provide. This is discussed in the section that follows.

8.3 Limitations of the ESC and EDC

The expiratory desflurane and sevoflurane concentrations, although modernly preferred over the use of the BIS, are not a direct measure of consciousness. As mentioned in Section 7.5.1, the minimum alveolar concentration (MAC) reference system, used in expiratory concentration monitoring, is dependant on historically collected statistical information. The EDC and ESC may give an indication of the amount of anaesthetic drug present in the patient's body, but they do not account for all the possible variables (such as gender, build and genetics) and are therefore flawed in this regard.

In this study, EDC and ESC have been shown to correlate with conciousness in a sigmoid-like fashion (concluded from the linear consciousness-latency of Fig. 8.1b and observed sigmoid-like nature of the latency-ESC / EDC plots of Chapter 7). This results in a sharp value change between the "Deep anaesthesia" and "Awake" concentration readings. This sudden steep gradient makes it difficult to respond, in-time, if such a monitor change unexpectedly occurs.

To illustrate the sigmoid-form conclusion, made in the previous paragraph, the same consciousness groupings, as shown in Fig. 8.1, can be applied to the ESC and EDC values obtained during the trials. Due to the differing ESC and EDC concentrations needed to induce and maintain anaesthesia, the minimum alveolar concentration (MAC as defined in Chapter 7) is used to normalise the data. To better depict their sigmoid nature the middle conciousness grouping, used in Fig. 8.1, is further divided up into two groups

(the one being closer to deep anaesthesia and the other being closer to the "awake" state). Figure 8.2 presents the results of such groupings, of expiratory values plotted against observed levels of anaesthesia, as clearly symbolising a sigmoid form. The sigmoid relationship is indicative of the anaesthetic washout basis of the monitoring technique.

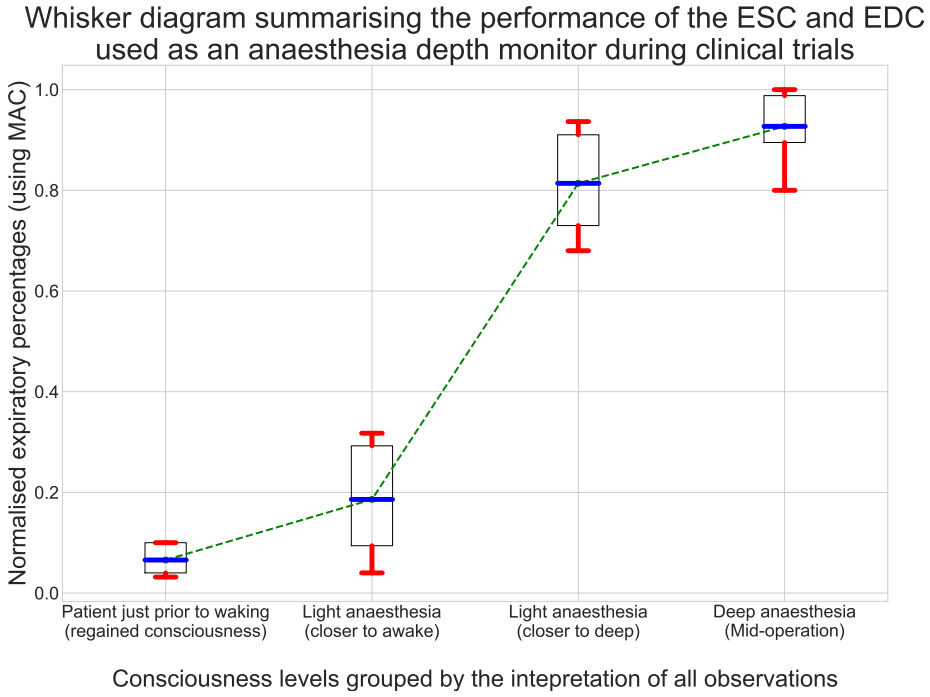

Figure 8.2: The overall performance of the expiratory desflurane and sevoflurane concentrations (normalised to their corresponding MAC value) to differentiate between the perceived conciousness groupings.

From the figure it becomes evident that although, for the cases of the patients measured, it is easy to differentiate between deep anaesthesia and a patient regaining conciousness, the sharp gradient and nature of the sigmoid make it difficult to differentiate between light anaesthesia groups from the former two groupings. The linear response of Fig. 8.1b therefore shows even more promise for addressing this downside through the use of expiratory values as a monitor of consciousness.

Possibly one of the largest limitations to the use of expiratory anaesthetic concentrations, is the fact that it can only be monitored during the use of vapour-type anaesthetics (such as desflurane and sevoflurane). Such a limitation means that the approach is not universal and can not be used in intravenous general anaesthetic applications. The only method currently recommended to monitor total intravenous anaesthesia (TIVA), with agents such as propofol and remifentanil, is the BIS. This points back to the shortcomings of Section 8.2 and reiterates the importance of a more universal consciousness monitoring

technique.

The following section discusses the case of the work in this investigation, in contrast to the limited BIS and expiratory monitoring.

8.4 Notation on the sample perspective

One may question the validity of only using the four MLAEP plots, for each of the four trial patients, to draw conclusive findings. For the sake of perspective, each of the four evoked potential plots presented, for each patient in Chapter 7, is itself a composition of between approximately 960 to 4800 period averages (or 8 Hz stimulus periods of between two and ten minutes, depending on the spike cleaning algorithm employed in Chapter 6 as well as the observed changes in the gradient of anaesthesia levels at that stage). Furthermore, every one of these averaged individual periods, contains 250 samples (each deriving from a 24-bit ADC resolution sampled at a rate of 2 kHz), which brings the total sample number composition of the deep anaesthesia's MLAEPs (from a ten minute recording during the stable mid-surgery anaesthesia levels) to about 1.2 million.

Every characteristic of the evoked potentials, as a result, should be observed as an average of numerous data points rather than a single period entity or characteristic. This larger perspective, of the average nature of each of the plots presented, gives greater credibility to the individual findings, and therefore, the overall summary of results.

8.5 A potentially better measure of consciousness

Auditory evoked potentials (AEPs), being more than merely an empirical or observational approach, have the potential to be utilised in the first feasible and universal anaesthesia monitoring device. The analysis of an AEP, delving deeper than the frequency observation of the BIS, gives an indication of the patient's mind's ability to process and be aware (or "be conscious") of the auditory stimulus. Although some patient-to-patient variations may be expected, the theoretical background thereof is constant. With the invention of machine learning, come a number of potential innovations for its application, which may include the analysis of in-ear AEPs to rigidly and accurately monitor consciousness. The more detailed implications thereof, to the future of research aligned with this thesis, are discussed in Section 8.6.

Due to the average-natured derivation of evoked potentials, the effects of EMI are attenuated to a negligible extent. The frequency of stimulation can be chosen to ensure that the frequency from the mains (being 50 Hz in South Africa) is averaged out over time. Such narrow-band EMI sources can alternatively be filtered out, using non-phase-distorting forward-reverse filters, as done in this project. The approach, in which a stereo-channel and Bluetooth audio device were utilised, to simultaneously provide audi-

tory stimulus and period synchronous ability, is unique to this dissertation. This provided the ability to streamline the averaging method using the designed algorithms from Chapter 6.

The easily and simultaneously streamable (with an additional WiFi unit not used in this thesis) synchronous signal and in-ear EEG data, mean that a relatively real-time MLAEP could be derived from the averaged data of a chosen past time-duration. The longer the past time-duration, the more the averaging algorithm will be able to remove other noise within the signal and zero in on the clean evoked potential. Inversely, the shorter the time-duration, the more real-time the evoked potentials become, at the expense of a larger noise presence. This trade-off is something that needs to be analysed, in detail, with further research.

In this thesis, a compromise between between real-time capability and signal quality was achieved by using a minimum data segment of two minutes (so in real-time terms it corresponds to the past two minutes) and applying a low-pass filter to remove any resilient high-frequency noise.

8.6 The future of anaesthesiology

It was observed in Fig. 8.1, that the alone latency of P_a outperformed a BIS system that has been optimised to determine consciousness in such an industry. An enticing thought as to where the future of the findings in this study may lead. If the P_a latency, alone, gives such a strong correlation to perceived levels of conciousness, imagine where a potential future machine learning system (that incorporates all the parameters) could lead. A system (such as a neural network) that can learn from inputs such as the MLAEP characteristics (latencies, amplitudes and form), in-ear spectral information (like-wise that of the BIS placed on the forehead) and perhaps even accelerometer data from the ear-piece (detecting patient head movements), could become the potential rigid baseline by which consciousness in patients are determined in the future.

The findings, discussed in this chapter, may excite further research in the field and as such, recommendations for further investigations are given in Chapter 9.

8.7 Summary of contributions

Ultimately the work done in this dissertation contributed to the larger understanding of evoked potentials and specifically so, within the ear. Based on a keywords passed through a search engine and the literature review of Chapter 2, this study is the first of its kind in recording in-ear evoked potentials of patients undergoing anaesthesia. The uniqueness of the approach followed in this thesis, provides useful insight into numerous future implications of like-wise research. The proven verification thereof as a strongly supported

anaesthesia (or consciousness) monitoring device, opens up further research in the field of anaesthesiology.

The implications are, however, not limited to the field of anaesthesiology. Fleet-driver drowsiness monitoring in an insurance setting, general fatigue monitoring for health or productivity research and the use thereof in becoming a wearable biometric identification device (that uses the uniqueness of the in-ear auditory evoked response to verify the wearer's identity) are all directions for further investigation into the potentially limitless opportunities possible.

It has been shown that it is possible to develop a minimally obtrusive in-ear device, that uses the theoretical basis of middle latency auditory evoked potentials, to be used as an accurate measure of consciousness levels (although such consciousness is expiratory anaesthetic concentration and perception based due to the lack of a true baseline). All of the research questions from Chapter 1, have thus been answered in this chapter.

8.8 Conclusion of discussion

This, hereby, concludes the additional discussions of the findings, other than those mentioned between the results and investigations of all of the preceding chapters. The following chapter provides recommendations for future research.

Chapter 9

Recommendations

This chapter gives recommendations to investigators that wish to further pursue this research. Possible other fields, in which the research could be utilised, are mentioned in Section 8.7.

9.1 Signal amplitude considerations

The obtained in-ear auditory evoked potentials had amplitudes that, although expected to be lower than conventional methods under similar signal-to-noise ratio conditions (as provided in the brief literature study of Section 1.6), were somewhat lower than expected. As a result, a low-pass filter was necessary to remove high-frequency noise and distinguish between the characteristic peak latencies. There are, however, various changes that can be considered to increase the amplitude of the evoked potential. The stimulus speaker (adapted from the JBL headphones [62]) volume was set to maximum, but, due to the electromagnetic interference (EMI) isolation design implemented, the sound intensity that ultimately reaches the ear is somewhat attenuated along the acoustic channel and overall route. Design alterations, that maintain EMI isolation whilst allowing for maximum volume from the headphones to reach the ear, may therefore increase evoked potential amplitudes and reduce the need for a low-pass filter. Another method that can be used to ensure maximum measurable amplitude, is to verify that optimal electrode-skin conductivity is obtained.

9.2 Sampling rate of data

After modifications to the Cyton board's firmware (Section 6.3), the maximum achievable sampling rate of EEG data was determined to be 2 kHz. Although this rate is sufficient for a proof-of-concept and probably also for a working end user system, a faster sampling rate would allow for smaller latency changes to be detectable. With the system in this thesis, with the period of sampling being $T_s = \frac{1}{2000\ \text{Hz}} = 0.5$ ms, the minimum step of latency change is one half of a millisecond. Faster sampling rates would allow for smaller detectable changes in latency and therefore possibly indicate even finer changes in con-

sciousness levels. It was, however, discovered that with desflurane and sevoflurane, large latency changes can be expected and the half millisecond intervals are more than sufficient to produce a definitive system.

9.3 Variabilities

The effects of patient variabilities and set-up changes could be investigated. A few examples of this would be to research the effect of:

- different general anaesthetics (both intravenous and vaporous);
- patient sleeping states;
- neurological development disorders (such as Down syndrome and autism);
- patient characteristics (age, build and gender);
- intoxication (alcohol and other mind effecting drugs);
- auditory impairment (therefore altered auditory evoked potentials);
- other stimulus methods (such as somatosensory defined in Chapter 2); and

various other research meaningful parameters on the in-ear evoked potentials. Further tests could be done to define expected changes (or the lack thereof), from the normal in-ear evoked response, of the various effects mentioned.

9.4 Machine learning implications

An in-depth investigation into the use of machine learning methods (such as a neural network), that can be trained by learning from all possible variabilities, could be conducted to produce a rigid consciousness monitoring device. All the parameters and inputs, mentioned in Section 8.6, as well as possible patient specific information (such as age, build and gender) and expiratory anaesthetic values (if available), can be fed into a neural network to, over-time, detect patterns that even the most trained data analysts would never pick up on (without the use of a computerised tool, that is). This could result in an anaesthesia monitoring device, that is truly universal and rigid, being able to become the baseline that the industry has been waiting for.

9.5 Conclusion of recommendations

The recommendations mentioned here, are in the viewpoint of the researcher, the most applicable to prospective future studies. Perhaps a brief final recommendation, although not critical to the functionality thereof, is that all of the circuit components and the general size of the device can be substantially downscaled to streamline the patient set-up and improve wearability. The following chapter concludes the findings of this dissertation.

Chapter 10

Conclusion

Auditory evoked potentials (and specifically the latencies denoted P_a), measured within the ear, showed a strong correlation with the levels of consciousness experienced by a patient undergoing a surgical procedure under general anaesthesia. The designed system showed the potential to outperform the existing bispectral index (BIS) monitor for the patients that formed part of the clinical trials. The findings could be of substantial importance to the design of a conciousness measuring baseline system, which does not yet exist. Therefore, this study encourages further research into such a system in the field of anaesthesiology and possibly into other applications as well.

The research questions have been answered and the problem statement has been addressed. The investigator successfully completed the phases of problem definition, literature analysis, methodical planning, design, implementation, verification, optimisation, ethical and clinical trials, presentation of results and an in-depth discussion of all of the findings. All of the details pertaining to these stages are conveyed in this documentation. The dissertation is thus concluded.

Appendices

Appendix A

Hospital consent form

The following four pages contain the hospital consent form that was provided to the patients prior to testing.

PARTICIPANT INFORMATION LEAFLET AND CONSENT FORM

TITLE OF THE RESEARCH PROJECT:

Design of an in-ear EEG device to provide drowsiness information, anaesthesia levels and responsiveness in order to determine the awareness of a user in a hospital, insurance or healthcare industry.

REFERENCE NUMBER: S18/06/128

PRINCIPAL INVESTIGATOR:
Mr Carel Wessels

ADDRESS:
Office E210, Electrical & Electronic Engineering
Cnr of Banghoek and Bosman
Stellenbosch Central
7600

CONTACT NUMBER:
076 190 8185

You are being invited to take part in a research project. Please take some time to read the information presented here, which will explain the details of this project. Please ask the study staff or doctor any questions about any part of this project that you do not fully understand. It is very important that you are fully satisfied that you clearly understand what this research entails and how you could be involved. Also, your participation is **entirely voluntary** and you are free to decline to participate. If you say no, this will not affect you negatively in any way whatsoever. You are also free to withdraw from the study at any point, even if you do agree to take part.

This study has been approved by the **Health Research Ethics Committee at Stellenbosch University** and will be conducted according to the ethical guidelines and principles of the international Declaration of Helsinki, South African Guidelines for Good Clinical Practice and the Medical Research Council (MRC) Ethical Guidelines for Research.

What is this research study all about?

The study will be conducted at Mediclinic Stellenbosch where a minimum of 3 and maximum of 15 participants will be recruited to take part in the study, depending on statistical requirements. The project aims to build a patient-friendly portable anaesthesia monitoring device to ultimately improve the safety of patients going in and coming out of surgery. The device will later be used in other healthcare industries to provide meaningful feedback. The procedure will require you to wear headphones which contains three EEG electrodes to be placed in contact with both the earlobes and inner-ear of one ear respectively. The device will be used pre-, intra- and post-anaesthesia along with the hospital's measuring devices to read information from the brain activity. During each test cycle an audio test-signal will be played to the patient in the form of

quick click noises. The test will be repeated in the three phases mentioned above to gather information of changing neurological responses. The device will then be easily removed from the patient and any medical conductive paste used with the electrodes can be wiped off with a wet cloth. Pre-cleaning of the inner-ear may be necessary to insure skin contact of the electrode. No randomization process will occur, and no medication will be used.

Why have you been invited to participate?

You are undergoing an anaesthesia surgery/procedure at Stellenbosch Mediclinic.

What will your responsibilities be?

To wear the headphones with EEG electrodes and have the audio stimulus played you during each respective test cycle while undergoing your procedure.

Will you benefit from taking part in this research?

You will not benefit.

Are there in risks involved in your taking part in this research?

You are not at risk.

If you do not agree to take part, what alternatives do you have?

You may continue the procedure as usual without having the extra measuring device connected.

Who will have access to your medical records?

All the neurological information collected will be treated as confidential and protected. Your contribution will remain completely anonymous in all publications and only the project investigator will have access to the information for the research purposes.

What will happen in the unlikely event of some form of injury occurring as a direct result of your taking part in this research study?

The project is registered with the University of Stellenbosch's insurance brokers who have a procedure in which such events can be claimed and the project investigator, Mr C Wessels and study supervisor, Prof PR Fourie will insure compensation claims takes place in the very unlikely event that injury does take place as a direct result of the device under testing.

Will you be paid to take part in this study and are there any costs involved?

No you will not be paid to take part in the study. There will also be no costs involved for you, if you do take part.

Is there any thing else that you should know or do?

All procedures will occur under the supervision of your doctor at Mediclinic Stellenbosch being Dr Johan Lourens.

You can contact Prof PR Fourie at 021-981 1200 if you have any further queries or encounter any problems.

You can contact the Health Research Ethics Committee at 021-938 9207 if you have any concerns or complaints that have not been adequately addressed by your study doctor.

You will receive a copy of this information and consent form for your own records.

Declaration by participant

By signing below, I ……..……. agree to take part in a research study entitled *(insert title of study)*.

I declare that:

- I have read or had read to me this information and consent form and it is written in a language with which I am fluent and comfortable.
- I have had a chance to ask questions and all my questions have been adequately answered.
- I understand that taking part in this study is **voluntary** and I have not been pressurised to take part.
- I may choose to leave the study at any time and will not be penalised or prejudiced in any way.
- I may be asked to leave the study before it has finished, if the study doctor or researcher feels it is in my best interests, or if I do not follow the study plan, as agreed to.

Signed at (*place*) .....……..…….. on (*date*) ……...…….. 2018.

.....	.....
Signature of participant	**Signature of witness**

Declaration by investigator

I *(name)* ……..…… declare that:

- I explained the information in this document to ……..
- I encouraged him/her to ask questions and took adequate time to answer them.

- I am satisfied that he/she adequately understands all aspects of the research, as discussed above
- I did/did not use a interpreter. (*If a interpreter is used then the interpreter must sign the declaration below.*

Signed at (*place*) .....…….. on (*date*) ……...…….. 2018.

....

Signature of investigator **Signature of witness**

Declaration by interpreter

I *(name)* ……..…… declare that:

- I assisted the investigator (*name*) ……. to explain the information in this document to (*name of participant*) ……..…….. using the language medium of Afrikaans/Xhosa.
- We encouraged him/her to ask questions and took adequate time to answer them.
- I conveyed a factually correct version of what was related to me.
- I am satisfied that the participant fully understands the content of this informed consent document and has had all his/her question satisfactorily answered.

Signed at (*place*) .....…….. on (*date*) ……...……..

....

Signature of interpreter **Signature of witness**

Appendix B

Ethical clearance research protocol

Department of Electrical and Electronic Engineering

Master's Thesis Research Protocol

Design of an in-ear EEG device to provide drowsiness information, anaesthesia levels and responsiveness to determine the awareness of a user in a hospital, insurance or healthcare industry.

C Wessels (17708133)

14 April 2018

Study leader	*Supporting Study Leader*
Prof WJ Perold	Prof PR Fourie

I. INTRODUCTION

In-ear electroencephalogram (EEG) devices have become increasingly more popular in the later stages of the last decade. Standard on-scalp EEG measuring methods have been around for quite a while, but these sensors become very obtrusive in their placement on the head as well as their numerosity. The time taken to set-up an EEG system on a user has been rather lengthy in the past and thus its feasibility in many fields has been rejected. An in-ear EEG system has the capability of becoming a much less obtrusive way of obtaining and analysing EEG signals that contain almost all the human body muscular, sensory and nervous information and therefore has the potential to provide a large diagnostic ability.

II. AIM

To design an in-ear EEG device that will be able to measure, analyse and process the electrical signals of the brain to provide meaningful insight in anaesthesia application environments. To use machine learning algorithms to intelligently identify characteristics in the signals and the changes thereof to provide such meaningful insight.

III. MOTIVATION

Such a device could offer valuable safety to future patients as the process of anaesthesia is often unpredictable for different patients. Drowsiness information could also be of immeasurable value to insurance companies in the future who wish to know the state of heavy vehicle fleet drivers whom they insure.

IV. RESEARCH PURPOSE

Such a device for such a purpose has in obtainable findings till thus far not been investigated in detail. The study will therefore provide meaningful insight into the feasibility of in-ear EEG devices in the use of medical and healthcare industries with the involvement of anaesthesiologists and related practitioners.

V. LITERATURE REVIEW

EEG has been around for quite some time as evident from [1] where Hans Berger, a researcher from Germany, studied the first human EEG signals 1924 following the discovery of brain tissue electrical activity of rabbits and monkeys in 1875 by physician Richard Caton. In-ear or ear EEG, being a new trend in the field of brain monitoring, provides various advantages over standard on-scalp measurements, but also comes with a cost. There exists a large database of EEG recordings from various medical departments as outlined in [2], but most of these are from conventional 10-20 electrode placement systems as well as not

necessarily having the stimulus being investigated. It therefore thus remains valuable to obtain validating data that is derivative of auditory stimulus (being the chosen method of analysis), ear EEG as well as acquisition during anaesthesia (being the investigation field). It is necessary to have all these factors present during the data to ensure that meaningful results can be obtained.

Automatic sleep monitoring has been done with ear EEG in [3]. The shortcoming of the approach used in this finding was it analysed raw EEG waves and simply looked at the power spectrum of the frequency bands to draw conclusions about sleep states. Nevertheless, the findings were indicative that ear EEG analysis could be used as an indication of sleep/wakefulness but with decreasing accuracy as one introduces sleep states and result in a decision that is more complex than binary. The findings in [4] and [5] are similar and from the same source and shows how auditory evoked potentials measured from the ear can be obtained. These publications compared on-scalp Auditory Evoked Potentials (AEPs) to the same AEPs taken within the ear and substantiates the feasibility of ear EEG as a viable way of obtaining and further researching evoked responses as well as its applications from ear electrodes. The paper [5] does note that one may expect a decreased amplitude in the response obtained from the scalp to the ear (between 10dB to 20dB attenuation) but both have a similar signal to noise ratio which therefore maintains the feasibility of accurately extracting the waveform.

A study done in [6] shows that a certain characteristic feature in AEPs can change in both amplitude and latency from patient to patient. What this means for the current investigation is that one should incorporate a system of reference when analysing such signals from different source patients. In simple terms, a differential AEP waveform input from a baseline measurement may be a better input to a machine learning algorithm than merely a single AEP waveform.

The material in [7] shows various filters, algorithms as well as techniques one should consider in processing EEG signals. It provides the theoretical background, detailed derivations as well examples of both EEG and event related potentials. This information will be of vital importance when optimizing the data analytics algorithms of the designed system. Having obtained an overview of the supporting research in this section, the following section provides the sample selection for this investigation's validation.

VI. SAMPLE

Statistically one shall require a sample number of 39 for a one-correlation test (using a Fisher Z refined algorithm) with an accuracy of 95% (derived from subtracting an type 1 error rate of 5% from 100%) and power goal of 90%. This will be obtainable by having 13 patients with 3 defined states of anaesthesia levels (13 patients × 3 levels/patient = 39 sample entities) with each combination of patient and anaesthesia level being treated as an independent entity on the output side of the statistical analysis. These recommendations were provided by Prof Daan Nel from the Department of Statistics and Actuarial Science of Stellenbosch University.

The 3 defined states of anaesthesia will relate to existing measuring equipment's interpretation of a 'fully awake / pre-anaesthesia', 'mild anaesthesia level' and 'full anaesthesia' patient. The power goal is defined as the probability to reject the null hypothesis for a chosen effect size (between 0.25 and 0.75) with a good value of the power goal being chosen as 90% and never less than 75%. This ultimately results in a viable test to show that the designed system can strongly correlate to existing measurement system (which may be obtrusive to the patient). This substantiates why the one correlation model was selected to validate the system that aims to one-to-one relationally correlate to the existing equipment at Netcare Kuilsriver. Figure 1 below shows the design of the statistical model as done with Prof Daan Nel in Statistica [8].

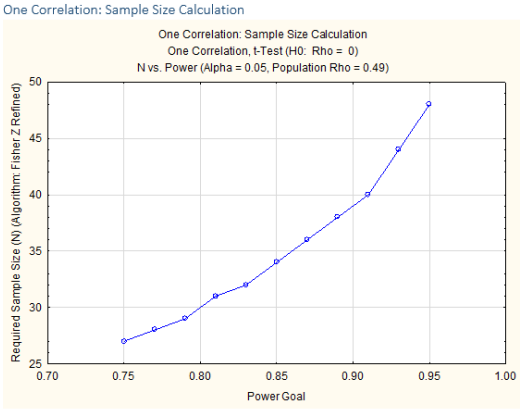

Sample Size Calculation ([No active dataset])

	Sample Size Calculation ([No active
	Value
Population Correlation (Rho)	0.4900
Type I Error Rate (Alpha)	0.0500
Power Goal	0.9000
Actual Power for Required N	0.9030
Required N (Refined Fisher Z)	39.0000

Figure 1: Fisher Z Transformation plots from Statistica

These patients shall all be above the age of 18 undergoing an anaesthesia procedure with Prof AR Coetzee. The sample aim is 13 patients as previously described to insure statistical soundness of the thesis analysis that will follow. All the patients will receive a consent form explaining the procedure to them in detail and all the data gathered from measurements will be treated with absolute confidentiality.

VII. VARIABLES

Basic variable anonymous characteristics such as patient age and gender shall be recorded for the sole purpose of their possible effect on data-analytics outcome and such information shall only be accessible by the principle investigator. The EEG data variable measurements recorded from within the ear will be a potential difference signal in the micro- and nano-volts range. The system ADC (analogue to digital converter) samples the analogue signals using a 24-bit resolution at a frequency of 2 kilohertz. These 24-bit numbers can be converted to a meaningful voltage with knowledge of the reference voltage and gain setting. This leads to the

raw data being a long time-domain chain of microvolt values which without processing may seem noisy and meaningless.

VIII. PROCEDURE

i. *Recruitment and inclusion/ exclusion criteria:* The only criteria necessary is being over the age of 18 and being prepared for surgery at Netcare Kuilsrivier with Prof AR Coetzee in which general anaesthetics (not local) is to be used. The patients will have the option to option out without any medical consequence and will undergo the procedure as per normal.

ii. *Methodology:* The method for the implementation of such a research system and the corresponding recording thereof can be broken up into the following methodical steps.

a. Pre-testing phase:

To adapt a designed in-ear EEG device to be able to detect the drowsiness, anaesthesia levels or awareness of a user or medical patient. The EEG recording device is designed and built with user and patient safety in-mind. This phase is completed before the research and testing phase can commence.

b. Testing and validation phase:

This is where data needs to be obtained from patients and is the reason for ethical application. The process of recording data from a patient once ethical clearance is given will commence with patient identification. Once a patient who is undergoing the appropriate medical procedure is identified at the specified hospital, he/she will be approached with the research opportunity whereby the exact details of the consent form and the option to refuse part-taking therein will be clearly communicated. If the patient agrees to take-part in this anonymous data analytical research, they will be clearly briefed and shown the exact setup of the measuring device before their surgery commences. The patient will also be given a copy of the consent form containing the information needed in the very unlikely event that there is an injury as a direct result of the in-ear EEG device.

On the date of the surgery the patient who has agreed to be a subject for the research will have the EEG headband connected to their head. Measurements will be taken at predetermined intervals throughout the operation commencing before the anaesthesia is applied and terminating after the patient has recovered from anaesthesia. Every test cycle will be clearly allocated to a time interval and the doctor's existing anaesthesia measuring device output at that specific time will be recorded. Once the patient has recovered from anaesthesia and it is deemed appropriate to remove the headband, the patient will be assisted with the removal. The patient will be thanked for their anonymous contribution and offered any post-surgery assistance if need be.

The above process will be repeated on various patients to create the sample size necessary for the statistical conclusions to be drawn within the formal documentation.

c. Machine-learning and validation process:

The data gathered will be partly used to train a machine learning algorithm to intelligently determine the state of anaesthesia for a patient. The algorithm will contain a calibrated signal for an 'awake' or patient not submitted to anaesthesia and monitor learn how this signal changes through the surgery process, specifically focusing on the latency and amplitude of neuron groups being triggered due to the audio stimulus involved. The remainder of the data which will be kept separate from the learning data will be used to verify the machine learning algorithm and produce statistical information. All the findings will be written up in the thesis report and all the patients will remain completely anonymous to any reader thereof.

iii. Measurement:

The designed device will play an audio stimulus in the form of click sounds at a predetermined rate around 8 hertz during the measurement phase. The electrical response of the audio signal being propagated through the neurological pathways will be averaged over time to produce a periodic time-domain waveform. The averaging time ranges from about 2 to 3 minutes in order to average out ambient noise and artefacts. This average waveform as well as the raw data frequency power spectrum can be used as input to the machine learning system. The measurements are recorded with high-resolution analogue-to-digital converters with built-in safety mechanisms that make it impossible to produce any electrical shock to a patient through the electrodes. These converters are also not configured in any way to produce a signal, but instead are solely configured to detect potential difference on a micro level.

iv. Safety Procedures and Design

Throughout the design process the safety of the user was considered. All the electronic circuitry was encapsulated in 3D printed insulated housing, all the wiring was done using shielded and insulated cables and all the soldering joints were insulted with heat-shrink covers. The parts of the headset that meets the head was smoothened and cushioned to provide optimal comfort. The electrodes contain safety circuitry and are thoroughly shielded from external noise. The in-ear electrode contains a layer of memory foam to comfortably take the shape of the patient's specific ear canal. The design has been approved by both Prof PR Fourie and Prof AR Coetzee who are both actively practicing medicine.

IX. DATA MANAGEMENT AND ANALYSIS PLAN

i. Data Management

All the raw and collected data and information will be saved offline on the password protected personal computer of the primary investigator. The data will be anonymous, and so will the findings be of the published thesis.

ii. *Analysis Plan*

The raw data will be first processed via a series of frequency filters to collectively remove DC offsets, remove speaker interference, remove mains interference as well as remove any frequencies that are note related to the auditory evoked potential range. The filtered data is also run through algorithms to remove corrupted data from muscle twitches or other non-related head electrical activity. The raw data is then divided and synchronised into period subsets correlating to the audio stimulus frequency. These data sets are then all averaged together to produce a single low micro- or high nano-volts waveform of stimulus period length (meaning with 8 hertz stimulus the waveform will be 125ms in length). The resulting signal is known as the auditory evoked potential waveform and contains a series of peaks and valleys correlating to the activation of neuron groups (which each produce a small yet detectable electrical ripple) from the eardrum up until auditory cortex where the stimulus is processed.

As the brain is subjected to anaesthesia, these peaks and valleys and the latency thereof is expected to defer from the normal ‘awake’ state and it is this change that will become the foundation of machine learning analysis. The peaks and valleys will reduce in amplitude as the neuron groups become sedated and the latency is expected to increase due to increase in propagation time from group to group. The exact machine learning algorithm used will only be selectable once data is available. The machine learning algorithm will be trained to take an auditory evoked potential waveform (as well as some reference perhaps) as input and output one of three anaesthesia states.

X. CONCLUSION

The data collected can thus be put through statistical testing and validation to outcome the feasibility of such a medical device. This research aims to provide new insight into the field of understanding medical technology and ultimately aims to be beneficial to the healthcare of the society in which it may be implemented. With the advantage of potential inexpensive manufacturing of such devices as well as its portability and reusability it may prove to be especially valuable for the African context where such accessible devices are a scarcity.

BIBLIOGRAPHY

[1] Schmitt, H. J. (2008). History of electroencephalography. *IEEE History of Telecommunications Conference, HISTELCON 2008*, 79–82. https://doi.org/10.1109/HISTELCON.2008.4668719

[2] Veloso, L., McHugh, J., von Weltin, E., Lopez, S., Obeid, I., & Picone, J. (2017). Big data resources for EEGs: Enabling deep learning research. *2017 IEEE Signal Processing in Medicine and Biology Symposium (SPMB)*, 1–3. https://doi.org/10.1109/SPMB.2017.8257044

[3] Nakamura, T., Goverdovsky, V., Morrell, M. J., & Mandic, D. P. (2017). Automatic sleep monitoring using ear-EEG. *IEEE Journal of Transilational Engineering in Health and Medicine*, *5*(June). https://doi.org/10.1109/JTEHM.2017.2702558

[4] Kidmose, P., Looney, D., Ungstrup, M., Rank, M. L., & Mandic, D. P. (2013). A study of evoked potentials from ear-EEG. *IEEE Transactions on Biomedical Engineering*, *60*(10), 2824–2830. https://doi.org/10.1109/TBME.2013.2264956

[5] Kidmose, P., Looney, D., & Mandic, D. P. (2012). Auditory evoked responses from Ear-EEG recordings. *Proceedings of the Annual International Conference of the IEEE Engineering in Medicine and Biology Society, EMBS*, 586–589. https://doi.org/10.1109/EMBC.2012.6345999

[6] Lombard, F. D. (2005). *An investigation of the Auditory P300 Event Related Potential across gender* . Univesity of Pretoria.

[7] Sanei, S., & Chambers, J. (2008). *EEG signal processing*. *Vasa*. John Wiley & Sons, Ltd.

[8] TIBCO Statistica™ | TIBCO Software. (n.d.). Retrieved September 10, 2018, from https://www.tibco.com/products/tibco-statistica

Appendix C

Ethical clearance approval letter

UNIVERSITEIT STELLENBOSCH UNIVERSITY

Health Research Ethics Committee (HREC)

Approval Notice

New Application

09/10/2018

Project ID : 6499

HREC Reference #: S18/06/128

Title: Design of a in-ear EEG device for clinical and health prognosis

Dear Mr Carel Wessels,

The **New Application** received on 13/09/2018 14:54 was reviewed by members of **Health Research Ethics Committee 2 (HREC2)** via **expedited** review procedures on 09/10/2018 and was approved.

Please note the following information about your approved research protocol:

Protocol Approval Period: **This project has approval for 12 months from the date of this letter.**

Please remember to use your **Project ID [6499]** on any documents or correspondence with the HREC concerning your research protocol.

Please note that the HREC has the prerogative and authority to ask further questions, seek additional information, require further modifications, or monitor the conduct of your research and the consent process.

After Ethical Review

Please note you can submit your progress report through the online ethics application process, available at: Links Application Form Direct Link and the application should be submitted to the HREC before the year has expired. Please see *Forms and Instructions* on our HREC website (www.sun.ac.za/healthresearchethics) for guidance on how to submit a progress report.

The HREC will then consider the continuation of the project for a further year (if necessary). Annually a number of projects may be selected randomly for an external audit.

Provincial and City of Cape Town Approval

Please note that for research at a primary or secondary healthcare facility, permission must still be obtained from the relevant authorities (Western Cape Departement of Health and/or City Health) to conduct the research as stated in the protocol. Please consult the Western Cape Government website for access to the online Health Research Approval Process, see: https://www.westerncape.gov.za/general-publication/health-research-approval-process. Research that will be conducted at any tertiary academic institution requires approval from the relevant hospital manager. Ethics approval is required BEFORE approval can be obtained from these health authorities.

We wish you the best as you conduct your research.

For standard HREC forms and instructions, please visit: Forms and Instructions on our HREC website https://applyethics.sun.ac.za/ProjectView/Index/6499

If you have any questions or need further assistance, please contact the HREC office at 021 938 9677.

Yours sincerely,

Francis Masiye,

HREC Coordinator,

Health Research Ethics Committee 2 (HREC2).

National Health Research Ethics Council (NHREC) Registration Number:

REC-130408-012 (HREC1)·REC-230208-010 (HREC2)

*The Health Research Ethics Committee (HREC) complies with the SA National Health Act No. 61 of 2003 as it pertains to health research. The HREC abides by the ethical norms and principles for research, established by the*World Medical Association (2013). Declaration of Helsinki: Ethical Principles for Medical Research Involving Human Subjects*;the South African* Department of Health (2006). Guidelines for Good Practice in the Conduct of Clinical Trials with Human Participants in South Africa (2nd edition); as well as the Department of Health (2015). Ethics in Health Research: Principles, Processes and Structures (2nd edition).

The Health Research Ethics Committee reviews research involving human subjects conducted or supported by the Department of Health and Human Services, or other federal departments or agencies that apply the Federal Policy for the Protection of Human Subjects to such research (United States Code of Federal Regulations Title 45 Part 46); and/or clinical investigations regulated by the Food and Drug Administration (FDA) of the Department of Health and Human Services.

Appendix D

Full software implementation

In-Ear EEG Data Analytics System - Auditory Evoked Potentials

Patient 1

The following Python code and plots thereof demonstrates the ability to retreive meaningful information from in-ear EEG of a anaesthesia patient (Example of patient 1)

Set-up and initialise the plot parameters

In [1]:

```
# IMPORTS
import matplotlib
import matplotlib.pyplot as pl
from cycler import cycler
%matplotlib inline

# Set plot colour scheme
pl.style.use('seaborn-whitegrid')
colors = [
    '#1f77b4', '#ff7f0e', '#2ca02c',
    '#d62728', '#9467bd', '#8c564b',
    '#e377c2', '#7f7f7f', '#bcbd22',
    '#17becf'
]

pl.rcParams['axes.prop_cycle'] = cycler('color', colors)
# pl.rcParams['axes.prop_cycle'] = pl.cycler(color=pl.cm.viridis(np.linspace(0,1,3)))

pl.rcParams['figure.figsize'] = (20,9)
pl.rcParams['axes.titlesize'] = 30   # fontsize of the axes title
pl.rcParams['axes.labelsize'] = 24  # fontsize of the x any y labels
pl.rcParams['xtick.labelsize'] = 18  # fontsize of the x any y labels
pl.rcParams['ytick.labelsize'] = 18  # fontsize of the x any y labels

print("Parameters set")
```

```
Parameters set
```

Generate the audio stimulus and synchronisation signal

In [2]:

```
# generate wav file containing sine waves
# FB36 - 20120617
import math, wave, array
import IPython.display as ipd
from scipy import signal as sig
import numpy as np


pip_len = 0.0001    # pip period = 100us
pip_rate = 8.0      # Hz
duration = 10.0     # How long is the total duration of the audio file
volume_out = 100    # percent
volume_sync = 1     # percent
freq = 1000         # frequency for math function generation

data = array.array('h')      # signed short integer (-32768 to 32767) data
sampleRate = 44100           # of samples per second (standard)
numChan = 2                  # of channels (1: mono, 2: stereo)
dataSize = 2                                # 2 bytes because of using signed short integers => bit depth = 16
numSamplesPerCyc = int(sampleRate / freq)   # determination of samples per cycle
numSamples = int(sampleRate * duration)     # total number of samples

alternating =                1 # Set to 1 if stimulus alternates or 0 if not

# Set text for file generation
if alternating == 1:
    alt_txt = "bipolar"
else:
    alt_txt = "polar"

t_stimulus = np.linspace(0, (1.0)/sampleRate * (duration*sampleRate - 1),int(duration*sampleRate))  # Set the time
sw_square_out = 0.5 * sig.square(2 * np.pi * pip_rate * t_stimulus, duty=pip_len*pip_rate)+0.5      # Set the stim
sw_square_sync = 0.5 * sig.square(2 * np.pi * pip_rate * t_stimulus, duty=100*pip_len*pip_rate)+0.5 # Set the sync

# ---------------------------- Apply the alternating algorithm if appropriate:
if alternating == 1:
    from_high = 0
    flag = 0
    for i in range(numSamples):
        if sw_square_out[i] != 0.0:
            from_high = 1
        else:
            if from_high == 1 and flag == 0:
                flag = 1
                from_high = 0
            elif from_high == 1 and flag == 1:
                flag = 0
                from_high = 0
        if flag == 0:
            sw_square_out[i] = (-1) * sw_square_out[i]
    from_high = 0
    flag = 0
    for i in range(numSamples):
        if sw_square_sync[i] != 0.0:
            from_high = 1
        else:
            if from_high == 1 and flag == 0:
                flag = 1
                from_high = 0
            elif from_high == 1 and flag == 1:
                flag = 0
                from_high = 0
        if flag == 0:
            sw_square_sync[i] = (-1) * sw_square_sync[i]


# ---------------------------- Apply the volume levels to the arrays:
for i in range(numSamples):
    if numChan==2:
        sample = 32767 * float(volume_out) / 100
        sample *= sw_square_out[i]
        data.append(int(sample))
    sample = 32767 * float(volume_sync) / 100
    sample *= sw_square_sync[i]
    data.append(int(sample))


# ---------------------------- Generate the audio file from arrays:
f = wave.open('Audio\SquareWave_' + str(int(pip_rate)) + 'Hz_'+ str(int(duration)) + 's_'+ str(volume_sync).replac
f.setparams((numChan, dataSize, sampleRate, numSamples, "NONE", "Uncompressed"))
f.writeframes(data.tostring())
f.close()
```

```
# ---------------------------- Load playable widget with the notebook:
print("\n\nThe audio file generated is " + 'SquareWave_' + str(int(pip_rate)) + 'Hz_'+ str(int(duration)) + 's_'+
ipd.Audio('Audio\SquareWave_' + str(int(pip_rate)) + 'Hz_'+ str(int(duration)) + 's_'+ str(volume_sync).replace('.
```

```
The audio file generated is SquareWave_8Hz_10s_1SyncVol_2chan_bipolar.wav
```

Out[2]:

0:00 / 0:10

Plot the audio file arrays for software verification

In [3]:

```
pl.rcParams['figure.figsize'] = (20,5)


sw_k = 32767 * float(volume_out) / 100
sw_out = np.multiply(sw_k,sw_square_out)
sw_k = 32767 * float(volume_sync) / 100
sw_sync = np.multiply(sw_k,sw_square_sync)

fig, ax1 = pl.subplots()

period = 20000

sw_out = sw_out[:period]
sw_sync = sw_sync[:period]
t_stim = t_stimulus[:period]

ax1.plot(t_stim, sw_sync,'r',linewidth=2)
ax1.set_xlabel('Time (s)')

# Make the y-axis label, ticks and tick labels match the line color.
ax1.set_ylabel('Synchronisation signal\n(16-bit value)', color='r')
ax1.tick_params('y', colors='r')

ax2 = ax1.twinx()
ax2.plot(t_stim, sw_out,'b',linewidth=2)
ax2.set_ylabel('Audio stimulation signal\n(16-bit value)', color='b')
ax2.tick_params('y', colors='b')

pl.title("Plot showing the duty cycle of the stimulus channels")
fig.tight_layout()

# pl.savefig("C:/Users/Carel/Google Drive/Master's Thesis/Latex Document/Carel Wessels - Master's Thesis/figs/veri
pl.show()
```

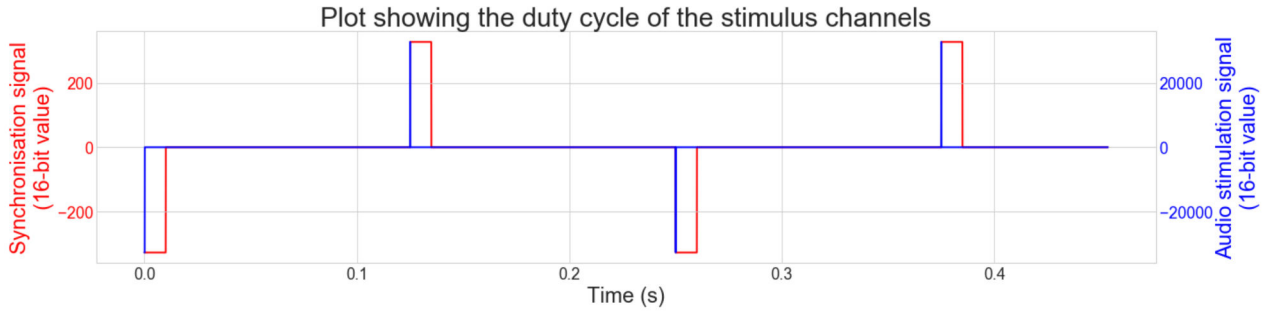

Create code that will streamline the FFT processes for plotting

In [4]:

```
from scipy import signal as sig
from scipy.fftpack import fft, ifft

pl.rcParams['figure.figsize'] = (20,5)

def shift_bit_len(input_data):
    return 1<<(input_data-1).bit_length()

def sym_pad(data, iterations = 1):
    temp_array = data
    for i in range(iterations):
        length = len(temp_array)
        diff = shift_bit_len(length+1) - length
        if length % 2 == 0:
            pad_width = (int(diff / 2),int(diff / 2))
        else:
            left_pad = int(diff/2)
            right_pad = int(diff - left_pad)
            pad_width = (left_pad, right_pad)
        temp_array = np.pad(temp_array,pad_width,'constant')
    return temp_array

N = len(sym_pad(sw_square_sync))
T = 1.0 / sampleRate
yf = fft(sym_pad(sw_square_sync))
xf = np.linspace(0.0, 1.0/(2.0*T) , N//2)

fig = pl.figure()
ax = fig.add_subplot(1, 1, 1)
major_ticks = np.arange(4, 200, 8)
ax.set_xticks(major_ticks)

pl.title('FFT of the bipolar signal for frequency verification')
pl.xlabel('Frequency (Hz)')
pl.ylabel('|Relative Amplitude|')
# pl.ylim([0,0.5])
pl.xlim([0,200])
ax.plot(xf,2.0/N * np.abs(yf[0:N//2]),'g-',linewidth=1)
# pl.savefig("C:/Users/Carel/Google Drive/Master's Thesis/Latex Document/Carel Wessels - Master's Thesis/figs/veri
pl.show()
```

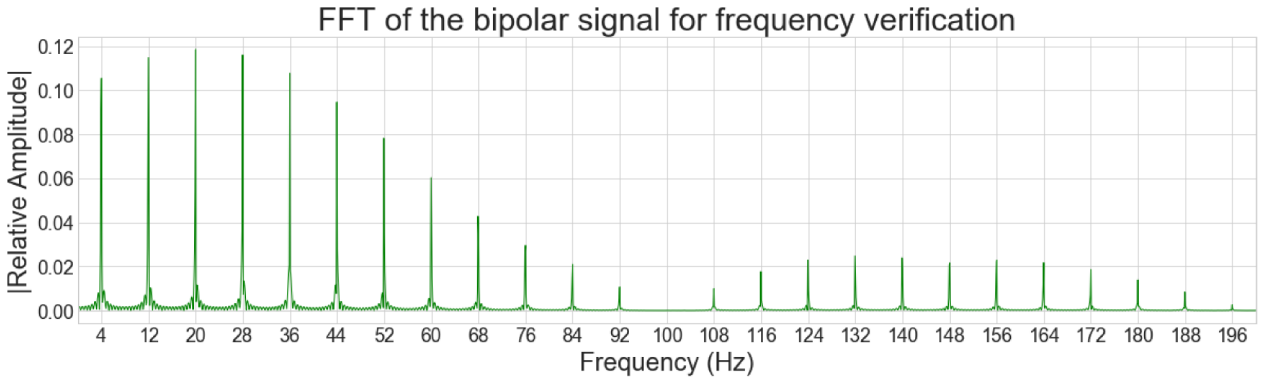

Attempt to play the previously generated audio file in-line

In [5]:
```
import pyaudio, wave
from scipy import signal as sig
import numpy as np

CHUNK_SIZE = 1024
pip_rate = 8.0 #Hz incase previous script not run

def play_wav(wav_filename, chunk_size=CHUNK_SIZE):
    '''
    Play (on the attached system sound device) the WAV file
    named wav_filename.
    '''

    try:
        print('Trying to play file ' + wav_filename)
        wf = wave.open(wav_filename, 'rb')
    except IOError as ioe:
        sys.stderr.write('IOError on file ' + wav_filename + '\n' + \
        str(ioe) + '. Skipping.\n')
        return
    except EOFError as eofe:
        sys.stderr.write('EOFError on file ' + wav_filename + '\n' + \
        str(eofe) + '. Skipping.\n')
        return

    # Instantiate PyAudio.
    p = pyaudio.PyAudio()

    # Open stream.
    stream = p.open(format=p.get_format_from_width(wf.getsampwidth()),
        channels=wf.getnchannels(),
        rate=wf.getframerate(),
                    output=True)

    data = wf.readframes(chunk_size)
    while len(data) > 0:
        stream.write(data)
        data = wf.readframes(chunk_size)

    # Stop stream.
    stream.stop_stream()
    stream.close()

    # Close PyAudio.
    p.terminate()

play_wav("Audio\SquareWave_8Hz_3s_10SyncVol_2chan.wav")

print("Done!")
```

```
Trying to play file Audio\SquareWave_8Hz_3s_10SyncVol_2chan.wav
Done!
```

Initialise parameters for recording

In [7]:
```
duration = 10*60.0 # s
SAMPLE_RATE = 2000.0  # Hz
print("Done - duration changed to " + str(duration) + "s")
```

```
Done - duration changed to 600.0s
```

Define the Cyton board control sequence

In [20]:

```
import serial
import time
import sys
import pdb
import open_bci_v3 as bci

stream_running = False

# Initialise the board
board = bci.OpenBCIBoard(port='COM3',
                                daisy=False,
                                filter_data=True,
                                scaled_output=True,
                                log=False,
                                aux=False)
# Definition of functions
def startLog():
    board.ser_write(b'b')
    global stream_running
    stream_running = True

def stopLog():
    board.ser_write(b's')
    global stream_running
    stream_running = False

# ---------------------------- Output to indicate start
print("\n---------------------------\n")
print("--- Recording Data EEG ----\n")
print("---------------------------\n")


# --------------- WRITE AND READ FEEDBACK-----------------
#---------------------------------------------------------
#---------------- Get User Sample Frequency---------------
choice = input("\n----- Sample Frequency options: -----\n'3' = 2kHz\n'2' = 1kHz\n'1' = 500Hz\n'0' = 250Hz"+ \
    "\nChoice number? --> ")

while choice not in ['0','1','2','3']:
    # ,'4','5','6'
    choice = input("\nPLEASE ENTER A VALID CHOICE (number between 0 and 3)? --> ")
#------------------------END READ-------------------------


# ---------------------------- Wait for user to attach the board (if needed)
for i in range (0,1):
    time.sleep(1)
    sys.stdout.write('\r' + "Waiting for user: " + str(i+1) + " sec." + ' ' * 20)
    sys.stdout.flush()
print("\n")

# ---------------------------- Define sampling frequency changing functions:
def freq2kHz():
    board.ser_write(b'~3')
    time.sleep(0.1)
    if (not stream_running):
        board.print_incoming_text()
def freq1kHz():
    board.ser_write(b'~4')
    time.sleep(0.1)
    if (not stream_running):
        board.print_incoming_text()
def freq500Hz():
    board.ser_write(b'~5')
    time.sleep(0.1)
    if (not stream_running):
        board.print_incoming_text()
def freq250Hz():
    board.ser_write(b'~6')
    time.sleep(0.1)
    if (not stream_running):
        board.print_incoming_text()

# ---------------------------- Set sampling rate:
set_freq = { '3' :freq2kHz,
             '2' :freq1kHz,
             '1' :freq500Hz,
             '0' :freq250Hz,
              }

set_freq[choice]()

```

```
# --------------- WRITE AND READ FEEDBACK-----------------
#---------------------------------------------------------
#---------------- create the SD file and check -----------

board.ser_write(b'H')
# board.ser_write(b'S')

board.print_incoming_text()

startLog()

time.sleep(0.1)

set_freq[choice]()

board.ser_write(b'x1060110Xx2000000Xx3100000Xx4100000Xx5100000Xx6100000Xx7100000Xx8100000X')

# Play the audio stimilus for duration
print("Playing Stimulus and recording data in progress...")
board.ser_write(b'o')

# ----------------------------- Play stimulus if note played externally, otherwise:
# play_wav("Audio\SquareWave_8Hz_180s_2chan.wav")
# ----------------------------- OR Loop the time duration while outputting the time ellapsed:
for i in range (0,int(duration)):
# for i in range (0,(10*60)):
    time.sleep(1)
    sys.stdout.write('\r' + "Recording data: " + str(i+1) + " sec." + ' ' * 20)
    sys.stdout.flush()
print("\n")
# ------------------------------

board.ser_write(b'j')

stopLog()

board.ser_write(b'~~')
board.print_incoming_text()

time.sleep(0.5)
board.disconnect()

#-----------------------END READ-------------------------

print("\n--------------------------\n")
print("-----     EXITING     -----\n")
print("--------------------------\n\n\n")

# ------------------------------------------------------------------------------------------------
#           Test measurements tracking log (file numbers and what was recorded)
# ------------------------------------------------------------------------------------------------

# A5 - A7 are tests with apartment (A7 being exterior to ear test)
# A8 - File with GND
# A9 - File without GND
# AB and AC - Signals full tests with GND attached
# AD and AE signals with speaker EMI improvement (moved to shielded compartment)
# AF, B0 - Signals full tests with GND attached gain at 3 (B1 gain at 24 - error in file) -> B0 falsely had no int
# B2 to B4 - tests with new laptop (connected to skin fully) shows sync interference -> figure_showing_sync_interf
# B5 and B6 -> meaningless data file -> forgot to play altered sync volume audio
# B7 - > signal with reduced sync volume (at 0.1 %)
# B9 and BA -> full tests with 0.1% volume (could not differentiate sync from noise)
# BB and BC -> floating nodes tests with 1% volume (could not differentiate sync from noise)
# BE normal volume
# BF 10% volume
# C0 1% volume
# C1 0.1% volume
# C5
# C8 and C7 -> Electrode and charger fixed
# C9 -> run without audio playing to test weird intermittent jump being obtained
# D1 - One channel / D2 - Two channel on 2 / D3 - Two channel on 8
# D9 - fixed sync with noise (3 minute recording)
# DB - fixed sync with noise (10 minute recording) - Carel - Home
# DC - fixed sync with noise (10 minute recording) - Daniel - office
# DD and DE - fixed sync with noise (10 minute recording) - Carel - Home
# E1 and E2 -> new audio system with 10s sync tests
# E9 first signal with new audio and sync alternation system 10 minutes
```

```
Connecting to V3 at port COM3
Serial established...
OpenBCI V3 8-16 channel
On Board ADS1299 Device ID: 0x3E
```

```
LIS3DH Device ID: 0x33
Firmware: v3.1.0


---------------------------

--- Recording Data EEG ----

---------------------------


----- Sample Frequency options: -----
'3' = 2kHz
'2' = 1kHz
'1' = 500Hz
'0' = 250Hz
Choice number? --> 3
Waiting for user: 1 sec.

Success: Sample rate is 2000Hz
Corresponding SD file OBCI_17.TXT

Playing Stimulus and recording data in progress...
Recording data: 600 sec.

Success: Sample rate is 2000Hz

WARNING:root:serial closed

Closing Serial...

---------------------------

-----     EXITING     -----

---------------------------
```

Read data from file

In [621]:

```
import time
import struct
import numpy as np



SAMPLE_RATE = 2000.0  # Hz
ADS1299_Vref = 4.5  #reference voltage for ADC in ADS1299.  set by its hardware
ADS1299_gain = 24.0  #assumed gain setting for ADS1299.  set by its Arduino code
scale_fac_uVolts_per_count = ADS1299_Vref/float((pow(2,23)-1))/ADS1299_gain*1000000.
scale_fac_accel_G_per_count = 0.002 /(pow(2,4)) #assume set to +/4G, so 2 mG
max_data_step = 500 # maximum difference between two data points
pip_rate = 8.0 # Hz

print("\n---------------------------\n")
print("------ Importing data -----\n")
print("---------------------------\n")

time.sleep(0.1)

# Get the file to be imported from the SD card
input_choice = input("\nPLEASE ENTER THE TEXT FILE HEX NUMBER (EXAMPLE '02' or 'C6')? --> ")

## ----------------------------------------
## To open directly from the SD card use:
## ----------------------------------------
# choice = "G:\OBCI_" + input_choice + ".txt"

## ----------------------------------------
## To open patient file use:
## ----------------------------------------
choice = "C:/Users/Carel/Documents/Patient Data/Patient 1/OBCI_" + input_choice + ".txt"

## ----------------------------------------
## To open back-up test files use:
## ----------------------------------------
# choice = "C:/Users/Carel/Documents/Data Files - Masters/OBCI_" + input_choice + ".txt"

sd_file = open(choice, 'r')
print("Success! Opened file at " + choice + "\n\n")

# Skip all the data up until the second '%STOP AT'
count = 0
while count != 2:
    next_line = sd_file.readline()
    if '%STOP AT' in next_line and count == 0:
        count = 1
    elif '%STOP AT' in next_line:
        count = 2
        sd_file.readline() # Skip the next non-data line

# Get all the data while the lines are full (Only Channel 1)
data_raw = []
data_raw_sync = []
loop = 0
line = sd_file.readline()
while line[51] == ',':#51
    data_raw.append(line[3:9])            #Channel 1 read
    data_raw_sync.append(line[10:16])     #Channel 2 read
#     data_raw_sync.append(line[17:23])   #Channel 3 read
#     data_raw_sync.append(line[24:30])   #Channel 4 read
#     data_raw_sync.append(line[31:37])   #Channel 5 read
#     data_raw_sync.append(line[38:44])   #Channel 6 read
#     data_raw_sync.append(line[45:51])   #Channel 7 read
#     data_raw_sync.append(line[52:58])   #Channel 8 read
    loop += 1
    line = sd_file.readline()

    if len(line) < 5:
        break
sd_file.close()

# Convert Hex values to uV
data_uV = []
sync_uV = []

# Set channel 1 scale factor
ADS1299_gain = 24.0  #assumed gain setting for ADS1299.  set by its Arduino code
scale_fac_uVolts_per_count = ADS1299_Vref/float((pow(2,23)-1))/ADS1299_gain*1000000.

# Convert Channel 1 data
for i in range(0,loop-1):
```

```
    literal_read = data_raw[i]
    onebyte = bytes(bytearray.fromhex(literal_read[0:2]))

    if (struct.unpack('>B',onebyte)[0] > 127):
        pre_fix = 'FF'
    else:
        pre_fix = '00'

    long_byte = pre_fix + literal_read;

    if i == 0:
        try:
            data_uV.append(struct.unpack('>i',bytes.fromhex(long_byte))[0] * scale_fac_uVolts_per_count)
        except:
            data_uV.append(data_uV[i-1])
    else:
        try:
            temp = (struct.unpack('>i',bytes.fromhex(long_byte))[0] * scale_fac_uVolts_per_count)
            if abs(temp-data_uV[i-1]) <= max_data_step:
                data_uV.append(temp)
            else:
                data_uV.append(data_uV[i-1])
        except:
            data_uV.append(data_uV[i-1])
            print("Error reading sync data")

# Set channel 2 scale factor
ADS1299_gain = 1.0  # Setting for ADS1299 for channel 2.  Set by the serial command
scale_fac_uVolts_per_count = ADS1299_Vref/float((pow(2,23)-1))/ADS1299_gain*1000000.

# Convert Channel 2 data (sync signal)
for i in range(0,loop-1):
    literal_read = data_raw_sync[i]
    onebyte = bytes(bytearray.fromhex(literal_read[0:2]))

    if (struct.unpack('>B',onebyte)[0] > 127):
        pre_fix = 'FF'
    else:
        pre_fix = '00'

    long_byte = pre_fix + literal_read

    if i == 0:
        try:
            sync_uV.append(struct.unpack('>i',bytes.fromhex(long_byte))[0] * scale_fac_uVolts_per_count)
        except:
            sync_uV.append(sync_uV[i-1])
    else:
        try:
            temp = (struct.unpack('>i',bytes.fromhex(long_byte))[0] * scale_fac_uVolts_per_count)
            if abs(temp-sync_uV[i-1]) <= max_data_step:
                sync_uV.append(temp)
            else:
                sync_uV.append(sync_uV[i-1])
        except:
            sync_uV.append(sync_uV[i-1])
            print("Error reading sync data")


print("Success! Data imported with "+str(len(data_uV))+" values")

print("\n---------------------------\n")
print("--------- Exiting ---------\n")
print("---------------------------\n")
```

```
---------------------------

------ Importing data -----

---------------------------


PLEASE ENTER THE TEXT FILE HEX NUMBER (EXAMPLE '02' or 'C6')? --> 08
Success! Opened file at C:/Users/Carel/Documents/Patient Data/Patient 1/OBCI_08.txt


Success! Data imported with 1199170 values

---------------------------

--------- Exiting ---------
```

Set-up and initialise the filter functions

In [622]:

```
from scipy import signal as sig
from scipy.fftpack import fft, ifft
import numpy as np
import math

import warnings
warnings.filterwarnings('ignore')
# warnings.filterwarnings('default')


def butter_bandpass(lowcut, highcut, fs, order=4):
    nyq = 0.5 * fs
    low = lowcut / nyq
    high = highcut / nyq
    b, a = sig.butter(order, [low, high], btype='band')
    return b, a

def butter_bandstop(freqs, swings, fs, order=4):
    nyq = 0.5 * fs
    low = (freqs-swings) / nyq
    high = (freqs+swings) / nyq
    b_s, a_s = sig.butter(order, [low, high], btype='bandstop')
    return b_s, a_s

def butter_lowpass(freq, fs, order=4):
    nyq = 0.5 * fs
    high = freq / nyq
    b_l, a_l = sig.butter(order, high, btype='low')
    return b_l, a_l

def butter_lowpass_filter(data, highcut, fs, order=4):
    b, a = butter_lowpass(highcut, fs, order=order)
    # apply forward and reverse filter to align phase
    y = sig.filtfilt(b, a, data)
    return y

def butter_bandpass_filter(data, lowcut, highcut, fs, order=4):
    b_l, a_l = butter_bandpass(lowcut, highcut, fs, order=order)
    # apply forward and reverse filter to align phase
    y = sig.filtfilt(b_l, a_l, data)
    return y

def butter_bandstop_filter(datas, freqs, swings, fs, order=4):
    b_s, a_s = butter_bandstop(freqs, swings, fs, order=order)
    # apply forward and reverse filter to align phase
    ys = sig.filtfilt(b_s, a_s, datas)
    return ys

def shift_bit_len(input_data):
    return 1<<(input_data-1).bit_length()

def sym_pad(data, iterations = 1):
    temp_array = data
    for i in range(iterations):
        length = len(temp_array)
        diff = shift_bit_len(length+1) - length
        if length % 2 == 0:
            pad_width = (int(diff / 2),int(diff / 2))
        else:
            left_pad = int(diff/2)
            right_pad = int(diff - left_pad)
            pad_width = (left_pad, right_pad)
        temp_array = np.pad(temp_array,pad_width,'constant')
    return temp_array

def replaceZeroes(data):
  min_nonzero = np.min(data[np.nonzero(data)])
  data[data == 0] = min_nonzero
  return data

# Sample rate and desired cutoff frequencies (in Hz).
fs = SAMPLE_RATE * 1.0
lowcut = 2.0
highcut = 800 # SAMPLE_RATE/2.1
order =2

print("Done defining filters and padding functions")


```

```
Done defining filters and padding functions
```

Plot the filter transfer functions

In [623]:

```
pl.rcParams['figure.figsize'] = (20,6)

# b_test,a_test = butter_bandpass(lowcut, highcut, fs, order)
# b_test,a_test =  butter_bandstop(50, 2, fs, order)
b_test,a_test = butter_lowpass(100, fs, order)


w, h = sig.freqz(b_test,a_test)

f = w * (2000/(2*math.pi))

fig = pl.figure()
pl.title('Low-pass digital filter frequency response')
ax1 = fig.add_subplot(111)
ax1.set_xscale('log')

# ax1.plot(47.5,-3, 'bo',markersize=12)
ax1.plot(100,-3, 'bo',markersize=12)

# ax1.annotate('$( 48Hz, -3dB )$',
#              xy=(47.5, -3), xycoords='data',
#              xytext=(-250, 0), textcoords='offset pixels',
#              arrowprops=dict(facecolor='blue', shrink=0.2),
#              horizontalalignment='left', verticalalignment='centre',fontsize=20)

ax1.annotate('$(100Hz,-3dB)$',
             xy=(100, -3), xycoords='data',
             xytext=(100, 0), textcoords='offset pixels',
             arrowprops=dict(facecolor='blue', shrink=0.2),
             horizontalalignment='left', verticalalignment='centre',fontsize=20)

major_ticks = [*np.arange(1, 10, 1),*np.arange(10, 100, 10) ,*np.arange(100, 1001, 100)]
# print(major_ticks)
ax1.set_xticks(major_ticks)

pl.plot(f, 20 * np.log10(replaceZeroes(abs(h))), 'b',linewidth=3)
pl.ylabel('Amplitude (dB)\n', color='b')
pl.xlabel('Frequency (Hz)')
pl.ylim([-18,2])
pl.xlim([10,1000])

ax2 = ax1.twinx()
angles = np.unwrap(np.angle(h)) * 57.296

pl.plot(f, angles, 'g',linewidth=3)
pl.ylabel('\nAngle (degrees)', color='g')
pl.grid()

# pl.savefig("C:/Users/Carel/Google Drive/Master's Thesis/Latex Document/Carel Wessels - Master's Thesis/figs/veri

pl.show()

```

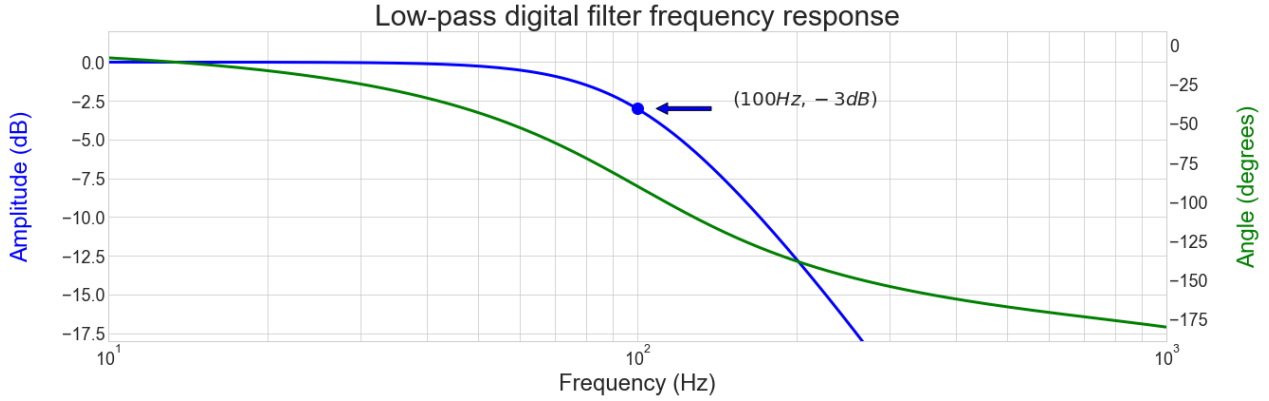

Synchronisation algorithm

In [624]:

```
sync_uV_bandstop=sync_uV
sync_uV_bandpass = butter_bandpass_filter(sync_uV_bandstop,2,800,fs,order)
sync_uV_abs = np.absolute(sync_uV_bandpass)
sync_uV_square = (-1)*np.square(sync_uV_abs)
t = np.linspace(0,(1.0/SAMPLE_RATE)*(len(sync_uV_bandpass)-1),len(sync_uV_bandpass))

# Detect the click positions
period_count = 0
stim_pos=[]
stim_thres = -50000 #uV
stim_grad_thres = 0 #uV
spacing_tolerance = 100 #35


# loop =  len(sync_uV_square)

for i in range(5,loop-15):
    if sync_uV_square[i-1] > stim_thres and sync_uV_square[i] < stim_thres and (sync_uV_square[i-1]-sync_uV_square
        if sync_uV_square[i+1] <= stim_thres: # Test whether duty cycle is correct
            if period_count != 0:
                if (i - stim_pos[period_count-1]) > int((SAMPLE_RATE/pip_rate)-spacing_tolerance):
                    stim_pos.append(i-5)
                    period_count += 1
            else:
                stim_pos.append(i-5)
                period_count += 1

# Plot raw uV data

# data_uV_bandpass = data_uV

print("Done detecting the synchronisation signal")

```

```
Done detecting the synchronisation signal
```

Plot synchronisation signal with detected positions

In [625]:
```
pl.rcParams['figure.figsize'] = (20,9)

pl.figure()
pl.title('Synchronisation signal (after negative of square taken) - Threshold set to -50 000')
pl.xlabel('Time (s)')
pl.ylabel('[Voltage (uV)]$^{2}$')
pl.plot(t,sync_uV_bandpass,'r-',linewidth=1)
pl.plot(np.multiply(stim_pos,(1/SAMPLE_RATE)),np.zeros(period_count),'bo',markersize=12)

pl.legend(['Negative square of absolute sync channel','Detected period start positions'],fontsize=18)

pl.xlim([0,1])
pl.ylim([-1000,1000])

# pl.savefig("C:/Users/Carel/Google Drive/Master's Thesis/Latex Document/Carel Wessels - Master's Thesis/figs/veri

pl.show()
```

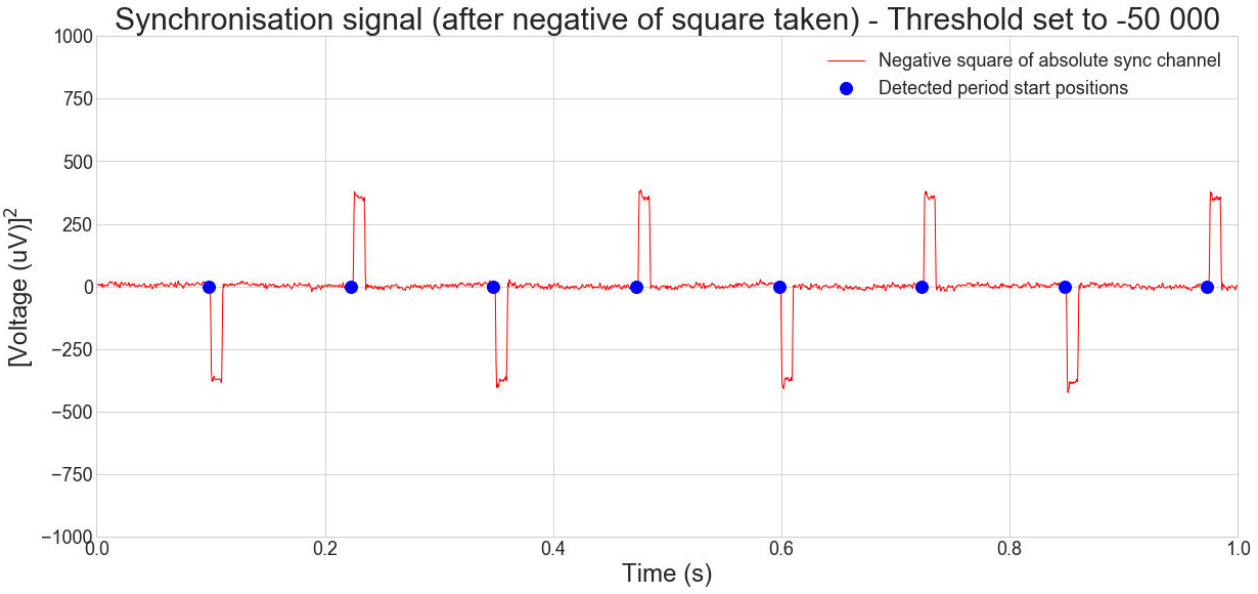

Detect the average frequency of the synchronisation (If close to 8 Hz - verified accurate)

In [626]:
```
sum_periods = 0

for i in range(1,period_count):
    sum_periods = sum_periods + (stim_pos[i]-stim_pos[i-1])*(1/SAMPLE_RATE)

print("\n\nDetected average stimulation frequency = " + str(1/(sum_periods/period_count))+"Hz\n\n")

```

```
Detected average stimulation frequency = 7.999159212462405Hz
```

Plot FFT of sync signal

In [627]:

```
from scipy import signal as sig
from scipy.fftpack import fft, ifft

pl.rcParams['figure.figsize'] = (20,5)

N = len(sym_pad(sync_uV_bandstop))
T = 1.0 / SAMPLE_RATE
yf = fft(sym_pad(sync_uV_bandpass))
xf = np.linspace(0.0, 1.0/(2.0*T) , N//2)

fig = pl.figure()
ax = fig.add_subplot(1, 1, 1)
major_ticks = np.arange(4, 200, 8)
ax.set_xticks(major_ticks)

pl.title('Frequency domain (band-pass filtered sync)')
pl.xlabel('Frequency (Hz)')
pl.ylabel('|Absolute Voltage (uV)|')
# pl.ylim([0,30])
pl.xlim([0,200])
ax.plot(xf,2.0/N * np.abs(yf[0:N//2]),'g-',linewidth=1)
# pl.savefig("C:/Users/Carel/Google Drive/Master's Thesis/Latex Document/Carel Wessels - Master's Thesis/figs/veri
pl.show()
```

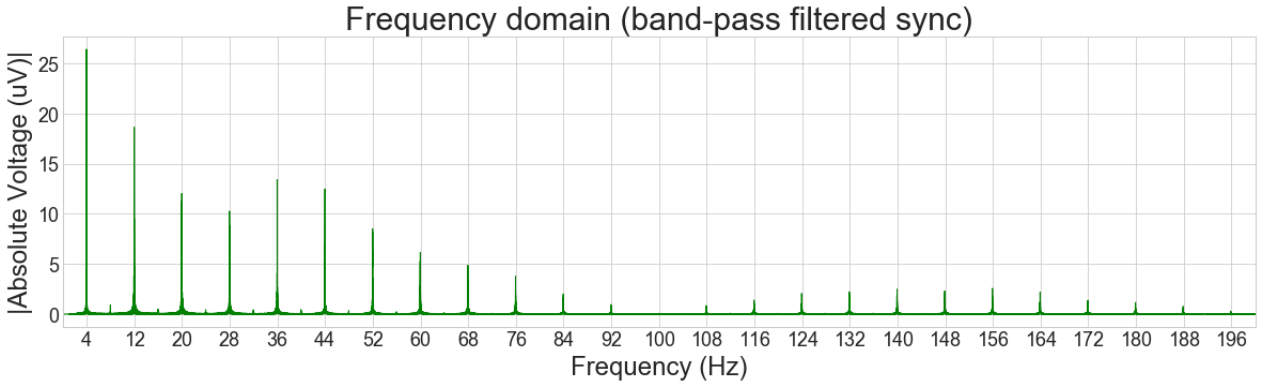

Plot time-domain of the EEG data after band-pass filter

In [628]:

```
pl.rcParams['figure.figsize'] = (20,5)

data_uV_bandpass = butter_bandpass_filter(data_uV, lowcut, 200, fs, order)
data_uV_cut = data_uV_bandpass

t = np.linspace(0,(1.0/SAMPLE_RATE)*(len(data_uV_cut)-1),len(data_uV_cut))
pl.figure()
pl.title('Band-pass filtered raw EEG data read from file')
pl.xlabel('Time (s)')
pl.ylabel('Voltage (uV)')
pl.plot(t,data_uV_cut,'r-',linewidth=0.5)
# pl.ylim([-15,15])
# pl.xlim([0,180])
# pl.savefig("C:/Users/Carel/Google Drive/Master's Thesis/Latex Document/Carel Wessels - Master's Thesis/figs/veri
pl.show()
```

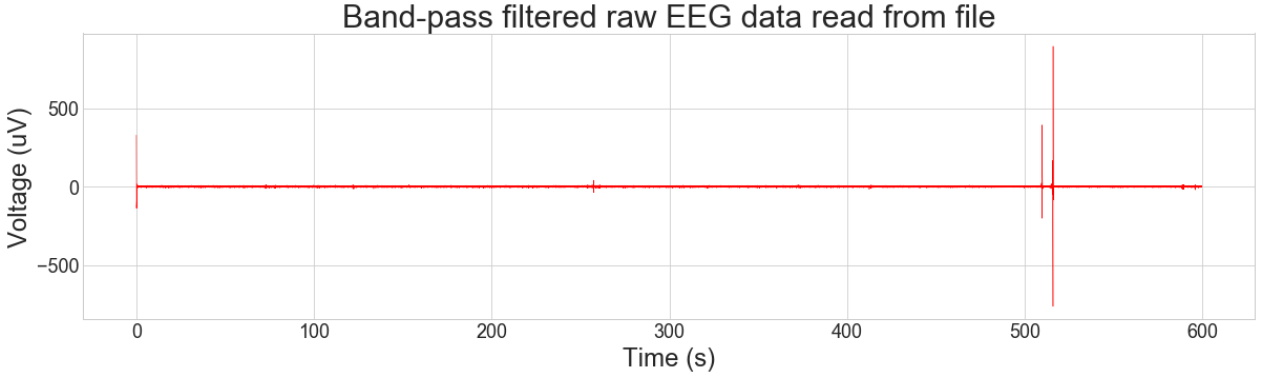

Plot frequency-domain of the EEG data after band-pass

In [629]:
```
N = len(sym_pad(data_uV_cut))
T = 1.0 / SAMPLE_RATE
yf = fft(sym_pad(data_uV_cut))
xf = np.linspace(0.0, 1.0/(2.0*T) , N//2)

pl.figure()
pl.title('FFT of band-passed raw EEG data read from file')
pl.xlabel('Frequency (Hz)')
pl.ylabel('|Voltage (uV)|')
pl.plot(xf,2.0/N * np.abs(yf[0:N//2]),'g',linewidth=1)
pl.xlim([0,200])
# pl.savefig("C:/Users/Carel/Google Drive/Master's Thesis/Latex Document/Carel Wessels - Master's Thesis/figs/veri
pl.show()
```

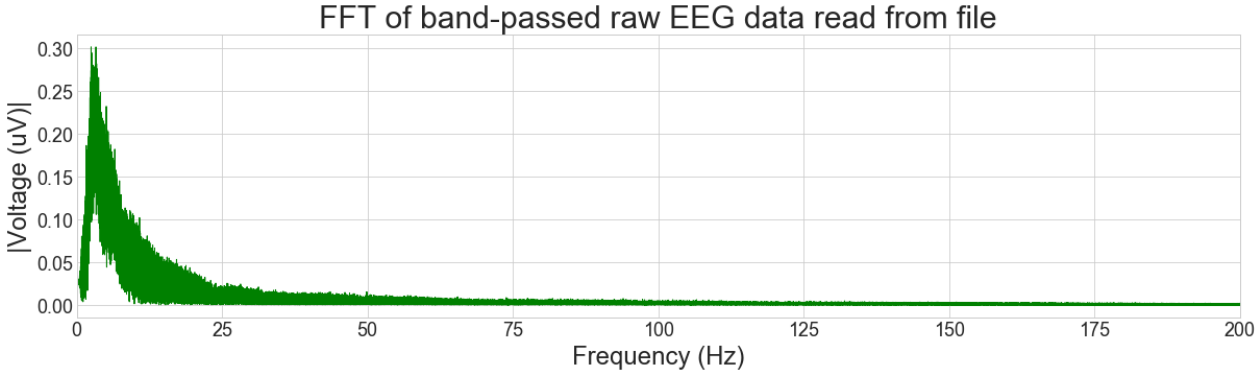

Plot time-domain of the EEG data after notch (if uncommented)

In [630]:
```
data_uv_filtered = data_uV_cut

#APPLY the notch at 50 Hz
# data_uv_filtered = butter_bandstop_filter(data_uV_cut, 50.0 , 1.0, fs, order)

t = np.linspace(0,(1.0/SAMPLE_RATE)*(len(data_uv_filtered)-1),len(data_uv_filtered))

pl.figure()
pl.title('Raw uV EEG Signal from ear')
pl.xlabel('Time (s)')
pl.ylabel('Voltage (uV)')
pl.plot(t,data_uv_filtered,'b-', linewidth=0.5)
pl.show()
```

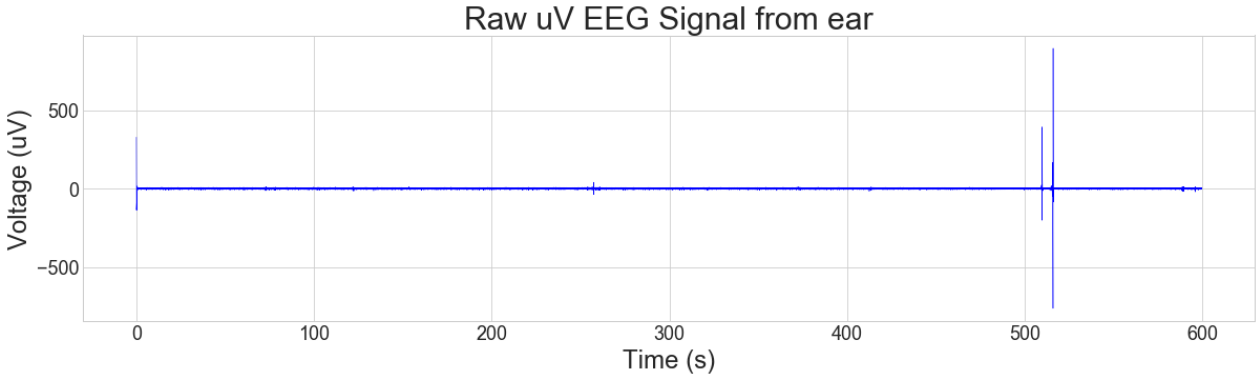

Plot frequency-domain of the EEG data after notch (if uncommented)

In [631]:

```
N = len(sym_pad(data_uv_filtered))
T = 1.0 / SAMPLE_RATE
yf = fft(sym_pad(data_uv_filtered))
xf = np.linspace(0.0, 1.0/(2.0*T) , N//2)

pl.figure()
pl.title('FFT of filtered uV signal')
pl.xlabel('Frequency (Hz)')
pl.ylabel('Absolute Voltage (uV)')
pl.plot(xf,2.0/N * np.abs(yf[0:N//2]),'g-',linewidth=1)
pl.xlim([0, 100])
pl.show()
```

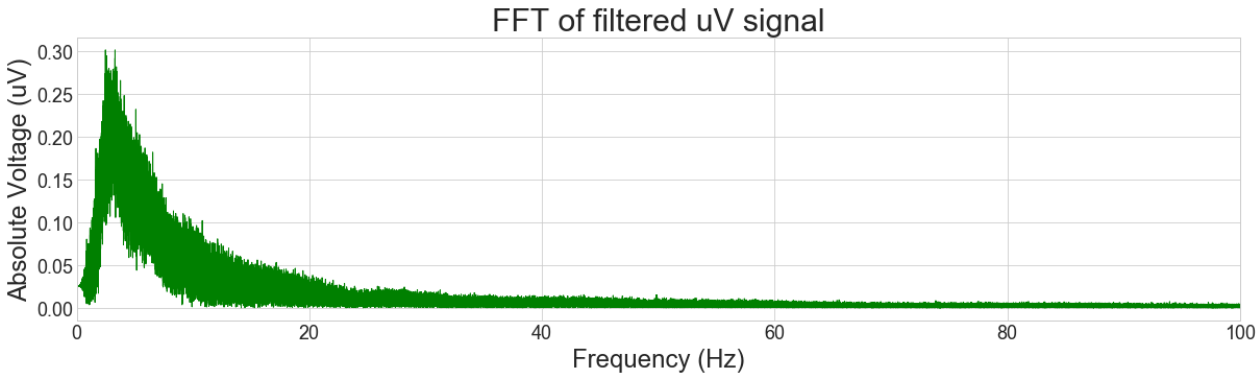

Define and generate the comb filter, plot transfer function and pole-zero plots

In [632]:

```
from scipy import signal as sig
import pylab as pl
import numpy as np
import math

def zplane(zeros, poles):
    """
    Plot the complex z-plane given zeros and poles.
    """
    zeros=np.array(zeros);
    poles=np.array(poles);
    ax = pl.gca()

    # Add unit circle and zero axes
    unit_circle = pl.matplotlib.patches.Circle((0,0), radius=1, fill=False,
                                 color='black', ls='solid', alpha=0.6)
    ax.add_patch(unit_circle)
    pl.axvline(0, color='0.7')
    pl.axhline(0, color='0.7')

    #Rescale to a nice size
    rscale = 1.2 * np.amax(np.concatenate((abs(zeros), abs(poles), [1])))
    pl.axis('scaled')
    pl.axis([-rscale, rscale, -rscale, rscale])

    # Plot the poles and zeros
    polesplot = pl.plot(poles.real, poles.imag, 'x', markersize=9)
    zerosplot = pl.plot(zeros.real, zeros.imag,  'o', markersize=9, color='none',
                            markeredgecolor=polesplot[0].get_color(),
                            )

    #Draw overlap text
    overlap_txt = []

def setup_plot(title, y_label, x_label):
    pl.box(False)
    pl.margins(*(pl.array(pl.margins())+0.05))
    pl.tight_layout()
    pl.title(title)
    pl.ylabel(y_label)
    pl.xlabel(x_label)

a_proto = (1,-0.9)
b_proto = (1,-1)

a_filter = (1,0,0,0,0,0,0,0,0,0,0,0,0,0,0,0,0,0,0,0,0,0,0,0,0,0,0,0,0,0,0,0,0,0,0,0,0,0,0,0,-0.95)#-0.95
b_filter = (1,0,0,0,0,0,0,0,0,0,0,0,0,0,0,0,0,0,0,0,0,0,0,0,0,0,0,0,0,0,0,0,0,0,0,0,0,0,0,0,-1)

z_proto, p_proto,k_proto = sig.tf2zpk(b_proto,a_proto)
z_filter,p_filter,k_filter = sig.tf2zpk(b_filter,a_filter)

pl.rcParams['figure.figsize'] = (12,6)
pl.figure()
pl.subplot(121)
pl.title('pole-zero plot of prototype\n')
zplane(z_proto, p_proto)
pl.subplot(122)
pl.title('pole-zero plot of filter\n')
zplane(z_filter,p_filter)

pl.savefig("C:/Users/Carel/Google Drive/Master's Thesis/Latex Document/Carel Wessels - Master's Thesis/figs/verify

freq_proto = sig.freqz(b_proto,a_proto, whole=True)
freq_filter = sig.freqz(b_filter,a_filter, whole=True)

pl.rcParams['figure.figsize'] = (20,6)

w, h = sig.freqz(b_filter,a_filter, whole=True)
w, h = sig.freqz(b_proto,a_proto, whole=True)

f = w * (2000/(2*math.pi))

fig = pl.figure()
pl.title('Comb digital filter frequency response')
ax1 = fig.add_subplot(111)
ax1.set_xscale('linear')

# ax1.plot(47.5,-3, 'bo',markersize=12)
# ax1.plot(100,-3, 'bo',markersize=12)

# ax1.annotate('$( 48Hz, -3dB )$',
#              xy=(47.5, -3), xycoords='data',
```

```
#             xytext=(-250, 0), textcoords='offset pixels',
#             arrowprops=dict(facecolor='blue', shrink=0.2),
#             horizontalalignment='left', verticalalignment='centre',fontsize=20)

# ax1.annotate('$(100Hz,-3dB)$',
#             xy=(100, -3), xycoords='data',
#             xytext=(100, 0), textcoords='offset pixels',
#             arrowprops=dict(facecolor='blue', shrink=0.2),
#             horizontalalignment='left', verticalalignment='centre',fontsize=20)

major_ticks = np.arange(0, 1000, 50)
# print(major_ticks)
ax1.set_xticks(major_ticks)

pl.plot(f, 20 * np.log10(replaceZeroes(abs(h))), 'b',linewidth=3)
pl.ylabel('Amplitude (dB)\n', color='b')
pl.xlabel('Frequency (Hz)')
pl.ylim([-5,2])
pl.xlim([0,1000])

ax2 = ax1.twinx()
angles = np.unwrap(np.angle(h)) * 57.296

pl.plot(f, angles, 'g',linewidth=3)
pl.ylabel('\nAngle (degrees)', color='g')
pl.grid()

# pl.savefig("C:/Users/Carel/Google Drive/Master's Thesis/Latex Document/Carel Wessels - Master's Thesis/figs/ver

pl.show()
```

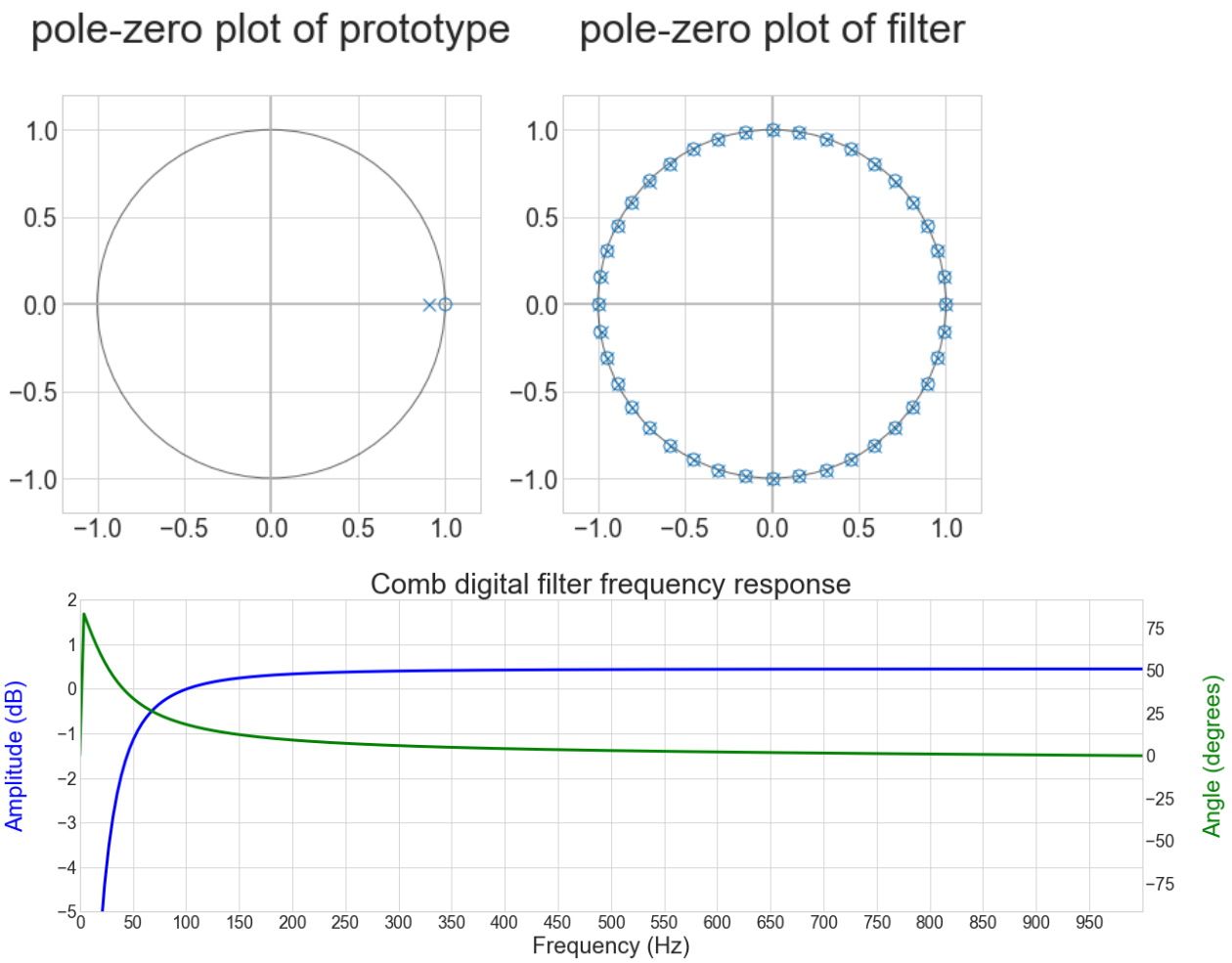

Plot frequency-domain of the EEG data after comb (if uncommented)

In [633]:

```
pl.rcParams['figure.figsize'] = (10,7)


t = np.linspace(0,(1.0/SAMPLE_RATE)*(len(data_uv_filtered)-1),len(data_uv_filtered))
data_uv_filtered = np.random.normal(0,2,len(data_uv_filtered))
data_uv_filtered = butter_bandpass_filter(data_uv_filtered,2,20,SAMPLE_RATE,2)+ 0.09*np.sin(2*np.pi*50*t) + 0.094*
data_uv_filtered = data_uv_filtered + np.random.normal(0,0.2,len(data_uv_filtered))
data_uv_filtered = butter_bandpass_filter(data_uv_filtered,2,250,SAMPLE_RATE,2)

N = len(sym_pad(data_uv_filtered))
T = 1.0 / SAMPLE_RATE
yf = fft(sym_pad(data_uv_filtered))
xf = np.linspace(0.0, 1.0/(2.0*T) , N//2)

data_uv_comb = sig.filtfilt(b_filter,a_filter,data_uv_filtered)
# data_uv_comb = sig.filtfilt(b_filter,a_filter,data_uv_comb)
# data_uv_comb = sig.filtfilt(b_filter,a_filter,data_uv_comb)


# data_uv_comb = butter_lowpass_filter(data_uv_filtered,100,SAMPLE_RATE,4)

## Bypass filters ------------------------------------------------------------------
data_uv_filtered = data_uV_cut
data_uv_filtered = butter_bandstop_filter(data_uv_filtered, 50, 1, SAMPLE_RATE, order=4)
data_uv_comb = data_uv_filtered

## ---------------------------------------------------------------------------------
pl.figure()
pl.title('Frequency-domain before and after comb \nfilter for mains harmonic components')
pl.xlabel('Frequency (Hz)')
pl.ylabel('|Voltage (uV)|')
# pl.ylim([0,10])
pl.xlim([0,320])
pl.plot(xf,2.0/N * np.abs(yf[0:N//2]),'b-',linewidth=1)
yf = fft(sym_pad(data_uv_comb))
pl.plot(xf,2.0/N * np.abs(yf[0:N//2]),'r-',linewidth=1)
pl.legend(['Before comb','After comb'],fontsize=18)
# pl.savefig(
#     "C:/Users/Carel/Google Drive/Master's Thesis/Latex Document/Carel Wessels - Master's Thesis/figs/verify/filt
pl.show()
```

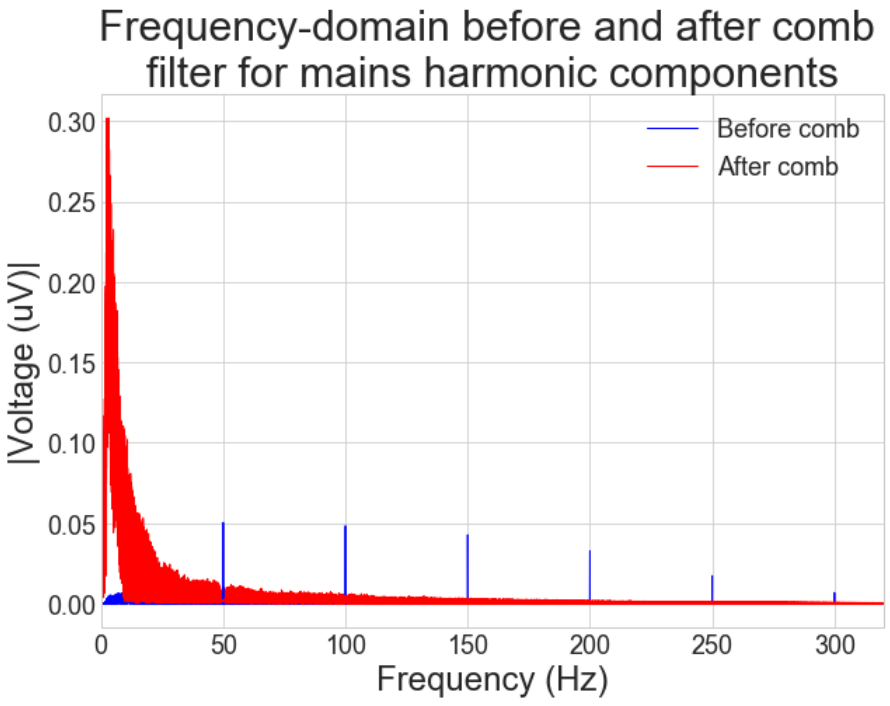

Plot time-domain of the EEG data after comb (if applied)

In [634]:

```
t = np.linspace(0,(1.0/SAMPLE_RATE)*(len(data_uv_comb)-1),len(data_uv_comb))

pl.rcParams['figure.figsize'] = (20,7)
pl.rcParams['figure.figsize'] = (10,7)

pl.figure()
pl.title('Plot of full data stream before cleaning algorithm is applied')
pl.title('Time-domain before and after comb \nfilter for mains harmonic components')
pl.xlabel('Time (s)')
pl.ylabel('Voltage (uV)')
pl.plot(t,data_uv_filtered,'b-', linewidth=1)
pl.plot(t,data_uv_comb,'r-', linewidth=2)
pl.xlim([47,47.5])
# pl.savefig("C:/Users/Carel/Google Drive/Master's Thesis/Latex Document/Carel Wessels - Master's Thesis/figs/veri
# pl.savefig("C:/Users/Carel/Google Drive/Master's Thesis/Latex Document/Carel Wessels - Master's Thesis/figs/veri
pl.show()
```

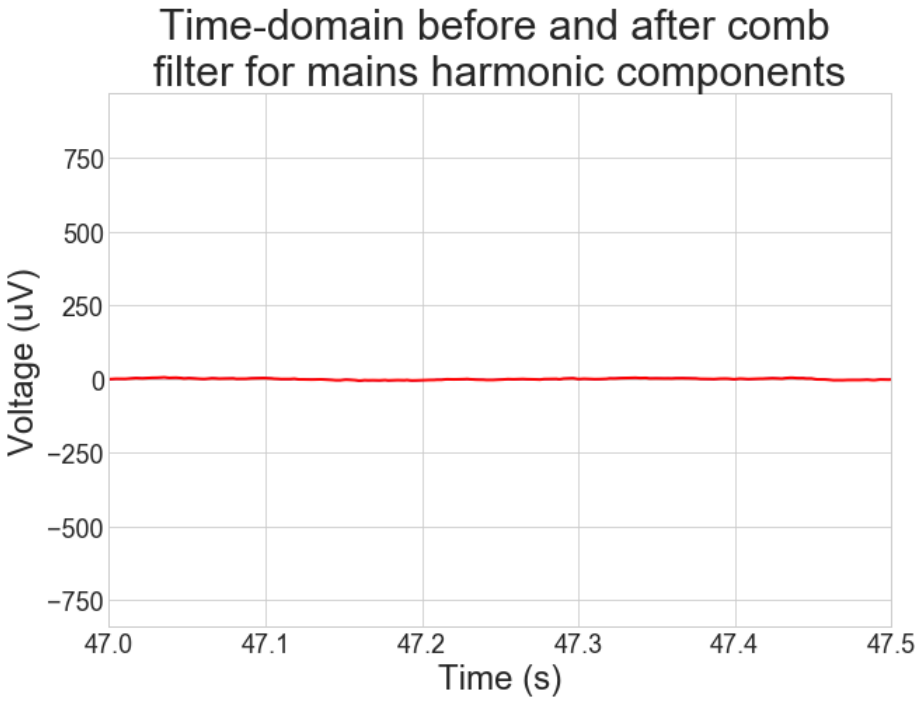

Old unused code that produced unsynchronised AEPs due to the lack of a synchronisation signal

In [635]:

```
#---------------------------------------------------

# Old code for averaging that contains clock drift

#---------------------------------------------------

# import numpy as np

# ave_len = int(SAMPLE_RATE/pip_rate)
# average_uV=np.zeros(ave_len)
# ave_num = 0 # How many periods are added to the average array to divide by ave_num at the end
# ave_count_full = 0 # count of all average data samples
# ave_count=0 # count of all average data samples minus the noisy spike-containing waveforms
# ave_range=500
# ave_thres=ave_range*2

# data_uv_ave=data_uv_comb[0:len(data_uv_comb)-20000]

# local_min=0
# local_max=0

# data_uV_cleaned = []
# local_mins = []
# pos_mins = []
# pos=0

# while ave_count_full < np.floor(len(data_uv_ave)-(ave_len)): # while there is still an averaging period ahead
#     local_min = data_uv_ave[ave_count_full]
#     local_max = data_uv_ave[ave_count_full]

#     for i in range(0,ave_len-1):
#         if data_uv_ave[ave_count_full] > local_max:
#             local_max = data_uv_ave[ave_count_full]
#         if data_uv_ave[ave_count_full] < local_min:
#             local_min = data_uv_ave[ave_count_full]
#             pos = ave_count_full
#         ave_count_full += 1

#     if local_min <= -750:
#         local_mins.append(local_min)
#         pos_mins.append(pos)

#     if (local_max-local_min)<ave_thres and local_max < ave_range and local_min > (-ave_range):
#         ave_count_full = ave_count_full - (ave_len-1)
#         for i in range(0,ave_len-1):
#             average_uV[i]=average_uV[i]+data_uv_ave[ave_count_full]
#             data_uV_cleaned.append(data_uv_ave[ave_count_full])
#             ave_count+=1
#             ave_count_full+=1
#         ave_num += 1

# average_uV=np.divide(average_uV,ave_num)

# t = np.linspace(0,(1.0/SAMPLE_RATE)*(len(data_uV_cleaned)-1),len(data_uV_cleaned))

# pl.figure()
# pl.title('Raw uV EEG Signal from ear')
# pl.xlabel('Time (s)')
# pl.ylabel('Voltage (uV)')
# pl.plot(t,data_uV_cleaned,'b-', linewidth=0.5)
# pl.show()

```

Define the used pip_rate for validation use

In [636]:

```
pip_rate = 8.0 # Hz

# print(len(data_uv_comb))
# print(ave_num)
```

Apply averaging and cleaning to the EEG data

In [810]:

```
#---------------------------------------------------------
# Code for implementing averaging on the filtered data
#---------------------------------------------------------
import numpy as np                                          # Import the numpy array library

start_time = int(len(data_uv_comb)*(1/3))                   # Define the start time in sample number terms
end_time = int(len(data_uv_comb)*(3/3))                     # Define the end time in sample number terms

ave_len_max = int(SAMPLE_RATE/pip_rate)+10                  # Define the maximum allowable period sample length
ave_len_min = int(SAMPLE_RATE/pip_rate)-10                  # Define the minimum allowable period sample length
average_uV = np.zeros(ave_len_max)                          # Initialise a length max array of zeroes for the evoked
ave_num = np.zeros(ave_len_max)                             # Array to track how many periods are added to average_u
ave_range=10.0                                              # Maximum threshold offset in uV from zero (remove spike
ave_thres=ave_range*2                                       # Maximum (max - min) range for any period in uV (remove
cut_periods = 5                                             # The amount of periods to cut from start and end (filte
data_uV_cleaned = []                                        # Empty array to hold all the cleaned data from start_ t

data_uv_ave=data_uv_comb                                    # Select data to be averaged (This case comb filter outp

local_min=0                                                 # Initialise local period minimum
local_max=0                                                 # Initialise local period mamimum

for i in range(0,period_count-2-cut_periods):
    local_max=data_uv_ave[stim_pos[cut_periods+i]]          # Redefine local period maximum to first value in a peri
    local_min=data_uv_ave[stim_pos[cut_periods+i]]          # Redefine local period minimum to first value in a peri

    # Test that the period lies within the start and end time specified
    if stim_pos[cut_periods+i] >= start_time and stim_pos[cut_periods+i+1] <= end_time:

        # Find the local minimum and maximum for the period and store into the variables
        for j in range(stim_pos[cut_periods+i],stim_pos[cut_periods+i+1]):
            if data_uv_ave[j] > local_max:
                local_max = data_uv_ave[j]
            if data_uv_ave[j] < local_min:
                local_min = data_uv_ave[j]

        # Test whether the data for period's range falls within the desired "spikeless" range, if so add to arrays
        if (local_max-local_min) < ave_thres and local_max < ave_range and local_min > (-ave_range):
            pos = 0
            if (stim_pos[cut_periods+i+1] - stim_pos[cut_periods+i]) < ave_len_max and (stim_pos[cut_periods+i+1]
                                                stim_pos[cut_periods+i]) > ave_len_min:
                for j in range(stim_pos[cut_periods+i],stim_pos[cut_periods+i+1]):
                    average_uV[pos]=average_uV[pos]+data_uv_ave[j]
                    ave_num[pos] += 1
                    data_uV_cleaned.append(data_uv_ave[j])
                    pos += 1

# Cut the average_uV array to only include index values that contain more than a thousand values
for i in range(0,len(ave_num)):
    if ave_num[i] <= 1000:
        ave_num = ave_num[:i]
        average_uV = average_uV[:i]
        break

# Divide the summed signals by the number of signals in each index to obtain the evoked potential average
average_uV = np.divide(average_uV,ave_num)

print("Done averaging - Evoked Potential Ready")


```

```
Done averaging - Evoked Potential Ready
```

Plot cleaning of the EEG data

In [811]:

```
t = np.linspace(0,(1.0/SAMPLE_RATE)*(len(data_uV_cleaned)-1),len(data_uV_cleaned))

pl.rcParams['figure.figsize'] = (20,7)

pl.figure()
pl.title('Plot of full data stream after cleaning algorithm is applied')
pl.xlabel('Time (s)')
pl.ylabel('Voltage (uV)')
pl.plot(t,data_uV_cleaned,'b-', linewidth=1)
# pl.xlim([47,47.5])
# pl.savefig("C:/Users/Carel/Google Drive/Master's Thesis/Latex Document/Carel Wessels - Master's Thesis/figs/veri
pl.show()
```

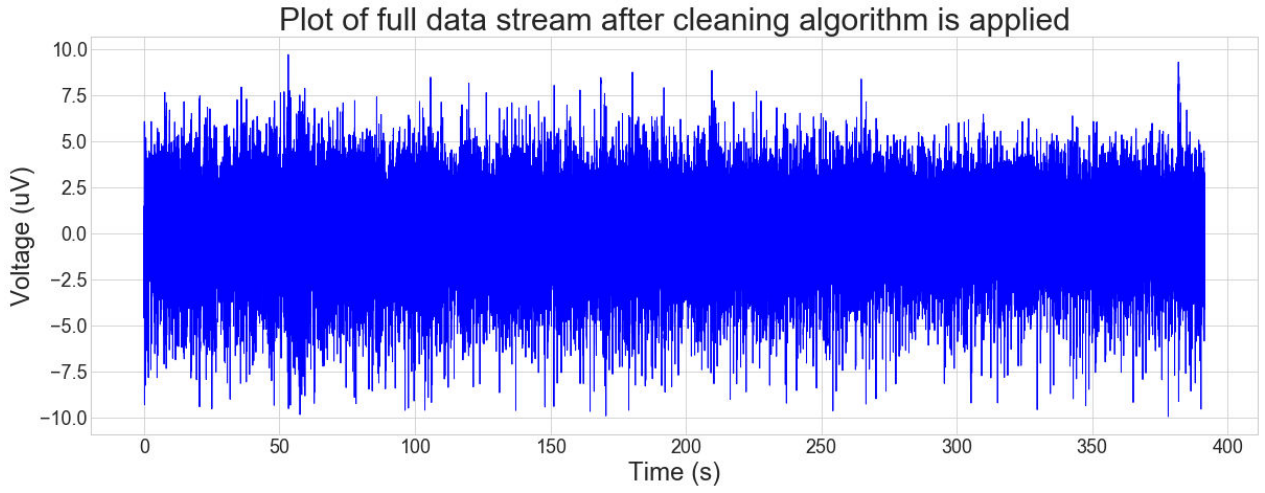

Apply averaging and cleaning to the Synchronisation data

In [812]:

```
#-------------------------------------------------
# Updated code for above cell implementing sync on filtered sync
#-------------------------------------------------

import numpy as np

ave_len_max = int(SAMPLE_RATE/pip_rate)+10
ave_len_min = int(SAMPLE_RATE/pip_rate)-10
sync_average_uV = np.zeros(ave_len_max)
ave_num = np.zeros(ave_len_max) # How many periods are added to the average array to divide by ave_num at the end
ave_range=2000.0
ave_thres=ave_range*2
cut_periods = 5
sync_uV_cleaned = []

sync_uv_ave=sync_uV_abs

local_min=0
local_max=0

for i in range(0,period_count-2-cut_periods):
    local_max=sync_uv_ave[stim_pos[cut_periods+i]]
    local_min=sync_uv_ave[stim_pos[cut_periods+i]]

    for j in range(stim_pos[cut_periods+i],stim_pos[cut_periods+i+1]):
        if sync_uv_ave[j] > local_max:
            local_max = sync_uv_ave[j]
        if sync_uv_ave[j] < local_min:
            local_min = sync_uv_ave[j]

    if (local_max-local_min) < ave_thres and local_max < ave_range and local_min > (-ave_range):
        pos = 0
        if (stim_pos[cut_periods+i+1] - stim_pos[cut_periods+i]) < ave_len_max and (stim_pos[cut_periods+i+1] - st
            for j in range(stim_pos[cut_periods+i],stim_pos[cut_periods+i+1]):
                sync_average_uV[pos]=sync_average_uV[pos]+sync_uv_ave[j]
                ave_num[pos] += 1
                sync_uV_cleaned.append(sync_uv_ave[j])
                pos += 1

for i in range(0,len(ave_num)):
    if ave_num[i] <= 1000:
        ave_num = ave_num[:i]
        sync_average_uV = sync_average_uV[:i]
        break

sync_average_uV = np.divide(sync_average_uV,ave_num)

print("Done averaging - Sync average ready")

```

```
Done averaging - Sync average ready
```

Plot cleaning to the sync data

In [813]:

```
t = np.linspace(0,(1.0/SAMPLE_RATE)*(len(sync_uV_cleaned)-1),len(sync_uV_cleaned))

pl.figure()
pl.title('Raw uV EEG Signal from ear')
pl.xlabel('Time (s)')
pl.ylabel('Voltage (uV)')
pl.plot(t,sync_uV_cleaned,'b-', linewidth=0.5)
pl.show()
```

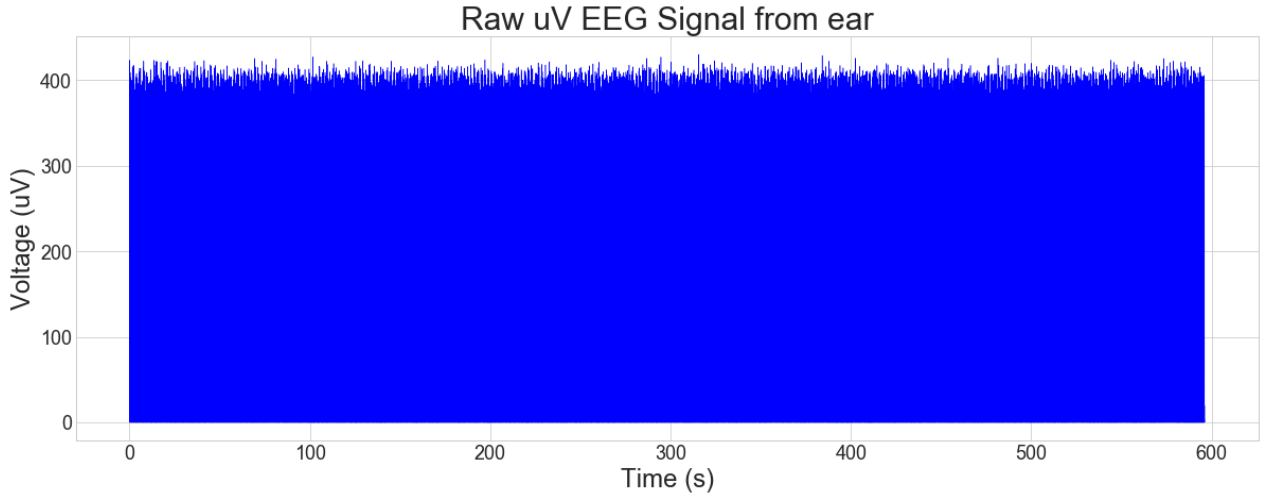

In [859]:

```
# ------------------------------------------------------------------------------------------
# ------------------------------ Time arrays for averages  -----------------------------------
#-------------------------------------------------------------------------------------------

t_av = np.linspace(0,(1.0/SAMPLE_RATE)*(len(average_uV)-1),len(average_uV))
t_av_sync = np.linspace(0,(1.0/SAMPLE_RATE)*(len(sync_average_uV)-1),len(sync_average_uV))

#-------------------------------------------------------------------------------------------
# ------------------------------ Variables to set output -------------------------------------
#-------------------------------------------------------------------------------------------

shift_back = 5                  # time shift to align the start position of stimulus to 0 (using sync average calcu
highcut = 50                    # lowpass filter set to 50 Hz cut off
pos_change = 33                 # time at which low-pass filter is applied in the AEPs

#-------------------------------------------------------------------------------------------
# ------------------------------ Compare sync steps ------------------------------------------
#-------------------------------------------------------------------------------------------

# shift1Sync = np.append(sync_average_uV[shift_back:],sync_average_uV[:shift_back])
# t_av_sync1 = t_av_sync

# shift2Sync = np.append(sync_average_uV[shift_back:],sync_average_uV[:shift_back])
# t_av_sync2 = t_av_sync

# shift3Sync = np.append(sync_average_uV[shift_back:],sync_average_uV[:shift_back])
# t_av_sync3 = t_av_sync

#-------------------------------------------------------------------------------------------
# ------------------------------ Compare AEPs       ------------------------------------------
#-------------------------------------------------------------------------------------------

# average1uV = average_uV
# shift1uV = np.append(average1uV[shift_back:],average1uV[:shift_back])
# sample1uV = np.append(shift1uV[0:pos_change],butter_lowpass_filter(shift1uV[pos_change:],highcut,fs,5))
# sample1t = t_av

# average2uV = average_uV
# shift2uV = np.append(average2uV[shift_back:],average2uV[:shift_back])
# sample2uV = np.append(shift2uV[0:pos_change],butter_lowpass_filter(shift2uV[pos_change:],highcut,fs,5))
# sample2t = t_av

# average3uV = average_uV
# shift3uV = np.append(average3uV[shift_back:],average3uV[:shift_back])
# sample3uV = np.append(shift3uV[0:pos_change],butter_lowpass_filter(shift3uV[pos_change:],highcut,fs,5))
# sample3t = t_av

# average4uV = average_uV
# shift4uV = np.append(average4uV[shift_back:],average4uV[:shift_back])
# sample4uV = np.append(shift4uV[0:pos_change],butter_lowpass_filter(shift4uV[pos_change:],highcut,fs,5))
# sample4t = t_av

# average5uV = average_uV
# shift5uV = np.append(average5uV[shift_back:],average5uV[:shift_back])
# sample5uV = np.append(shift5uV[0:pos_change],butter_lowpass_filter(shift5uV[pos_change:],highcut,fs,5))
# sample5t = t_av

#-------------------------------------------------------------------------------------------
# ------------------------------    Plot average period     ---------------------------------
#-------------------------------------------------------------------------------------------

fig=pl.figure()
ax1 = fig.add_subplot(111)
pl.title('BAEP (first 10ms) and MLAEP response - Patient 1')
pl.xlabel('Time (ms)')
pl.ylabel('Voltage (uV)')


# pl.plot(sample1t*1000,-sample1uV,'g-', linewidth=3)
# pl.plot(sample2t*1000,-sample2uV,'g-', linewidth=3)
# pl.plot(sample3t*1000,-sample3uV,'g-', linewidth=3)
# pl.plot(sample4t*1000,-sample4uV,'g-', linewidth=3)

#-------------------------------------------------------------------------------------------
# ------------------------------    Annotations             ---------------------------------
#-------------------------------------------------------------------------------------------

ax1.plot(44.0,0.045294481097411333, 'bo',markersize=12)
ax1.annotate('$P_a$',
             xy=(44.0,0.045294481097411333), xycoords='data',
             xytext=(-50, 50), textcoords='offset pixels',
             arrowprops=dict(facecolor='blue', shrink=0.2),
```

```
            horizontalalignment='center', verticalalignment='bottom',fontsize=24)

ax1.plot(15.5,-0.02857058365494162, 'bo',markersize=12)
ax1.annotate('$N_a$',
            xy=(15.5,-0.02857058365494162), xycoords='data',
            xytext=(0, -50), textcoords='offset pixels',
            arrowprops=dict(facecolor='blue', shrink=0.2),
            horizontalalignment='center', verticalalignment='top',fontsize=24)

ax1.plot(85.0,-0.03459880747489874, 'bo',markersize=12)
ax1.annotate('$N_b$',
            xy=(85.0,-0.03459880747489874), xycoords='data',
            xytext=(50, -50), textcoords='offset pixels',
            arrowprops=dict(facecolor='blue', shrink=0.2),
            horizontalalignment='center', verticalalignment='top',fontsize=24)

# ax1.annotate('BAEP',
#              xy=(0.01*1000,0.2), xycoords='data',
#              xytext=(-50, 20), textcoords='offset pixels',fontsize=20)

# pl.legend(['BAEP (first 10ms) / MLAEP (remainder)','Characteristic MLAEP points'],fontsize=18)

#-------------------------------------------------------------------------------------------------
# ------------------------------    Show figure             ----------------------------------
#-------------------------------------------------------------------------------------------------
ax1.plot([44.0,44.0],[-1,1], 'r--',markersize=1)
ax1.plot([85.0,85.0],[-1,1], 'm--',markersize=1)

pl.ylim([np.min(-sample2uV)-0.05,np.max(-sample2uV)+0.05])
pl.xlim([0,125])

pl.rcParams['figure.figsize'] = (20,6)

# pl.savefig('Figures/in_ear_first_clinical_test_no_offsets.pdf')
# pl.savefig("C:/Users/Carel/Google Drive/Master's Thesis/Latex Document/Carel Wessels - Master's Thesis/figs/resu

pl.show()
```

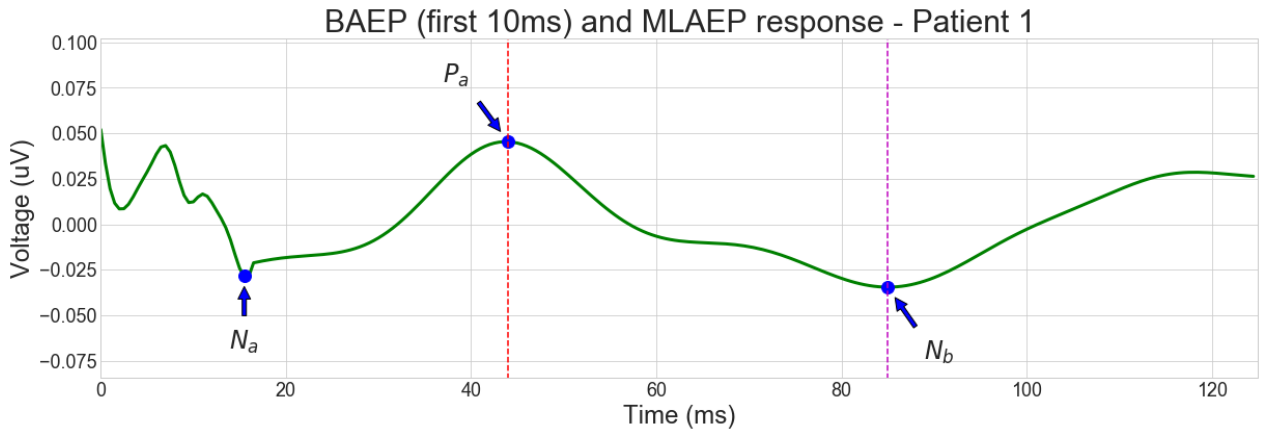

Detect the local and maximums within a time range (to find P_a and N_a etc)

In [855]:

```
# Find local max and minimums

signal_in = -sample2uV
time_in = sample2t
time_start = 10
time_end = 50

first = 1
for i in range(0,len(signal_in)-1):
    if (0.5)*i >= time_start and (0.5)*i <= time_end:
        if first == 1:
            time_max = (1/2)*i
            amp_max = signal_in[i]
            first = 0
        else:
            if signal_in[i]>amp_max:
                time_max = (1/2)*i
                amp_max = signal_in[i]

print("Max time: " + str(time_max))
print("uV value: " + str(amp_max))
print(""+str(time_max)+","+str(amp_max)+"\n\n")

first = 1
for i in range(0,len(signal_in)-1):
    if (0.5)*i >= time_start and (0.5)*i <= time_end:
        if first == 1:
            time_min = (1/2)*i
            amp_min = signal_in[i]
            first = 0
        else:
            if signal_in[i]<amp_min:
                time_min = (1/2)*i
                amp_min = signal_in[i]

print("Min time: " + str(time_min))
print("uV value: " + str(amp_min))
print(""+str(time_min)+","+str(amp_min)+"")
```

```
Max time: 44.0
uV value: 0.045378468353022644
44.0,0.045378468353022644


Min time: 15.5
uV value: -0.02857058365494162
15.5,-0.02857058365494162
```

All the other plots of the results are done below

In [856]:

```
N = len(sym_pad(data_uV_cleaned))
T = 1.0 / SAMPLE_RATE
yf = fft(sym_pad(data_uV_cleaned))
xf = np.linspace(0.0, 1.0/(2.0*T) , N//2)

y_freq = 2.0/N * np.abs(yf[0:N//2])

max_value = np.max(y_freq)
for i in range(0,len(y_freq)):
    if y_freq[i] == max_value:
        freq_max = x_freq[i]

print("Max frequency at " + str(freq_max) + "Hz")

delta = 0
d_n = 0
theta = 0
t_n = 0
alpha = 0
a_n = 0
beta = 0
b_n = 0
gamma = 0
g_n = 0

for i in range(0,len(y_freq)):
    if xf[i] < 4:
        delta = delta + y_freq[i]
        d_n = d_n + 1
    elif xf[i] < 8:
        theta = theta + y_freq[i]
        t_n = t_n + 1
    elif xf[i] < 13:
        alpha = alpha + y_freq[i]
        a_n = a_n + 1
    elif xf[i] < 30:
        beta = beta + y_freq[i]
        b_n = b_n + 1
    elif xf[i] < 50:
        gamma = gamma + y_freq[i]
        g_n = g_n + 1

total = (delta/d_n)+(theta/t_n)+(alpha/a_n)+(beta/b_n)+(gamma/g_n)
print(str(delta/d_n)+','+str(theta/t_n)+','+str(alpha/a_n)+','+str(beta/b_n)+','+str(gamma/g_n))
print(str(delta/d_n/total)+','+str(theta/t_n/total)+','+str(alpha/a_n/total)+','+str(beta/b_n/total)+','+str(gamma


pl.figure()
pl.title('FFT')
pl.xlabel('Frequency (Hz)')
pl.ylabel('Absolute Voltage (uV)')
pl.plot(xf,y_freq,'g-',linewidth=1)
pl.xlim([0, 100])
pl.show()
```

```
Max frequency at 1.6727479414900617Hz
0.021860999297241196,0.02633388624474373,0.022550872925885618,0.009357641351429085,0.004228354668506601
0.25922618864050956,0.31226536676112226,0.26740666149838394,0.1109622515061291,0.05013953159385521
```

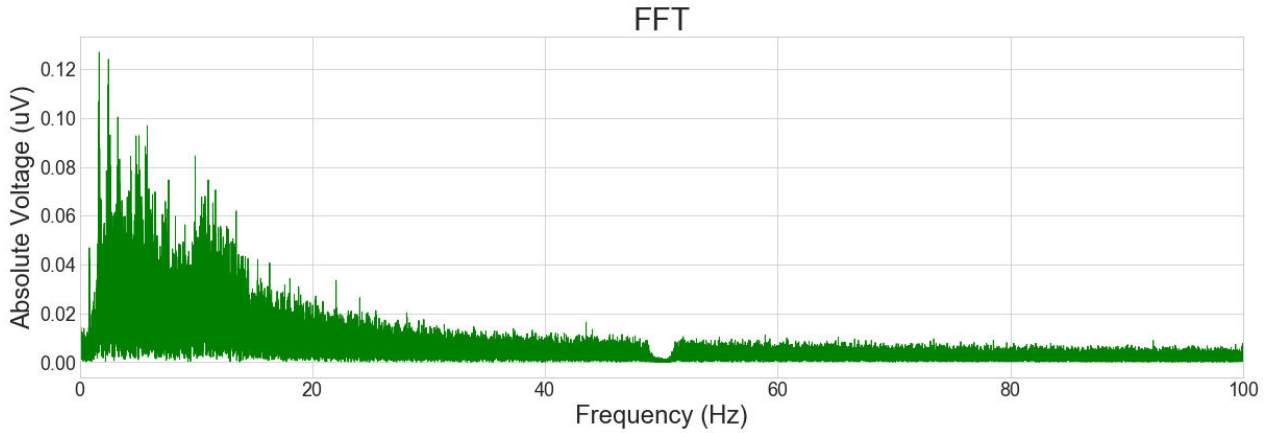

In [2]:

```
import numpy as np
# Patient 1 data

Na=[17.5,15.0,15.5,11]
Pa=[83.0,49.0,44.0,26.5]
Nb=[124.0,88.0,85.0,65.5]
BIS=[43,50,52,62]
Pa_m_Nb=[0.024992514623068587+0.030981192215155134,0.06572740614964405+0.0041625380529621316,0.045294325947411333
perc=[1.9,1.7,0.23,0.1]

freq=[3.4389561442492376,5.130777608447282,1.720431748260018,1.6727479414900617]

d=[0.014677638461527047,0.012736960378200036,0.022292202535397744,0.01789244969228331]
t=[0.019410019776513486,0.017683396024146477,0.02717918023104369,0.021206448317451696]
a=[0.013436033387957581,0.013974906736738284,0.01871692338800389,0.019567444221121236]
b=[0.005357632594949195,0.005475963130179157,0.007887844598124036,0.008111754820991518]
g=[0.002315864016845413,0.002358900396197936,0.003575100049104262,0.003672553530442008]

tot=np.add(d,t)
tot=np.add(tot,a)
tot=np.add(tot,b)
tot=np.add(tot,g)

# d=np.divide(d,tot)
# t=np.divide(t,tot)
# a=np.divide(a,tot)
# b=np.divide(b,tot)
# g=np.divide(g,tot)

# Max frequency at 3.4389561442492376Hz - BIS 43
# 0.014677638461527047,0.019410019776513486,0.013436033387957581,0.005475963130179157,0.002315864016845413

# Max frequency at 10.0040626603368Hz - BIS 50
# 0.012736960378200036,0.017683396024146477,0.013974906736738284,0.005357632594949195,0.002358900396197936

# Max frequency at 1.720431748260018Hz - BIS 52
# 0.022292202535397744,0.02717918023104369,0.019567444221121236,0.007887844598124036,0.003575100049104262

# Max frequency at 1.6727479414900617Hz - BIS 62
# 0.01789244969228331,0.021206448317451696,0.01871692338800389,0.008111754820991518,0.003672553530442008



# Nb=Nb/(np.min(Nb))
# Pa=Pa/(np.min(Pa))

pl.rcParams['figure.figsize'] = (15,7)

fig=pl.figure()


# ---------------------------------------------------------------------
# ------------------- Bands vs BIS / perc
# ---------------------------------------------------------------------
# pl.title('Frequency band relative power change against BIS readings')
# pl.xlabel('BIS (%)')
# pl.ylabel('|Average spectrum amplitude|')

# pl.plot(BIS,d, 'go--',linewidth=3,markersize=12)
# pl.plot(BIS,t, 'bo--',linewidth=3,markersize=12)
# pl.plot(BIS,a, 'ro--',linewidth=3,markersize=12)
# pl.plot(BIS,b, 'mo--',linewidth=3,markersize=12)
# pl.plot(BIS,g, 'co--',linewidth=3,markersize=12)

# pl.legend(['delta','theta','alpha','beta','gamma'],fontsize=24)
# pl.xlim([40, 70])

# pl.savefig("C:/Users/Carel/Google Drive/Master's Thesis/Latex Document/Carel Wessels - Master's Thesis/figs/resu

# ---------------------------------------------------------------------
# ------------------- Na/Pa/Nb vs BIS / perc
# ---------------------------------------------------------------------
pl.title('Latency of characteristic points plotted against ESC readings')
pl.xlabel('ESC (%)')
pl.ylabel('Latency or difference (ms)')

pl.plot(perc,Na, 'go--',linewidth=3,markersize=12)
pl.plot(perc,Pa, 'bo--',linewidth=3,markersize=12)
pl.plot(perc,Nb, 'ro--',linewidth=3,markersize=12)
pl.plot(perc,np.subtract(Nb,Pa), 'mo--',linewidth=3,markersize=12)
pl.plot(perc,np.subtract(Pa,Na), 'co--',linewidth=3,markersize=12)

```

```
pl.legend(['$N_a$','$P_a$','$N_b$','$N_b - P_a$','$P_a - N_a$'],fontsize=24)
pl.xlim([0, 2.5])

# pl.savefig("C:/Users/Carel/Google Drive/Master's Thesis/Latex Document/Carel Wessels - Master's Thesis/figs/resu
pl.show()

# ------------------------------------------------------------------
# ------------------- Na/Pa/Nb vs BIS perc
# ------------------------------------------------------------------

# pl.title('Latency of characteristic points plotted against BIS readings')
# pl.xlabel('BIS (%)')
# pl.ylabel('Latency or difference (ms)')

# pl.plot(BIS,Na, 'go--',linewidth=3,markersize=12)
# pl.plot(BIS,Pa, 'bo--',linewidth=3,markersize=12)
# pl.plot(BIS,Nb, 'ro--',linewidth=3,markersize=12)
# pl.plot(BIS,np.subtract(Nb,Pa), 'mo--',linewidth=3,markersize=12)
# pl.plot(BIS,np.subtract(Pa,Na), 'co--',linewidth=3,markersize=12)

# pl.legend(['$N_a$','$P_a$','$N_b$','$N_b - P_a$','$P_a - N_a$'],fontsize=24)
# pl.xlim([40, 70])

# pl.savefig("C:/Users/Carel/Google Drive/Master's Thesis/Latex Document/Carel Wessels - Master's Thesis/figs/resu
# pl.show()

```

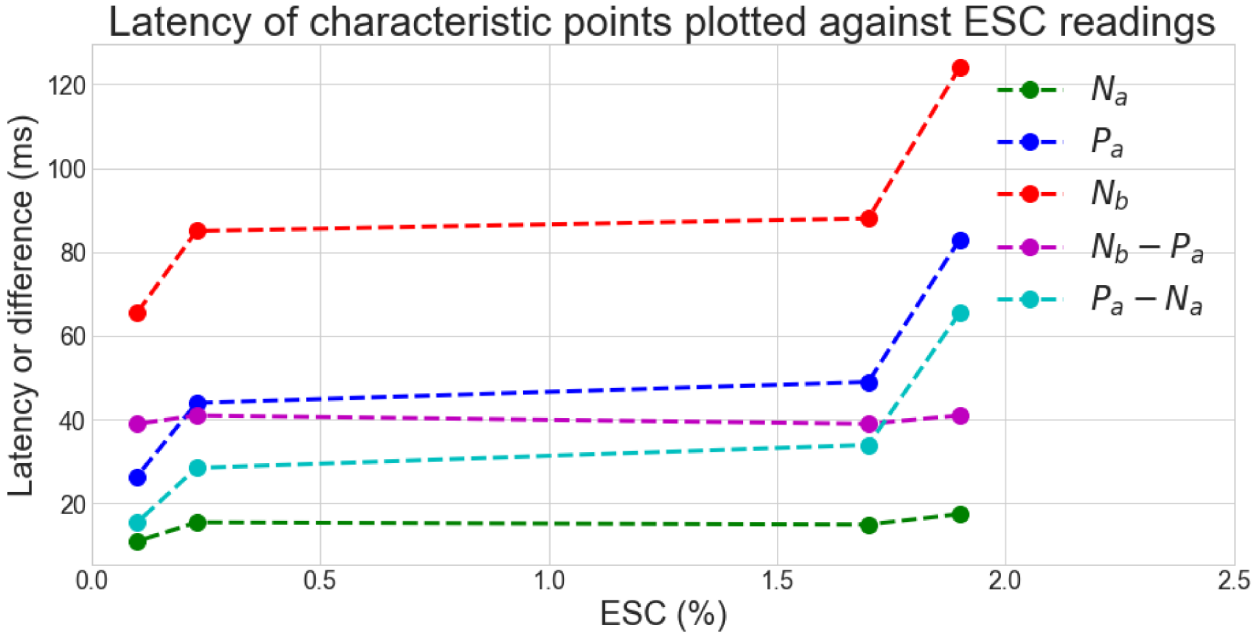

In [18]:

```
# ----------------------------------------------------------------------
# ------------------- BIS vs perc
# ----------------------------------------------------------------------

pl.rcParams['figure.figsize'] = (20,7)

pl.title('Expiratory sevoflurane plotted against the BIS readings')
pl.xlabel('BIS (%)')
pl.ylabel('ESC (%)')

pl.plot(BIS,perc, 'mo--',linewidth=3,markersize=12)

# pl.savefig("C:/Users/Carel/Google Drive/Master's Thesis/Latex Document/Carel Wessels - Master's Thesis/figs/resu
pl.show()
```

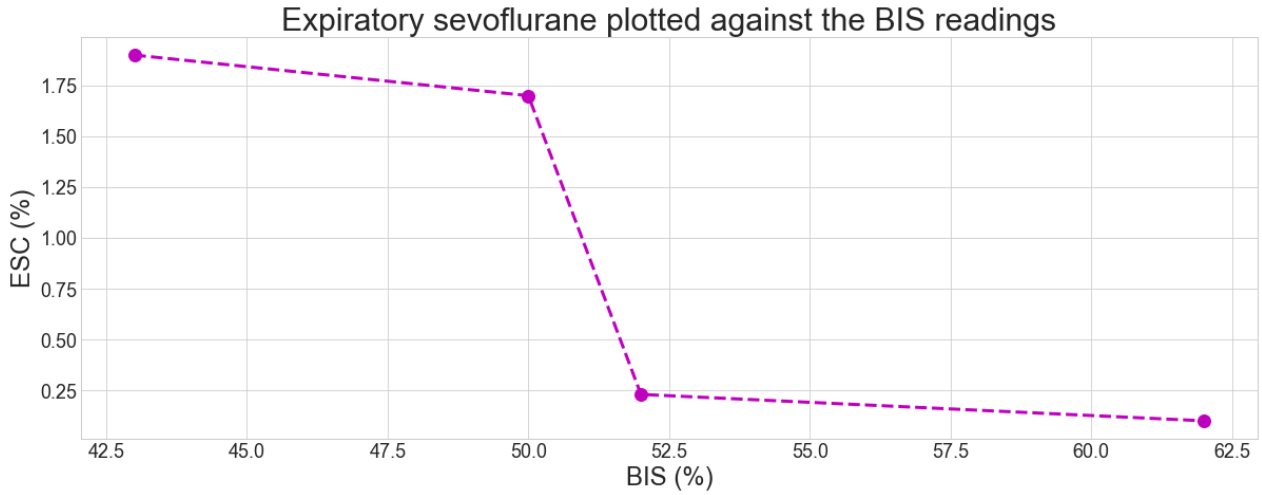

In [3]:

```
# ------------------------------------------------------------------------
# ------------------- Peak difference vs perc
# ------------------------------------------------------------------------

# pl.rcParams['figure.figsize'] = (20,7)

# fig=pl.figure()

# pl.title('Voltage range between Pa and Nb for the various ESC readings')
# pl.xlabel('ESC reading (%)')
# pl.ylabel('Pa - Nb (in uV)')

# pl.plot(perc,Pa_m_Nb, 'bo--',linewidth=3,markersize=12)

# pl.savefig("C:/Users/Carel/Google Drive/Master's Thesis/Latex Document/Carel Wessels - Master's Thesis/figs/resu

# pl.show()

# ------------------------------------------------------------------------
# ------------------- Peak difference vs perc
# ------------------------------------------------------------------------

# pl.rcParams['figure.figsize'] = (20,7)

# fig=pl.figure()

# pl.title('Voltage range between Pa and Nb for the various BIS readings')
# pl.xlabel('BIS reading (%)')
# pl.ylabel('Pa - Nb (in uV)')

# pl.plot(BIS,Pa_m_Nb, 'go--',linewidth=3,markersize=12)

# pl.savefig("C:/Users/Carel/Google Drive/Master's Thesis/Latex Document/Carel Wessels - Master's Thesis/figs/resu

# pl.show()
```

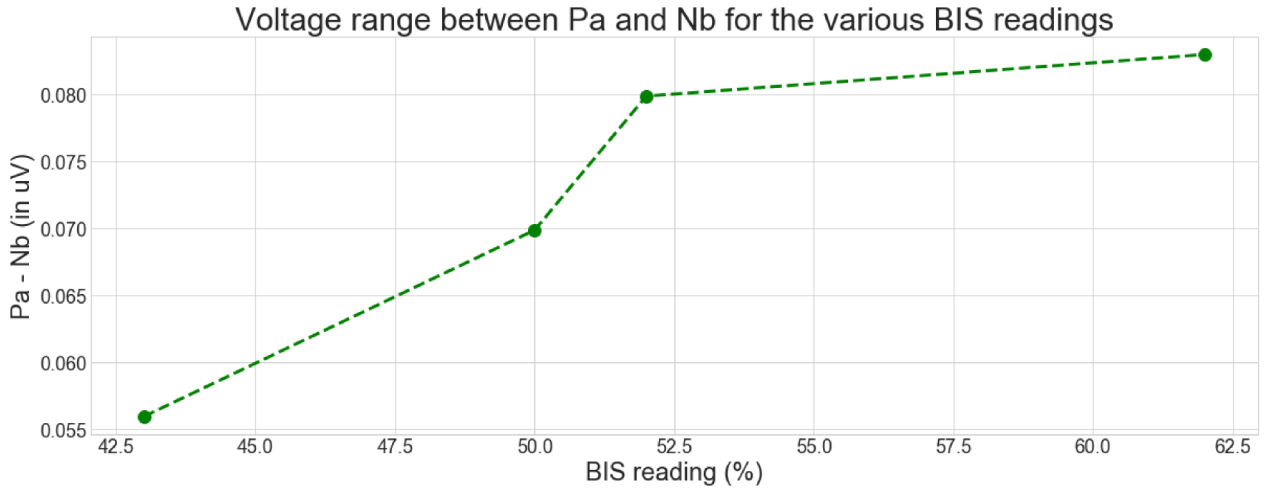

In [778]:

```
num = 3

d=[0.014677638461527047,0.012736960378200036,0.022292202535397744,0.01789244969228331]
t=[0.019410019776513486,0.017683396024146477,0.02717918023104369,0.021206448317451696]
a=[0.013436033387957581,0.013974906736738284,0.01871692338800389,0.019567444221121236]
b=[0.005357632594949195,0.005475963130179157,0.007887844598124036,0.008111754820991518]
g=[0.002315864016845413,0.002358900396197936,0.003575100049104262,0.003672553530442008]

tot=np.add(d,t)
tot=np.add(tot,a)
tot=np.add(tot,b)
tot=np.add(tot,g)

d=np.divide(d,tot)
t=np.divide(t,tot)
a=np.divide(a,tot)
b=np.divide(b,tot)
g=np.divide(g,tot)

data = (d[num],t[num],a[num],b[num],g[num])
ind = np.arange(5)    # the x locations for the groups
width = 0.8       # the width of the bars: can also be len(x) sequence

pl.rcParams['axes.prop_cycle'] = pl.cycler(color=pl.cm.viridis(np.linspace(0,1,5)))

colors = color=pl.cm.viridis(np.linspace(0,1,8))


for i in range (0,5):
    p1 = pl.bar(ind[i], data[i], width, color=colors[i])

pl.ylabel('Normalised Power')
pl.title('Power spectral density at BIS reading of ' + str(BIS[num]))
pl.xticks(ind, ('Delta\n(0-4 Hz)', 'Theta\n(4-8 Hz)', 'Alpha\n(8-13 Hz)', 'Beta\n(13-30 Hz)', 'Gamma\n(30-50 Hz)')
pl.yticks(np.arange(0, 0.4, 0.05))
pl.ylim([0,0.4])
# pl.legend((p1[0]), ('Men', 'Women'))
pl.savefig("C:/Users/Carel/Google Drive/Master's Thesis/Latex Document/Carel Wessels - Master's Thesis/figs/result

pl.show()

```

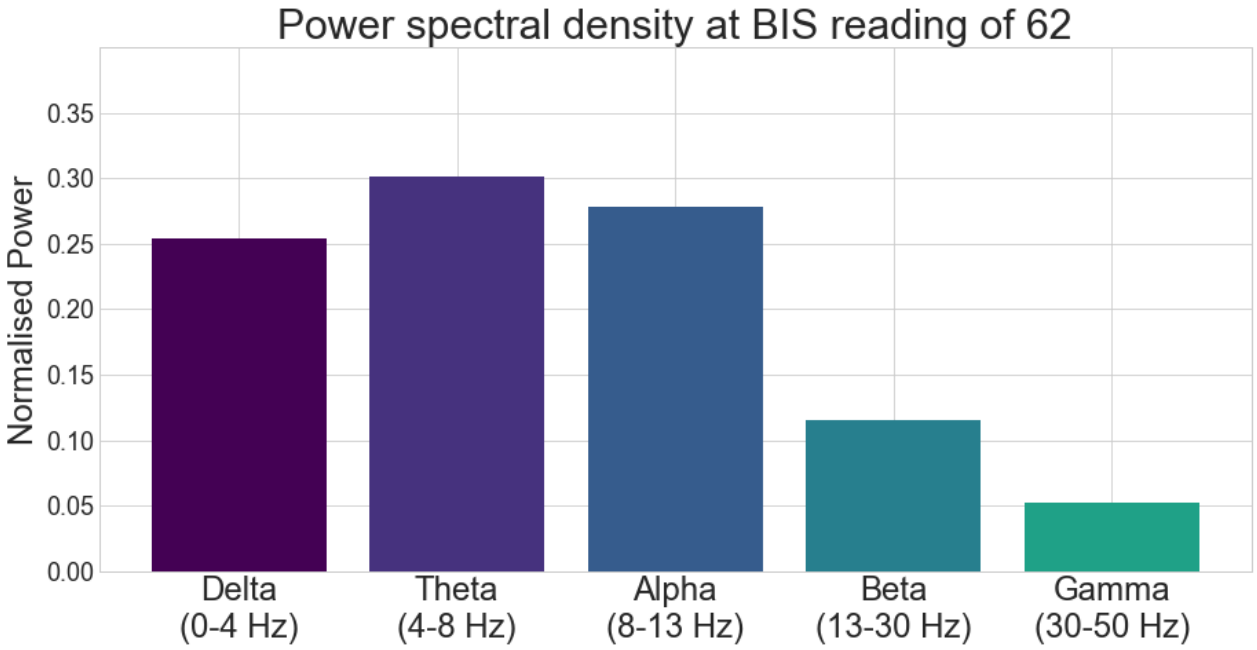

In [497]:

```
# Max frequency at 3.4389561442492376Hz
# 0.014677638461527047,0.019410019776513486,0.013436033387957581,0.005475963130179157,0.002358900396197936
# 0.26513767241805064,0.35062367005582296,0.24270924974423028,0.09891810064598851,0.04261130713590752

# Max frequency at 10.0040626603368Hz
# 0.012736960378200036,0.017683396024146477,0.013974906736738284,0.005357632594949195,0.002315864016845413
# 0.24461808652903275,0.33961623262685486,0.26839330922419863,0.10289533725371111,0.04447703436620266

# Max frequency at 1.720431748260018Hz
# 0.022292202535397744,0.02717918023104369,0.019567444221121236,0.007887844598124036,0.003575100049104262
# 0.27691567629753355,0.33762213773811517,0.24306849183260268,0.09798349077220923,0.04441020335953933

# Max frequency at 1.6727479414900617Hz
# 0.01789244969228331,0.021206448317451696,0.01871692338800389,0.008111754820991518,0.003672553530442008
# 0.25707494737100056,0.3046897813822517,0.2689208117205621,0.11654798418084805,0.052766475345337654

# ax1.plot(44.0,0.10363408769555306, 'bo',markersize=12)    0.10363408769555306+0.07897063413873524
# ax1.annotate('$P_a$',
#             xy=(44.0,0.10363408769555306), xycoords='data',
#             xytext=(-50, 50), textcoords='offset pixels',
#             arrowprops=dict(facecolor='blue', shrink=0.2),
#             horizontalalignment='center', verticalalignment='bottom',fontsize=24)

# ax1.plot(15.5,-0.05357058365494162, 'bo',markersize=12)
# ax1.annotate('$N_a$',
#             xy=(15.5,-0.05357058365494162), xycoords='data',
#             xytext=(0, -50), textcoords='offset pixels',
#             arrowprops=dict(facecolor='blue', shrink=0.2),
#             horizontalalignment='center', verticalalignment='top',fontsize=24)

# ax1.plot(85.0,-0.07897063413873524, 'bo',markersize=12)
# ax1.annotate('$N_b$',
#             xy=(85.0,-0.07897063413873524), xycoords='data',
#             xytext=(50, -50), textcoords='offset pixels',
#             arrowprops=dict(facecolor='blue', shrink=0.2),
#             horizontalalignment='center', verticalalignment='top',fontsize=24)



# ax1.plot(83.0,0.024992514623068587, 'bo',markersize=12)   0.024992514623068587+0.030981192215155134
# ax1.annotate('$P_a$',
#             xy=(83.0,0.024992514623068587), xycoords='data',
#             xytext=(-50, 50), textcoords='offset pixels',
#             arrowprops=dict(facecolor='blue', shrink=0.2),
#             horizontalalignment='center', verticalalignment='bottom',fontsize=24)

# ax1.plot(17.5,-0.02872843556813182, 'bo',markersize=12)
# ax1.annotate('$N_a$',
#             xy=(17.5,-0.02872843556813182), xycoords='data',
#             xytext=(0, -50), textcoords='offset pixels',
#             arrowprops=dict(facecolor='blue', shrink=0.2),
#             horizontalalignment='center', verticalalignment='top',fontsize=24)

# ax1.plot(124.0,-0.030981192215155134, 'bo',markersize=12)
# ax1.annotate('$N_b$',
#             xy=(124.0,-0.030981192215155134), xycoords='data',
#             xytext=(-50, -50), textcoords='offset pixels',
#             arrowprops=dict(facecolor='blue', shrink=0.2),
#             horizontalalignment='center', verticalalignment='top',fontsize=24)




# ax1.plot(49.0,0.06572740614964405, 'bo',markersize=12)     0.06572740614964405+0.0041625380529621316
# ax1.annotate('$P_a$',
#             xy=(49.0,0.06572740614964405), xycoords='data',
#             xytext=(-50, 50), textcoords='offset pixels',
#             arrowprops=dict(facecolor='blue', shrink=0.2),
#             horizontalalignment='center', verticalalignment='bottom',fontsize=24)

# ax1.plot(15.0,-0.05607362045160389, 'bo',markersize=12)
# ax1.annotate('$N_a$',
#             xy=(15.0,-0.05607362045160389), xycoords='data',
#             xytext=(0, -50), textcoords='offset pixels',
#             arrowprops=dict(facecolor='blue', shrink=0.2),
#             horizontalalignment='center', verticalalignment='top',fontsize=24)

# ax1.plot(88.0,-0.0041625380529621316, 'bo',markersize=12)
# ax1.annotate('$N_b$',
#             xy=(88.0,-0.0041625380529621316), xycoords='data',
#             xytext=(50, -50), textcoords='offset pixels',
#             arrowprops=dict(facecolor='blue', shrink=0.2),
```

Bibliography

[1] H. J. Schmitt, "History of electroencephalography", *IEEE History of Telecommunications Conference, HISTELCON 2008*, pp. 79–82, 2008. DOI: 10.1109/HISTELCON.2008.4668719.

[2] L. Veloso *et al.*, "Big data resources for EEGs: Enabling deep learning research", *2017 IEEE Signal Processing in Medicine and Biology Symposium (SPMB)*, pp. 1–3, 2017. DOI: 10.1109/SPMB.2017.8257044.

[3] T. Nakamura *et al.*, "Automatic sleep monitoring using ear-EEG", *IEEE Journal of Transilational Engineering in Health and Medicine*, vol. 5, no. June, 2017, ISSN: 2168-2372. DOI: 10.1109/JTEHM.2017.2702558. arXiv: 1701.04398.

[4] P. Kidmose *et al.*, "Auditory evoked responses from Ear-EEG recordings", *Proceedings of the Annual International Conference of the IEEE Engineering in Medicine and Biology Society, EMBS*, pp. 586–589, 2012, ISSN: 1557170X. DOI: 10.1109/EMBC.2012.6345999.

[5] P. Kidmose *et al.*, "A study of evoked potentials from ear-EEG", *IEEE Transactions on Biomedical Engineering*, vol. 60, no. 10, pp. 2824–2830, 2013, ISSN: 00189294. DOI: 10.1109/TBME.2013.2264956.

[6] F. D. Lombard, "An investigation of the Auditory P300 Event Related Potential across gender .", PhD thesis, Univesity of Pretoria, 2005, pp. 1–96.

[7] S. Sanei and J. Chambers, *EEG signal processing*. John Wiley & Sons, Ltd, 2008, pp. 10–12, ISBN: 9780470025819.

[8] B. E. Swartz, "The advantages of digital over analog recording techniques", *Electroencephalography and Clinical Neurophysiology*, vol. 106, no. 2, pp. 113–117, Feb. 1998, ISSN: 0013-4694. DOI: 10.1016/S0013-4694(97)00113-2.

[9] F. A. Azevedo *et al.*, "Equal numbers of neuronal and nonneuronal cells make the human brain an isometrically scaled-up primate brain", *The Journal of Comparative Neurology*, vol. 513, no. 5, pp. 532–541, Apr. 2009, ISSN: 00219967. DOI: 10.1002/cne.21974.

[10] M. A. Patestas and L. P. Gartner, *A Textbook of Neuroanatomy*, First. Baltimore, Maryland: Blackwell Science Ltd, 2006, pp. 20–40, ISBN: 1-4051-0340-X.

[11] B. Bruce. (). Multipolar neuron - Wikipedia, [Online]. Available: https://en.wikipedia.org/wiki/Multipolar_neuron#/media/File:Blausen_0657_MultipolarNeuron.png (visited on 09/28/2018).

[12] Multiple. (2016). Electroencephalogram (EEG) | Johns Hopkins Medicine Health Library, [Online]. Available: https://www.hopkinsmedicine.org/healthlibrary/test_procedures/neurological/electroencephalogram_eeg_92,P07655 (visited on 09/27/2018).

[13] B. Musizza and S. Ribaric, "Monitoring the depth of anaesthesia", *Sensors*, vol. 10, no. 12, pp. 10 896–10 935, 2010, ISSN: 14248220. DOI: 10.3390/s101210896.

[14] M. T. Alkire *et al.*, "Consciousness and Anesthesia", *Science*, vol. 322, no. 5903, pp. 876–880, Nov. 2008, ISSN: 0036-8075. DOI: 10.1126/science.1149213.

[15] G. Schneider and P. S. Sebel, "Monitoring depth of anaesthesia.", *European journal of anaesthesiology. Supplement*, vol. 15, pp. 21–8, May 1997, ISSN: 0952-1941.

[16] B. Heyse *et al.*, "Comparison of contemporary EEG derived depth of anesthesia monitors with a 5 step validation process", *Acta Anaesthesiol. Belg.*, vol. 60, pp. 19–33, 2009.

[17] J. C. Sigl and N. G. Chamoun, "An introduction to bispectral analysis for the electroencephalogram.", *Journal of clinical monitoring*, vol. 10, no. 6, pp. 392–404, Nov. 1994, ISSN: 0748-1977. DOI: 10.1007/bf01618421.

[18] H. Kaul and N. Bharti, "Monitoring depth of anaesthesia", *Indian J Anaesth*, vol. 46, no. 4, pp. 323–332, 2002.

[19] K. Hirota, "Special cases: Ketamine, nitrous oxide and xenon", *Best Pract. Res. Clin. Anaesthesiol*, vol. 20, pp. 69–79, 2006.

[20] J. Sleigh *et al.*, "Comparison of changes in electroencephalographic measures during induction of general anaesthesia: influence of the gamma frequency band and electromyogram signal", *British Journal of Anaesthesia*, vol. 86, pp. 50–58, 2001.

[21] P. Myles, "Prevention of awareness during anaesthesia", *Best Pract. Res. Clin. Anaesthesiol*, vol. 21, pp. 345–355, 2007.

[22] B. Palanca *et al.*, "Processed electroencephalogram in depth of anesthesia monitoring", *Curr. Opin. Anaesthesiol*, vol. 22, pp. 553–559, 2009.

[23] G. H. Klem *et al.*, "The ten-twenty electrode system of the International Federation. The International Federation of Clinical Neurophysiology.", *Electroencephalography and clinical neurophysiology. Supplement*, vol. 52, pp. 3–6, 1999, ISSN: 0424-8155.

[24] Unknown. (2018). JPEG image of Anatomy Of Ear Pinna Ear Anatomy Pinna - Anatomy Sciences - The Anatomy Body, [Online]. Available: https://theanatomybody.com/anatomy-of-ear-pinna/anatomy-of-ear-pinna-ear-anatomy-pinna-anatomy-sciences/ (visited on 09/28/2018).

[25] H. H. Jasper, "The ten-twenty electrode system of the International Federation", *Electroencephalography and clinical neurophysiology*, vol. 10, pp. 371–375, 1958.

[26] (2012). 10/20 System Positioning Manual, [Online]. Available: https://www.trans-cranial.com/local/manuals/10_20_pos_man_v1_0_pdf.pdf.

[27] R. W. Proctor and T. Van Zandt, *Human factors in simple and complex systems*, 3rd ed. CRC Press, 2017, pp. 101–109, ISBN: 9781482229561.

[28] J. Malmivuo and R. Plonsey, *Bioelectromagnetism*, January 1995. New York, Oxford: Oxford University Press, 1995, pp. 364–374, 197–232.

[29] T. Nakamura *et al.*, "In-ear EEG biometrics for feasible and readily collectable real-world person authentication", 2017. arXiv: 1705.03742v2.

[30] E. N. Marieb and K. Hoehn, *Human anatomy & physiology*, 9th ed. Pearson Education, Inc, 2012, pp. 570–581, ISBN: 0321743261.

[31] J. E. Hawkins. (Jul. 2017). Human ear, [Online]. Available: https://www.britannica.com/science/ear/Tympanic-membrane-and-middle-ear (visited on 08/02/2017).

[32] W. W. Clark and K. K. Ohlemiller, *Anatomy and physiology of hearing for audiologists*. Clifton Park, NY: Thomson Delmar, 2008, pp. 93–108, ISBN: 1401814441.

[33] P. Walsh *et al.*, "The clinical role of evoked potentials", *Neurology in Practice*, vol. 76, no. 2, pp. 16–22, 2005, ISSN: 14737086. DOI: 10.1136/jnnp.2005.068130.

[34] G. D. Dawson, "Investigations on a patient subject to myoclonic seizures after sensory stimulation.", *Journal of neurology, neurosurgery, and psychiatry*, vol. 10, no. 4, pp. 141–62, Nov. 1947, ISSN: 0022-3050.

[35] S. Sherman, "Thalamus", *Scholarpedia*, vol. 1, no. 9, p. 1583, 2006, ISSN: 1941-6016. DOI: 10.4249/scholarpedia.1583.

[36] B. Roger, "Myoclonus", *Advances in Clinical Neuroscience & Rehabilitation*, vol. 3, no. 5, pp. 20–22, 2003.

[37] P. S. Sebel *et al.*, "Evoked Potentials During Isoflurane Anaesthesia", Tech. Rep., 1986, pp. 580–585. DOI: 10.1093/bja/58.6.580.

[38] C. P. H. Heneghan *et al.*, "The effects of Althesin on the auditory evoked response in man", *Br. J. Anaesth*, vol. 56, p. 792, 1984.

[39] M. Navaratnarajah *et al.*, "Effect of etomidate on the auditory evoked response in man", *Br.J. Anaesth*, vol. 55, p. 1157, 1983.

[40] K. Tae Min, "Evoked potentials", *Yonsei University Health System*, pp. 1–28, 2007.

[41] T. Picton *et al.*, "Human auditory evoked potentials", *Electroencephalography and Clinical Neurophysiology*, vol. 36, pp. 179–190, 1974.

[42] D. Schwender *et al.*, "Midlatency auditory evoked potentials and motor signs of wakefulness during anaesthesia with midazolam", Tech. Rep., 1997, pp. 53–58. DOI: 10.1093/bja/79.1.53.

[43] C. Thornton *et al.*, "Effects of halothane or enflurane with controlled ventilation on auditory evoked potentials", *British Journal of Anaesthesia*, vol. 56, pp. 315–323, 1984.

[44] C. Thornton *et al.*, "Effect of etomidate on the auditory evoked response in man", *British Journal of Anaesthesia*, vol. 57, pp. 554–561, 1985.

[45] C. Madler *et al.*, "Sensory information processing during general anaesthesia: Effect of isoflurane on auditory evoked neuronal oscillations", *British Journal of Anaesthesia*, vol. 66, pp. 81–87, 1991.

[46] C. Heneghan *et al.*, "Effect of isoflurane on the auditory evoked response in man", *British Journal of Anaesthesia*, vol. 59, pp. 277–282, 1987.

[47] D. Newton *et al.*, "The early cortical auditory evoked response in anaesthesia: comparison of the effects of nitrous oxide and isoflurane", *British Journal of Anaesthesia*, vol. 62, pp. 61–65, 1989.

[48] D. Schwender *et al.*, "Mid-latency auditory evoked potentials and purposeful movements after thiopental bolus injection", *Anaesthesia*, vol. 49, pp. 99–104, 1994.

[49] D. Schwender *et al.*, "Effects of anaesthesia with increasing end expiratory concentrations of sevoflurane on mid-latency auditory evoked potentials", *British Journal of Anaesthesia*, vol. 81, pp. 817–822, 1995.

[50] D. Schwender *et al.*, "Mid-latency auditory evoked potentials during anaesthesia with increasing end expiratory concentrations of desflurane", *Acta Anaesthesiologica Scandinavica*, vol. 40, pp. 171–176, 1996.

[51] C. Thornton *et al.*, "Selective effect of althesin on the auditory evoked response in man.", *British Journal of Anaesthesia*, vol. 58, pp. 422–427, 1986.

[52] C. Thornton *et al.*, "Effect of propofol on the auditory evoked response and oesophageal contractility", *British Journal of Anaesthesia*, vol. 63, pp. 411–822, 1989.

[53] E. W. Jensen *et al.*, "On-line analysis of middle latency auditory evoked potentials (MLAEP) for monitoring depth of anaesthesia in laboratory rats", *Medical Engineering & Physics*, vol. 20, no. 10, pp. 722–728, Feb. 1999, ISSN: 13504533. DOI: 10.1016/S1350-4533(98)00089-7.

[54] A. Kumar *et al.*, "Comparison of auditory evoked potential parameters for predicting clinically anaesthetized state", *Acta Anaesthesiologica Scandinavica*, vol. 50, no. 9, pp. 1139–1144, Oct. 2006, ISSN: 0001-5172. DOI: 10.1111/j.1399-6576.2006.01137.x.

[55] Natus. (2017), [Online]. Available: https://natus.com/ (visited on 09/16/2017).

[56] Natus Neurology - Natus Neuro France. (2017). Natus EP Webinar: Clinical Auditory Evoked Potentials, [Online]. Available: https://www.youtube.com/watch?v=16nuoHzbL9s (visited on 09/16/2017).

[57] Tiertime. (Nov. 2013). Up plus 2, [Online]. Available: https://www.tiertime.com/up-plus-2/ (visited on 06/17/2018).

[58] MakerBot. (Jun. 2014). Replicator z18, [Online]. Available: https://www.makerbot.com/3d-printers/replicator-z18/ (visited on 06/17/2018).

[59] LPKF. (2017). Protomat s63, [Online]. Available: https://www.lpkf.com/products/rapid-pcb-prototyping/circuit-board-plotter/protomat-s63.htm.

[60] OpenBCI. (2015). Cyton Biosensing Board, [Online]. Available: https://shop.openbci.com/products/cyton-biosensing-board-8-channel?variant=38958638542 (visited on 05/11/2017).

[61] OpenBCI. (2015). Gold Cup Electrodes, [Online]. Available: https://shop.openbci.com/collections/frontpage/products/openbci-gold-cup-electrodes?variant=9056028163 (visited on 05/11/2017).

[62] JBL. (2016). T450BT Wireless on-ear headphones, [Online]. Available: https://uk.jbl.com/headphones-wireless/JBL+T450BT.html (visited on 03/29/2018).

[63] Geist. (2016). 36BL Bluetooth Earphones for Running and Sport, [Online]. Available: https://www.geistaudiosa.co.za/copy-of-geist-18bl (visited on 01/11/2018).

[64] 3M. (2014). Peltor X2 Earmuffs X2A, [Online]. Available: https://www.3m.com/3M/en_US/company-us/all-3m-products/~/3M-PELTOR-X2-Earmuffs-X2A-37271-AAD-Over-the-Head-10-EA-Case/?N=5002385+3294326341&rt=rud (visited on 09/11/2017).

[65] Weaver and company. (2016). Ten20 Conductive Paste, [Online]. Available: http://www.weaverandcompany.com/ten20.html (visited on 05/01/2018).

[66] Weaver and company. (2016). NuPrep skin prep gel, [Online]. Available: http://www.weaverandcompany.com/nuprep.html (visited on 05/01/2018).

[67] Python. (Mar. 7, 2018). Python programming language. version latest version 3.7.1, [Online]. Available: https://www.python.org/.

[68] Anaconda. (Mar. 7, 2018). Anaconda python programming environment. version latest version 5.3, [Online]. Available: https://www.anaconda.com/.

[69] MathWorks. (May 11, 2017). Matlab. version 2017a and 2018b, [Online]. Available: https://www.mathworks.com/products/matlab.html.

[70] Trimble Inc. (May 19, 2017). Sketchup pro trial and sketchup make. version 2017, [Online]. Available: https://www.sketchup.com/download/all.

[71] Autodesk. (Apr. 18, 2018). Inventor 3D CAD Software. version 2018, [Online]. Available: https://www.autodesk.com/products/eagle/free-download.

[72] Autodesk. (Apr. 18, 2018). Eagle PCB Design Software. version 2018, [Online]. Available: https://www.autodesk.com/products/eagle/overview.

[73] ON Semiconductors. (2012). 2N3903 - General Purpose NPN Transistors, [Online]. Available: https://www.onsemi.com/pub/Collateral/2N3903-D.PDF (visited on 04/07/2018).

[74] Texas Instruments. (2004). LM386 Low Voltage Audio Power Amplifier, [Online]. Available: http://www.ti.com/lit/ds/symlink/lm386.pdf (visited on 04/07/2018).

[75] Texas Instruments. (2012). ADS1299-x Low-Noise, 4-, 6-, 8-Channel, 24-Bit, Analog-to-Digital Converter for EEG and Biopotential Measurements, [Online]. Available: http://www.ti.com/lit/ds/symlink/ads1299.pdf (visited on 05/18/2017).

[76] OpenBCI. (2016). Ultracortex Mark IV, [Online]. Available: https://github.com/OpenBCI/Docs/blob/master/Headware/01-Ultracortex-Mark-IV.md (visited on 08/23/2017).

[77] OpenBCI. (2016). Python Hardware Communication, [Online]. Available: https://github.com/OpenBCI/OpenBCI_Python (visited on 08/23/2017).

[78] OpenBCI. (2015). OpenBCI Cyton SDK - Serial Command Protocols, [Online]. Available: http://docs.openbci.com/OpenBCI%20Software/04-OpenBCI_Cyton_SDK (visited on 08/24/2017).

[79] SciPy Cookbook. (Apr. 17, 2018). Filtfilt, [Online]. Available: https://scipy-cookbook.readthedocs.io/items/FiltFilt.html.